I. Group 14 Metal Alkoxides: Synthesis and Reactivity Studies

II. Synthesis of Novel Planar Chiral Complexes Based on [2.2]Paracyclophane

Lorenzo Ferro

DPhil Chemistry

University of Sussex

May 2011

I hereby declare that this thesis has not been and will not be, submitted in whole or in part to another University for the award of any other degree.

Signature_____

UNIVERSITY OF SUSSEX

LORENZO FERRO, DPHIL CHEMISTRY

I. GROUP 14 METAL ALKOXIDES: SYNTHESIS AND REACTIVITY STUDIES

II. SYNTHESIS OF NOVEL PLANAR CHIRAL COMPLEXES BASED ON [2.2]PARACYCLOPHANE

ABSTRACT

I. A series of group 14 β-diketiminate alkoxides (BDI)EOR (BDI = [CH{(CH_3)CN-2,6-$^{i}Pr_2C_6H_3$}$_2$; E = Ge, Sn, Pb; R = ^{i}Pr, ^{s}Bu, ^{t}Bu) was synthesised and characterised. The reactivity towards aliphatic and unsaturated electrophiles was investigated. For the tin and lead systems, an unexpected trend was observed. For instance, they do not or very sluggishly react with aliphatic electrophiles, but readily activate carbon dioxide. The slower tin system was used to investigate the mechanism of carbon dioxide insertion through detailed kinetic, thermodynamic and DFT studies.

The isostructural germanium system showed a different reactivity pattern. Treatment with aliphatic electrophiles and iodine leads to cationic Ge(IV) oxidative addition products, whereas reactivity towards heterocumulenes was not observed. The Lewis basic behaviour was also investigated, revealing that the germanium lone pair coordinates to copper(I) iodide.

The synthesis of an isostructural mercury system was also attempted, resulting in the formation of the first homoleptic bis-β-diketiminate complex bound through the γ-carbons.

II. Monosubstituted paracyclophane was exploited in the synthesis of a novel β-diketimine and enaminone both possessing planar chirality. These were used to stabilise *N,N'*- and *N,O*-chelated scandium and zirconium complexes, potentially suitable for asymmetric hydroamination catalysis. Preliminary tests show no catalytic activity.

Al nonno Enzo e al nonno Liliano,
che mi hanno guidato con il loro esempio.

Acknowledgements

First of all I would like to express my sincere gratitude to Robin, my supervisor, for giving me the opportunity of living such an important and beneficial experience for both my scientific and personal growth. It is hard to overstate how precious she has been, always being present, ready to answer to any question and discuss any of my ideas. For me, she has not been only a teacher, but a friend and an advisor too.

My special thanks also go to Martyn, for introducing Robin to me when I applied for an MSc with him, for the big help he has given with X-ray crystallography and for letting me win our last bowling match, and to Iain, for all the help with any NMR related issue. Sincere thanks are extended to Geoff, my co-supervisor, for his generousity; Peter, for X-ray crystallography; Ali, for mass-spec; and Hazel, for helping me with calculations.

I should give a special mention to Morgan, Eric, Lisa, Lamin, Mat, Phil, Ben, Tara, Nikki and Jess for their help and advice, as well as for the wonderful time I had in and outside the lab… and at the pub. If I will miss Brighton, it is mainly thanks to them!

I am extremely grateful to my flatmates Vale and Fulvio, for always being such good friends and making me feel at home, as well as to all of my friends who came visiting during these cold and rainy years, especially Fab and Deer.

My best appreciation goes to my parents, Fabrizio and Isi, and my sister Livia, for their love, unconditioned support and understanding, and for never failing faith in me.

Lastly, a special thanks goes to the Swan for their exquisite gammon, egg & chips, to the Evening Star, for their awesome beers, and to EPSRC, for fundings.

This thesis is also dedicated to the memory of my cat Wednesday.

Table of Contents

List of Figures, Schemes and Tables

List of Abbreviations

χ_g	mole fraction solubility
BAr^F	tetrakis(pentafluorophenyl)borate
BDE	bond dissociation energy
BDI	β-diketiminate
CSA	camphorsulfonic acid
CSC	camphorsulfonyl chloride
Cp	cyclopentadiene
DCM	dichloromethane
de	diasteroisomeric excess
Dipp	diisopropylphenyl
DOSY	diffusion ordered NMR spectroscopy
dppe	1,2-bis(diphenylphosphino)ethane
DFT	density functional theory
EA	elemental analysis
ee	enantiomeric excess
GIAO	gauge invariant atomic orbital
HSQC	heteronuclear single quantum coherence
HMBC	heteronuclear multiple bond correlation
IR	infrared
ma	maleate
Mes	trismethylphenyl
nacnac	β-diketiminate

NMR	nuclear magnetic resonance
papo	4-([2.2]paracyclophenylamino)pent-3-en-2-one
PacNac	*N*-[2.2]paracyclophenyl-4-([2.2]paracyclophenylimino)pent-2-en-2-amine
PC	paracyclophenyl
pK_a	acidity in aqueous solution
pz	pyrazolyl
Tbt	tris-(bis(trimethylsilyl)methyl)phenyl
THF	tetrahydrofuran
Tp	trispyrazolyl-hydroborate
Trip	triisopropylphenyl
UV	ultraviolet

I. Group 14 Metal Alkoxides: Synthesis and Reactivity Studies

1 Introduction

1.1 Genesis and evolution

Germanium, tin and lead are all members of a single family, called the 'silicon subgroup', 'the heavier elements of Group 14' or also "tetrels" or "mesoids", the latter due to their central position in the short version of Mendeleev's periodic table.

These elements were discovered at very different stages: while tin and lead were both discovered before the third millennium BC, germanium's physical and chemical properties – despite being predicted by Mendeleev in 1870 – had been unknown until 1886, when Winkler experimentally confirmed Mendeleev's prediction isolating a new element from the novel mineral argirodit (Ag_6GeS_5) and named it in honour of his motherland.[1] Only one year after its discovery, Winkler synthesised Et_4Ge,[2] officially giving birth to the organometallic chemistry of germanium. However, due to the scarcity and high prices of germanium and its derivatives, Et_4Ge remained the only organogermanium compound until 1925, when the discovery of new germanium sources (germanite, rhenierite and processing wastes of coal ashes and sulfide ores)[3] stimulated the actual start of organometallic germanium chemistry in the second quarter of the 20th century.[4] This chemistry was predominantly regarding hypervalent (tetravalent) germanium; in fact, the first kinetically stable diorganylgermylenes $[(Me_3Si)_2CH]_2Ge$ and $[(Me_3Si)_2N]_2Ge$ had been synthesised for the first time only in the last quarter of the twentieth century.[5,6]

The bioinorganic chemistry of germanium started in 1922, when it was discovered that GeO_2 stimulates erythropoesis (red blood cells production),[7] which led to the development of the organogermanium drug Ge-132 in 1968 and to the establishment of a special Germanium Research Institute in Tokyo.[8] It should be also mentioned that the cytotoxic antitumor drug 'spyrogermanium' was developed in 1974.[9] In the last 40 years organogermanium chemistry has found many practical applications in medicine and agriculture as drugs and biostimulants,[10] as well as in the microelectronic industry.[11,12]

In contrast to the relatively recently discovered germanium, tin and lead were two of the seven main elements known to ancient man. Until the 17th century these elements were often confused with each other, as witnessed by their latin names *Plumbum album* (Sn) and *Plumbum nigrum* (Pb), literally translatable as 'white lead' and 'black lead' respectively.[1] The Swiss chemist Carl Löwig, also known for the discovery of bromine,[13] can be considered the forefather of organometallic chemistry of these two elements. After 1852, year of the synthesis of polyethylstannylene $(Et_2Sn)_n$ and hexaethyldiplumbane $Et_3PbPbEt_3$,[14] Löwig developed methods for the synthesis of several organic (and toxic) derivatives of tin and lead in the complete absence health and safety precautions, and ironically died at the age of 87 because of an unrelated accident. Despite the early synthesis of $(Et_2Sn)_n$, it is necessary to specify that this class of "divalent" tin alkyls synthesised for over a century were not monomers, as originally thought, but the cyclic oligomers or polymers of tetravalent tin.[15] Only in 1976, in the Lappert laboratory, was the synthesis of the first stable truly divalent organotin derivative $[(Me_3Si)_2CH]_2Sn$ accomplished.[16] In contrast, divalent organolead compounds had

been known quite early in the 19th century with the isolation of the red powder-like diphenylplumbylene Ph_2Pb in 1922.[17]

Investigations into the bioinorganic chemistry of tin and lead are the ones that have received the most attention among all the other metals, being comparable only to that of mercury compounds.[18] Investigations into the organotin compounds initially regarded their toxicity[19] and subsequently their fungicidal,[20] antimicrobial and insecticide[21] action. During World War II, organotin compounds were also studied as poisoning substances,[22] but none of them were employed as poisoning agents in the war. These studies however led to the conclusion that toxicity of R_3SnX (X = halide) was caused by the R_3Sn^+ ion. In the second half of the 20th century, tin was used for both technological and agriculture purposes finding practical application as photo- and thermo-stabiliser, olefines polymerisation catalyst, biocide, pesticide and bioprotecting agent.[23] As such, organotin compounds world production reached 35,000 tons in 1980.[12]

Organic lead compounds toxic action was known even to the first researchers in the middle of 19th century;[24] the harmful physiological effect of Et_4Pb was studied for over a century, and especially at the end of the 20th century due to its vast usage as an anti-knock agent of motor fuels,[25] and, similarly to the isostructural tin analogue, its toxicity depends on the cleavage of one Pb–C bond *in vivo* producing the highly toxic Et_3Pb^+ cation.[26] Saunders investigated organolead compounds as sternutators and irritating agents for the Ministry of Supply of England during WWII. Remarkably, the author and his co-workers voluntarily tested the effects of a wide series of toxic compounds on themselves, making big progress in the development and preparation of lead organic derivatives.[27] Despite having found use as components of paints, fungicides and herbicides in the past, practical

employment of organometallic lead will only decrease in the future due to its toxicity and its release in the environment.[28] Lead poisoning can also count some famous personalities among its victims, such as Caravaggio, Beethoven, Van Gogh and Goya, who used to wet their paintbrush with their mouths, and it became the most common environmentally caused disease in the United States.[29] However, large amounts of lead are still used in the automobile industry for lead-acid batteries.[30]

1.2 Recent advances in tetrylenes organometallic chemistry

The chemistry of low-valent germanium,[5,31,32] tin[16,33-35] and lead[6,32,34,36] has attracted much attention in the last quarter of the past century. It has become evident in the last decades that monomeric tetrylenes complexes can be stabilised, either kinetically or thermodynamically, by using sterically encumbering or electron-donating ligands respectively. A wide range of ligand systems have been successfully employed with this aim. Exhaustive reviews on heavier analogues of carbenes and alkynes have been recently published respectively by Tokitoh and Power and Fischer.[37] This chapter will discuss the most remarkable examples of recently published stable monomeric tetrylenes (i.e. divalent tetrels), not possessing E–E or E–TM (E = Ge, Sn, Pb; TM = transition metal) bonds, and their reactivity. For clarity, trivial reaction byproducts will not be reported in schemes.

Power and co-workers developed a series of substituted terphenyl ligands $[C_6H_3\text{-}2,6\text{-}Ar_2]^-$ (Ar^1 = Mes = C_6H_2-2,4,6-Me_3; Ar^2 = Trip = C_6H_2-2,4,6-$^iPr_3$; Ar^3 = Dipp = C_6H_3-2,6-$^iPr_2$) used to stabilise both homo- and heteroleptic tetrylene complexes.[38] Not only do such ligand systems prove to be very effective for the

formation of heavier analogues of alkenes and alkynes,[39] but they are also useful for the synthesis of elusive compounds, such as the quasi one-coordinate lead cation $[(C_6H_3\text{-}2,6\text{-}Trip_2)Pb\cdot(\eta^2\text{-}MeC_6H_5)][B(Me)(C_6F_5)_3]$,[40] as well as for the activation of small molecules by low coordinate germanium, tin and lead complexes. For instance, heteroleptic terphenyl germylene **I** activates carbon monoxide, affording α-germyloxy ketones **II** via a CO double insertion into the Ge–Ar bond and alkyl migration from one of the flanking rings (Scheme 1).[41]

Scheme 1 Carbon monoxide activation by heteroleptic diarylgermylenes.

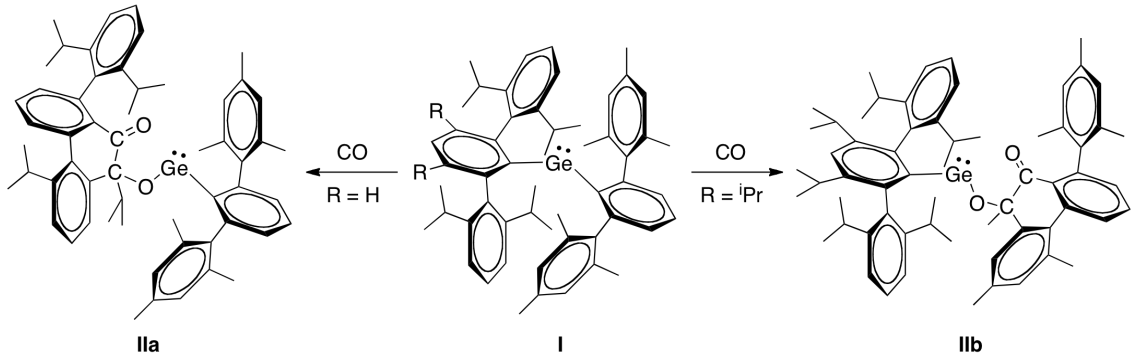

Molecular hydrogen and ammonia are also activated by series of homoleptic terphenyl germylenes and stannylenes. Dihydrogen activation resulted in the formation of the oxidative addition germanium(IV) complex. On the other hand, reaction with ammonia produced a bridging amide with concomitant arene elimination. The reactivity also proved to be dependent on small variations of the steric bulk of the ligands.[42] More recently, a phosphinidene terphenyl ligand $[PC_6H_3\text{-}2,6\text{-}Dipp_2]^{2-}$ has been developed affording the $\{E(\mu\text{-}PC_6H_3\text{-}2,6\text{-}Dipp_2)\}_2$ (E = Ge, Sn) dimer.[43]

Baines and co-workers have exploited the strong donor ability of the *N*-heterocyclic carbene $[(MeCN^iPr)_2C:]$ to stabilise a germanium(II)-centered dication bound to three carbene ligands, **IV**, prepared from the NHC stabilised germanium

dichloride, **III** (Scheme 2). The lack of colour of the crystals suggests the absence of back-bonding from the germanium lone pair to the carbenes; this theory is backed up also by DFT calculations.[44]

Scheme 2 Synthesis of stabilised germanium dications. R = [(MeCN^{i}Pr)$_2$C:]

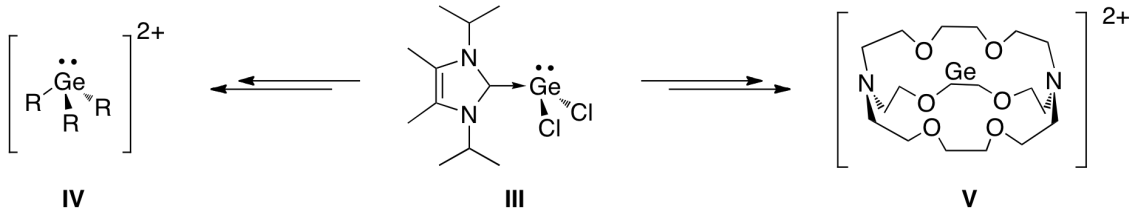

IV **III** **V**

The dichloride precursor, **III**, was also used to isolate the free Ge^{2+} cation as the salt (Ge·cryptand[2.2.2])$(O_3SCF_3)_2$, **V** (Scheme 2). The germanium centre is stabilised by numerous weak donor–acceptor interactions, and it did not exhibit a stereochemically active lone pair of electrons.[45] Baines and co-workers also used other crown ethers to stabilise a Ge^{2+} center, showing the structure to be dependent on the cavity size.[46]

The bulkier NHC carbene [(HCNDipp)$_2$C:] was employed by Rivard and co-workers to prepare the donor/acceptor-stabilised germylene dihydride complex [(HCNDipp)$_2$C·GeH$_2$·BH$_3$], **VII** (Scheme 3).[47]

Scheme 3 Synthesis of germylene dihydride and Ge^0 NHC-stabilised complexes.

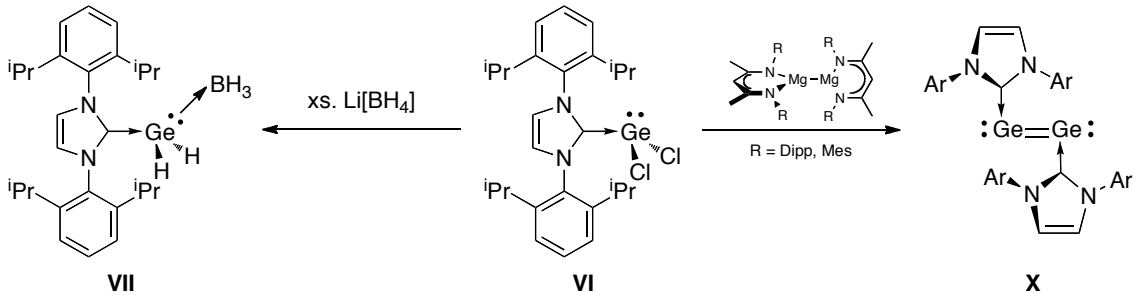

VII **VI** **X**

Rivard also synthesised very recently stable monomeric two-coordinate germylene and stannylene complexes supported by two bis(amido)silyl ligands [{$^{i}Pr_2Si(NDipp)_2$}E:] and [{$^{i}Pr_2Si(NSiPh_3)_2$}E:] (E = Ge, Sn).[48] The germanium system **VIII** reacts with chalcogens undergoing oxidative addition and yielding dimeric oxo- and sulfido compounds, **IX** (Scheme 4). The bis(amido)silyl ligand system, thanks to its easily tuneable steric properties, is a good candidate for the stabilisation of other low-coordination environments.

Scheme 4 Synthesis of oxo- and sulfido bridged bis(amido)silyl germylenes.

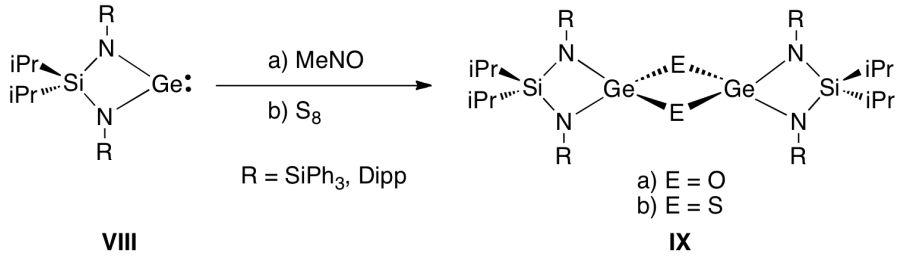

The NHC stabilised $GeCl_2$ complex **VI** was reported by Jones and co-workers and the carbene nucleophilic power was exploited for the stabilisation of the digermanium(0) species $[(HCNDipp)_2C{\cdot}Ge]_2$, **X**, obtained by reduction of the chloride precursor by a bulky β-diketiminate magnesium(I) dimer (Scheme 3).[49] A series of monomeric homoleptic amidinate and guanidinate tetrylenes complexes [{$RC(NDipp)_2$}$_2$E:] (R = H, ^{t}Bu, N$^{i}Pr_2$; E = Ge, Sn, Pb) was also successfully synthesised.[50,51] The amidinate ligands bearing a *tert*-butyl and a di-*iso*-propylamido group in the backbone have also been employed in the synthesis of the heteroleptic germylidene chloride complex **XI**, used as a precursor for the synthesis of germanium(I) dimers [{$RC(NDipp)_2$}Ge]$_2$ (R = ^{t}Bu, N$^{i}Pr_2$), **XII**, by reduction with potassium (Scheme 5).[50]

The less sterically hindered amidinate ligand $[PhC(N^tBu)_2]^-$ was used by Roesky and co-workers to stabilise a monomeric heteroleptic germanium(II) chloride complex **XI**.[52] Reduction of **XI** with potassium afforded the germanium(I) dimer $[\{PhC(N^tBu)_2\}Ge]_2$ **XIII**, which, due to the lower steric pressure, crystallises in the unusual *gauche*-bent geometry (Scheme 5). This is in contrast to the *trans*-bent geometry of the previously mentioned complexes having an E–E bond.

Scheme 5 Reduction of amidinate and guanidinate germylene chlorides.

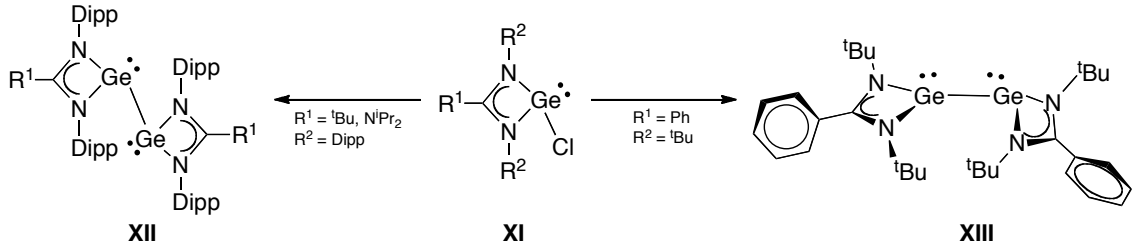

A few other remarkable coordination examples of divalent germanium, tin and lead, shown in Scheme 6, are worth mentioning. Breher and co-workers, reported the synthesis of the pyrazolyl stannylene $[\{Sn(3,5\text{-}R_2pz)_2\}_2]$ (R = ^{t}Bu, CF_3) **XIV**, which is formally described as an 'inside-out distannene' and representing the first quadruply R-bridged olefin isomer of a heavier Group 14 element.[53] Wright and co-workers synthesised the stannylene 6π-dianion $[\{C_6H_4\text{-}1,2\text{-}P_2\}Sn]^{2-}$, **XV**, which is stabilised by a non-sterically hindered phosphide.[54] This complex is a heavier analogue of an Arduengo-type carbene. Izod and co-workers recently developed sterically demanding phosphorus-based ligands for the stabilisation of germylenes and stannylenes, both with (**XVI**)[55] and without (**XVII**)[56] peripheral donor groups. Agostic B–H···E (E = Sn, Pb) interactions were also exploited for the synthesis of stable seven-membered cyclic heavy tetrylenes (**XVIII**).[57] Lastly, Hahn and co-workers managed to trap the heavier tetrylene analogues of carbon monoxide

thanks to the hydrolysis of a benzannulated lutidine-bridged bistannylene to give complex **XIX**.[58]

Scheme 6 More tetrylene coordination examples.

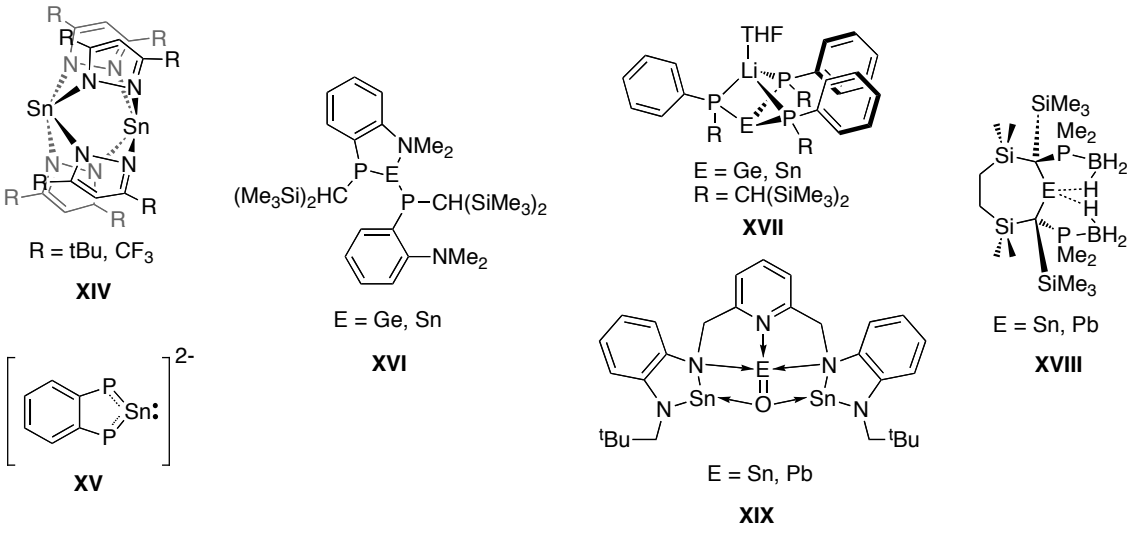

1.2.1 β-diketiminate ligands

Alongside the cyclopentadienyl ligand (Scheme 7, R = H, Me, plus other varieties), the β-diketiminate ligand – generally denoted as "$(R^1)_2$-nacnac"[59] (R^2 = Me, R^3 = H) or, in its bulkier and more popular and version, "BDI"[60] (R^1 = Dipp, R^2 = Me, R^3 = H) – occupies one of the seats of honour in the list of ancillary ligands, thanks to its ability to stabilise and generate unique coordination environments around metal center.

Scheme 7 Cyclopentadienide (left) and β-diketiminate (right) anionic ligands.

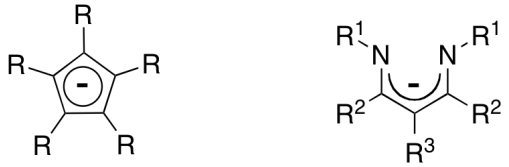

The β-diketiminate backbone is analogous to the acetylacetone (acac) one, with the oxygen atoms being substituted by nitrogen-based groups NR (R = aryl, alkyl, silyl), thus providing a steric protection of the metal centre not given by acac. The most popular BDI ligand (R^1 = Dipp, R^2 = Me, R^3 = H), thanks to its steric and electronic versatility, its monoanionic nature and the ease in preparation in multigram scale has seen an explosion in popularity in the last decade. For instance, it has been successfully employed in the stabilisation of main group and transition metals, as well as actinides and lanthanides metal centers.[61]

Outside of group 14 chemistry, a few representative examples of the use of this class of ligands are shown in Scheme 8. Group 13 analogues of a singlet carbene (**XX**) were reported by Roesky and Power. The aluminium(I) complex was obtained by the reduction of (BDI)AlI_2 with potassium,[62] while the gallium(I) system was synthesised by salt metathesis between (BDI)Li and 'GaI'.[63] Hill and co-workers exploited small variations of the aryl groups substituent to produce a series of indium(I) complexes. A monomeric In(I) complex (**XX**) was isolated when using the bulkier BDI ligand (Ar = Dipp). When the steric hindrance of the aryl group was reduced to Ar = Mes, a dimer was obtained; finally, utilising the less bulky aryl group (Ar = 3,5-MeC_6H_3) the linear hexaindium chain complex **XXI** was isolated.[64]

Jones and co-workers reduced (BDI)MgI with elemental potassium to produce a dimeric magnesium (I) complex **XXII**, possessing a magnesium-magnesium single bond.[65] Tsai and co-workers isolated the dichromium(I)[66] and divanadium(I)[67] inverted-sandwich complexes **XXIII**, via reduction of the (BDI)MCl_n (M = Cr, n = 1 or M = V, n = 2) with KC_8.

Scheme 8 β-diketiminate stabilised complexes.

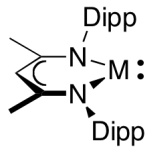

M = Ga, Al, I

XX

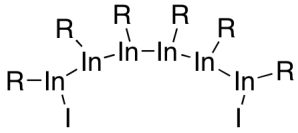

R = [CH{(CH$_3$)CN(3,5-MeC$_6$H$_3$)}$_2$]

XXI

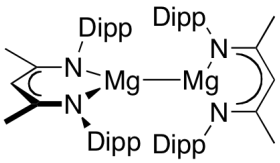

XXII

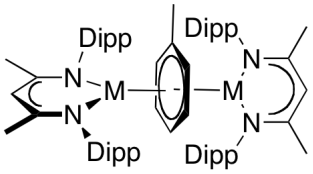

M = Cr, V

XXIII

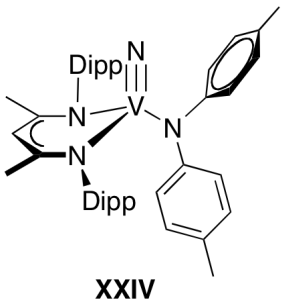

XXIV

Mindiola and co-workers synthesised a very rare example of neutral low-coordinate vanadium terminal nitrido complex **XXIV** by means of a metathesis reaction of (BDI)V(NAr$_2$)Cl with sodium azide and the concomitant evolution of N_2.[68] Holland and Limberg used a bulkier BDI version, in which the methyl groups in the backbone were substituted by *tert*-butyl groups (^{tBu}BDI), to stabilise dimeric nickel(I)[69] and iron(I)[70] dinitrogen complexes **XXV** (Scheme 9).

The nickel complex was obtained by treatment of (^{tBu}BDI)NiBr **XXVI** with KHBEt$_3$ in hexane under a N_2 atmosphere, while the iron complex was obtained by the reduction of (^{tBu}BDI)FeCl **XXVII** with naphthalenide. Both the dinitrogen complexes **XXV** (M = Fe, Ni) were further reduced to K$_2$[(^{tBu}BDI)MNNM(^{tBu}BDI)] **XXVIII**, in which the potassium atoms coordinate to both the dinitrogen fragment and the aryl groups. Impressively, Limberg managed to isolate the oddly charged complex K[(^{tBu}BDI)NiNNNi(^{tBu}BDI)] **XXIX** and found that this can be prepared also by comproportionation reactions using the appropriate stoichiometry of the Ni^{I} **XXV** and Ni^0 **XXVIII** or Ni^{II} **XXVI** and Ni^0 **XXVIII** complexes.[69]

Scheme 9 Stepwise dinitrogen reduction mediated by iron- and nickel-based complexes.

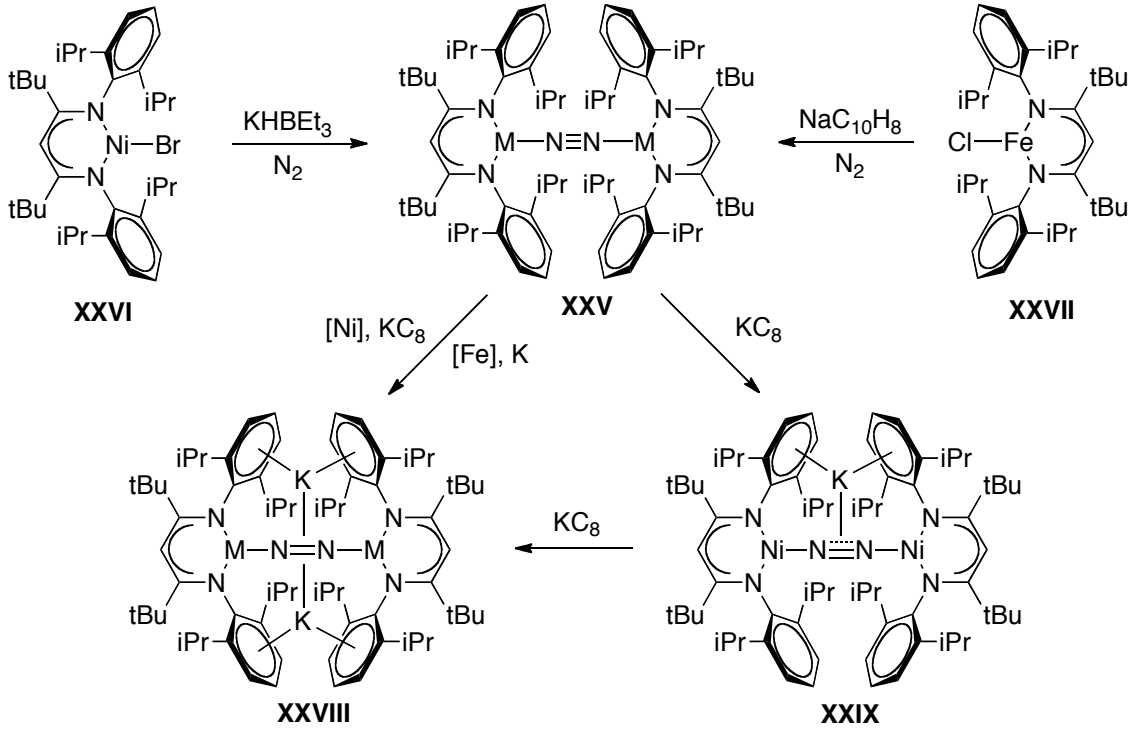

The first tetrylene β-diketiminate complexes were independently reported at the beginning of 2001 by three research groups, who reported the synthesis and derivatisation of β-diketiminate divalent germanium and tin chloride, with the ligand differing only in the steric hindrance of the aryl groups: phenyl (Barrau),[71] mesityl (Dias)[72] and 2,6-di-*iso*-propylphenyl (Roesky and Power).[73] The series of β-diketiminate Group 14 complexes was completed only in 2007 with the synthesis of the lighter silylene (Driess),[74] and the heavier plumbylene (Fulton and Lappert),[75] both utilising the bulkier ligand version (BDI). As $(Ph)_2$- and $(Mes)_2$-nacnac tetrylene chemistry does not differ from the BDI one, only the latter chemistry, being also the more developed one, will be discussed here.

The most common precursor for BDI Group 14 heavier complexes are the metal halide (BDI)ECl (E = Ge, Sn, Pb) complexes, **XXX**, which have been extensively utilised generally exploiting simple halide-metathesis reactions to produce a wide

series of complexes (Scheme 10). This has included the synthesis of alkyl **XXXI**,[76,77] alkoxide and aryloxide **XXXII**,[78-81] amide[75,77,82] and phosphide **XXXIII**[83,84], which were all synthesised by the treatment of (BDI)ECl with the appropriate alkali metal derivative for all the tetrylene series. The hydride and azide complexes **XXXIV**,[85] and **XXXV**[73] were generated only as germanium and tin analogues. The triflate complexes **XXXVI**[73,76] were generated by salt metathesis with silver triflate.

Scheme 10 (BDI)ECl (E = Ge, Sn, Pb) reactivity pattern.

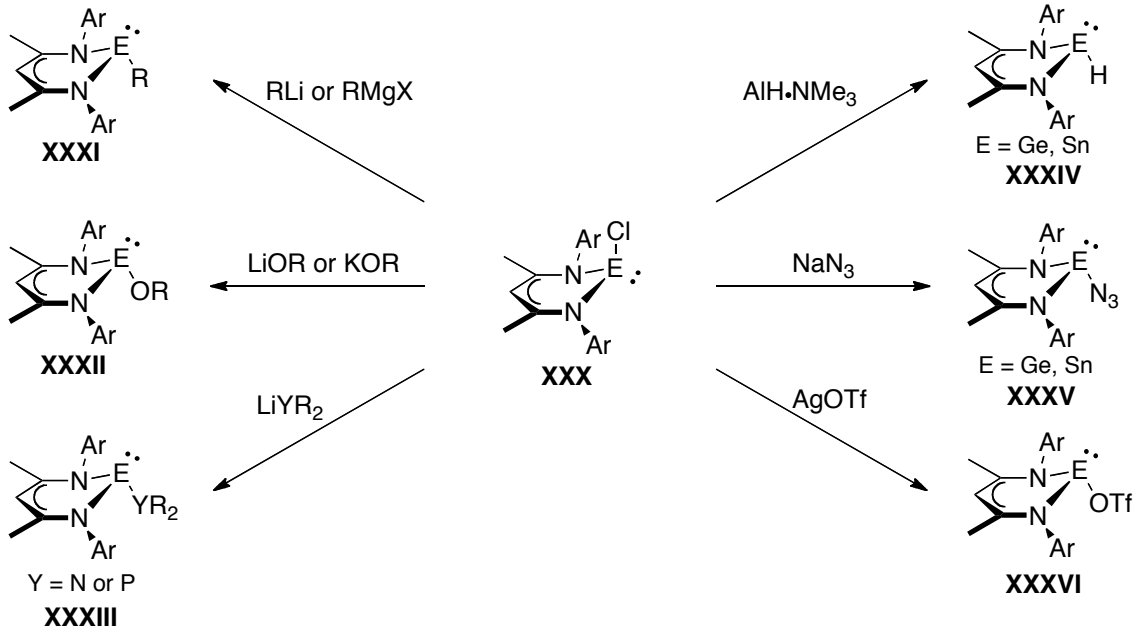

The hydrido complex (BDI)GeH reacts facilely with unsaturated compounds (Scheme 11). For instance, reactions with diazo-derivatives proceeds via an end-on nitrogen insertion into the Ge–H bond, with subsequent hydrogen transfer to give the substituted hydrazone derivative **XXXVII**.[86] The hydride ligand of (BDI)GeH is transferred to unsaturated bonds, such as alkynes or carbon dioxide.

Treatment of the germanium hydride **XXXV** with alkynes produced the first example of germanium(II)-substituted alkenes **XXXVIII**, while treatment with CO_2 resulted in the heavier analogue ester of formic acid **XXXIX** via formal

hydrogermylation reactions. Similar reactivity is also observed with elemental sulfur at room temperature, with the formation of the germanium analogue of dithiocarboxylic acid **XL**.[87] The hydride **XXXV** also reacts with nitrous oxide to form the hydroxide complex **XLI**, and with fluorinated-ketones to produce the alkoxide complex **XLII** via a hydride nucleophilic addition to the carbonyl.[88]

Scheme 11 BDI-germanium(II) hydride reactivity pattern.

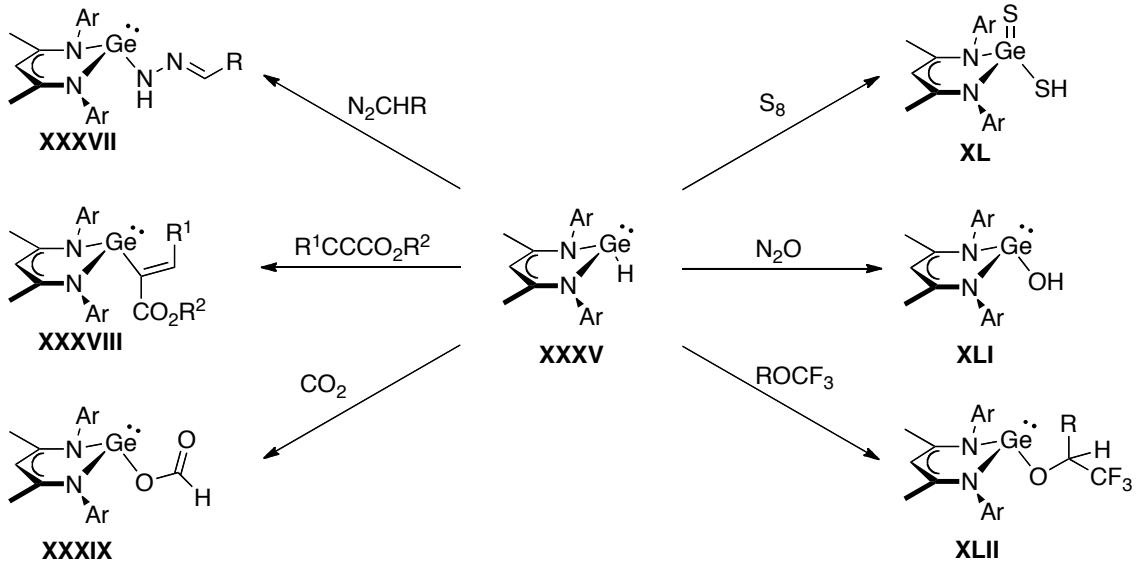

The reactivity of the isostructural tin analogue (BDI)SnH towards carbon dioxide, ketones, alkynes and other nitrogen-based unsaturated compounds is analogous to the germanium system, giving the corresponding hydrostannylation products.[89]

The hydroxide (BDI)GeOH, **XLI**, can also be synthesised by the reaction of (BDI)GeCl **XXX** with water in the presence of a bulky *N*-heterocyclic carbene (Scheme 12).[90] The similar tin alkoxide was also isolated via the hydrolysis of the iron tetracarbonyl adduct of the β-diketiminate tin amide **XLIII** to give the bimetallic hydroxide complex **XLIV**.[91]

The reactivity of other germylenes and stannylenes derivatives has not been fully examined, with the exception of the tin(II) alkoxide (BDI)SnO^iPr. This compound was isolated by Gibson and co-workers and utilised as an initiator for the polymerisation of *rac*-lactide. This group also investigated the role of the $5s^2$ lone pair in the catalysis mechanism.[60]

Scheme 12 Synthesis of BDI-germylene and –stannylene hydroxides.

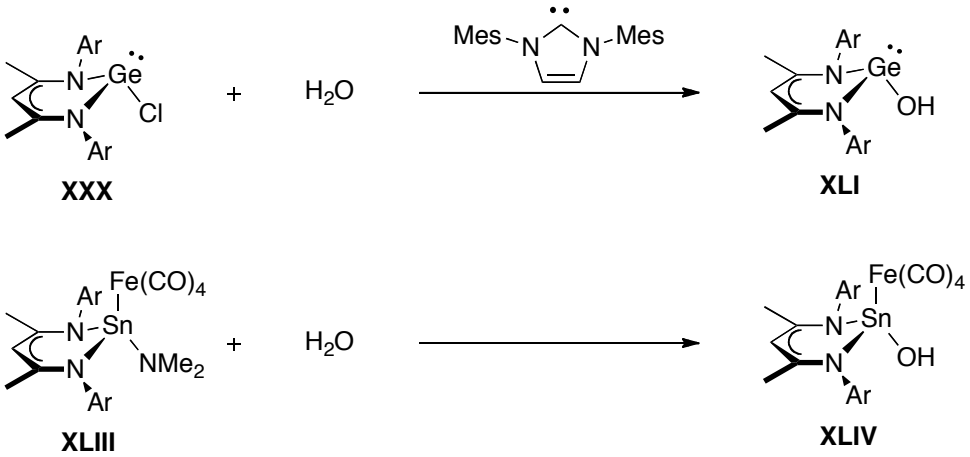

The reduction of β-diketiminate germylene and stannylene can be compared to the amidinate and guanidinate germanium(II) chloride complexes **XI** (Scheme 5); however, treatment of (BDI)GeCl **XXX** with excess potassium afforded the heavier cyclopentadienide analogue **XLV** and the amide **XLVI** (Scheme 13), with cleavage of one of the *N*-aryl groups of the BDI ligand. A reaction mechanism was proposed, which consists of initial K–Cl halogen-metal exchange reaction, followed by ring contraction, K–Cl salt metathesis and final Ge–N reductive fission yielding **LVII**. Protonation of the K salt of the secondary product gives amide **LVIII**.[92]

Salt metathesis of the nucleophilic *N*-heterocyclic germylidene **LVII** with (BDI)ECl (E = Ge, Sn), **XLI**, afforded the asymmetric *trans*-bent digermylene or germylene-stannylene complexes **LIX** (Scheme 13), the latter presenting Ge–Sn σ-

bonding interactions with some ionic character. This was supported by DFT analysis.[93] The heavier *N*-heterocyclic stannylene analogue was isolated and stabilised by the utilisation of the bulkier β-diketiminate ligand (^{tBu}BDI) and metallic lithium as a milder reducing agent.[94]

Scheme 13 Proposed mechanism for the reduction of (BDI)GeCl.

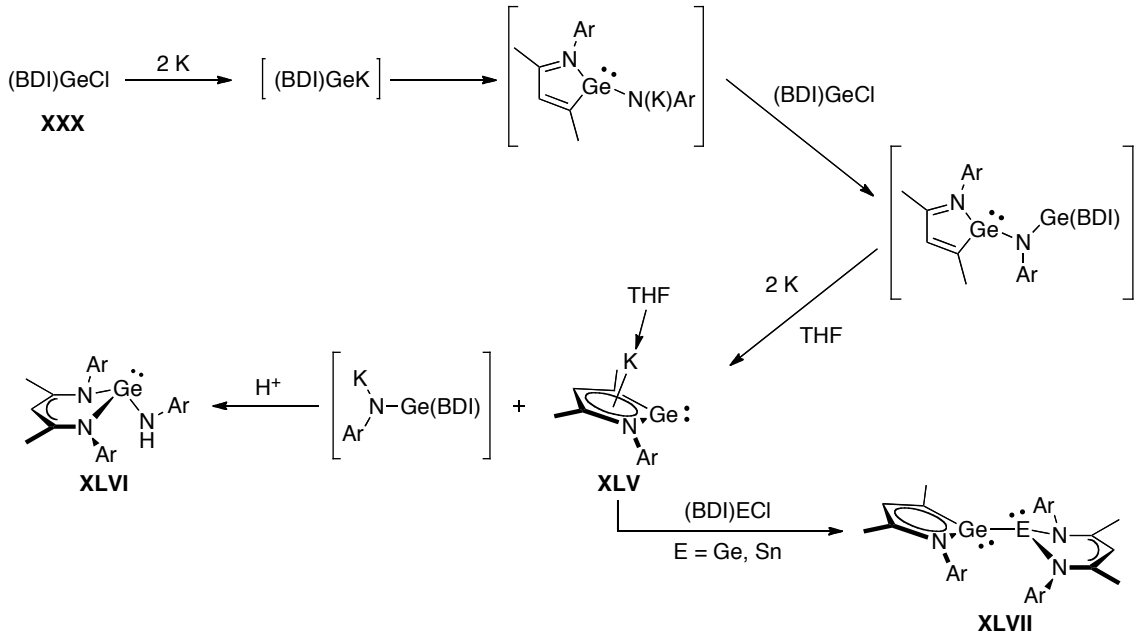

β-Diketiminate lead(II) chemistry has been subject of much less attention, not only due to its much decreased stability, but also because of the later synthesis of a stable and accessible precursor. Therefore, the whole plumbylene BDI chemistry present in the literature to date can be summarised in Schemes 14 and 15.

Fulton and co-workers developed the synthesis of a β-diketiminate lead(II) halogens series (BDI)PbX (X = Cl, Br, I) **XLVIII**,[75] and used it as precursor for the amide **XLIX**,[75] the alkoxide **L**[78] and the aryloxide **LI**.[80] Driess and co-workers showed that the latter complex can also be isolated from the direct reaction of (BDI)Li with a bulky lead diphenolate, which reacts with lithium amides and

phosphides to yield the corresponding lead(II) amido and phosphanido complexes **XLIX** and **LII**; treatment of the amide **XLIX** with a bulky *P*-phosphasilene afforded the *P*-plumbyleniophosphasilene complex **LIII**.[84] Roesky and co-workers completed the picture with the synthesis of a series of alkyl, alkynyl and triflate derivatives **LIV** and **LVI** the latter presenting a polymeric structure in the solid phase.[76] They also investigated the reactivity of the amide **XLIX** with 2-benzoyl pyridine to afford the alkoxide **L**.

Scheme 14 β-diketiminate plumbylenes reactivity pattern.

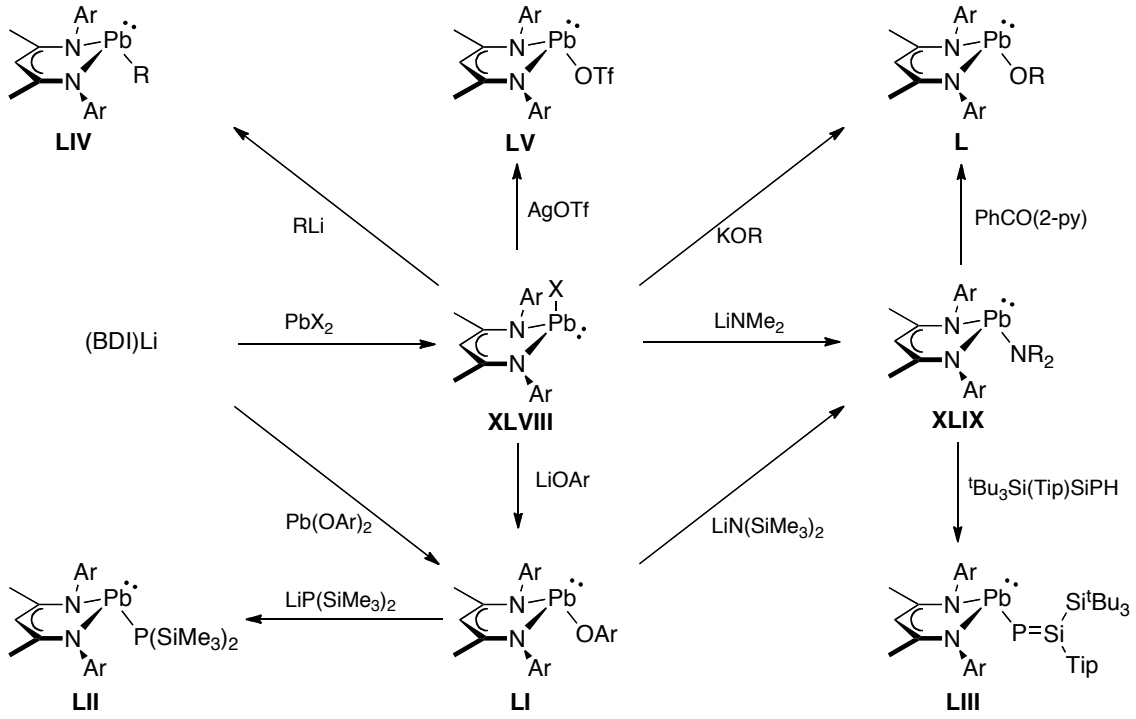

In addition, Roesky and co-workers attempted the synthesis of the plumbylene hydride (BDI)PbH (Scheme 15) by treating the chloride **XLVII** with AlH_3NMe_3, $KBEt_3H$ and $PhSiH_3$, as well as the amide **XLIX** with $PhSiH_3$. In all cases lead black and protonated ligand (BDI)H were observed, with small traces of the heteroleptic complex **LVI**, which suggests the initial formation of the desired plumbylene hydride as an intermediate, decomposing to Pb^0 and (BDI)H; in a side reaction

(BDI)H reacts with the transient (BDI)PbH, forming **LVI** and eliminating dihydrogen.[82]

Scheme 15 Attempted (BDI)PbH synthesis (top) and (BDI)PbOR reactivity pattern towards heterocumulenes (bottom). R = ^{i}Pr, ^{s}Bu, ^{t}Bu.

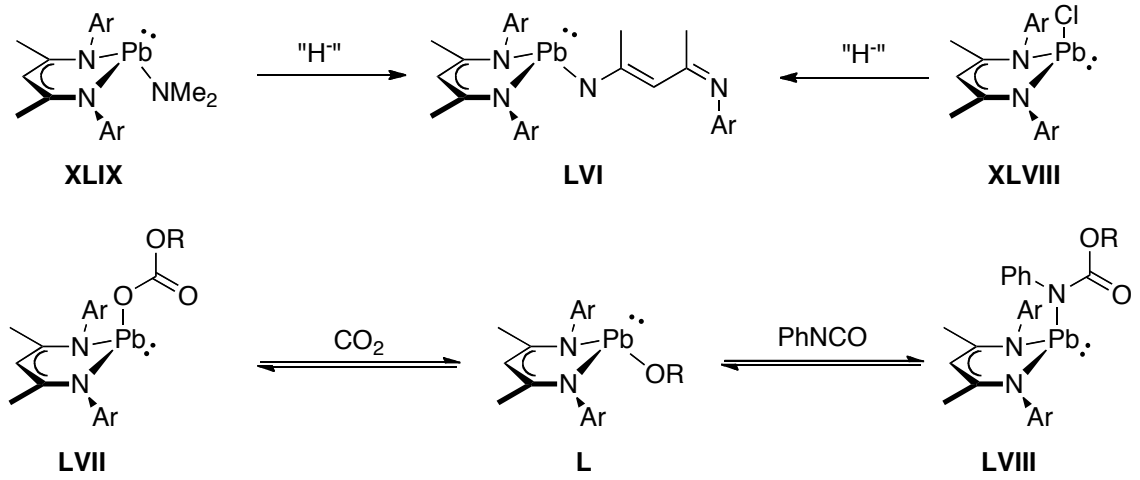

Fulton and co-workers investigated the reactivity of a series of alkoxides **L** towards heterocumulenes showing the facile and reversible activation of carbon dioxide and phenylisocyanate giving the carbonate **LVII** and the carbamate **LVIII**, despite the sluggishness towards strong aliphatic electrophiles.[78] Part of this reactivity is subject of this thesis, therefore it will be discussed more in detail in the 'Results and Discussion' section.

1.3 Carbon Dioxide Activation

Over the past decade the world's attention has focused on a small multiply-bonded molecule called carbon dioxide, both for its potential impact on climate change and its employment as readily available C_1 synthon: it has the advantage of being abundant, cheap and nontoxic.[95] Therefore, it is of no surprise that the

activation of carbon dioxide has become a subject of growing interest over the recent years.

Because carbon is in the most oxidised state in carbon dioxide, the biggest obstacle in its activation is its low energy level. It is in fact so thermodynamically and kinetically stable that it can rarely be used to its full potential. However, thanks to the high electron deficiency of the carbon, carbon dioxide has a strong affinity towards nucleophilic reagents. In fact, the organometallic activation of carbon dioxide is generally operated by complexes bearing ligands such as alkoxides or amides, converted respectively to the metallo-alkylcarbonate and -alkylcarbamate derivatives.[78,96,97-101]

The driving force of the reaction is widely agreed to be the electron-donating power of the oxygen or nitrogen atom, which undergoes a nucleophilic attack to the *sp* carbonylic carbon of carbon dioxide (Scheme 16); concomitant coordination of one of the oxygen atoms of CO_2 to the metal centre leads to the formation of a four membered ring M–O–C–O (or M–N–C–O) transition state. Final cleavage of the original M–O (or M–N) bond yields the metallo-alkylcarbonate (or -alkylcarbamate) product.

Scheme 16 Proposed mechanism for the insertion of carbon dioxide into M–O bonds.

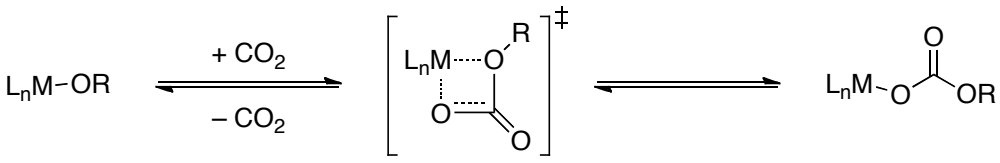

Darensbourg and co-workers observed no variation of the reaction rate between $(CO)_5WOAr$ (Ar = 2,6-$Ph_2C_6H_3$) and CO_2 upon added CO. Formation of $W(CO)_6$ was not observed either. This proved that the aryloxide ligand remains

coordinated to the metal during the insertion process and CO dissociation from the metal center is not rate determining, indicating that this mechanism, despite the appearance, does not require an open coordination site on the metal.[102]

For divalent metal ions, there is a good correlation between their acidity in aqueous solution (pK_a) and their charge-to-size ratio (q^2/r).[103] Moreover, divalent lead has a pK_a of 7.2, higher than predicted by theory.[104] As such, divalent lead hydroxide (and alkoxides) should be weakly basic and quasi non-nucleophilic, making the reported facile activation of carbon dioxide by β-diketiminate plumbylene alkoxide complexes absolutely surprising (Scheme 15). Although hypervalent tin alkoxides are known to react with CO_2,[99] the reactivity of stannylene alkoxides has not been investigated outside of polymerisation studies,[60,81] and considering Sn^{2+} astonishingly high aqueous acidity (pK_a = 2), its alkoxides derivatives should be assumed to be virtually non-nucleophilic.

For this reason, attention was drawn to the synthesis of a series of β-diketiminate stannylene alkoxides to explore their reactivity, especially towards carbon dioxide, also in the hope of clarifying the reaction mechanism. A similar reasoning can be done for divalent mercury (pK_a = 3.5), therefore the synthesis of an isostructural mercury system was also attempted.

2 Results and discussion

2.1 CO_2 activation by β-diketiminate Sn(II) and Pb(II) alkoxides

2.1.1 BDI-plumbylene sec-butoxide synthesis and characterisation

Treatment of a toluene solution of (BDI)H, **1**, with *n*-butyllithium produced the lithiated β-diketiminate complex (BDI)Li, **2**. This was added *in situ* to $PbCl_2$, resulting in the formation of (BDI)PbCl in 82% yield after stirring overnight at room temperature (Scheme 17).[75]

Scheme 17 BDI-lead chloride synthesis.

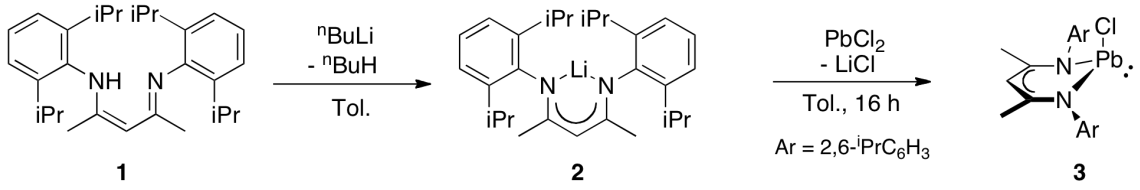

Subsequent treatment of a toluene solution of **3** with potassium *sec*-butoxide afforded (BDI)-lead *sec*-butoxide (BDI)PbO^{s}Bu **4** in 83% yield (eq 1).

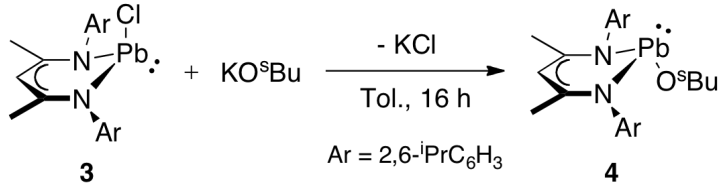

(1)

The ^{1}H NMR spectrum of **4** shows four doublets (δ 1.47, 1.21, 1.15 and 1.42 ppm) and two septets (δ 3.10 and 3.79 ppm) corresponding to the ligand *iso*-propyl groups, indicating a non-planar environment around the three-coordinate metal center. The ^{209}Pb NMR spectra shows a singlet a δ = 1543 ppm.

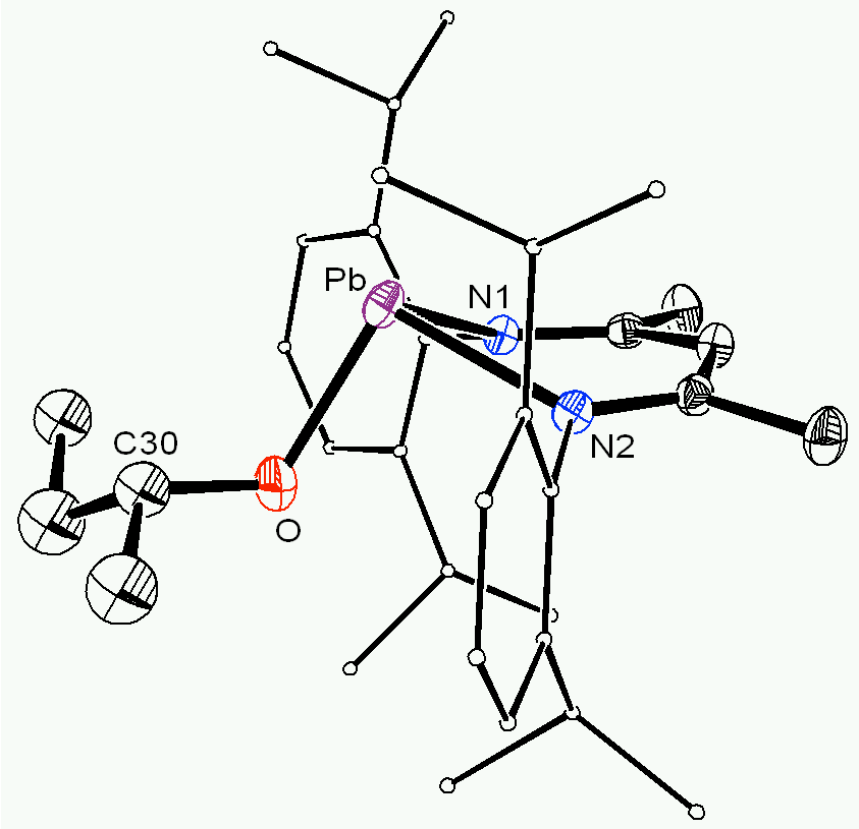

Figure 1 ORTEP diagram of (BDI)PbO^{s}Bu **4**. Aryl groups are minimised and hydrogen atoms are not shown for clarity. Thermal ellipsoids are shown at 30%.

Yellow brick-like crystals of **4** suitable for X-ray structural analysis were grown overnight from pentane saturated solution at -27 ˚C (Figure 1). There is a distorted pyramidal geometry environment around the metal center and the *sec*-butyl group disordered over two overlapping orientations. The former is due to hybridisation of lead *s* and *p* orbitals, resulting in the formation of a stereochemically active lone pair which occupies a large and diffuse region of space. The alkoxide ligand points away from the (BDI)Pb core and it lies in a different portion of space with respect to the N_2C_3 plane, in a so called 'exo' fashion. This is in contrast with (BDI)PbCl, in which the Pb and Cl atom both lie on the same side ('exo' fashion). The Pb–O bond is 2.117 Å, slightly shorter than the similar β-diketiminate lead *iso*-propoxide **4b** (2.135 Å) and *tert*-butoxide **4c** (2.126 Å).[78] The bond angles around the metal

centre show an ^{i}Pr-^{s}Bu-^{t}Bu trend, with the N(1)–Pb–N(2) angle increasing and the N(1,2)–Pb–O angles decreasing along the series (Table 1).

Table 1 Selected bond lengths (Å) and angles (deg) for (BDI)PbOR (R = ^{i}Pr, ^{s}Bu, ^{t}Bu).

	(BDI)PbO^{s}Bu **4**	(BDI)PbO^{i}Pr **4b**	(BDI)PbO^{t}Bu **4c**
Pb–O	2.117(3)	2.135(3)	2.126(3)
N1–Pb	2.304(3)	2.307(3)	2.317(3)
N2–Pb	2.305(3)	2.311(3)	2.299(3)
O–C30	1.421(8)	1.413(5)	1.415(4)
N1–Pb–N2	80.76(10)	80.56(9)	81.04(10)
N1–Pb–O	93.33(10)	94.94(10)	92.74(10)
N2–Pb–O	94.08(11)	93.49(10)	92.26(10)

2.1.2 Reactivity towards electrophiles

The nucleophilicity of the alkoxide **4** was investigated, revealing some unexpected trends. Similar to **4b** and **4c**,[78] no reactivity was observed towards benzyl bromide. Treatment with stronger electrophiles such as methyl iodide under forcing conditions (70 ˚C, 2 d), or methyl triflate at room temperature, afforded respectively the known lead iodide, **5**, or triflate, **6**, complexes and methyl-*sec*-butyl ether (eq 2),[75,76] as confirmed by ^{1}H NMR spectroscopy.

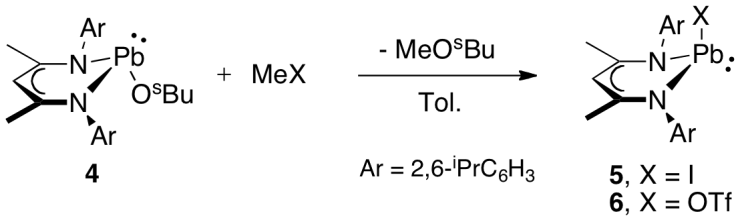

(2)

In contrast, **4** readily activates carbon dioxide. Treatment of **4** with 1 eq of CO_2 resulted in the quantitative and reversible conversion to BDI-lead carbonate **7** (Scheme 18). The ^{1}H NMR spectroscopic analysis shows a broad peak (3.30 ppm)

corresponding to the *iso*-propyl groups protons of the ligand, which splits into two distinct septets by cooling the sample down to -50 ˚C. The ^{13}C NMR spectrum shows a spectral resonance at 160.7 ppm, typical for a carbonate group; this functionality was further confirmed by IR spectroscopy, showing a stretch at 1645 cm^{-1} (CCl_4). The ^{209}Pb NMR spectroscopic analysis shows an upfield shift of ~700 ppm to δ = 810 ppm. Unfortunately, it was not possible to carry out any solid-state characterisation on compound **7** because of the reversibility of the insertion reaction (*vide infra*). Further confirmation of the nature of compound **7** was given by treatment of (BDI)PbCl **3** with potassium mono-*sec*-butyl carbonate, producing (BDI)Pb$OCO_2{}^s$Bu **7**, as confirmed by ^1H and ^{13}C NMR spectroscopy.

Scheme 18 Synthesis of the carbonate **7** via carbon dioxide insertion or salt metathesis.

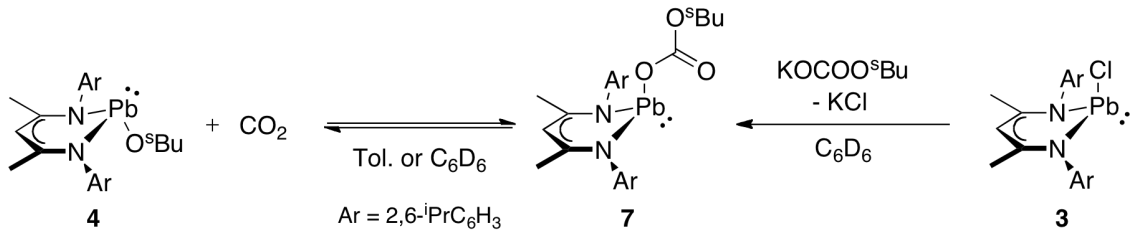

The degree of reversibility of **7** is intermediate between the *iso*-propoxide and the *tert*-butoxide system: in fact, both **4b** and **4c** readily react with carbon dioxide to give the corresponding lead carbonates **7b** and **7c**: apparently non-reversibly for the first, reversibly for the latter. For instance, applying a vacuum on the carbonates results in the almost complete conversion to the alkoxide for the *tert*-butyl system, only 20% conversion is observed for the *sec*-butyl, while no formation of the alkoxide was observed for the *iso*-propyl system. A similar trend is observed in the stability of the carbonates: a solution of the lead *iso*-propylcarbonate is stable at 60 ˚C, while the *sec*-butylcarbonate very slowly

decomposes at the same temperature and the *tert*-butylcarbonate decomposes overnight at room temperature.

Reactivity towards unsaturated electrophiles was further investigated. For instance, treatment of **4** with carbon disulfide gave in an intractable mixture of products, consisting of a black precipitate, protonated ligand and other unidentifiable products.

Compound **4** cleanly reacts with maleic anhydride affording the ring-opening and insertion product (BDI)Pb(ma^{sBu}) (ma^{R} = $OCOC_2H_2COOR$), **8**, in 72% yield (eq 3).

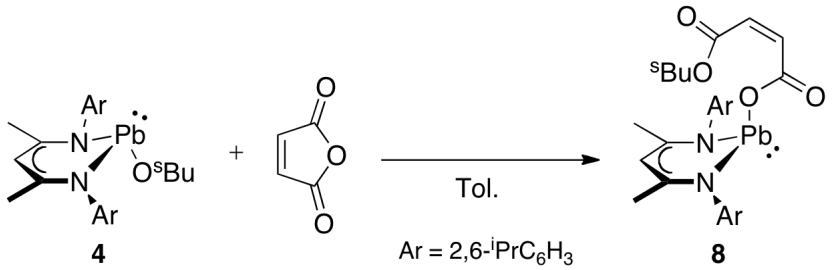

(3)

Similarly to **7**, ^{1}H NMR analysis of **8** shows the characteristic maleate pattern with two sets of doublets at 6.00 and 5.90 ppm, and the isopropyl groups protons of the ligand merging at room temperature into a broad signal at 3.25 ppm and splitting into two distinct septets by cooling the sample down to -50 °C. The ^{209}Pb NMR spectroscopy shows a singlet at 871 ppm, very close to **7**, indicating a similar coordination environment around the lead atom.

Compound **8** crystallises as deep orange crystals from a saturated hexanes solution at -27 °C after one week (Figure 2). Similarly to the chloride **3**, and in contrarst to the alkoxide **4**, the maleate ligand are arranged in an 'endo' fashion with respect to the ligand backbone. Pb–O1 bond length is 2.279(5) Å, considerably longer than the alkoxide. The elongation could be attributed to a

secondary long range interaction between the metal centre and the carbonylic oxygen Pb···O2 = 2.88 Å, well within the sum of their van der Waals radii (3.54 Å), indicating a pseudo η^2 coordination mode.

Table 2 Selected bond lengths (Å) and angles (deg) for (BDI)PbO(ma^{sBu}) **8**.

Pb–O1	2.279(5)	C30–O2	1.236(10)
Pb–N1	2.284(5)	N1–Pb–N2	83.76(19)
Pb–N2	2.291(5)	N1–Pb–O1	86.07(18)
O1–C30	1.278(9)	N2–Pb–O1	87.62(18)

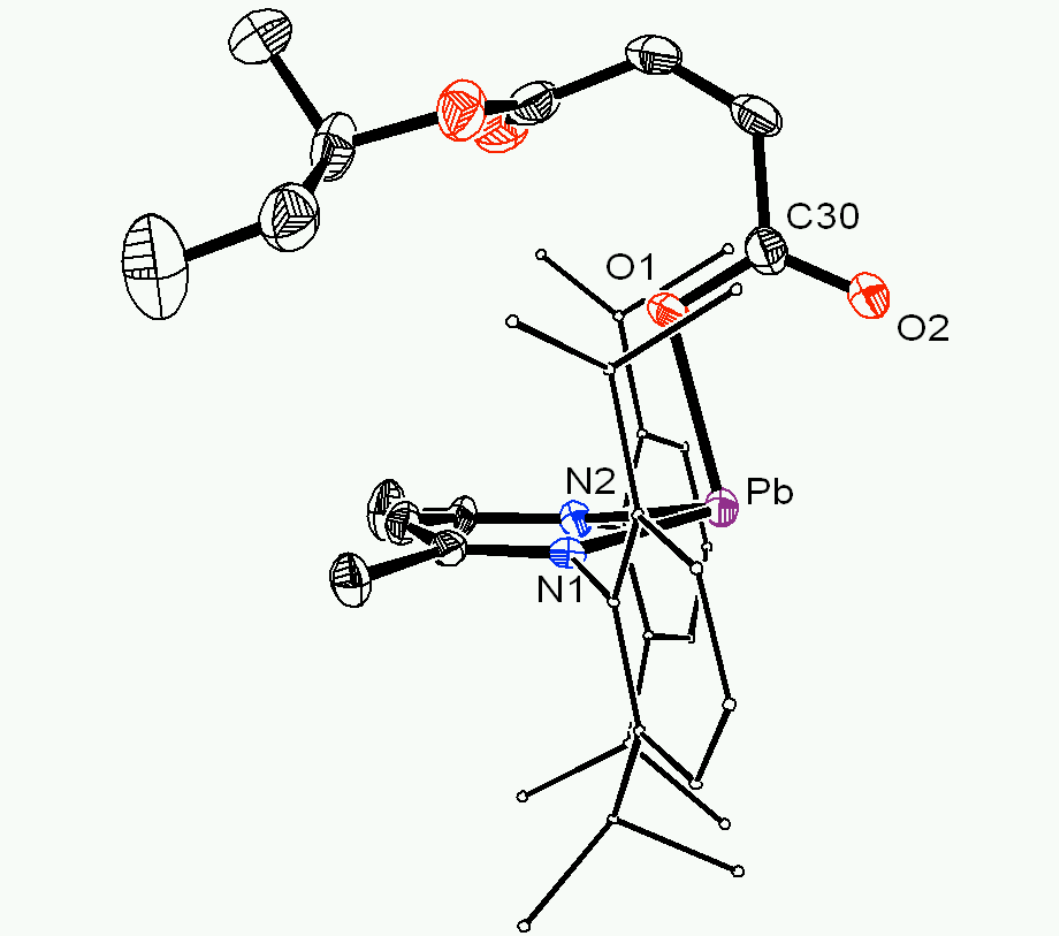

Figure 2 ORTEP diagram of (BDI)Pb(ma^{sBu}) **8**. Aryl groups are minimised and hydrogen atoms are not shown for clarity. Thermal ellipsoids are shown at 30%.

Addition of 1 eq of phenyl isocyanate to a toluene solution of lead alkoxide **4** readily results in a transient product, that slowly converts into a secondary

product characterised by the presence of a low-field singlet (13.61 ppm) and two sets of doublets (6.41 and 7.58 ppm) in the ^{1}H NMR spectrum. After 1 day in solution at -27 ˚C, the conversion reaches about 20%, thwarting any attempt to isolate and characterise any of the products; unfortunately, only 70% conversion was reached after a month. Attempts to accelerate the formation of the thermodynamic product by storing the reaction at room temperature resulted in the formation of (BDI)H after two days. IR spectroscopy shows the presence of an N–H stretching frequency, which could be associated with the singlet at low field observed by ^{1}H NMR spectroscopy.

In an attempt to confirm the nature of this unknown product (BDI)H was treated with 1 eq of triflic acid, however resulting in the near quantitative conversion to the protonated [(BDI)H$_2$]OTf **9** (eq 4).

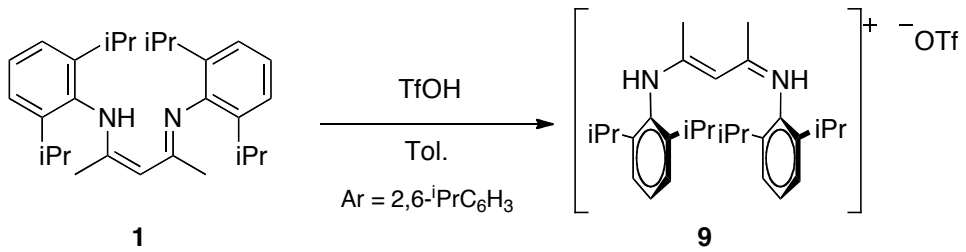

1 **9** (4)

The ^{1}H NMR spectrum exhibits a singlet at 9.30 ppm, corresponding to the CN*H* iminic protons. Unfortunately this resonance does not correspond with the unknown compound. The connectivity was confirmed by the crystallisation of colourless air-stable single crystals of **9** (Figure 3). The β-diketimine, protonated at both nitrogen atoms, is arranged in an open structure, derived from the rotation around the C1–C2 and C2–C3 bonds, with the aryl rings facing each other and the C–N bonds pointing in opposite directions. One of the iminic protons forms a hydrogen bonding interaction (2.024 Å) with one of the oxygen atoms (O2) of the

triflate counteranion. The positive charge is delocalised along the ligand backbone, as evidenced by the pattern of C–C and C–N bond lengths (Table 3 and Figure 4).

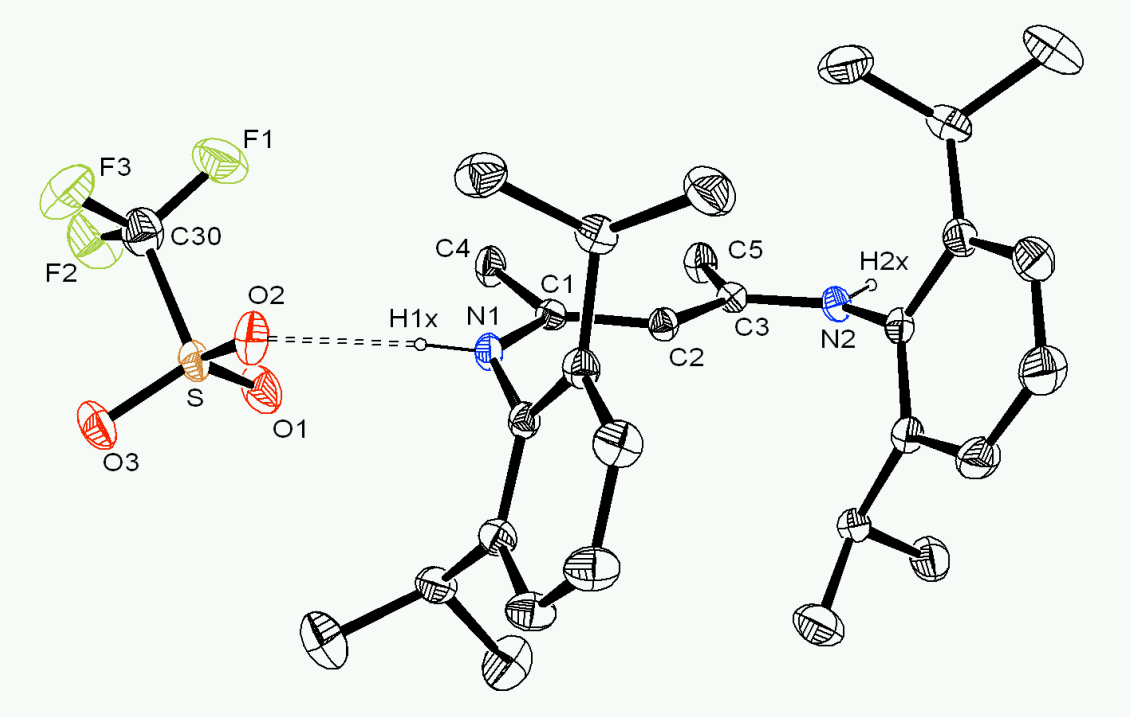

Figure 3 ORTEP diagram of [(BDI)H_2]OTf **9**. Thermal ellipsoids are shown at 30%.

Table 3 Selected bond lengths (Å) and angles (deg) for [(BDI)H_2]OTf **9**.

	[(BDI)H_2]OTf **9**	(BDI)H **1**[105]
N1–C1	1.331(2)	1.318(3)
N2–C3	1.337(2)	1.341(3)
C1–C2	1.397(2)	1.418(4)
C2–C3	1.395(2)	1.386(4)
N1–C1–C2	120.21(15)	120.6(2)
N1–C1–C4	113.85(14)	121.9(2)
N2–C3–C2	120.43(15)	121.0(3)
N2–C3–C5	113.50(14)	119.0(2)
C1–C2–C3	127.44(16)	126.3(3)

In fact, differently from (BDI)H **1**,[105] C1–C2 (1.397(2) Å) and C2–C3 (1.395(2) Å) bonds of **9** are identical, respectively shorter and longer than the corresponding bond lengths of **1** (1.418(4) and 1.386(4) Å), in between a single and a double

bond order. Analogous comparison and reasoning is applicable to C–N bonds: 1.331(2) and 1.337(2) Å of **9** versus 1.318(3) and 1.341(3) Å of **1**. Bond angles are generally not comparable due to the different geometry adopted by the ligand.

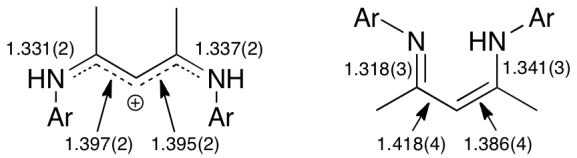

Figure 4 Bond lengths (Å) of compound **9** (left) and **1** (right).

Similar structures were previously reported by Hill and co-workers, differing for the counteranion (BAr^F) and characterised only by X-ray structural analysis, and by Richards and co-workers, differing for the aryl groups (Mes) and the counteranion.[106] The C–N bond lengths reported by Hill of 1.334(5) Å are very similar to **9**, while the C1–C2 and C2–C3 bond lengths are shorter by 0.012 and 0.014 Å. In contrast, the complexes reported by Richards showed a bond length pattern more similar to (BDI)H, with considerably shorter C–C bond lengths (1.367 (16) and 1.379(15) Å). The C–N bond lengths are 1.337(14) and 1.362(15) Å, evidencing a marked deviation from symmetry. Interestingly, the ^{1}H NMR spectra of the cationic species reported by Richards, show the iminic proton spectral resonance at δ 3.72 ppm (in C_6D_6), more than 5 ppm different from **9**. This can be plausibly attributed to a different hydrogen bonding between the iminic proton and the counteranion, possibly due to the different deuterated solvent used.

2.1.3 BDI-stannylene alkoxides synthesis and characterisation

A series of β-diketiminate stannylene alkoxides was synthesised by metathesis reaction of (BDI)SnCl **10** with the appropriate potassium (or sodium) alkoxide in

THF (Scheme **19**). The synthesis of (BDI)SnO^{i}Pr **11a** was previously reported by Gibson and co-workers.[81] All the tin alkoxides (BDI)SnOR **11** (R = ^{i}Pr, ^{s}Bu, ^{t}Bu, ^{t}Bu^{F}) are air-sensitive compounds, isolable in good yield by crystallisation and characterised by multinuclear NMR, IR and UV-vis spectroscopic, elemental analysis and X-ray crystallography.

Scheme 19 Synthesis of β-diketiminate tin alkoxides **11a-d.**

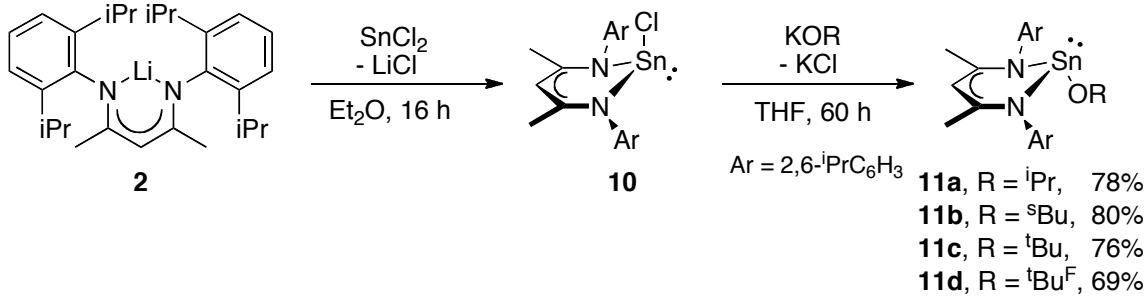

The ^{1}H and ^{13}C NMR spectra do not show unexpected features and were fully assigned. For instance, ^{1}H NMR spectroscopic analysis of (BDI)SnO^{t}Bu, **11c**, shows the presence of a non-planar environment around the metal center, indicated by the presence of two sets of septets (δ 3.89 and 3.21 ppm) and four doublets (δ 1.53, 1.28, 1.17 and 1.12 ppm) spectral resonances. Two singlets corresponding to the γ-C*H* proton and the *tert*-butyl group resonate respectively at δ 4.61 and 0.86 ppm. The other alkoxides all showed a similar pattern. The perfluorinated alkoxide **11d** presented a singlet spectral resonance in the ^{19}F NMR spectrum at δ -73.0 ppm. The ^{119}Sn NMR exhibits a singlet spectral resonance and shows a correlation between the chemical shift and the basicity of the alkoxide group, that is the lower the electron donating nature of the alkoxide, the lower the ^{119}Sn chemical shift. It spans, in fact, from -253 ppm, for the weakly basic perfluorinated alkoxide **11d**, to -149 ppm for the most basic *tert*-butyl alkoxide **11c**, with **11a** and **11b** in between,

resonating respectively at -189 and -181 ppm. The molecular structure of the alkoxides is depicted in Figure 5.

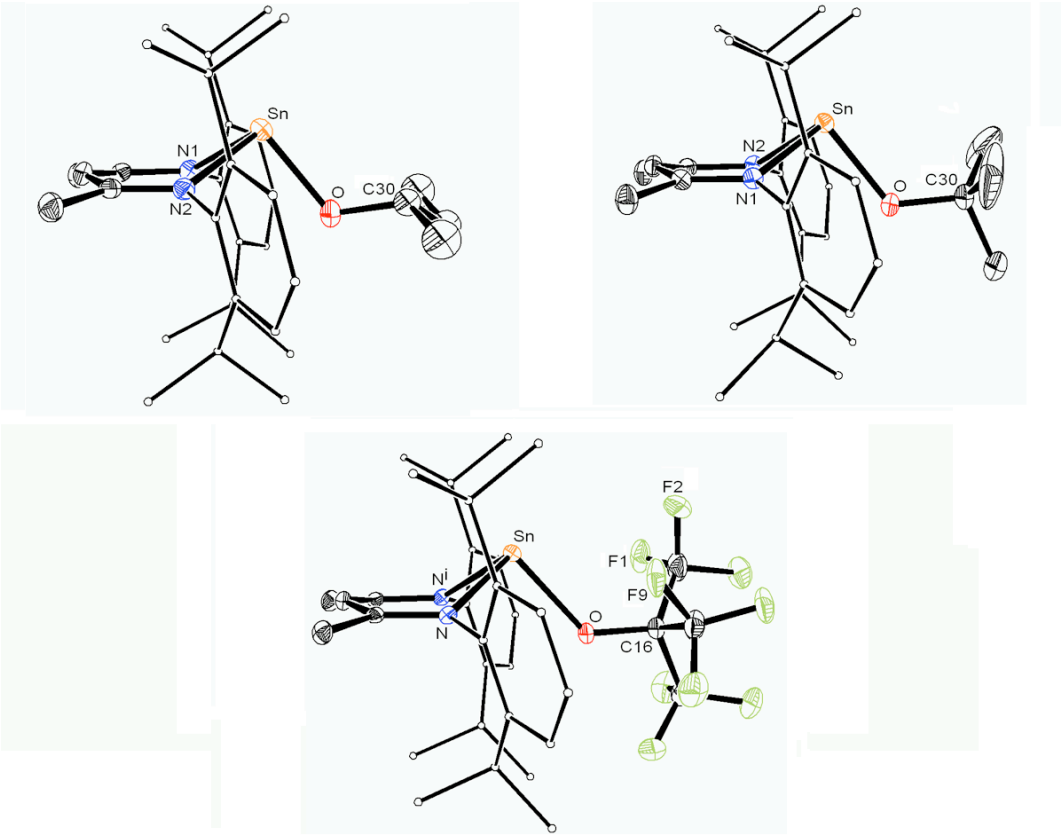

Figure 5 ORTEP diagram of (BDI)SnOR (**11b**, R = ^{s}Bu, left; **11c**, R = ^{t}Bu, right; **11d**, R = ^{t}Bu^{F}, middle). Aryl groups are minimised and hydrogen atoms are not shown for clarity. Thermal ellipsoids are shown at 30%.

Compounds **11b** and **11c** crystallise from pentane saturated solution at -27 ˚C as yellow bricks. The former shows the *sec*-butyl group to be disordered over two partially overlapping orientations. Single crystals of **11d** suitable for X-ray analysis were grown overnight by maintaining a saturated tetrahydrofurane solution at -27 ˚C; the molecule lies on a mirror plane with the alkoxide group disordered over two positions. Similar to plumbylene alkoxides **4**, tin alkoxides **11a-c** exhibit a distorted trigonal pyramidal geometry around the metal centre, presumably the result of a $5s^2$ based stereochemically active lone pair, arising from the hybridisation of tin *s* and *p* orbitals. The alkoxide group points away from the

(BDI)Sn core and is arranged in an 'exo' fashion with respect to the N_2C_3 plane of the ligand.

Selected bond lengths and angles are reported in Table 4. Only minor differences are observed between the alkoxides **11a-c**, with the Sn–O bond increasing with the steric bulk of the alkoxide. More significant differences are observed for the perfluorinated alkoxide **11d**: compared to its perprotonated analogue **11c**, it shows a significant elongation of the Sn–O bond (2.110(2) vs. 2.0179(16) Å), attributed to the more ionic nature of the Sn–O bond, which is reflected in the shorter Sn–N bond lengths (2.1837(16) vs. average 2.2058(19) Å). The O–C bond length is also shorter, potentially due to the strong electron-withdrawing nature of the fluorinated alkyl group. A potential long-range Sn···F interaction is observed between Sn and F1 (3.20 Å), F2 (3.35 Å) and F9 (3.43 Å) as all of these distances are shorter than the sum of the Sn-F radii of 3.64 Å, consistent with other fluoroalkoxide complexes.[107]

Table 4 Selected bond lengths (Å) and angles (deg) for alkoxides **11a-d**.

	(BDI)SnO^{i}Pr **11a**	(BDI)SnO^{s}Bu **11b**	(BDI)SnO^{t}Bu **11c**	(BDI)SnO^{t}Bu^{F} **11d**
Sn–O	2.000(5)	2.013(3)	2.0179(16)	2.110(2)
Sn–N1	2.206(4)	2.202(3)	2.2015(19)	2.1837(16)
Sn–N2	2.208(4)	2.202(3)	2.2100(19)	2.1837(16)
O–C30	1.418	1.442(7)	1.419(3)	1.360(3)
N1–Sn–N2	83.6(2)	82.79(11)	83.02(7)	83.53(8)
N1–Sn–O	94.1(2)	94.08(12)	92.66(7)	93.65(6)
N2–Sn–O	95.2(2)	94.29(12)	93.89(7)	93.65(6)
Sn–O–C30	118.58	118.1(3)	122.40(16)	128.97(18)

Compared to the heavier isostructural lead system, the main difference of tin alkoxides **11a-c** is the longer bond lengths around the metal center (E–O and E–N), due to the bigger ionic radius of divalent lead.

2.1.4 Reactivity towards electrophiles

The reactivity of the alkoxides **11a-d** toward aliphatic electrophiles was examined, revealing no reactivity towards methyl iodide, even under forcing conditions (eq 5).

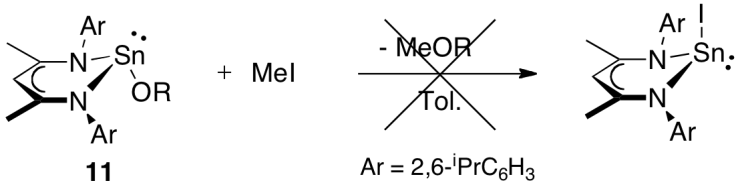

(5)

This is in contrast to the behaviour exhibited by (BDI)PbOR **4**, which reacted at elevated temperature, and in stark contrast to transition metal alkoxides, which readily reacted with aliphatic electrophiles.[101] Treatment of **11a-c** with a more potent electrophile, methyl triflate, resulted in the formation of the nucleophilic substitution product (BDI)SnOTf **12** and the corresponding methyl ether (eq 6).[73]

(6)

The half life of this reaction was measured by ^{1}H NMR spectroscopy and was found to be dependent on the alkoxide group, with tin *iso*-propoxide **11a** proving to be the most reactive ($t_{½}$ = 8 min), tin *sec*-butoxide **11b** to be slightly slower ($t_{½}$ = 15 min) and the tin *tert*-butoxide **11c** to be the most sluggish ($t_{½}$ = 150 min). Treatment of (BDI)SnO^{t}Bu^F **11d** with methyl triflate produces an intractable mixture of products; no evidence for either (BDI)SnOTf or MeOC(CF$_3$)$_3$ was found.

Reactivity towards unsaturated electrophiles was also investigated. Treatment with carbon disulfide and phenyl isocyanate gave intractable product mixtures;

however, addition of 1 eq of maleic anhydride to (BDI)SnO^{i}Pr **11a** resulted in the ring-opening product (BDI)Sn(ma^{iPr}) **13** in high yield (eq 7).

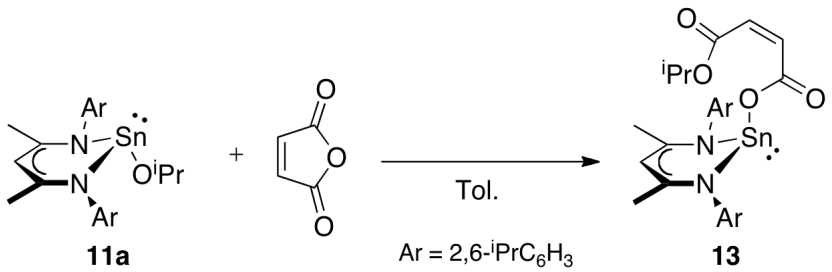

(7)

The ^{1}H NMR spectrum shows the expected two sets of doublets resonating at δ 5.96 and 5.83 ppm, corresponding to the vicinal methine protons of the maleate ligand. ^{119}Sn NMR analysis exhibits a singlet at -374 ppm, about 200 ppm lower than **11a**, with an upfield shift in the same direction observed in the lead system.

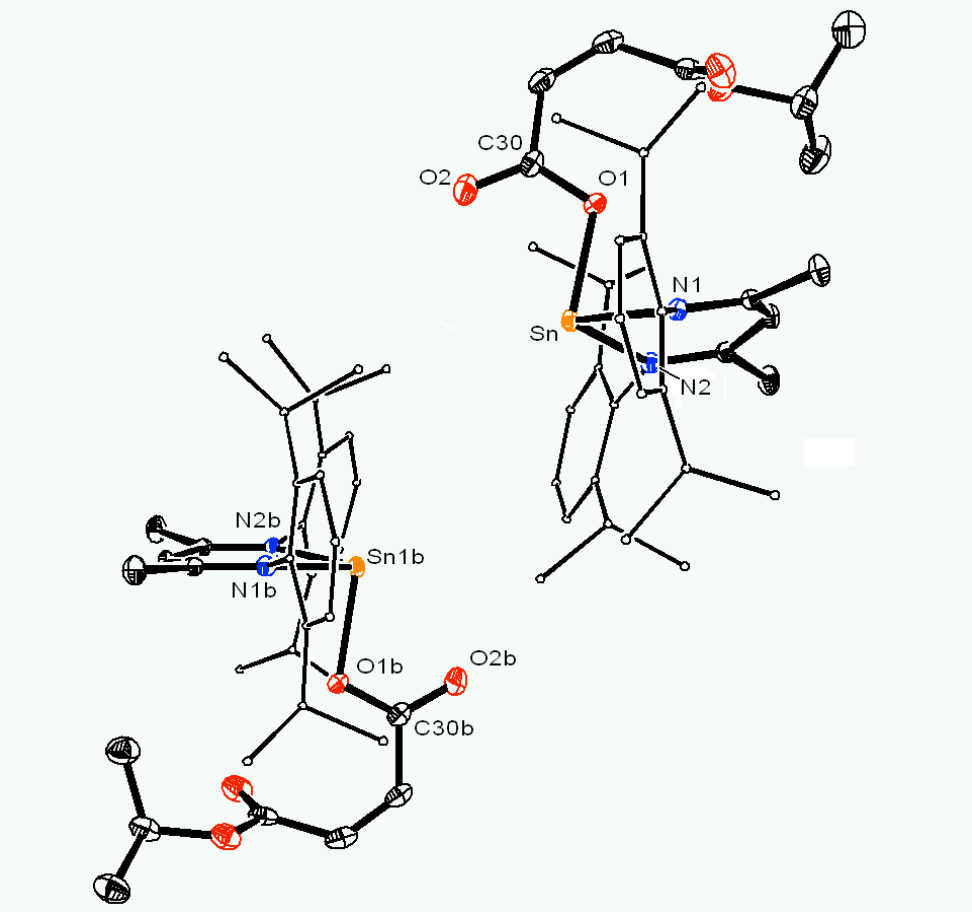

Figure 6 ORTEP diagram of (BDI)Sn(ma^{iPr}) **13**. Aryl groups are minimised and hydrogen atoms are not shown for clarity. Thermal ellipsoids are shown at 30%.

Red crystals of **13** suitable for X-ray structural analysis were grown by storage of a saturated hexane solution at -27 ˚C for three days. Compound **13** crystallises with two independent molecules in the unit cell, differing in the conformation of the maleate ligand (Figure 6). Selected bond lengths and angles are reported in Table 5.

Table 5 Selected bond lengths (Å) and angles (deg) for tin maleate **13**.

molecule A		molecule B	
Sn–O1	2.1489(16)	Sn1b–O1b	2.1534(16)
Sn–N1	2.1812(17)	Sn1b–N1b	2.1866(17)
Sn–N2	2.1784(18)	Sn1b–N2b	2.1851(18)
Sn–O2	2.898	Sn1b–O2b	2.954
N1–Sn–N2	84.88(7)	N1b–Sn1b–N2b	86.09(7)
N1–Sn–O1	87.32(7)	N1b–Sn1b–Ob	88.78(6)
N2–Sn–O1	87.90(7)	N2b–Sn1b–Ob	86.09(7)

Tin alkoxides **11a-c** readily activate carbon dioxide at room temperature with the formation of the tin-alkylcarbonate (BDI)SnOCO$_2$R **14a-c** (R = ^{i}Pr, ^{s}Bu, ^{t}Bu) (Scheme 20).

Scheme 20 Reaction of alkoxides **11a-c** with carbon dioxide to form carbonates **14a-c** and the various equilibria involved.

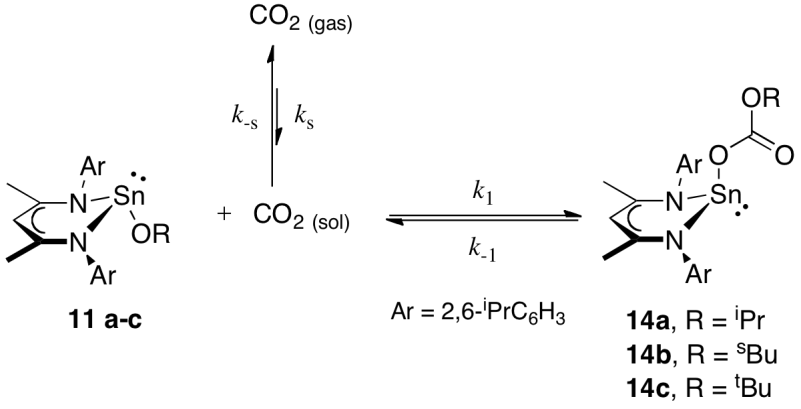

In contrast, perfluoro alkoxide **11d** does not react with CO_2. Application of a dynamic vacuum to the carbonates **14a-c** resulted in the conversion to the alkoxide. Unfortunately, the facile reversibility of the process prevented any solid-state characterization.

The ^{1}H NMR spectra of the alkylcarbonates **14**, compared the corresponding alkoxides **11**, show a similar and slightly shifted resonances pattern. For instance, compound **14c** exhibits two sets of septets (δ 3.68 and 3.05 ppm) and four doublets (δ 1.44, 1.18, 1.13 and 1.02 ppm) spectral resonances, corresponding to the aryl *iso*-propyl groups. Two singlet spectral resonances corresponding to the γ-C*H* proton and the *tert*-butyl group are found respectively at δ 4.89 and 0.87 ppm. The ^{13}C NMR spectrum exhibits a singlet at δ 158.9 ppm indicative of a carbonate carbon, the IR spectrum of the products shows a characteristic carbonate stretching frequency at 1621 cm^{-1}. Addition of $^{13}CO_2$ to all the alkylcarbonates resulted in an increase of the ^{13}C NMR carbonate resonance.

Further conformation of the nature of the product was given by treatment of tin chloride **10** with the potassium salt of monoalkyl carbonate (KO_2COR, R = ^{s}Bu, ^{t}Bu), which produced a mixture of tin alkoxide **11** and tin carbonate **14**, not only supporting the nature of the product, but also confirming the presence of the alkoxide-carbonate equilibrium. Although KO_2COR does revert to KOR and CO_2, this latter reaction only occurs at elevated temperatures.

Similarly to the lead system, the reactivity towards CO_2 is influenced by the minor differences of the alkyl group of the alkoxide ligand. For instance, under 1 atm of carbon dioxide, the half life of the complete conversion of tin *iso*-propoxide **11a** and *sec*-butoxide **11b** to the corresponding alkylcarbonate is less than 10 min,

while tin *tert*-butoxide **11c** reacts significantly slower with carbon dioxide and only reaches 74% conversion to the alkylcarbonate.

2.1.5 Equilibrium studies

To gauge the influence of the alkyl group on the reaction, the equilibrium between reagents and product was examined. This investigation is complicated by the presence of an additional equilibrium between gas phase and solution phase carbon dioxide. This was partially overcome by working with low alkoxide concentration and flooding with CO_2 (1 atm), which allowed us to keep a constant concentration of CO_2 in solution, which can be calculated from its mole fraction (χ_g) solubility corrected to a partial pressure of 1 atm (in the 283 – 313 K temperature range) from eq 8:[108]

$$\ln \chi_g = -73.824 + \frac{3804.8}{T} + 9.8929 \ln T \qquad (8)$$

Tin *iso*-propoxide **11a** is completely converted to the alkylcarbonate **14a** at room temperature under 1 atm of carbon dioxide ($[CO_2]_{298K}$ = 0.103 M); however, running the reaction at a more elevated temperature (313 K, $[CO_2]_{313K}$ = 0.091 M) resulted in a 92% conversion. This is consistent with entropic factors becoming more influential at higher temperature, resulting in a shift of the equilibrium towards the reagents, as well as a lower concentration of carbon dioxide in solution.

The ratio of **11** and **14** was measured under these conditions, and K_{eq} (eq 9) and ΔG° were calculated for each system and summarised in Table 6.

$$K_{eq} = \frac{[\mathbf{14}]}{[\mathbf{11}][CO_2]} \quad (9)$$

The tin *iso*-propoxide conversion to *iso*-propyl carbonate is the most energetically favoured with a ΔG°_{313K} of –3.27 kcal/mol, followed by the *sec*-butyl and the *tert*-butyl system, ΔG°_{313K} = –3.22 and –1.88 kcal/mol respectively. The sluggishness of the conversion of (BDI)SnO^tBu **11c** to the corresponding tin-alkylcarbonate was exploited to determine both the entropic and enthalpic contribution to this reaction.

Table 6 Ratio of alkoxide **11** to carbonate **14**, K_{eq}, ΔG°_{313K} (kcal mol^{-1}), and relative time to equilibrium (t_{eq}) for the equilibrium between **11** and carbon dioxide.[a]

	11 : **14**	K_{eq}	ΔG°_{313K}	t_{eq}
2a/5a	7.6 : 92.4	191	–3.27	3 h
2b/5b	11.1 : 88.9	178	–3.22	1d
2c/5c	45.4 : 54.6	20	–1.88	3 d

[a] All measurements were performed in C_6D_6 at 313 K using 36.4 mM alkoxide in a sealed NMR tube with a 50 cm^3 headspace (to maintain a steady CO_2 concentration). The calculated CO_2 concentration at this temperature is 0.091 M.

The equilibrium was measured at four different temperatures under 1 atm of carbon dioxide, and the ΔH° (–13.8 kcal mol^{-1}), ΔS° (–39.6 cal mol^{-1}) and ΔG°_{298K} (–2.0 kcal mol^{-1}) for the insertion of CO_2 into the Sn–O^{t}Bu bond were calculated via van 't Hoff plot (Figure 7). Due to the limited solubility data of CO_2, it was not possible to determine ΔH° and ΔS° for the *iso*-propoxide and *sec*-butoxide systems, because of the lack of solubility data at more elevated temperature or different pressure.

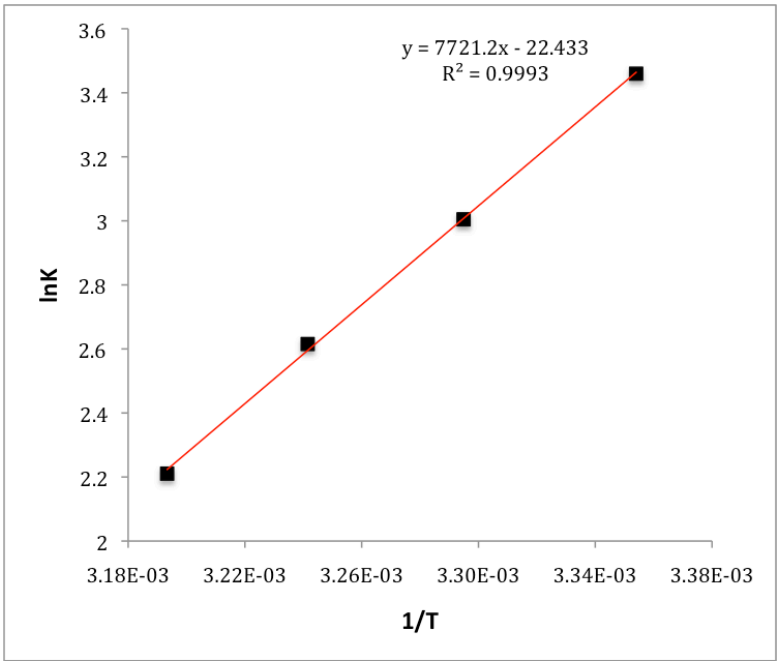

Figure 7 Van 't Hoff plot of the equilibrium between alkoxide **11c** and carbonate **14c**. All measurements were performed in C_6D_6 in a sealed NMR tube with a 50 cm^3 headspace (to maintain a steady CO_2 concentration).

2.1.6 Kinetic measurements

Despite being able to maintain a steady carbon dioxide concentration over the course of reaction, determination of the reaction rate using NMR spectroscopy was impossible because of limited ability to mix the solution, resulting in diffusion of carbon dioxide being rate influencing. However, the reaction rate was qualitatively measured at 313 K and flooding with CO_2 (1 atm): for the *iso*-propoxide system, equilibrium was established after 3 hours, for the *sec*-butoxide system after 1 day, and for the *tert*-butoxide system after 3 days (Table 6); however, all reactions proceeded faster when the NMR tube was shaken.

The rate constant of the system depicted in Scheme 20 is shown in eq 10.

$$v = k_{-1}[\mathbf{14}] - k_1[\mathbf{11}][CO_2] \qquad (10)$$

A kinetic experiment that reduces the system to the case of opposing first-order reaction is achieved by flooding with CO_2. As such, if $[CO_2] \gg [\mathbf{11}]$, a plot of $\ln([\mathbf{11}]_t - [\mathbf{11}]_{eq})$ versus time will be linear with $k_{obs} = k_1[CO_2] + k_{-1}$,† if our proposed rate equation is correct. Rate constants k_1 and k_{-1} can be obtained by the introduction of the previously measured equilibrium constant K_{eq} into the calculations as shown in eq 11 and 12.

$$k_1 = \frac{k_{obs}}{[CO_2] + K_{eq}^{-1}} \tag{11}$$

$$k_{-1} = \frac{k_{obs}}{1 + [CO_2]K_{eq}} \tag{12}$$

---

† As $v = 0$ at the equilibrium, k_1 and k_{-1} are related to the equilibrium constant K_{eq} by equation (*i*)

$$(i) \qquad K_{eq} = \frac{[\mathbf{14}]}{[\mathbf{11}][CO_2]} = \frac{k_1}{k_{-1}}$$

If $[CO_2]_0 \gg [\mathbf{11}]_0$ it is possible to consider $d[CO_2]/dt = 0$; therefore eq 10 and (*i*) can be rewritten as

$$(ii) \qquad K'_{eq} = \frac{[\mathbf{14}]_{eq}}{[\mathbf{11}]_{eq}} = \frac{k_1'}{k_{-1}}$$

$$(iii) \qquad v' = k_{-1}[\mathbf{14}] - k_1'[\mathbf{11}]$$

with $k' = k[CO_2]_0$. If no carbonate is initially present, then at all the times $[\mathbf{11}] + [\mathbf{14}] = [\mathbf{11}]_0$. Therefore

$$(iv) \qquad \frac{d[\mathbf{11}]}{dt} = -k_1'[\mathbf{11}] + k_{-1}[\mathbf{14}] = -(k_1' + k_{-1})[\mathbf{11}] + k_{-1}[\mathbf{11}]_0$$

The solution of the first-order differential equation (*iv*) is

$$(v) \qquad [\mathbf{11}] = \frac{k_{-1} + ke^{-(k_1' + k_{-1})}}{k_1' + k_{-1}}[\mathbf{11}]_0$$

As $t \to \infty$ the concentrations reach their equilibrium values, which aregiven by equations (*vi*) and (*vii*)

$$(vi) \qquad [\mathbf{11}]_{eq} = \frac{k_{-1}[\mathbf{11}]_0}{k_1' + k_{-1}}$$

$$(vii) \qquad [\mathbf{14}]_{eq} = [\mathbf{11}]_0 - [\mathbf{11}]_{eq} = \frac{k_1'[\mathbf{11}]_0}{k_1' + k_{-1}}$$

The integrated form of the reaction rate (*iv*) becomes

$$(viii) \qquad \ln\left(\frac{[\mathbf{11}]_0 - [\mathbf{11}]_{eq}}{[\mathbf{11}]_t - [\mathbf{11}]_{eq}}\right) = -(k_1' + k_{-1})$$

Therefore, a plot of $\ln([\mathbf{11}]_t - [\mathbf{11}]_e)$ will be linear with $k_{obs} = k_1' + k_{-1} = k_1[CO_2] + k_{-1}$

To examine the reaction rate in greater detail, a UV-vis spectroscopy experiment was designed using a customized quartz UV cell (see Experimental section), which allowed us both to overcome the diffusion-limit of carbon dioxide into benzene and to maintain a constant pressure of the gas during the reaction.

Reaction of tin alkoxides **11** with carbon dioxide (1 atm) at 313 K was monitored and analysed via UV-vis spectroscopy. The high molar extinction coefficient ε allowed us to run the reaction with a very low concentration of the alkoxides **11** ($2.4 \cdot 10^{-5}$ M), which was singnificantly lower than the concentration of dissolved carbon dioxide ($9.1 \cdot 10^{-2}$ M), satisfying the required flooding conditions needed for a correct measurement of the reaction rate. Scanning kinetic spectra showed an isosbestic point in all cases (Figure 8), evidence for the lack of any side reaction, consistent with what was observed by ^{1}H NMR spectroscopy. Inexplicably, under these conditions, the reaction of all the tin-alkoxides **11a-c** with carbon dioxide goes to completion, in contrast both with theory (equilibrium constant K_{eq} does not dependent on concentration) and with what is observed by ^{1}H NMR spectroscopy.

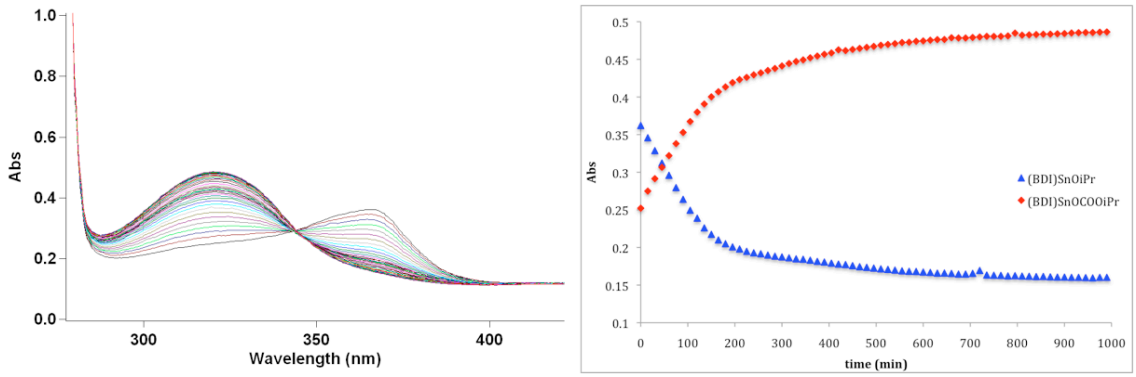

Figure 8 Scanning kinetic plot (left) and linear plot (right) for the conversion of **11a** to **14a**.

A plausible explanation for the variation of K_{eq} at different concentrations of the reagents could be the presence of an aggregation process in solution, with the formation of dimeric (or oligomeric) species. A similar behaviour was observed for BDI-lead *iso*-propylcarbonate, which was reported as a dimer in the solid phase.[78] In order to verify the presence of this process, diffusion ordered NMR spectroscopy (DOSY) was run on tin *iso*-propoxide **11a** in deuterated benzene, before and after the addition of carbon dioxide. The observed diffusion coefficient of both **11a** and **14a** is $\sim 6 \cdot 10^{-10}$ m^2 s^{-1}. This value is in agreement with a monomeric structure in solution, disproving the presence of any aggregation process.

The logarithmic plot of the reaction between the alkoxides **11a-c** and CO_2 is shown in Figure 9. The plot exhibits a linear trend after ~ 300 min, and linear interpolation shows the *iso*-propyl to be the fastest system, followed by the *sec*-butyl and *tert*-butyl ones. This result is in agreement with the qualitative measurement collected by NMR spectroscopy, previously discussed and summarised in Table 6.

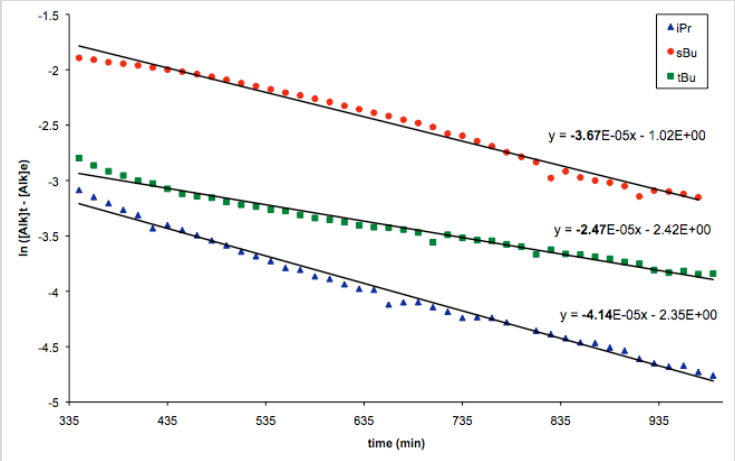

Figure 9 Logarithmic plot for the conversion of **11a-c** to **14a-c** (335–1000 min).

Unexpectedly, for all the alkoxides the reaction proceeds faster and with approximately the same rate for the initial 3 hours (Figure 10). The identical reaction rate indicates that this is plausibly not depending on the alkoxide, however any eventual diffusion process or non-detectable side reaction would result in a slower reaction rate.

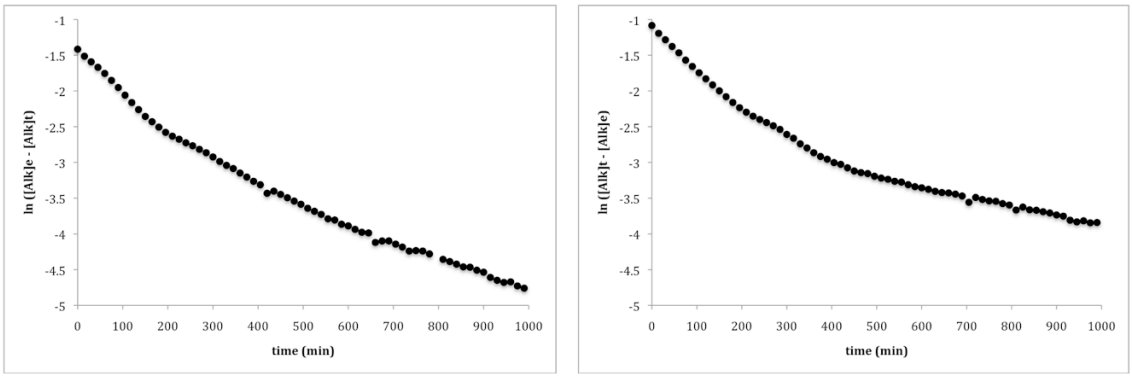

Figure 10 Logarithmic plot for the conversion of **11a** to **14a** (left) and **11c** to **14c** (right).

In order to detect and prevent any catalytic process possibly happening on the quartz surface, which would explain the initial faster rate, the quartz cell was treated with trimethylsilylchloride before running the reaction. Results however did not clarify the reasons for the unexpected trend.

2.1.7 Computational study

Density Functional Theory (DFT) studies were performed to further understand the influence of the alkyl group on both the thermodynamics and kinetics for the formation of tin alkylcarbonates from the reaction of tin alkoxides with carbon dioxide. Geometry optimization calculations on the entire molecule were performed on tin alkoxides **11a-d** and the corresponding alkylcarbonates **14a-d** using a B3LYP/Lanl2dz/3-21 g level of theory. Calculated structural

parameters for the alkoxide complexes are in good agreement with the experimental results, although the N–Sn–O bond angles are overestimated by 5–7% for the nonfluorinated alkoxide complexes (Table 7).

Table 7 X-ray crystallography data of alkoxides **11a-c** compared with computed bond distances (Å) and angles (deg) at the B3LYP/Lanl2dz/3-21g level of theory for L = BDI, and at the B3LYP/Lanl2dz/6-31g* level of theory for L = BDI*.

		L = BDI				L = BDI*			
		^{i}Pr	^{s}Bu	^{t}Bu	^{t}Bu^{F}	^{i}Pr	^{s}Bu	^{t}Bu	^{t}Bu^{F}
Sn-O	Expt	2.000	2.013	2.018	2.110	2.000	2.013	2.018	2.110
	Calcd	2.005	2.005	2.010	2.061	2.000	1.996	1.997	2.079
	% Diff	-0.26	0.40	0.41	2.30	-0.00	0.82	1.04	1.45
Sn-N1	Expt	2.206	2.202	2.202	2.184	2.206	2.202	2.202	2.184
	Calcd	2.208	2.208	2.211	2.188	2.204	2.205	2.205	2.183
	% Diff	-0.08	-.029	-0.43	-0.20	0.10	-0.12	-0.17	0.03
Sn-N2	Expt	2.208	2.202	2.210	2.184	2.208	2.202	2.210	2.184
	Calcd	2.208	2.214	2.213	2.177	2.204	2.202	2.202	2.176
	% Diff	0.01	-0.54	-0.15	0.33	0.19	0.00	0.34	0.33
C1-N1	Expt	1.323	1.328	1.328	1.334	1.323	1.328	1.328	1.334
	Calcd	1.344	1.345	1.344	1.343	1.326	1.326	1.326	1.328
	% Diff	-1.59	-1.27	-1.23	-0.67	-0.23	0.14	0.14	0.46
C3-N2	Expt	1.323	1.328	1.328	1.334	1.323	1.328	1.328	1.334
	Calcd	1.344	1.343	1.344	1.349	1.326	1.327	1.326	1.328
	% Diff	-1.59	-1.14	-1.18	-1.10	-0.23	0.11	0.14	0.43
N1-Sn-N2	Expt	83.60	82.79	83.02	83.53	83.60	82.79	83.02	83.53
	Calcd	84.25	84.24	84.54	85.64	81.71	81.60	81.69	82.75
	% Diff	-0.78	-1.75	-1.83	-2.53	2.26	1.43	1.60	0.93
N1-Sn-O	Expt	94.10	94.08	92.66	93.65	94.10	94.08	92.66	93.65
	Calcd	99.32	99.25	98.68	94.37	91.30	92.60	91.58	91.46
	% Diff	-5.55	-5.50	-6.49	-0.76	2.98	1.57	1.17	2.34
N2-Sn-O	Expt	92.50	94.29	93.89	93.65	92.50	94.29	93.89	93.65
	Calcd	99.34	99.40	98.80	96.70	91.29	91.87	90.72	86.77
	% Diff	-7.39	-5.42	-5.22	-3.25	1.30	2.56	3.37	7.35

Single point energy calculations, using the larger basis set [4333111/433111/43] for the Sn atom (see Experimental section for further details) and 6-31g(d,p) for all the others, were performed on the previously optimized geometries and used for the calculation of the ΔG°_{298K} for the insertion of carbon dioxide into the tin alkoxide. This value was calculated to be closer to

neutrality than our experimental results, with a positive ΔG°_{298K} for the *sec*-butyl and *tert*-butyl systems and a negative ΔG°_{298K} for the *iso*-propyl system (Table 8). However, the trends in reactivity of the different alkyl groups correspond to what was experimentally observed; that is, the ΔG°_{298K} was more positive for the *tert*-butoxide system and the least positive for the *iso*-propoxide system. In agreement to what experimentally observed, the perfluorinated system (**8d/11d**) exhibits a significantly more positive value of ΔG°_{298K}.

Table 8 Calculated thermodynamic (kcal mol^{-1}) parameters at the B3LYP/[4333111/433111/43]/6-31g(d,p) level of theory for the transformation of LSnOR to $LSnOCO_2R$ (L = BDI, BDI*).

	L = BDI			L = BDI*					
	ΔG°	ΔH°	ΔE°	ΔG°	ΔH°	ΔE°	$\Delta G^{\ddagger}$	$\Delta H^{\ddagger}$	$\Delta E^{\ddagger}$
^{i}Pr	- 0.03	-9.72	-9.53	- 4.05	+ 7.00	- 13.73	+10.42	+ 0.82	+ 0.77
^{s}Bu	+ 0.54	-10.76	-10.18	- 2.88	-12.44	- 12.39	+12.42	+ 2.54	+ 2.52
^{t}Bu	+ 1.05	- 9.97	-9.41	- 0.34	-11.96	- 11.34	+15.60	+ 3.57	+ 4.21
$^{t}Bu^{F}$	+17.51	+ 7.00	+ 7.57	+20.38	+ 9.4	+10.08	NA	NA	NA

An abbreviated molecule in which the N-aryl groups, as well as the backbone methyl groups, are replaced with protons, $[CH\{CHCNH\}_2]^-$ (BDI*) was used to give further mechanistic insight into the insertion of carbon dioxide into the tin-oxygen bond. This smaller ligand was utilised in looking for transition states in the reaction pathway, providing information about the different electronic contributions from each of the different alkoxide substituents, due to the minimal steric influence of BDI*. Calculated structural parameters for the alkoxide complexes supported by the abbreviated BDI* ligand are in good agreement with the experimental results, with all the bond lengths within a 1% error and the bond angles within 3% error, and only one over 7% (Table 7).

Single point energy calculations on the optimized structures, using the larger basis set, were performed and the ΔG°_{298K} of the reaction between (BDI*)SnOR and CO_2 were calculated for all the alkoxides. The trend is similar to what is observed with the larger sysyem; that is, the *iso*-propyl system has the most negative ΔG°_{298K}, followed by the *sec*-butyl and *tert*-butyl system, respectively. The fluorinated system has a significantly positive ΔG°_{298K} , which is in agreement with our experimental results in which the nonafluoro-*tert*-butoxide **11d** did not react with carbon dioxide.

Because of the low reactivity of the tin alkoxides with aliphatic electrophiles, as well as the sterical low accessibility of the alkoxide's oxygen atom, a non-nucleophilic pathway, in which carbon dioxide coordinates directly to the metal center, followed by insertion into the Sn-O bond, was initially examined. Although rare, coordination of carbon dioxide to coordinatively unsaturated metal centers has been observed, most commonly in an η^2-fashion, but end-on coordination has also been found. A high energy transition state (**TS^{NP}** $\Delta G^{\ddagger}$ = 56.6 kcal mol^{-1}) was located in which carbon dioxide coordinates in an η^2-fashion to the tin metal center of *iso*-proxide **Alk-a** (Figure 11).

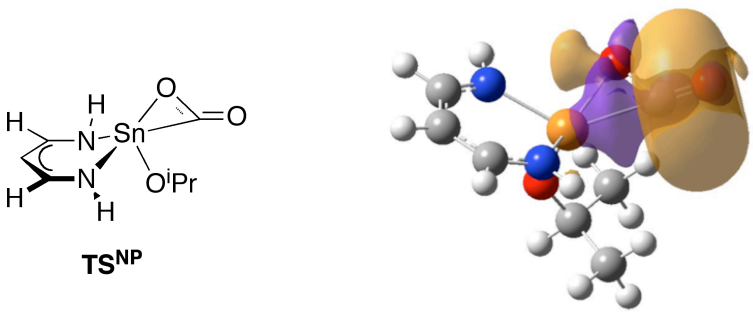

TS^{NP}

Figure 11 Chemdraw diagram of **TS^{NP}** (left) and HOMO molecular orbital diagram (right).

This interaction involves the tin $5s^2$ lone pair binding to an antibonding orbital located on the carbon dioxide molecule (Figure 11). As a result, there is a predictable decrease in electron density at the metal center and an increase in electron density at the carbon atom (see Figure 12 for Mulliken charge distribution). The C–O2 bond length is significantly longer than experimentally derived η^2-CO_2 complexes, opening up the possibility that this transition state structure is best described as a metallacycle in which there has been an oxidative addition of C=O to the metal center, generating a tin(IV) complex. The formal oxidation is further confirmed by Wiberg Bond Index (WBI) analysis, which shows a significant increase of the total WBI for the Sn atom from 1.49 in **Alk-a** to 2.78 in **TS^{NP}**, as result of the strong bonding interactions Sn–C and Sn–O2 (WBI = 0.62 and 0.50 respectively).

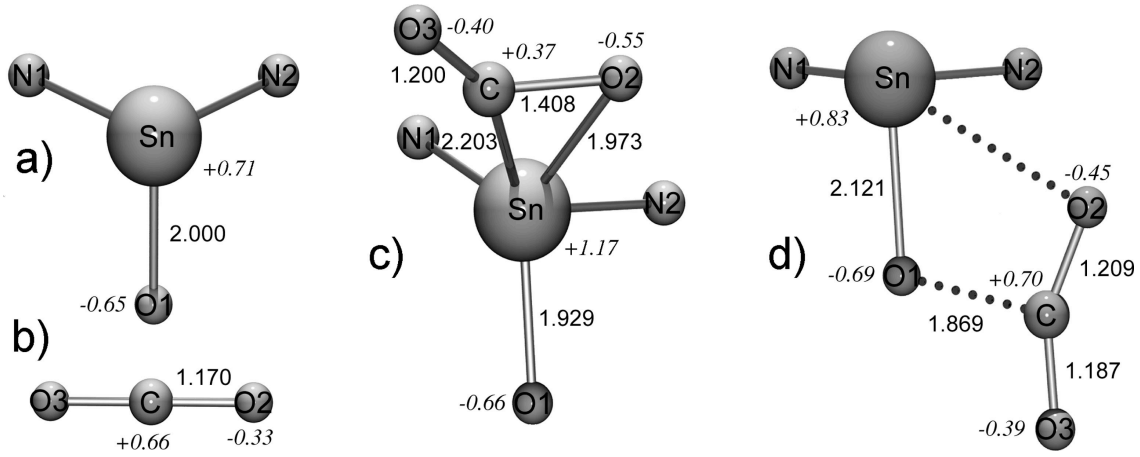

Figure 12 Optimised geometries and Mulliken charges for a) **Alk-a**, b) **CO_2**, c) **TS^{NP}** and d) **TS-a**. Only Sn, N, O and carbon dioxide atoms of the model complex are shown for clarity.

Because of both the high-energy nature of this structure and our inability to find a pathway from **TS^{NP}** to the corresponding carbonate (**Carb-a**), this transition state was deemed nonproductive. An alternative and more energetically accessible

transition state (**TS-a**, $\Delta G^{\ddagger}$ = 16.6 kcal mol^{-1}) was found arising from an interaction between the oxygen lone pair (HOMO -1) on the tin alkoxide and the LUMO of CO_2 (Figure 13).

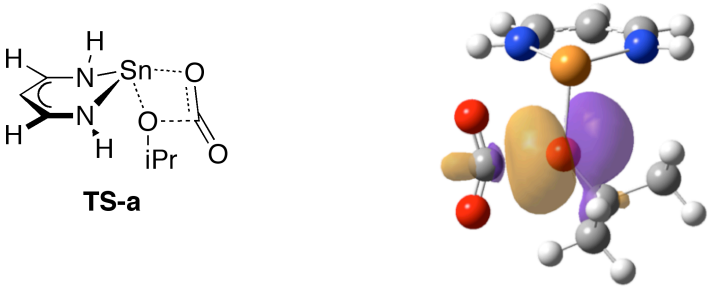

Figure 13 Chemdraw diagram of **TS^{NP}** (left) and HOMO -1 molecular orbital diagram (right).

This four-membered transition state involves formation of a new C–O1 bond, weakening of the C=O2 double bond, formation of a new Sn–O2 bond and a weakening of the Sn–O1 bond. The C···O1 interaction of 1.869 Å results in a slight C=O bond elongation of 0.017 Å (C–O2) and 0.039 Å (C–O3), a decrease in the O2–C–O3 bond angle to 151˚ and an elongation of the Sn–O bond by 0.121 Å. The WBI of the formation C–O1 bond is 0.33, whereas the WBI of the Sn–O1 bond has decreased by 0.19–0.37, indicating that although there has been minimal geometric change within the Sn–O1 bond, there has been significant weakening.

The Sn···O2 interaction of 2.733 Å is well within their combined Van der Waal radii of 3.69 A˚ and is shorter than the long-range interaction observed for maleate **13**. Although the WBI of 0.09 shows very little direct electronic interaction, the Mulliken population analysis shows there is a build-up of negative charge on O2 (-0.45 for the O2 atom in **TS-a** compared to -0.33 fro the free carbon dioxide). Taken with the increase of positive charge from +0.71 to +0.83 of the tin atom, there could be an electrostatic Sn–O2 interaction that has not been accounted for in our

calculations. Mulliken population analysis also confirms the electron donation to carbon dioxide, indicated by the increasing from 0.00 of free CO_2 to -0.17. Interestingly, there is a small increase in electron population on O1 from -0.65 to -0.69, despite the electron donation to the carbonylic carbon, which shows an electron population decrease of +0.04.

Coordination of CO_2 results then in a higher nucleophilic character of O1 and O2 and a higher electrophilic character of C and Sn. Carbon dioxide, otherwise inert, is activated by this process, which allows the reaction to proceed towards the formation of the tin alkylcarbonate via the expected four-membered ring intermediate. As such, once **TS-a** is formed, a smooth transition to the metallo-alkylcarbonate intermediate, **INT-a**, is observed and no intermediates between **TS-a** and **INT-a** were found during Intrinsic Reaction Coordinate (IRC) calculations. **INT-a** possesses a formal Sn–O2 bond, the Sn···O1 distance is 2.913 Å, which is shorter than the sum of the combined van der Waals radii (WBI = 0.05) and no interaction exists between Sn and O3. A similar intermediate has also been observed by Wakamatsu and Otera.[109] After formation of **INT-a**, the Sn–O2 bond rotates such that the bulky alkyl group points away from the metal center and a new Sn···O3 interaction is formed (2.728 Å, WBI = 0.11). The final product, **Carb-a**, is analogous to that reported and structurally characterised for the β-diketiminate lead isopropylcarbonate system, in which there is a long distance Pb···O3 interaction. The reaction profile for the conversion of (BDI*)SnO^iPr to the corresponding tin-alkylcarbonate (BDI*)Sn$OCO_2{}^iPr$ is shown in Figure 14, and includes the relative energies of the reactants (**Alk-a**), transition state (**TS-a**), intermediate (**INT-a**) and carbonate (**Carb-a**).

The corresponding calculations were performed on the other alkoxide complexes, *sec*-butoxide **Alk-b**, *tert*-butoxide **Alk-c** and their corresponding transition state **TS-b** and **TS-c**. It has not been possible to locate a stable transition state for the reaction of the nonafluoro-tert-butoxide **Alk-d** with carbon dioxide. Results are summarised in Table 8 and the $\Delta G^{\ddagger}$ trend is in agreement with the experimental kinetic measurements, that is the *iso*-propyl system is the fastest, followed by the *sec*-butyl and the *tert*-butyl, in this order.

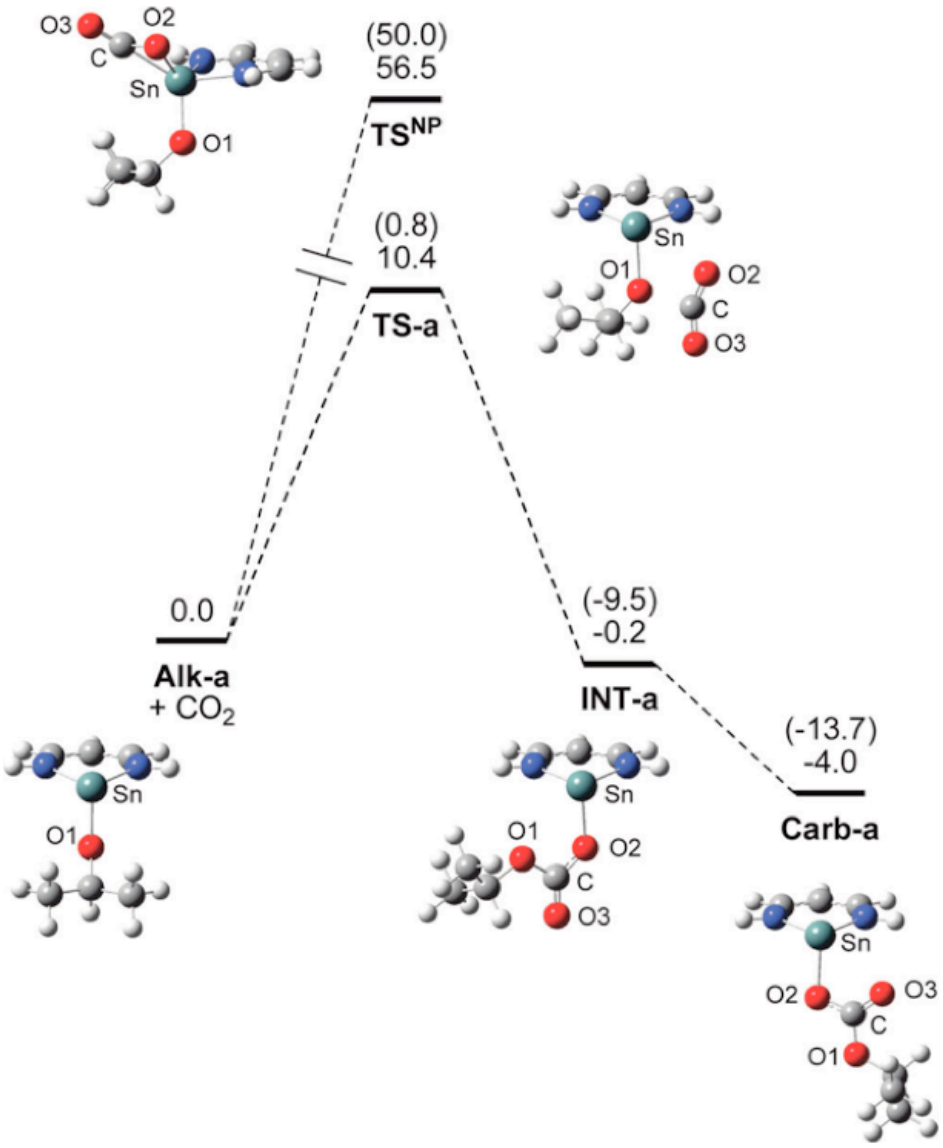

Figure 14 Gibbs free energy diagram (kcal mol^{-1}) and drawings for the reaction of (BDI*)SnO^{i}Pr and CO_2 at the BP3LYP level of theory. Electronic energies are given in parenthesis.

Table 9 Computed total electronic energies (***E***, au), zero-point energies (***ZPE***, kcal/mol), enthalpies (***H***, au/298 K) and Gibbs free energies (***G***, au/298 K) for the optimized structures at the b3lyp/Lanl2dz/6-31+g* level of theory for L$^{\#}$SnOR (**Alk**) L$^{\#}$SnOR+CO_2 (**TS1**) and L$^{\#}$Sn$O(CO_2)$R (**Carb**). The value in braces represents the energies for the single point energy calculations at the b3lyp/[4333111/433111/43]/6-31G(d,p) level. The value in parenthesis represents the energies for the optimized structure at the b3lyp/Lanl2dz/3-21g level of theory and, in square brackets, for the single point energy calculations at the b3lyp/[4333111/433111/43]/6-31G(d,p) level for LSnOR and L$SnO(CO_2)$R.

	^{i}Pr	^{s}Bu	^{t}Bu	^{t}Bu^{F}
Alk	***E*** = -423.849834 {-6441.438508} (-1615.552012) [-7453.399959]	***E*** = -463.137705 {-6480.727882} (-1467.082857) [-7492.686003]	***E*** = -463.139880 {-6480.730349} (-1467.086372) [-7492.687506]	***E*** = -1356.41765 {-7373.939694} (-2355.493909) [-8385.885695]
	ZPE = 113.29156 {113.42637} (475.96871) [461.53327]	***ZPE*** = 131.17584 {131.37568} (484.81474) [479.66861]	***ZPE*** = 130.68276 {130.81579} (484.31143) [479.20085]	***ZPE*** = 86.13822 {86.78156} (439.78046) [435.40441]
	H = - 423.837257 {-6441.426149} (-1615.506935) [-7453.358457]	***H*** = - 463.122820 {-6480.714228} (-1467.039356) [-7492.642570]	***H*** = - 463.125056 {-6480.715814} (-1467.042811) [-7492.644034]	***H*** = -1356.396496 {-7373.918791} (-2355.444347) [-8385.836901]
	G = - 423.888769 {-6441.477286} (-1615.629609) [-7453.470844]	***G*** = - 463.181424 {-6480.768401} (-1467.157406) [-7492.759731]	***G*** = - 463.182459 {-6480.772155} (-1467.160680) [-7492.760590]	***G*** = -1356.469625 {-7373.991117} (-2355.573988) [-8385.962394]
TS1	***E*** = -612.421091 {-6630.003213}	***E*** = -651.705441 {-6669.289820}	***E*** = -651.703680 {-6669.289596}	***E*** = -1544.948254 {-7562.468402}
	ZPE = 121.46040 {121.57133}	***ZPE*** = 139.39984 {139.54244}	***ZPE*** = 139.03779 {139.12862}	***ZPE*** = 95.63472 {96.23081}
	H = -612.404814 {-6629.987191}	***H*** = -651.687857 {-6669.272544}	***H*** = -651.686254 {-6669.272493}	***H*** = -1544.930168 {-7562.450529}
	G = -612.465605 {-6630.047336}	***G*** = -651.751675 {-6669.335279}	***G*** = -651.748996 {-6669.333966}	***G*** = -1544.994247 {-7562.514173}
Carb	***E*** = -612.443633 {-6630.026323} (-1615.552012) [-7641.980913]	***E*** = -651.728766 {-6669.313582} (-1654.626301) [-7681.268171]	***E*** = -651.728752 {-6669.314365} (-1654.629629) [-7681.268449]	***E*** = -1544.97366 {-7562.489586} (-2542.998650) [-8574.439582]
	ZPE = 123.12110 {123.24549} (475.96871) [471.32039]	***ZPE*** = 141.08486 {141.19175} (494.03334) [489.14424]	***ZPE*** = 140.44914 {140.54837} (493.53508) [488.53756]	***ZPE*** = 95.48026 { 96.08874 } (449.03099) [444.65003]
	H = -612.427528 {-6630.010482} (-1615.506935) [-7641.936176]	***H*** = - 651.711313 {-6669.296415} (-1654.579868) [-7681.222080]	***H*** = - 651.711333 {-6669.297245} (-1654.583239) [-7681.222292]	***H*** = -1544.949934 {-7562.466041} (-2542.946461) [-8574.388109]
	G = -612.488368 {-6630.070394} (-1615.629609) [-7642.056833]	***G*** = - 651.775499 {-6669.359656} (-1654.705322) [-7681.345545]	***G*** = - 651.774437 {-6669.359357} (-1654.708112) [-7681.345580]	***G*** = -1545.029295 {-7562.545302} (-2543.082405) [-8574.521157]

2.1.8 Discussion

In contrast to transition metal alkoxides, β-diketiminate stannylene and plumbylene alkoxides showed a similar reactivity. Despite showing slow to non-existent reactivity towards methyl iodide, indicating that the oxygen atom is essentially non-nucleophilic toward anything but very strong electrophiles such as methyl triflate, they all readily and reversibly react with carbon dioxide. The heavier lead system is reactive towards both aliphatic and unsaturated electrophiles than the isostructural tin system. Small variations of the electronic and steric properties of the alkoxide ligand (R = ^{i}Pr, ^{s}Bu, ^{t}Bu) resulted in notable differences in the reactivity; this can be attributed to both steric and electronic factors. On the one side, a bulkier alkyl group on the alkoxide ligand results in a more hindered approach to the oxygen atom (most reactive: ^{i}Pr); on the other side, the greater the basicity of the alkoxide, i.e. the greater the pK_a in solution of the corresponding alcohol (^{i}PrOH = 30.2; ^{t}BuOH = 32.5),[110] the more reactive is the alkoxide (most reactive: ^{t}Bu).[111] It is reasonable to attribute the differences of reactivity showed by the lead and tin system, predominantly to the higher polarisation and lability of the E–O bond: the tin system will be primarily discussed as it was more amendable to both experimental and theoretical studies; however, analogous arguments can apply to the lead system.

The perfluoro alkoxide **11d**, possessing at the same time a bulky and electron withdrawing alkyl group was employed to gauge the sterics and electronic influence in the activation of CO_2. Unfortunately, calculation showed that the conversion to the corresponding tin perfluoroalkylcarbonate is a strongly thermodynamically unfavoured process. Moreover, a direct comparision with the

perprotonated systems cannot be done, because of the heavy influence of fluorine atoms on the basicity of the alkoxide group, substantially lowering its basicity.[112]

It has previously been shown for transition metal complexes that the nucleophilicity of the alkoxide ligand drives insertion reactions.[98] Studies on rhenium alkoxide and aryloxide complexes, (*fac*)-$(CO_3)(PMe_3)_2ReOR$, revealed that only the alkoxide (R=Me) reacts with carbon dioxide, yet both alkoxide and aryloxide (R=4-MeC_6H_4) react with carbon disulfide. Darensbourg observed that (*fac*)-$(CO)_3$(dppe)MnOMe reacts more readily with carbon dioxide than $(CO)_3$(dppe)$MnOCH_2CF_3$, a less nucleophilic alkoxide ligand.[100] The mechanism of carbon dioxide insertion in this case was postulated to proceed via a four-membered transition state, similar to what we observed in our calculations and have been proposed by others.[97,100,102,109]

A few transition metal systems have been reported to react with both methyl iodide and carbon dioxide, unfortunately most reports have been vague on the reaction conditions.[113] Vahrenkamp's pyrazolylborate-zinc methoxide complex, ($Tp^{Ph,Me}$)ZnOMe, reacts readily with methyl iodide but very slowly with carbon dioxide, in sharp contrast to our results.[101] The former reaction is attributed to the nucleophilicity of the zinc-alkoxide. Thus, it cannot only be the nucleophilicity of the alkoxide ligand that is governing the reactivity of alkoxides with carbon dioxide. An explanation could be given by the anomalous high acidities of divalent lead and tin, which could differently polarise the metal–oxygen bond possibly making it more labile. Also, the higher acidity could have an important role in the coordination of carbon dioxide, due to the enhanced affinity of the acidic metal center and the nucleophilic oxygen of carbon dioxide.

DFT calculations on the non sterically hindered model complex allowed us to consider only the electronic factors of the insertion of carbon dioxide into the Sn–O bond. The observed trend shows a counterintuitive result, that is the less basic *iso*-propoxide system to be the most thermodynamically and kinetically favoured process. This strong and apparently strange influence on the equilibrium and kinetic rate, exerted by small variations of the alkyl group on the alkoxide ligand, can be explained in terms of the bond dissociation energy (BDE) of the Sn–O bond. Electronic influence of the different alkyl groups is apparent upon considering the pK_a's of aliphatic alcohols;[110,114] however, these electronic influences are not apparent upon considering either the BDE's or pK_a's of the corresponding carboxylic acids.[115] Therefore, in considering the total ground state energy of the alkoxides and the alkylcarbonates, the alkyl group has a much less pronounced inductive influence on the energy of the latter ones. As such, the relative energies of the alkylcarbonates can be all set to zero, and other energies be compared to these. An energy diagram using the values reported in Table 8 can easily be constructed (Figure 15).

As steric arguments cannot be brought into consideration due to the nature of the model complex, tin–oxygen BDE can be evaluated and utilised to explain the different ground state energies of the alkoxides, which result to be lower with the more electron donating (or more basic) alkoxide group, i.e. with the greater pK_a of the alkoxide's corresponding alcohol. The higher the basicity of the alkoxide, the higher the BDE, the lower the ground state energy and therefore the less favoured the reaction. As such, the conversion of tin *tert*-butoxide **Alk-c** to the corresponding carbonate is close to neutrality, followed by the more favoured conversion for the *sec*-buyl and *iso*-propyl systems.

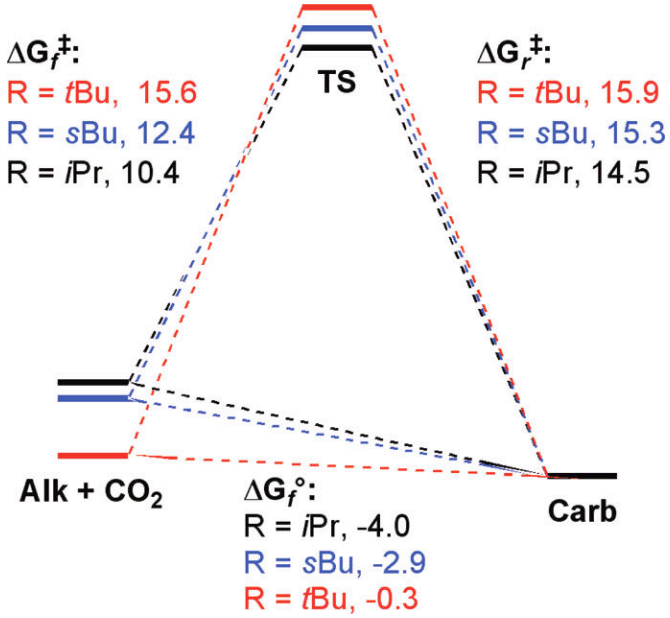

Figure 15 Energy diagram for the interconversion of **Alk** + CO_2 and **Carb** via transition state **TS**. Energies are reported in kcal mol^{-1}. ΔG°_f is the change in Gibbs energy in the forward sense, $\Delta G^{\ddagger}_f$ is the activation energy for the forward reaction, $\Delta G^{\ddagger}_r$ is the activation energy for the the reverse reaction.

In the forward sense of the reaction, the Sn–O BDE is translated in more energy required to reach the transition state. Therefore, the energy required is greater for the *tert*-butoxide than the *iso*-propoxide system, thus the Sn–O bond of *iso*-propoxide **Alk-a** must be weaker than the Sn–O bond of *tert*-butoxide **Alk-c**. Although the activation barriers to the reverse reaction follow a similar pattern in which the *tert*-butoxide system has a greater activation barrier than the *iso*-propoxide system, the difference is not as great and can be attributed to a combination of steric arguments and the differences in the C–O1 bond strengths. For the real molecule, (BDI)SnOR, the reverse reaction should be more affected by the sterics of the alkoxide group due to the interactions of both the BDI *N*-aryl groups and the alkoxide.

These observations are in accordance not only with the experimental thermodynamic and kinetic measurements of the tin system, but also with the

higher reactivity observed for the lead system, whose metal–oxygen BDE is lower than the tin one.

2.1.9 Conclusions

In conclusion, a series of tin(II) and lead(II) β-diketiminate alkoxide was successfully synthesised. They all showed low to non-reactivity towards aliphatic electrophiles, while they readily reacted with unsaturated electrophiles, such as maleic anhydride or carbon dioxide, producing respectively a rare case of structurally characterised terminal maleate and the metallo-alkylcarbonate. The latter process was reversible and dependent on small variations of the alkyl group on the alkoxide ligand. DFT calculations showed the reaction to proceed via a four-membered transition state and although sterics might play a role, there is a significant electronic contribution to both the activation energy and the established equilibrium. In contrast to what was reported for transition metal alkoxides, it has been shown that it is not just the nucleophilicity of the alkoxide ligand that determines its reactivity with carbon dioxide, but this is consistently depending on the E–O bond dissociation energy, which was higher with the higher basicity of the alkoxide ligand. This also explains the observed general higher reactivity of the lead system compared to the tin system. Reassuringly, the calculation and experimental results are in agreement.

2.2 Germanium chemistry

2.2.1 BDI-germylene alkoxides synthesis

A series of BDI-germanium(II) alkoxides was synthesised by treatment of a THF solution of (BDI)GeCl with the appropriate potassium alkoxide, affording germanium alkoxides (BDI)GeO^{i}Pr (**15a**) (BDI)GeO^{s}Bu (**15b**) and (BDI)GeO^{t}Bu (**15c**) (Scheme 21).

Scheme 21 Synthesis of β-diketiminate germanium alkoxides **15a-c**.

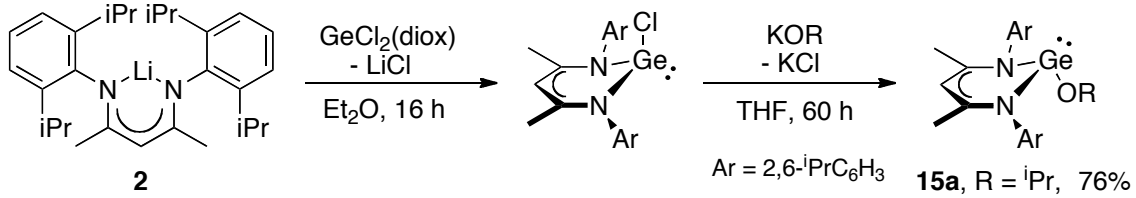

All germanium alkoxides complexes **15a-c** are air and moisture sensitive compounds, isolable in good yields and characterised by ^{1}H and ^{13}C NMR, IR spectroscopy, elemental analysis and X-ray crystallography. The ^{1}H and ^{13}C NMR spectra do not show any unexpected singularities and were fully assigned. For instance, ^{1}H NMR spectrum of *iso*-propoxide **15a** exhibits a single resonance at δ 4.64 ppm, corresponding to the ligand backbone γ-C*H* proton. Two sets of septets (δ 3.73 and 3.34 ppm) and four doublets (δ 1.51, 1.49, 1.17 and 1.10 ppm) are also observed, corresponding to the aryl *iso*-propyl groups. As observed for the isostructural tin and lead systems, this shows a deviation from planarity due to the presence of a stereochemically active lone pair. This lack of planarity is also

supported by X-ray crystallography. The ^{13}C NMR spectroscopic analysis shows a signal at δ 64.9 corresponding to the alkoxide O*C*Me$_2$ carbon.

Single crystals of germanium alkoxides **15a-c** were grown overnight from a saturated hexane solution at -27 ˚C (Figure 16). The structures are isomorphous with the Sn analogues **11a-c**. The *sec*-butyl group and one of the *iso*-propyl groups of the ligand of alkoxide **15b** are disordered and were modelled over two positions with loose restraints applies to C–C distances.

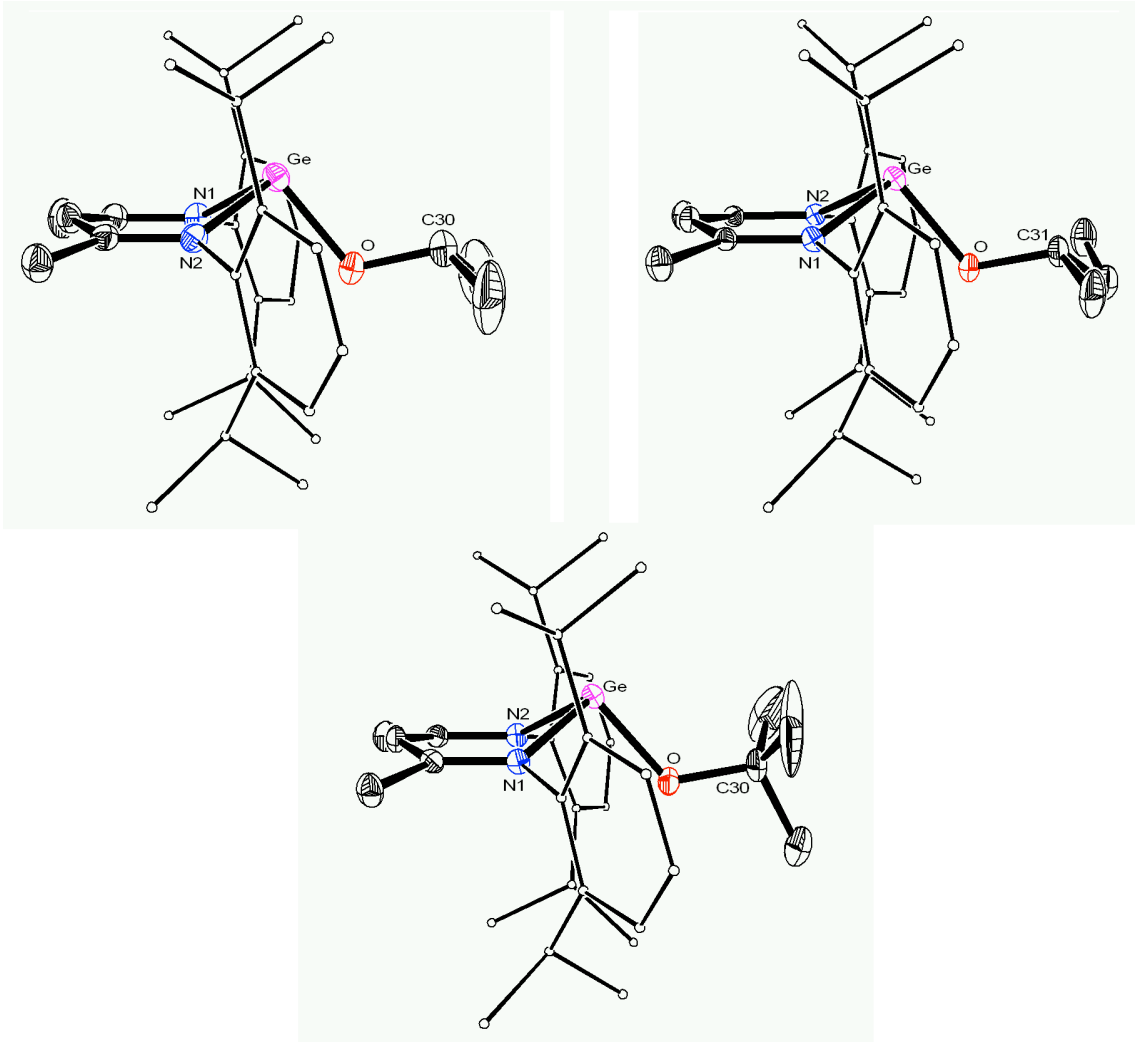

Figure 16 ORTEP diagram of (BDI)GeOR (**15a**, R = ^{i}Pr, left; **15b**, R = ^{s}Bu, right; **15c**, R = ^{t}Bu, middle). Aryl groups are minimised and hydrogen atoms are not shown for clarity. Thermal ellipsoids are shown at 30%.

Selected bond lengths and angles are reported in Table 10. Similar to the isostructural tin and lead analogues, germylene alkoxides **15** exhibit a pyramidal geometry around the germanium center, due to the presence of a $4s^2$ based stereochemically active lone pair, with the alkoxide ligand pointing away from the (BDI)-metal core of the molecule arranged in an 'exo' fashion. The Ge–O bond length is higher with the bulkier alkoxide group, probably due to steric repulsion between the alkyl group on the alkoxide ligand and the bulky aryl groups of the β-diketiminate ligand.

Table 10 Selected bond lengths (Å) and angles (deg) for alkoxides **15a-c**.

	(BDI)GeO^{i}Pr **15a**	(BDI)GeO^{s}Bu **15b**	(BDI)GeO^{t}Bu **15c**
Ge–O	1.821(2)	1.8249(12)	1.8287(15)
N1–Ge	2.016(2)	2.0134(14)	2.0222(16)
N2–Ge	2.020(2)	2.0244(14)	2.0263(17)
O–C30	1.432(4)	1.429(4)	1.432(3)
N1–Ge–N2	87.74(9)	87.48(5)	87.62(7)
N1–Ge–O	94.63(10)	96.31(6)	94.44(7)
N2–Ge–O	96.10(10)	96.70(6)	95.98(7)

Compared to the heavier isostructural systems some general trends can be observed; for instance, the E–O and E–N (E = Ge, Sn, Pb) bond lengths increase with the radius of the metal center and the N–E–N and N–E–O angles increase with the smaller metal center, plausibly due to the lower steric pressure exerted by the less diffuse lone pair. The observed Ge–O bond lengths of germanium alkoxides **15a** (1.821(2) Å), **15b** (1.8249(12) Å) and **15c** (1.8287(15) Å) are shorter than aryloxides (BDI)GeOPh (1.860(4) Å) and (BDI)GeOC$_6$F$_5$ (1.9515(14) Å), previously prepared by Roesky and co-workers by nucleophilic addition reaction of L'Ge (L' = CH{(C=CH$_2$)-(CMe)(2,6-^{i}Pr$_2$C$_6$H$_3$N)$_2$}) with PhOH or C$_6$H$_5$OH.[79] A similar

consideration can be done for Ge–N bond lengths, while the angles around the metal center are wider for alkoxides **15a-c** than Roesky's aryloxides.

2.2.2 Reactivity studies

Deuterated benzene solutions of germanium *iso*-propoxide **15a** and *tert*-butoxide **15c** were treated with carbon dioxide (1.5 atm). No reaction was observed for either alkoxides after 3 days at room temperature or 50 ˚C. Although this might look in contrast with what was observed for the tin and lead system, this is in accordance with a proposed carbon dioxide insertion mechanism that depends on the E–O bond dissociation energy, which increases going up the group.[116] Addition of carbon disulphide to **15a-c** resulted in an intractable mixture of products. In contrast with the heavier isostructural systems, treatment of germanium alkoxides with maleic anhydride resulted in no reaction, even under forcing conditions.

Addition of phenyl isocyanate to **15a-c** also resulted in no reaction at room temperature (eq 13). However, addition of phenyl isocyanate **15a** at 50 ˚C resulted in the partial formation of a new compound (**16a**) in 42% conversion, as seen by ^{1}H NMR spectroscopy. A doublet (δ 7.01 ppm) and two sets of triplets (δ 6.89 and 6.67 ppm) spectral resonances in a 2:2:1 ratio were observed in the aromatic region. The ^{1}H NMR spectrum also exhibits a singlet (δ 5.03 ppm) and two sets of septets (δ 5.22 and 3.56 ppm) spectral resonances in a 1:1:4 ratio corresponding to the γ-C*H*, the OC*H*Me$_2$ and the Ar–C*H*Me$_2$ protons respectively.

Increasing the temperature to 60 ˚C resulted in a smaller conversion into **16a** (36%), while leaving the reaction to cool down overnight, from 60 ˚C to room

temperature, resulted in the highest conversion (47%). Unfortunately, addition of 5 eq of phenyl isocyanate, in order to shift the equilibrium towards the product, resulted in an intractable mixture of products. This behaviour thwarted us from isolating the product.

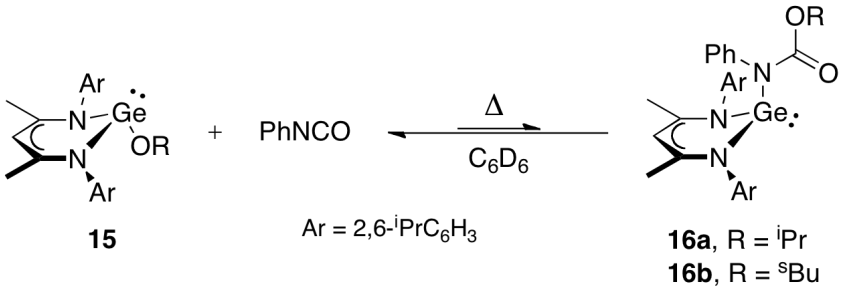

(13)

The germanium *tert*-butoxide **15c** does not react even at elevated temperatures, while germanium *sec*-butoxide **15b** is partially converted to **16b** (34% at 50 ˚C, 24% at 60 ˚C). After cooling down the sample overnight, the conversion to **16b** was 41%. A similar ^{1}H NMR resonance pattern and chemical shifts were observed for the isostructural lead system (BDI)PbN(Ph)$CO_2{}^{i}$Pr, resulting from the treatment of BDI-lead *iso*-propoxide with PhNCO.[78] The ^{1}H NMR spectrum exhibits a singlet (δ 5.03 ppm) and two sets of septets (δ 4.91 and 3.13 ppm) spectral resonances in a 1:1:4 ratio corresponding to the γ-C*H*, the OC*H*Me_2 and the Ar–C*H*Me_2 protons respectively, very similar to the previously discussed compound **16a**. For this reason, compounds **16a-b** were attributed to correspond to a germanium carbamate molecular structure.

This behaviour is presumably the result of a relatively high activation barrier, causing the lack of reactivity at room temperature, and the entropic factors, which favour the reagents at a more elevated temperature. Attempts to quantitatively measure the equilibrium were thwarted by the appearance of a precipitate after a few hours. In order to fully convert the alkoxide to an isolable product, complexes

15a-c were treated with the more reactive PhNCS, resulting however in no reactivity at room temperature, and an intractable mixture of products at 50 ˚C.

The reactivity towards aliphatic electrophiles differs sharply to the reactivity of the BDI tin and lead systems. Treatment of germanium *tert*-butoxide **15c** with methyl iodide results in the formation the germane cation [(BDI)Ge(Me)O^{t}Bu]I **17**, as a pale yellow powder in 90% yield (eq 14). The methyl group resonates at δ 1.58 ppm in the ^{1}H NMR spectrum and 6.0 ppm in the ^{13}C NMR spectrum. Colourless flake-like crystals suitable for X-ray structural analysis were obtained by leaving the reaction mixture overnight at room temperature without stirring.

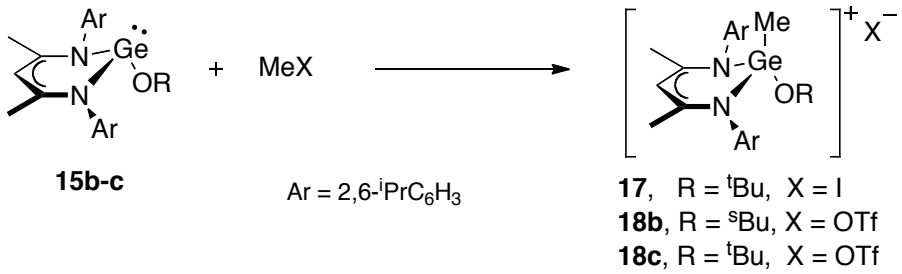

15b-c Ar = 2,6-^{i}PrC$_6$H$_3$ **17**, R = ^{t}Bu, X = I; **18b**, R = ^{s}Bu, X = OTf; **18c**, R = ^{t}Bu, X = OTf (14)

Compound **17** crystallises with half a molecule in the unit cell; the structure lies on a mirror plane with the *tert*-butyl group included as disordered across the mirror plane and with restraints on the C–C(Me) and C(Me)···C(Me) distances (Figure 17). The metal center is in a distorted tetrahedral coordination environment. The methyl group occupies the coordination site previously occupied by the lone pair. As result of the higher oxidation state, the bond lengths around the metal center (Ge–O = 1.723(3) Å, Ge–N = 1.877(2) Å) are significantly shorter than the precursor **15c**, while the bond angles (N–Ge–N' = 98.63(12)˚, N–Ge–O = 105.94(8)˚) are wider (Table 11). The Ge–C20 bond length is 1.905(4), significantly shorter than both the divalent (BDI)GeMe (2.002(4) Å) and the tetravalent (BDI)Ge(S)Me (2.009(2) Å) germanium complexes,[117,118] possibly due

to the cationic nature of **17**. Oxidative addition of (BDI)GeMe by methyl iodide has already been reported by Roesky and co-workers, however the product was not structurally characterised.[117]

The reactivity of compound **17** was briefly investigated, attempting to coordinate to the cationic metal center a non-sterically demanding ligand, such as azo- or oxo- group, by treatment with sodium azide or pyridine *N*-oxide respectively. However, these attempts proved to be unsuccessful.

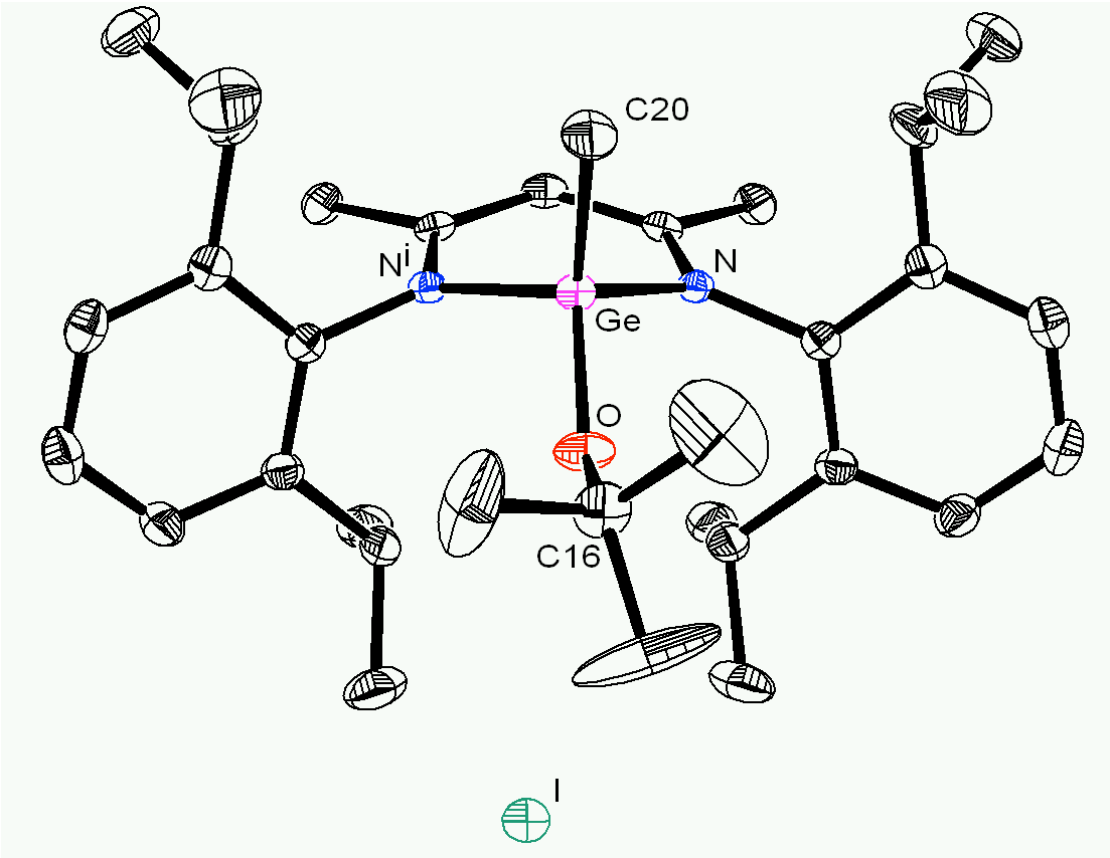

Figure 17 ORTEP diagram of [(BDI)Ge(Me)O^{t}Bu]I **17**. Hydrogen atoms are not shown for clarity. Thermal ellipsoids are shown at 30%.

Similar reactivity was observed by treatment of (BDI)GeO^{s}Bu **15b** and (BDI)GeO^{s}Bu **15c** with the stronger electrophile MeOTf (eq 14), resulting in the formation of the cationic germanium(IV) complex [(BDI)Ge(Me)OR]OTf **18b-c** (R = ^{s}Bu, ^{t}Bu). Compounds **18b** and **18c** were characterised by multinuclear NMR and

IR spectroscopy and elemental analysis. The ^{1}H NMR spectroscopic analysis shows the terminal methyl group resonating at δ 1.44 (**18b**) and 1.62 (**18c**) ppm. The corresponding ^{13}C spectral resonances are observed at 6.1 (**18b**) and 6.0 (**18c**) ppm. The ^{19}F NMR spectra shows a singlet at δ -78.19 (**18b**) and -78.31 (**18c**) ppm, corresponding to the triflate group. Colourless crystals of **18b** suitable for X-ray analysis were obtained from a saturated solution of tetrahydrofuran at -27 ˚C after two weeks (Figure 18).

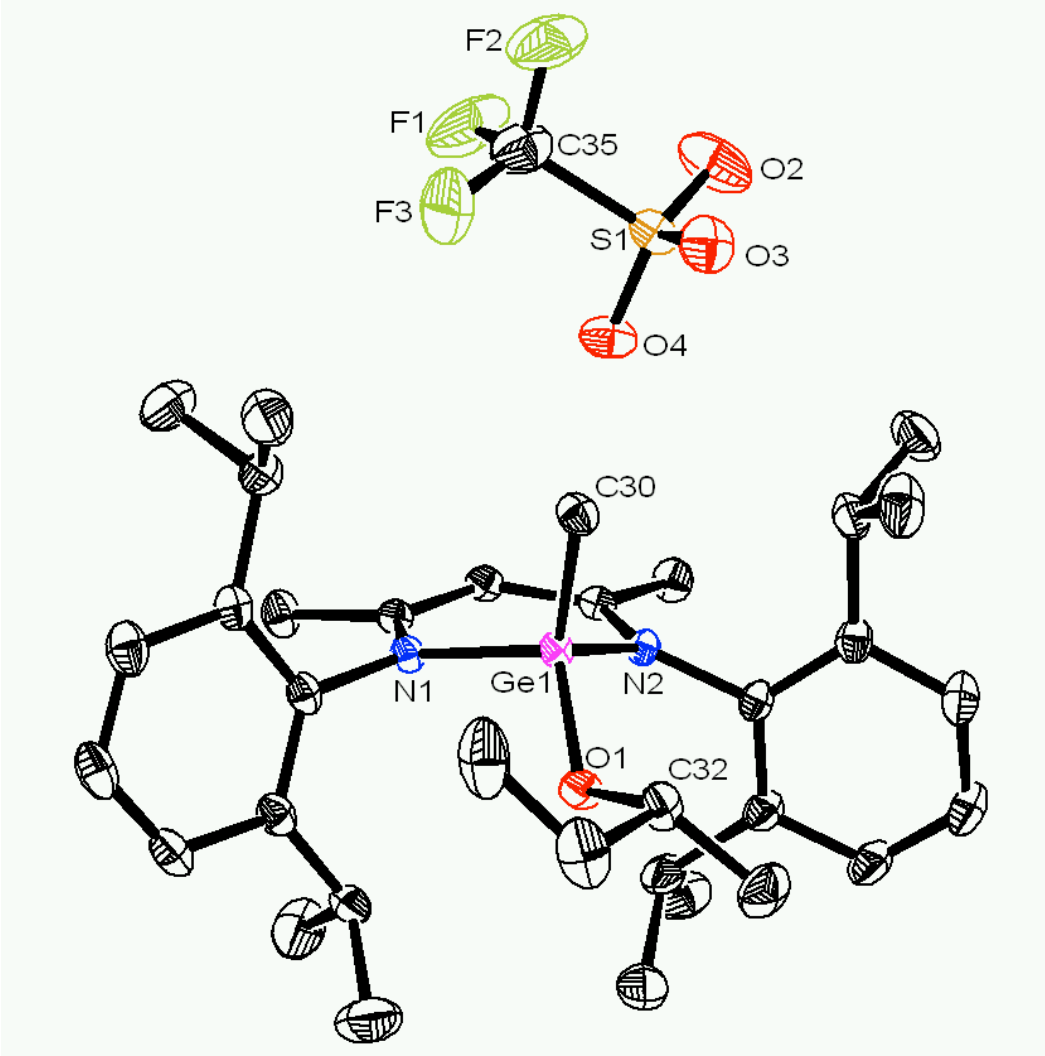

Figure 18 ORTEP diagram of [(BDI)Ge(Me)O^{s}Bu]OTf **18b**. Hydrogen atoms are not shown for clarity. Thermal ellipsoids are shown at 30%.

The metal center is in a distorted tetrahedral coordination geometry. The bond length and angles of **17** and **18b** are very similar, if not identical within experimental error, with the exception of the Ge–O bond length and O–Ge–C bond angle, presumably due to the different alkoxide groups. Interestingly, treatment of germanium alkoxides **15** with benzyl bromide did not result in any reaction, even under forcing conditions. This behaviour could be ascribed to either steric factors or a relatively reduced reactivity of the electrophile.

Table 11 Selected bond lengths (Å) and angles (deg) for cations **17** and **18b**.

[(BDI)Ge(Me)O^{t}Bu]I **17**		[(BDI)Ge(Me)O^{s}Bu]OTf **18b**	
Ge–O	1.723(3)	Ge1–O1	1.7418(15)
Ge–C20	1.905(4)	Ge1–C30	1.910(2)
Ge–N	1.877(2)	Ge1–N1	1.8809(16)
Ge–N'	1.877(2)	Ge1–N2	1.8684(16)
N–Ge–N'	98.63(12)	N1–Ge–N2	98.39(7)
N–Ge–O	105.94(8)	N1–Ge1–O1	107.11(7)
N'–Ge–O	105.94(8)	N2–Ge1–O1	106.87(8)
N–Ge–C20	110.72(10)	N1–Ge1–C30	112.48(9)
N'–Ge–C20	110.72(10)	N2–Ge1–C30	115.93(9)
O–Ge–C20	132.1(2)	O1–Ge1–C31	114.56(9)

Oxidative addition was further investigated by treatment of germanium *tert*-butoxide **15c** with molecular iodine. This results in the formation of the cationic complex [(BDI)Ge(I)O^{t}Bu]I$_3$ **19** (eq 15), presumably formed by the reaction of the iodide counteranion of the transient species [(BDI)Ge(I)O^{t}Bu]I with a further equivalent of iodine, to give the more stabilising counteranion $(I_3)^-$.

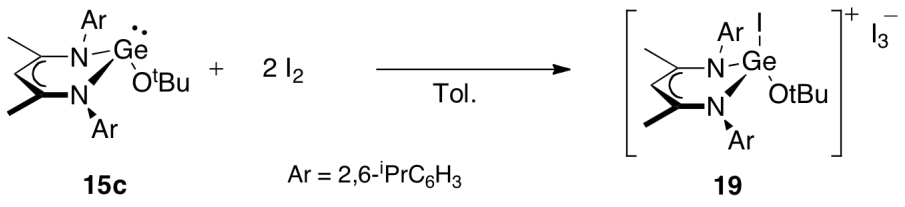

15c Ar = 2,6-^{i}PrC$_6$H$_3$ **19** (15)

Compound **19** can be obtained in 92% yield as a dark orange powder and was characterised by IR and multinuclear NMR spectroscopic and elemental analysis. The very low field singlet resonance of the methinic γ-C*H* proton in the ^{1}H NMR spectrum (δ 6.47 ppm) is reminiscent of cationic hypervalent germanium BDI complexes **15** (δ 6.10 ppm), **16b** (δ 5.99 ppm) and **16c** (δ 6.04 ppm). Deep orange single crystals suitable for X-ray crystallography were grown from a tetrahydrofuran/fluorobenzene mixture. Single-crystal X-ray diffraction study of complex **19** did not result in a high quality structure solution, but the connectivity proposed for the molecule was confirmed and further supported by elemental analysis (Figure 19).

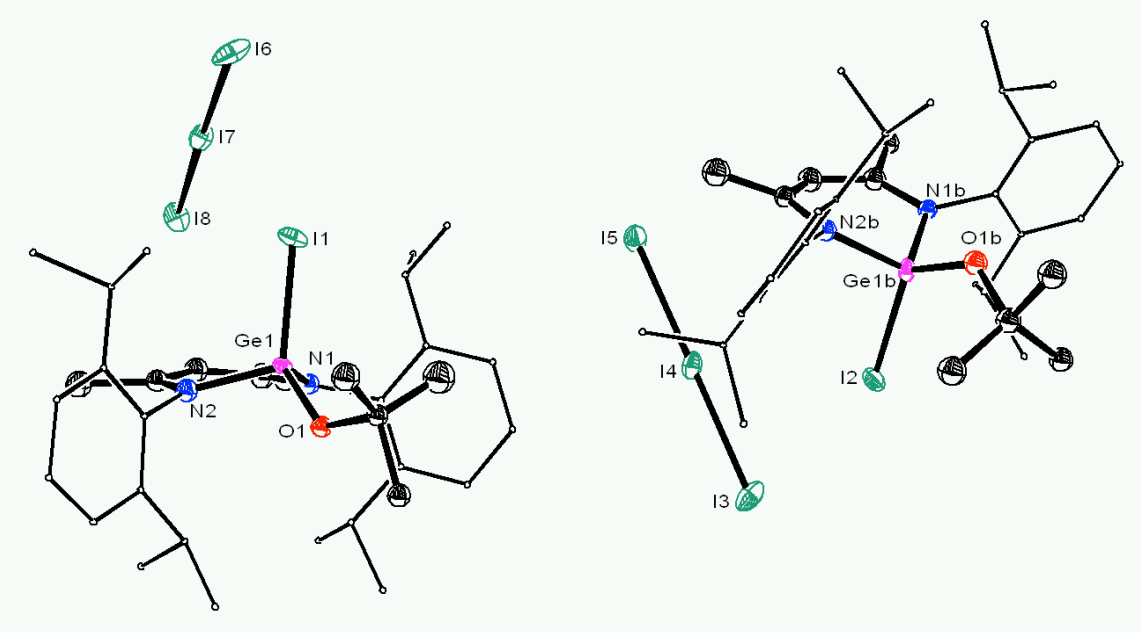

Figure 19 ORTEP diagram of [(BDI)Ge(I)O^{t}Bu]I_3 **19**. Aryl groups are minimised and hydrogen atoms are not shown for clarity. Thermal ellipsoids are shown at 30%.

Following the encouraging results obtained in oxidative addition of small molecules to germylene alkoxides **15**, dihydrogen (1.5 atm) was added to a C_6D_6

solution of **15a-c** in sealed NMR tube. Unfortunately, no reaction was observed, even at more elevated temperatures (80 ˚C).

Reactivity of the isostructural tin and lead system towards diiodine was also investigated. Treatment of lead *tert*-butoxide **4c** with 1 eq of iodine in toluene resulted in a white precipitate, insoluble in most organic solvents. The residue could be dissolved only in dichloromethane after the addition of 18-crown-6. Although crystals could be obtained from fractional crystallisation, it has not still be possible to structurally characterise the product. The ^{1}H NMR spectrum showed only one septet spectral resonance for the *iso*-propyl methine protons (δ 2.81 ppm), suggesting a symmetric molecular structure.

Treatment of tin *tert*-butoxide **11c** with iodine in pentane resulted in the precipitation of the oxidative addition product (BDI)Sn(I)$_2$O^{t}Bu **20** in good yield (eq 16).

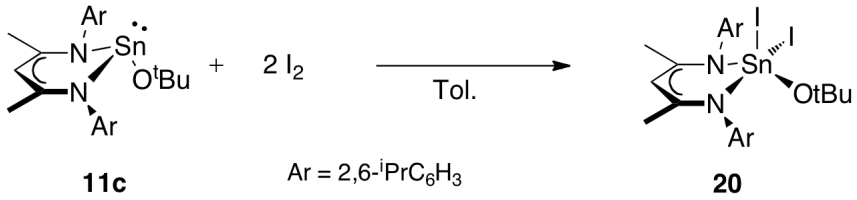

11c Ar = 2,6-^{i}PrC$_6$H$_3$ **20** (16)

Compound **20** is insoluble in non polar aromatic and aliphatic solvents and was characterised by multinuclear NMR and IR spectroscopic, elemental and X-ray structural analysis. The ^{1}H NMR spectrum shows the presence of an asymmetric environment, indicated by two distinct multiplets at δ 3.42 and 3.15 ppm, corresponding to the *iso*-propyl groups methine protons. The ^{119}Sn NMR spectroscopic analysis exhibits a singlet at -1095 ppm. Orange crystals of **20** suitable for X-ray structural analysis were grown after 3 days from a saturated tetrahydrofuran solution at -27 ˚C (Figure 20). In contrast to **19**, the complex is

neutral with a pentacoordinated tin(IV) center in a distorted trigonal bipyramidal environment. Selected bond lengths and angles are reported in Table 12. The bond lengths around the metal center are shorter than (BDI)SnO^{t}Bu **11c** as well as the O–C30 bond. This can be attributed to the increased polarization of the bonds around the hypervalent Sn atom. The Sn–I1 (2.7104(5) Å), Sn–I2 (2.8047(5) Å) bond lengths are similar to those reported by Roeksy and co-workers (2.7041(9) and 2.7903(7) Å) for (BDI)SnI$_3$.[119] The N2 and I2 atoms occupy a pseudo-axial positions (N2–Sn–I2 = 168.87(11)°) in the trigonal bipyramidal geometry.

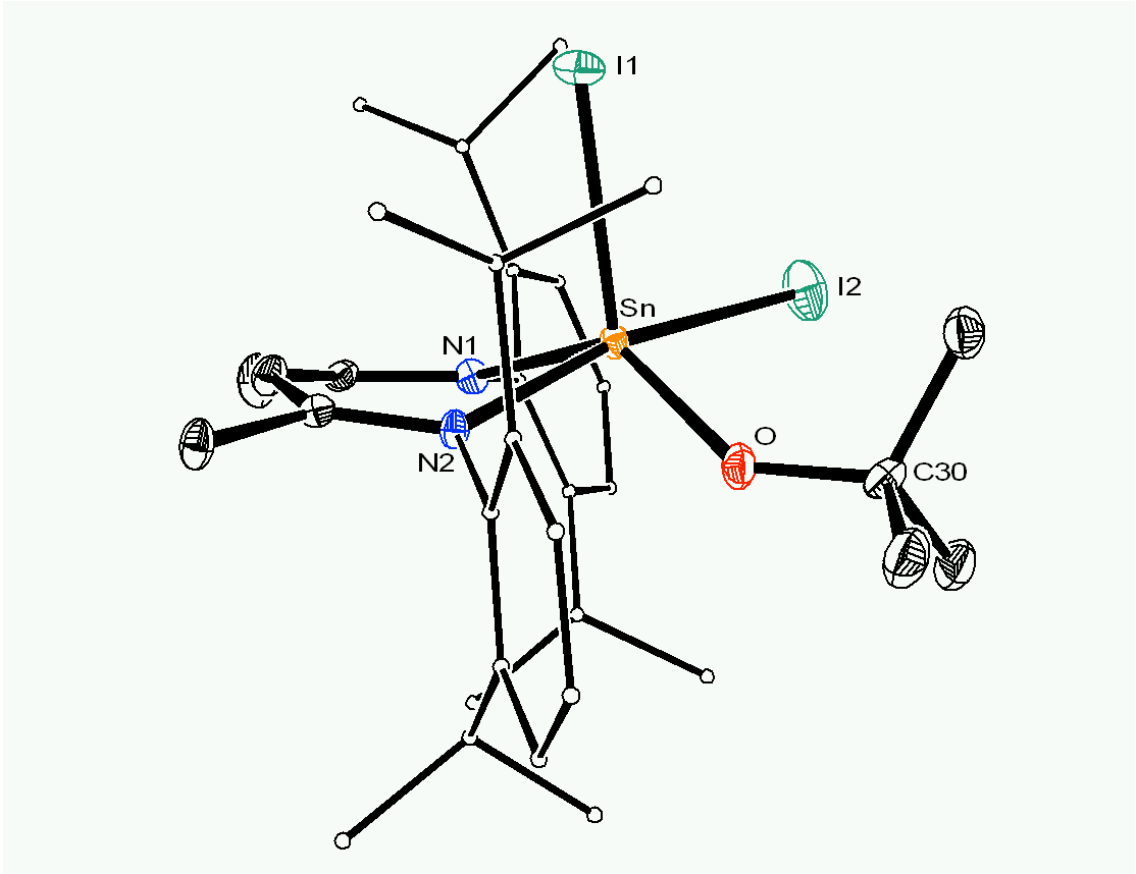

Figure 20 ORTEP diagram of (BDI)Sn(I)$_2$O^{t}Bu **20**. Aryl groups are minimised and hydrogen atoms are not shown for clarity. Thermal ellipsoids are shown at 30%.

Table 12 Selected bond lengths (Å) and angles (deg) for compound **20**.

Sn–O	1.971(4)	N1–Sn–I1	104.40(11)
Sn–N1	2.165(4)	N1–Sn–I2	89.96(11)
Sn–N2	2.194(4)	N2–Sn–O	80.59(15)
Sn–I1	2.7104(5)	N2–Sn–I1	96.69(11)
Sn–I2	2.8047(5)	N2–Sn–I2	168.87(11)
O–C30	1.390(7)	O–Sn–I1	120.64(12)
N1–Sn–N2	86.44(15)	O–Sn–I2	94.51(11)
N1–Sn–O	134.13(16)	I1–Sn–I2	94.401(17)

To gauge the Lewis base behaviour of the alkoxides **15**, a tetrahydrofuran solution of germylene *tert*-butoxide **15c** was treated with copper(I) iodide, affording the germanium(II)-copper(I) adduct $\{\mu^1\text{-}Cu_2I_2\}[(BDI)GeOtBu]_2$ **20** in 67% yield (eq 17).

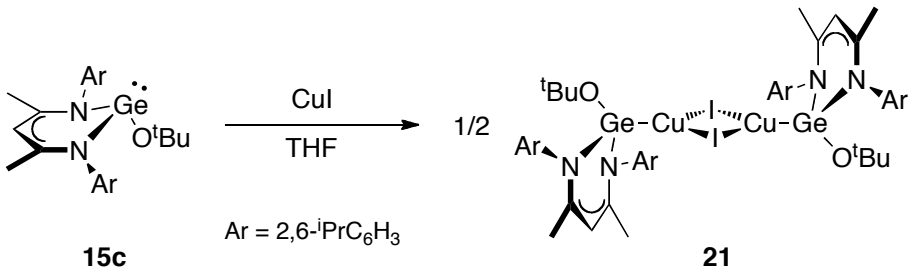

(17)

The ^{1}H NMR spectroscopic analysis shows a broad resonance for the *iso*-propyl groups methine protons (δ 3.46 ppm); unfortunately, both heating up (60 ˚C) and cooling (-70 ˚C) the d_8-THF NMR sample did not result in a sharper signal.

Complex **21** crystallises from a saturated solution of toluene at -27 ˚C after a month with half a molecule in the unit cell (Figure 21). The molecule lies on a mirror plane and an inversion center. As such, the germanium, oxygen, carbon (C16), copper and iodine atoms all lie on the same plane (Figure 22). The *tert*-butyl groups are disordered about a mirror plane and refined with carbon atoms left

isotropic. Selected bond lengths and angles are reported in Table 13. The bonds around the metal center (Ge–O = 1.781(4) Å, Ge–N = 1.964(3) Å) are shorter than (BDI)GeO^{t}Bu **15c** by 0.048 Å and 0.060 Å respectively, but longer than [(BDI)Ge(Me)O^{t}Bu]I **17** by 0.058 Å and 0.087 Å respectively. This can be attributed increased positive partial charge of the germanium atom, resulting from electron donation into the empty *s* orbital of Cu(I).

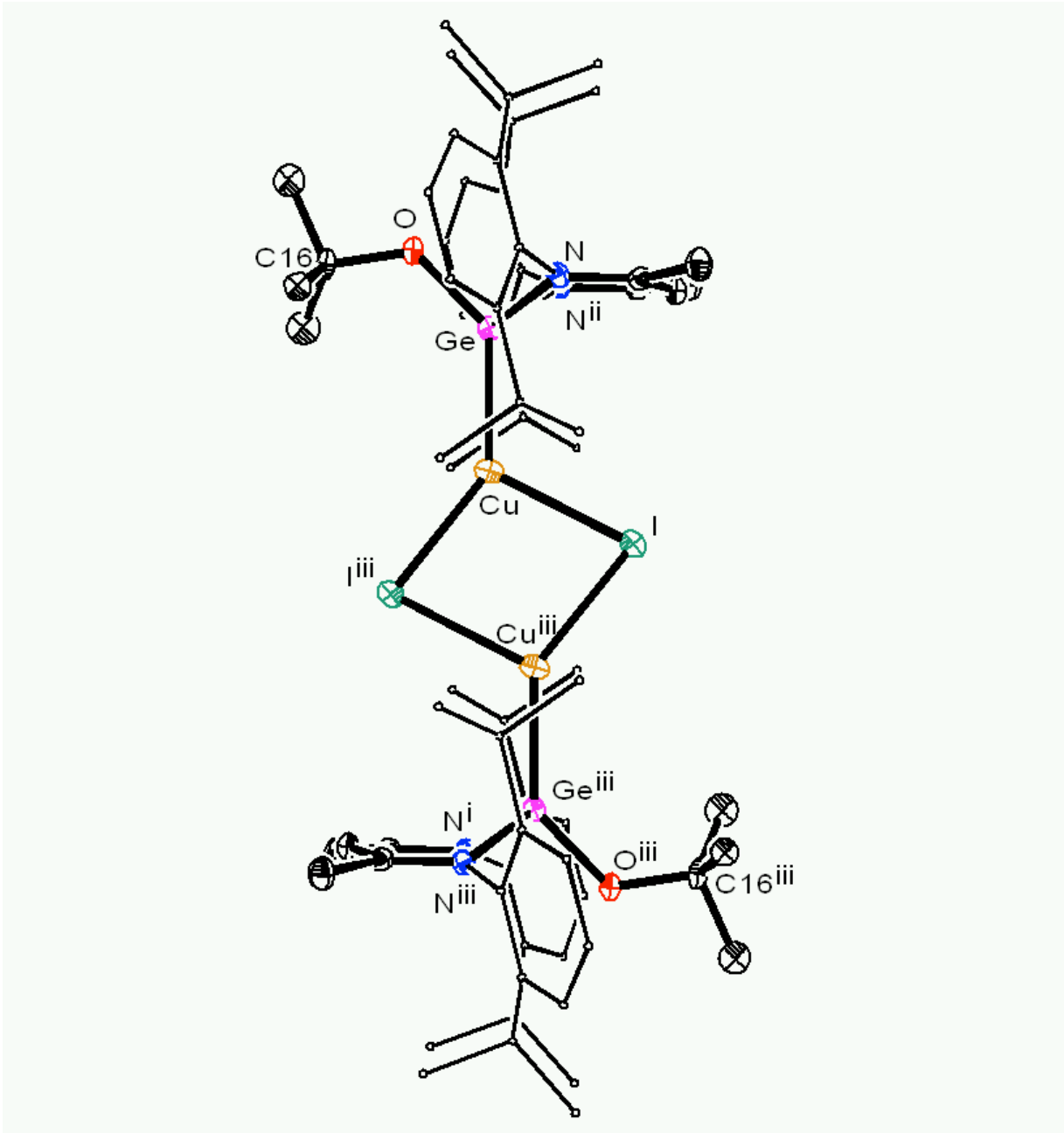

Figure 21 ORTEP diagram of complex **21**. Aryl groups are minimised and hydrogen atoms are not shown for clarity. Thermal ellipsoids are shown at 30%.

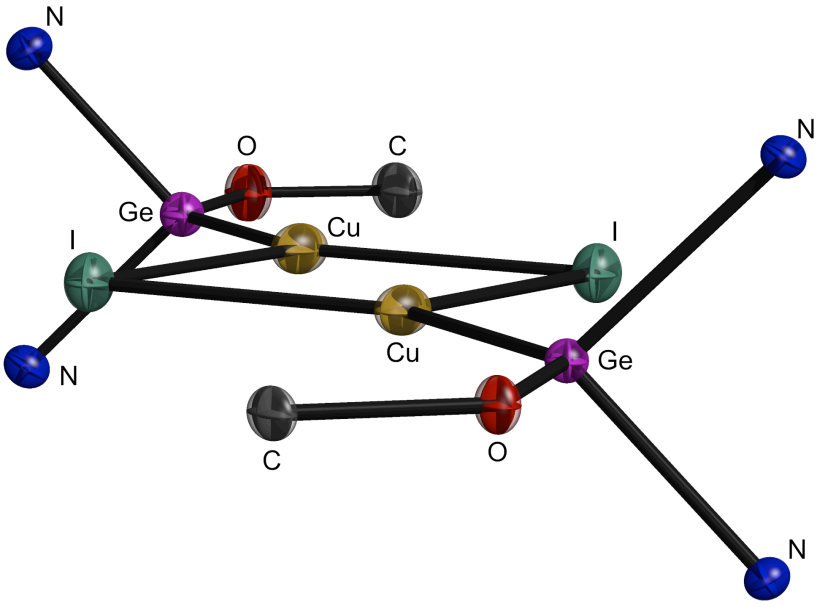

Figure 22 Raster3D diagram of the mirror plane of molecule **21**. Only N, O, I, Cu, Ge and C16 atoms are shown for clarity.

Table 13 Selected bond lengths (Å) and angles (deg) for compound **21**.

		N–Ge–N''	91.3(2)
Ge–O	1.781(4)	N–Ge–O	96.87(14)
Ge–N	1.964(3)	N–Ge–Cu	113.29(10)
Ge–Cu	2.3341(10)	O–Ge–Cu	135.71(14)
Cu–I	2.6382(9)	Ge–Cu–I	116.99(4)
Cu–I'	2.5791(9)	Ge–Cu–I'	141.37(4)
O–C16	1.447(7)	Cu–I–Cu'	78.37(3)
		I–Cu–I'	101.63(3)

Only a few other complexes possessing Cu–Ge bonds are known.[120,121] The Ge–Cu distance of 2.3341(10) Å in compound **20** is longer than what theoretical calculations predict for Ge^{II}–Cu^{I} bonds (2.250 Å),[122] however it is similar to what experimentally observed by Mochida and co-workers of 2.3165 Å for [(^{i}Pr-nacnac)Cu–Ge(Cl)(^{i}Pr-nacnac)] and by Leung and co-workers of 2.359(2) Å for $[LGe(CuI)Cl]_4$ (L = {$N(SiMe_3)C(Ph)(SiMe_3)(C_5H_4N$-2)}).[121]

The Cu_2I_2 ring is in a rhomboidal shape with the Cu–I and Cu–I' bond lengths being 2.6382(9) and 2.5791(9) Å, and the Cu–I–Cu' and I–Cu–I' angles are 78.37(3)° and 101.63(3)° respectively. The Cu···Cu' distance is 3.297 Å, well above the sum of their van der Waals radii (2.80 Å), excluding any metal-metal bonding interactions. Although the Cu_2I_2 unit is not extremely rare in coordination chemistry,[123,124] in only three examples the copper atom is bound to another metal center.[125-127] In the first case, reported by Xin and co-workers, two nest-shaped fragments $[MoOS_3Cu_2BrI]$ are interconnected through a Cu_2I_2 bridge, in which the copper atom is coordinating to one molybdenum and two sulfur atoms.[126] In the second case, reported by White and co-workers, crystallization of 1 : 2 mixtures of copper(I) iodide with triphenylstibine (Ph_3Sb) resulted in the formation of the dimer $[(Ph_3Sb)_2CuI]_2$, with the copper atom bound to two antimony and two iodine atoms.[127] In the third case, reported by Bulychev and co-workers, $Cp_2Re(H)CuI$ dimerises forming a non-planar Cu_2I_2 unit, also possessing Cu–Cu bonding interactions.[125]

Complex **20** is therefore the only example, to our knowledge, of Cu_2I_2 ring in which the copper atom is tricoordinate and bonding with a metal. Also, while the bond lengths and angles are similar to those found in the literature, the difference between Cu–I and Cu–I' (0.059 Å), usually equal to zero, is the highest found.

2.2.3 Conclusions

A series of germylene alkoxides were synthesised. In contrast to the isostructural lead and tin system, germanium(II) β-diketiminate alkoxides do not activate carbon dioxide, further supporting the dependence on the metal–oxygen

bond dissociation energy (BDE); that is, the reactivity towards insertion increases with the decreasing BDE, i.e. going down the group. (BDI)-germanium(II) alkoxides also present a different reactivity towards aliphatic electrophiles, showing the germanium lone pair to be more energetically accessible than the oxygen's one. This resulted in the formation of cationic oxidative addition products, also accessible by reaction with molecular iodine. The pronounced Lewis base behaviour of the germanium center was also confirmed by the addition of copper(I) iodide, which resulted in the formation of a Ge(II)–Cu(I) adduct presenting an unusual planar Cu_2I_2 ring bridging two metal centres.

2.3 Mercury chemistry

2.3.1 Introduction

Mercury, together with tin, lead, iron, copper, gold and silver, is one of the seven metals known to ancient man. As mercury's red ore, cinnabar, it was employed in China more than 3000 years ago for the production of red ink, and it has been found in Egyptian tombs dating back to 1500 and 1600 BC.[128] Metallic mercury, also known as *quicksilver*, found a wide range of applications in various technological fields: in the production of caustic soda and chlorine, in the manufacture of thermometers, thermostats, mercury arc lamps, fluorescent and incandescent lights, batteries and barometers, as well as in the extraction of gold and silver from their respective ores.[128] Inorganic and organic mercury derivatives are used especially in medicinal fields, from the addition of calomel (Hg_2Cl_2) to teething powders, to mercurochrome, an antiseptic preservative, and Thimerosal, still used for vaccines and many other purposes (Scheme 22).[128,129]

Scheme 22 Molecular structures of mercurochrome (left) and Thimerosal (right).

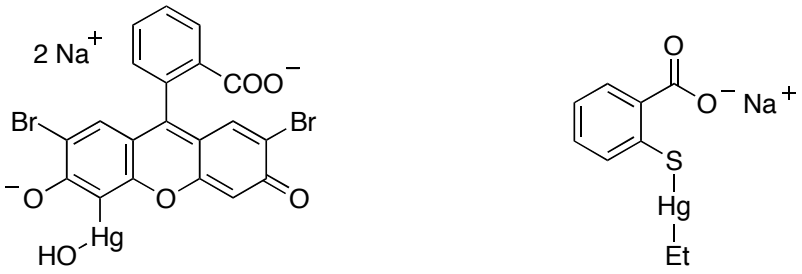

Mercury-based compounds are known for their high toxicity, which is generally attributed to the high affinity of mercury for sulfur.[128,130] For instance, mercury

easily binds to the thiol group of cysteine residues in proteins and enzymes, thereby perturbing their actions.[131] Another mechanism for mercury toxicity is attributed to its interaction with selenium,[128,132] an essential trace element.[133] Two explanations have been proposed: one consists in the lowering of the bioavailability of selenium via the formation of insoluble HgSe species;[128,134] the other in the inhibition of selenoenzymes functions caused by the binding of mercury to the enzyme's active site.[135] Detoxification of mercury is operated by the combined actions of two enzymes: organomercurial lyase (*MerB*) and mercuric ion reductase (*MerA*). *MerB* cleaves the otherwise inert Hg–C bond, while *MerA* reduces Hg(II) to the less toxic Hg(0).[136]

Similarly to divalent tin and lead cations, mercury(II) exhibits a pK_a in aqueous solution of ~ 3.5, lower than what predicted by theory (~ 10).[104] Following the somewhat surprising described results for the activation of carbon dioxide by tin(II) and lead(II) alkoxide, attention was drawn towards the isostructural mercury, in order to gauge the eventual influence of the high acidity of the metal centre.

Before this work, only two examples of β-diketiminate mercury(II) complexes were present in the literature (Scheme 23). Lappert and co-workers reported an homoleptic sila-β-diketiminate mercury complex L_2Hg (L = [{N(2,6-$^{i}Pr_2C_6H_3$)C(Me)}$_2$Si(SiMe$_3$)]$^-$), in which the BDI methine group is replaced by a Si(SiMe$_3$) and the mercury bound through the silicon atoms.[137] Layh and co-workers reported a β-diketiminate complex L'HgCl (L' = [{N(3,5-$^{t}Bu_2C_6H_3$)C(SiMe$_3$)}$_2$CH]$^-$), in which the *N*-aryl substituent possesses a *tert*-butyl group in the *meta* positions and the methyl group of the backbone are substituted with SiMe$_3$ groups.[138]

Scheme 23 Lappert's (left) and Layh's (right) β-diketiminate mercury(II) complexes.

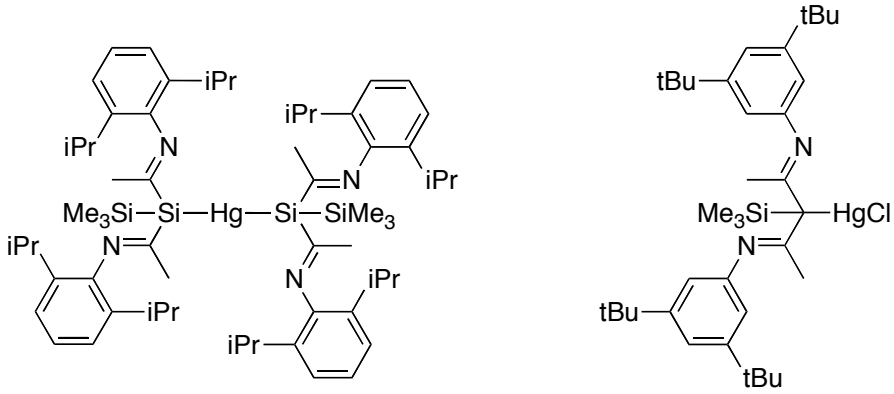

2.3.2 Synthesis and characterisation

Similarly to the described Group 14 β-diketiminate alkoxides synthesis, simple salt metathesis reaction of (BDI)Li and $HgCl_2$ was attempted to produce (BDI)HgCl, a useful precursor for the synthesis of the alkoxide derivative. However, this attempt resulted in an intractable mixture of products. Similar results were obtained from the lithiation of (BDI)H *in situ*, followed by the addition of mercury dichloride. Due to the difficulty in preparing the chloride derivative, a new synthetic route was envisioned, which involved the direct formation of a BDI–mercury amide followed by alcoholysis to lead to the desired alkoxide. Treatment of (BDI)H **1** with LiN^{i}Pr (2 eq), followed by addition of a suspension of $HgCl_2$ (0.5 eq) in toluene resulted in the formation of a white powdery product, **22** (eq 18). Proton NMR analysis of the product revealed the presence of multiple products. However, washings with pentane, toluene or tetrahydrofuran, or as recrystallisation from a saturated dichloromethane solution, never resulted in a modification of the ratio of products.

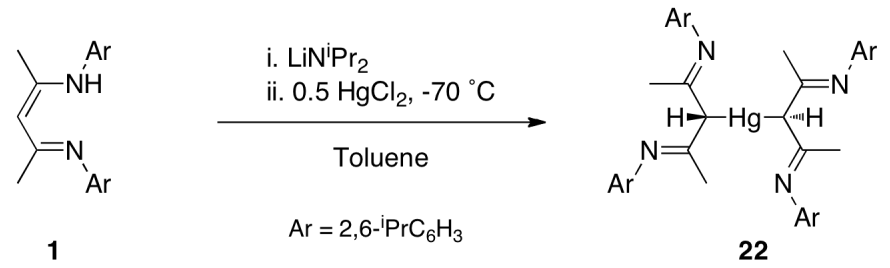

(18)

Compound **22** is a relatively air stable compound, which undergoes thermal decomposition after 2 days at room temperature in solution, and it was characterised by multinuclear NMR and IR spectroscopy, elemental and structural analysis. Colourless single crystals suitable for X-ray diffraction analysis were obtained by slowly cooling a saturated dichloromethane solution. Compound **22** crystallises with half a molecule in the unit cell, and the mercury atom is located on the center of inversion and bound through the γ-carbon of the BDI ligand (Figure 23).

Although there are a few other examples of C-bound β-diketiminate complexes in the literature, this is the first structurally characterised compound in which two β-diketiminate ligands are C-bound to a single metal center.[119,124,138,139] This structure is reminiscent to what was reported by Lappert for the sila-β-diketiminate homoleptic mercury complex L_2Hg (L = [{N(2,6-$^{i}Pr_2C_6H_3$)C(Me)}$_2$Si(SiMe$_3$)]$^-$).[137] The geometry around the metal center is linear, similarly to other R_2Hg complexes too,[140] with the ligands adopting a staggered conformation to each other. Although the Hg–C bond length of 2.127(3) Å (Table 14) is similar to other dialkylmercury complexes,[140] it is significantly shorter than that reported by Layh and co-workers (2.337(2) Å) for the β-diketiminate complex L'HgCl (L' = [{N(3,5-$^{t}Bu_2C_6H_3$)C(SiMe$_3$)}$_2$CH]$^-$), in which the *N*-aryl substituent

possesses a *tert*-butyl group in the *meta* positions and the methyl group of the backbone are substituted with $SiMe_3$ groups.[138]

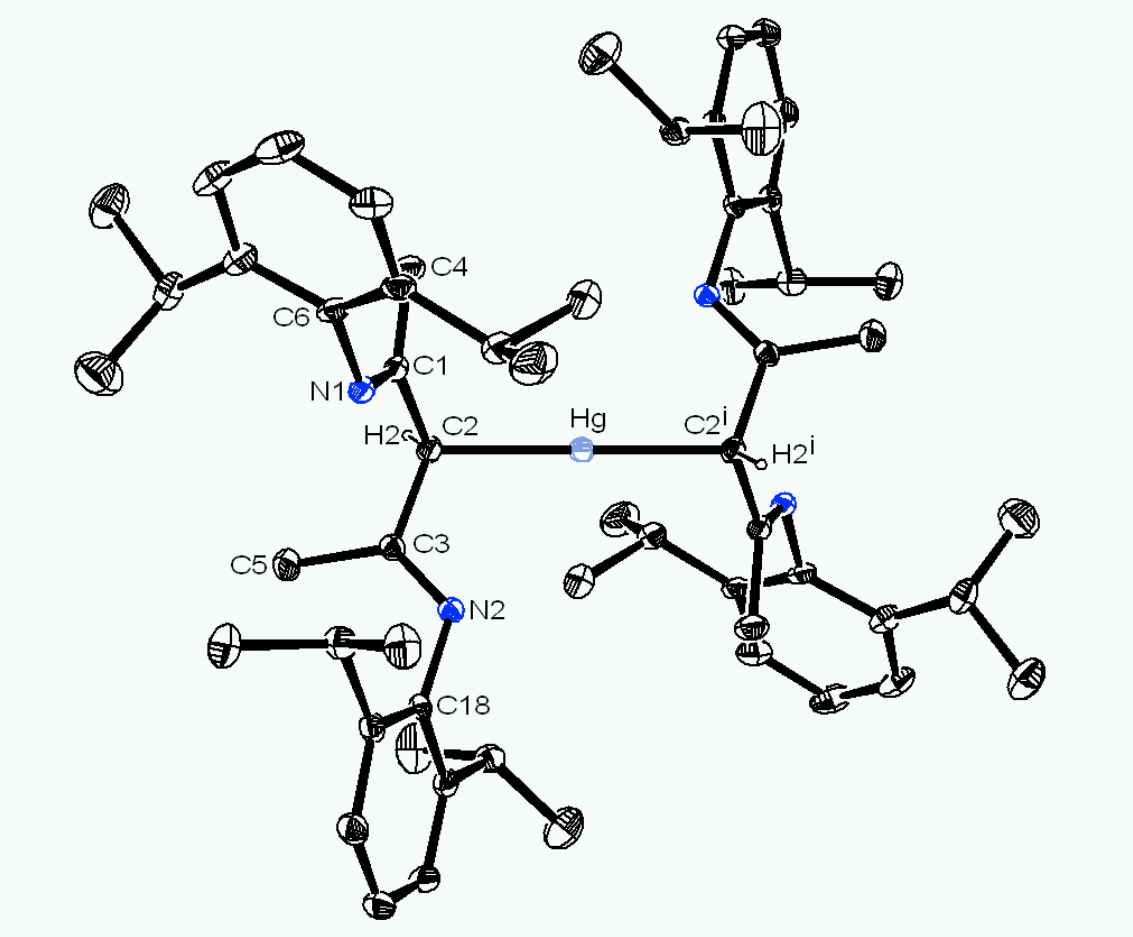

Figure 23 ORTEP diagram of $(BDI)_2Hg$. Only H2 hydrogen atoms are shown for clarity. Thermal ellipsoids are shown at 30%. Atoms marked with a prime (^{i}) are at equivalent positions (*–x*, *–y*, *–z*).

Table 14 Selected bond lengths (Å) and angles (deg) for compound **22**.

Hg–C2	2.128(3)	C2–Hg–C2’	180.00(10)
C1–N1	1.227(3)	Hg–C2–C1	107.75(18)
C3–N2	1.272(3)	Hg–C2–C3	109.81(18)
N1–C6	1.428(3)	C1–C2–C3	114.2(2)
N2–C18	1.430(3)	C2–C1–N1	118.2(2)
C2–C1	1.500(4)	C2–C1–C4	115.6(2
C2–C3	1.501(4)	C4–C1–N1	126.1(3)
C1–C4	1.505(4)	C2–C3–C5	115.9(2)
C3–C5	1.510(4)	C2–C3–N2	119.0(2)

Similar to Lappert's L_2Hg and Layth's L'HgCl, a long range intramolecular nitrogen–mecury interaction is observed (N2···Hg = 2.99 Å), within the sum of their van der Waals radii of 3.10 Å.

As ^{1}H NMR analysis did not directly correspond to this relatively simple structure, two dimensional ^{1}H-^{13}C HSQC and HMBC NMR correlation experiments (Figure 24 and Figure 25) were performed to clarify the behaviour of compound **22** in solution, two compounds in a 3:2 ratio were identified. The major compound can be assigned to the dialkyl species, with a γ-CH resonance at δ 3.98 ppm, similar to that reported for L'HgCl, correlating to a carbon found at δ 77.7 ppm. The resonances corresponding to the minor compound are reminiscent of an *N*,*N*'-bound β-diketiminate ligand, with a backbone γ-C*H* resonance at δ 4.75 ppm. Integrating in an approximately 1:1 ratio with this resonance is a coupling pattern at δ 3.71 ppm. The former proton correlates with a carbon at δ 96.2 ppm, which is in the same range as for other *N*,*N*-bound β-diketiminate compounds,[60,78,141] the latter with a carbon at δ 66.7 ppm, similarly to the major isomer.

Analysis of ^{199}Hg NMR spectrum showed a broad singlet at both room temperature (δ -990 ppm) and -60 ˚C (δ -1086 ppm). The corresponding resonance line widths at half-height are 144 and 236 Hz, respectively (the data were processed with 75 Hz exponential line broadening prior to Fourier transformation). The observed broad line width can be attributed to the close proximity of the (broad) resonances for the two species, leading to the appearance of a single signal, as well as fast relaxation caused by the chemical shift anisotropy of the ^{199}Hg.[142] The latter contribution can be confirmed by the observation that the ^{199}Hg line width at half-height is 30% larger at 14.1 T than at 9.4 T (190 Hz, with identical processing parameters). As the line width for this system is larger

than the expected magnitude of the coupling constant, no mercury–proton (^{119}Hg–^{1}H) or mercury–carbon (^{119}Hg–^{13}C) coupling could be observed at either temperature.

The solid-state IR spectrum (Nujol) revealed three strong bands at 1648, 1624, and 1589 cm^{-1}; although these bands are similar to those for other β-diimine compounds,[137,143] these data are not conclusive for either isomer, as *N*,*N*′-bound β-diketiminate complexes have a wide range of stretching frequencies in the same region.[75,78,119] The solution-phase IR spectrum was equally inconclusive. These data are consistent with an equilibrium mixture between the major homoleptic isomer **22** and a minor isomer **23** in which one ligand is bound through the γ-carbon and the other ligand is chelated through the nitrogen atoms (eq 19).

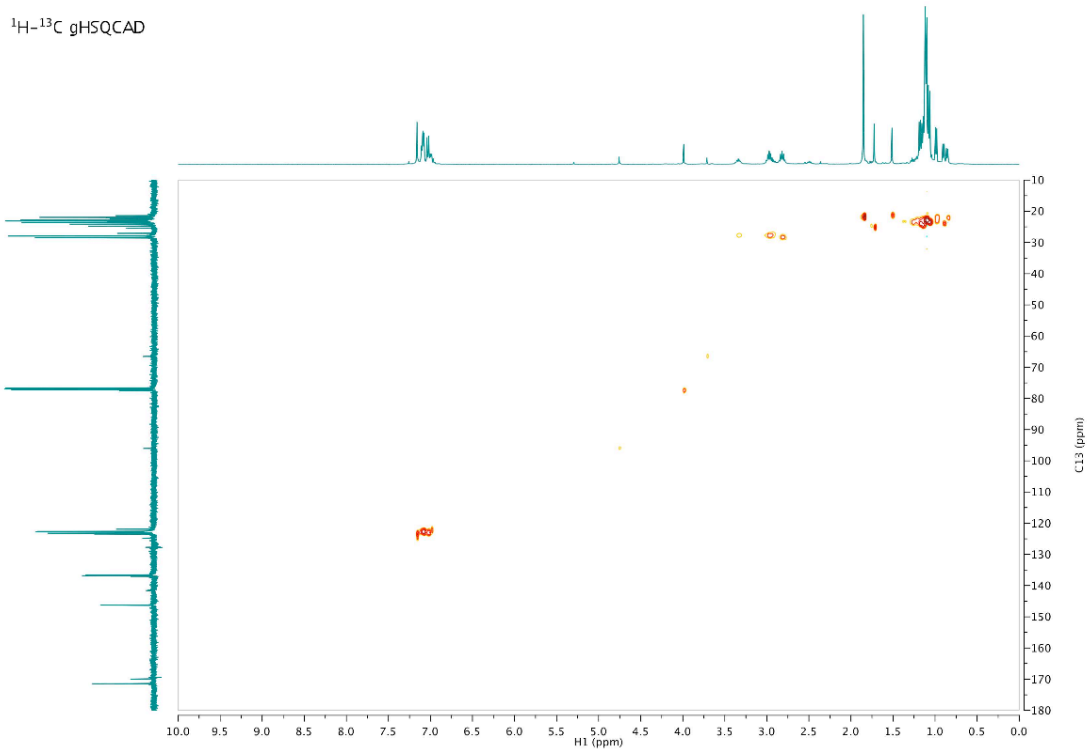

Figure 24 ^{1}H-^{13}C HSQCAD NMR spectrum of compound **22**.

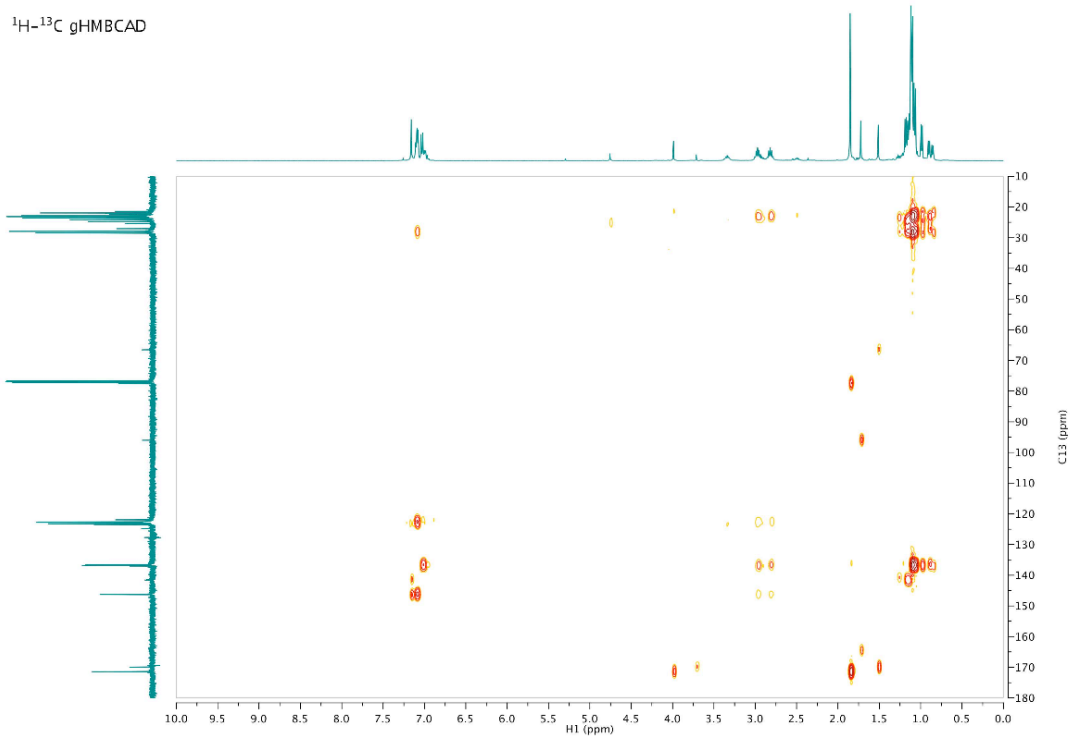

Figure 25 ^{1}H-^{13}C HMBCAD NMR spectrum of compound **22**.

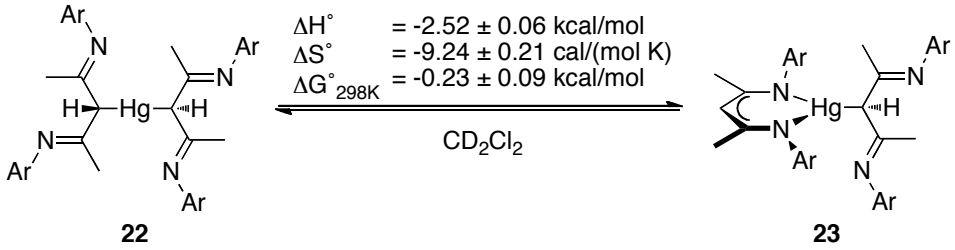

(19)

The thermodynamic parameters of the established equilibrium were measured by variable temperature ^{1}H NMR spectroscopy, revealing the heteroleptic complex to be more favoured at lower temperature (Figure 26): $\Delta H°$ (−2.52 ± 0.06 kcal mol^{-1}), $\Delta S°$ (−9.24 ± 0.21 cal mol^{-1} K^{-1}), $\Delta G°_{298}$ (0.23 ± 0.09 kcal mol^{-1}). A similar equilibrium was previously reported for L^{2}Hg (L^{2} = 2,2,6,6-tetramethylheptane-3,5-dione), in which an equilibrium was observed, but not measured, between an homoleptic bis-C-bound mercury isomer and an heteroleptic isomer in which one ligand is bound through the γ-carbon and the other through an oxygen atom.[144]

Interestingly, mercury–proton coupling was observed at -40 ˚C; however, a lower field NMR spectrometer was used, significantly decreasing the line width contribution of relaxation due to chemical shift anisotropy.

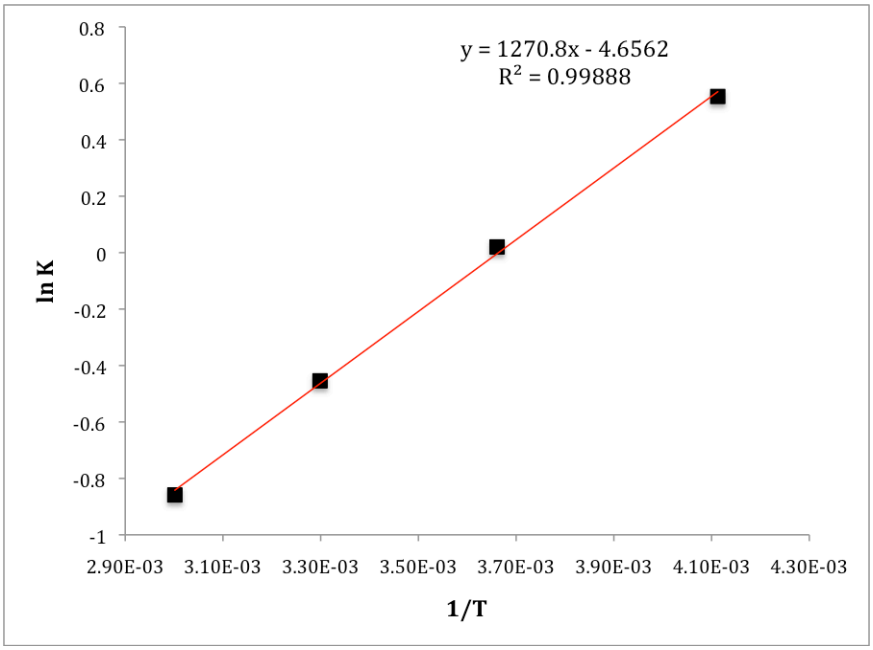

Figure 26 Van 't Hoff plot of the equilibrium between isomers **22** and **23**.

Variable temperature ^{1}H NMR spectroscopy also revealed a fluxional behaviour of **23** on the NMR time scale (Figure 27). Above room temperature, three different septets are present at δ 3.33, 2.91 and 2.49 ppm, corresponding to the isopropyl methine protons, integrating respectively four, two and two; the first spectral resonance corresponds to the *N*,*N*'-bound ligand, while the other corresponds to the carbon bound one. Cooling the sample down to -60 ˚C resulted in the splitting of the most deshielded septet into two broad signals. This can be attributed to the relatively high energy of rotation around the Hg–C bond, which causes the formation of an asymmetric structure, resulting in two different environments for the four methine protons. A $\Delta G^{\ddagger}$ value for the rotation around the Hg–C bond was calculated to be 11 kcal mol^{-1} from the variable temperature study.

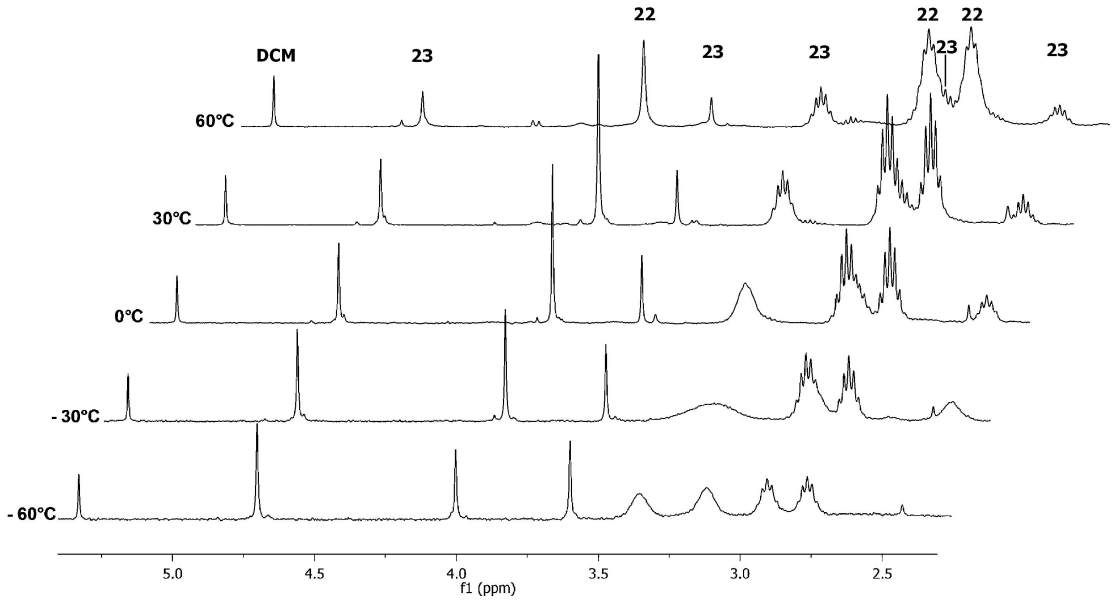

Figure 27 Variable temperature ^{1}H NMR spectra of **22** and **23** in CD_2Cl_2.

This equilibrium was further confirmed by density functional theory (DFT) calculations at the B3LYP/Lanl2dz/3-21g level of theory, used to determine the optimized geometry of compound **23**, which shows the asymmetric structure of the carbon bound ligand, resulting in different environments for the aryl substituents (Figure 27). Thermodynamic parameters for the interconversion of the isomers were also calculated from the ground state energies of compounds **22** and **23**.

Unfortunately, presumably due to the low level of theory, the calculated $\Delta H°$ (0.60 kcal mol^{-1}) was higher than the experimentally measured value and the magnitude of $\Delta S°$ (−14 cal mol^{-1} K^{-1}) greater (but still negative). Because of these discrepancies $\Delta G°_{298K}$ (4.9 kcal mol^{-1}) was also greater.

Gauge Invariant Atomic Orbital DFT (GIAO-DFT) calculations were performed on the optimized structures to predict ^{1}H NMR chemical shifts, showing a good agreement between experimental and theoretical values (Figure 28).

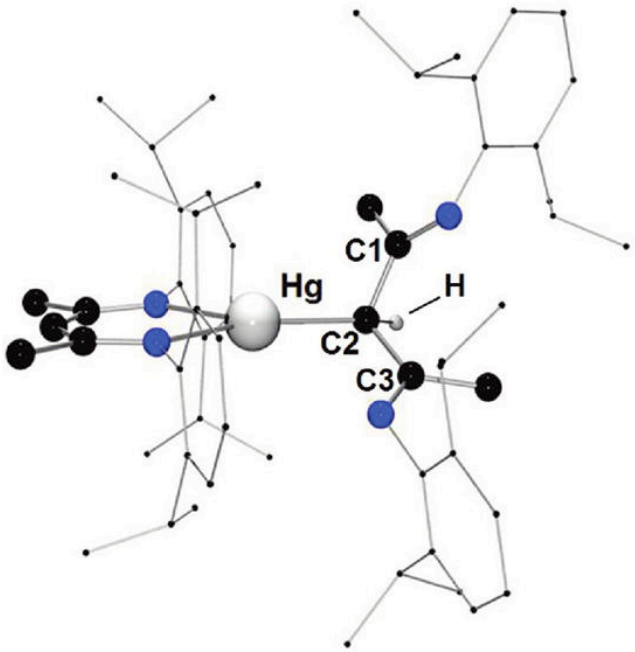

Figure 27 Optimised geometry of compound **23** at the B3LYP/Lanl2dz/3-21g level of theory.

For compound **22** the γ-C*H* proton was calculate to resonate at δ 4.21 ppm (expt: 3.98 ppm) and the NC*Me* protons at δ 1.91 and 1.67 ppm (expt: 1.85 ppm). For compound **23**, the γ-C*H* proton for the C-bound and *N*-*N*' ligands were calculated to resonate at δ 3.72 and 4.48 ppm respectively (expt: 3.71 and 4.75 ppm); while the NC*Me* protons were calculated to resonate at δ 1.70 and 1.47 ppm for the C-bound ligand (expt: 1.72 ppm) and at δ 1.31 and 1.27 ppm for the *N*-*N*'-chelated ligand (expt: 1.51 ppm).

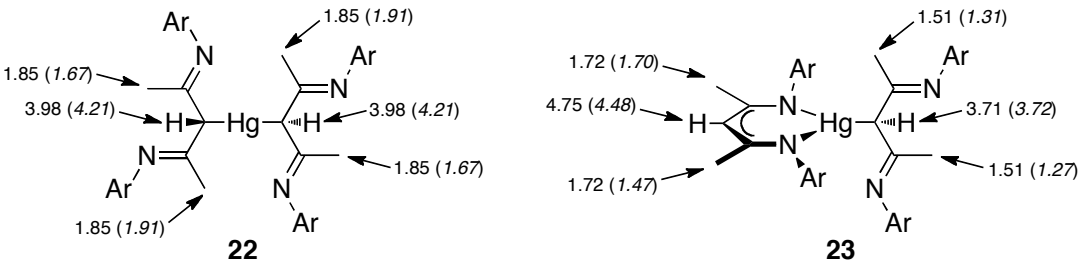

Figure 28 Experimental and calculated chemical shifts for isomers **22** and **23**. Calculated values are shown in parenthesis.

The chemistry of compound **22** has been explored aiming to selectively cleave one of the Hg–C bond, mimicking the action of organomercurial lyase (*MerB*). Therefore, reactivity studies towards protonation of one of the ligands were conducted. Unfortunately, addition of *iso*-propanol or 4-methylbenzenethiol to compound **22**, in the attempt of protolytically cleaving the mercury–carbon bond, producing an alkoxide or sulfide respectively, proved to be unsuccessful, leading only to intractable mixture of products.

3 Experimental

3.1 General considerations

All manipulations, except those involving the synthesis of **1**, were carried out in an atmosphere of dry nitrogen using standard Schlenk techniques or in an inert-atmosphere glovebox. Solvents were dried from the appropriate drying agent, distilled, degassed, and stored over 4 Å sieves. (BDI)H,[105] (BDI)Li,[105] (BDI)SnCl,[145] (BDI)SnO^{i}Pr,[81] (BDI)PbCl,[75] (BDI)PbO^{t}Bu,[78] (BDI)GeCl[145] and (papo)H[146] were prepared according to the literature. Synthesis of $GeCl_2$(diox)[33] was slightly modified. Chemicals were commercially purchased from Acros, Fisher or Aldrich and used as received, unless otherwise stated. Potassium alkoxide salts were prepared by the slow addition of the relevant alcohol (dried and distilled) to a suspension of potassium hydride, except NaO^{t}Bu^{F} that was prepared by the treatment of a water solution of $(CF_3)_3COH$ with 1eq of NaOH and dried overnight under vacuum over P_2O_5. Potassium monoalkylcarbonate salts were synthesised by bubbling carbon dioxide for 4 hours into a diethyl ether solution of the corresponding potassium alkoxide. Methyl iodide, methyl trifluoromethanesulfonate, phenyl isocyanate, phenyl isothiocyanate and carbon disulfide were freshly dried and distilled before use. Maleic anhydride and copper(I) iodide were purified before use following literature procedures.[147] Carbon dioxide was used as received (Union Carbide, 99.999%), and $^{13}CO_2$ was 99 atom %. NMR deuterated solvents were purchased from Cambridge Isotope Laboratories Inc., and degassed by freeze-pump-thaw technique and stored over

sieves. ^{1}H, ^{13}C, ^{19}F, ^{119}Sn, ^{199}Hg and ^{207}Pb NMR spectra were recorded on a Varian 400 MHz, Varian 500 MHz or Varian 600 MHz spectrometer. All the spectrometers were equipped with X{^{1}H} broadband-observe probes. ^{1}H and ^{13}C NMR spectroscopy chemical shifts are given relative to residual solvent peaks, ^{19}F, ^{119}Sn, ^{199}Hg and ^{207}Pb chemical shifts were determined from the deuterium lock signal and quoted relative to $CFCl_3$, $SnMe_4$, $HgMe_2$ and $PbMe_4$ respectively at 0 ppm. The $^{1}H-^{13}C$ HSQC and $^{1}H-^{13}C$ HMBC spectra were recorded using the Varian ChemPack 4.1 sequences gHSQCAD and gHMBCAD. The UV spectra were recorded in Varian Cary 50 UV-vis spectrophotometer using a quartz cuvette equipped with a Young's tap. IR spectrophotometry was carried out on a Perking-Elmer 1600 FT-IR instrument. Mass spectroscopy was carried out at the Centre of Mass Spectroscopy, University of Sussex. Elemental analyses were carried out by London Metropolitan University. The data for X-ray structures were collected at 173 K on a Nonius KappaCCD diffractometer, *k*(Mo-Kα) = 0.71073 Å and refined using the *SHELXL-97* software package.[148]

3.2 Computational details

All the calculations were carried out with the density functional theory (DFT) in the Gaussian 03 program.[149] Geometry optimization for the full complexes (BDI)SnOR **11** was performed at the b3lyp level by using a double-ζ basis set (Lanl2dz) plus a d type polarization function (d exponent 0.183) along with the effective core potential (Lanl2 ECP)[150] for Sn atoms and 3-21g for all other atoms. Geometry optimization for the model complexes (BDI)*SnOR was performed at the b3lyp level by using a double-ζ basis set (Lanl2dz) plus a d type polarization

function (d exponent 0.183) along with the effective core potential (Lanl2 ECP) for Sn atoms and 6-31+g* for all other atoms. Single point calculations were carried on all the found saddle points with the larger basis set [4333111/433111/43] plus two d polarization function (d exponents 0.253 and 0.078) for Sn and 6-31g(d,p) for all the other atoms.[151] The geometry optimization for $(BDI)_2Hg$ **22** was performed at the B3LYP level by using a double-ζ basis set (LanL2dz) along with the effective core potential (Lanl2 ECP) for the Hg atom and the 3-21G basis set for all other atoms. Zero-point vibrational energy corrections were also included. ^1H NMR spectra were estimated with the gauge invariant atomic orbital DFT (GIAO-DFT) calculations at the B3LYP/LanL2DZ/3-21G level. All the transition structures (TS) were located on the potential energy surfaces and verified by one imaginary frequency. Intrinsic reaction coordinates (IRC) calculations confirmed the connectivity of TS with reactants and products.

3.3 Synthetic procedures

$[CH\{(CH_3)CN\text{-}2,6\text{-}^iPr_2C_6H_3\}_2H]$ (**1**). 2,4-pentanedione (14 mL, 136 mmol) and 2,6-diisopropylamine (58.4 mL, 310 mmol) in an ethanol solution (500 mL) were treated with 12N HCl (11.2 mL). The reaction mixture was refluxed for 3 days, after which the volatiles were evacuated affording a pale pink solid. Saturated aqueous Na_2CO_3 (400 mL) and dichloromethane (400 mL) were added and the slurry was stirred until complete dissolution. The organic phase was separated, dried with $MgSO_4$, filtered and the solvents were evacuated to afford a solid pale brown residue, which was washed with cold methanol and recrystallised from hot hexane, affording 42g of (BDI)H **1** (73%). ^1H and ^{13}C NMR spectra are in agreement

with literature data.[105] ^{1}H NMR (400 MHz, C_6D_6) δ 12.41 (s, 1H), 7.12 (s, 6H), 4.85 (s, 1H), 3.27 (sept, 4H, *J* = 6.8), 1.63 (s, 6H), 1.18 (d, 12H, *J* = 6.9), 1.12 (d, 12H, *J* = 6.8).

[CH{(CH$_3$)CN-2,6-^{i}Pr$_2$C$_6$H$_3$}$_2$Li(Et$_2$O)] (**2**). 2.00 g (4.8 mmol) of (BDI)H **1** were dissolved in diethyl ether (25 mL) and treated dropwise with 2.05 M ^{n}BuLi (2.4 mL), and the solution was left stirring at room temperature overnight. The resulting yellow solution was concentrated and stored overnight in the freezer, to afford colourless crystals of (BDI)Li **2** in 89% yield (2.13 g). ^{1}H NMR is in agreement with literature data.[105] ^{1}H NMR (500 MHz, C_6D_6) δ 7.07 (m, 6H), 4.96 (s, 1H), 3.37 (sept, 4H, *J* = 6.7), 2.71 (s, 4H), 1.86 (s, 6H), 1.24 (d, 12H, *J* = 6.9), 1.14 (d, 12H, *J* = 6.8), 0.88 (s, 6H).

[CH{(CH$_3$)CN-2,6-^{i}Pr$_2$C$_6$H$_3$}$_2$PbCl] (**3**). 2.05 M ^{n}BuLi (3.5 mL) was added dropwise to a toluene solution of (BDI)H **1** (3.00g, 7.18 mmol). The resulting yellow solution was left stirring for 30 minutes and added dropwise to a stirred suspension of $PbCl_2$ (2.0 g, 7.18 mmol) in toluene (20 mL). The reaction mixture was left stirring at room temperature overnight and the resulting gray/green solution was filtered through celite. The solvents were evacuated and the orange residue was washed with cold pentane several times affording (BDI)PbCl **3** as a yellow powder in 82% yield (3.90 g). ^{1}H NMR spectrum is in agreement with literature data.[75] ^{1}H NMR (500 MHz, C_6D_6) δ 7.17 (d, 2H, *J* = 7.6), 7.08 (t, 2H, *J* = 7.6), 7.02 (d, 2H, *J* = 7.6), 4.84 (s, 1H), 3.92 (sept, 2H, *J* = 6.7), 3.01 (sept, 2H, *J* = 6.9), 1.64 (s, 6H), 1.47 (d, 6H, *J* = 6.6), 1.20 (d, 6H, *J* = 6.8), 1.12 (d, 6H, *J* = 6.9), 1.04 (d, 6H, *J* = 6.8).

[CH{(CH$_3$)CN-2,6-^{i}Pr$_2$C$_6$H$_3$}$_2$PbO^{s}Bu] (**4**). A suspension of KO^{s}Bu (0.085 g, 0.76 mmol in 3 mL of toluene) was added dropwise to a stirred solution of (BDI)PbCl **3** (0.500 g, 0.76 mmol) in toluene (10 mL) at room temperature. The reaction mixture was stirred overnight. The deep-yellow solution was filtered through Celite, and the solvent was removed under vacuum. The resulting yellow solid was dissolved in the minimum amount of pentane (7 mL) and stored at −27 °C overnight, yielding yellow crystals of (BDI)PbO^{s}Bu **4** (0.441 g, 83%). ^{1}H NMR (toluene-d_8, 303 K): δ 7.17 (d, 2H, *J* = 7.5, Ar-*H*), 7.03 (t, 2H, *J* = 16.9, Ar-*H*), 7.02 (d, 2H, *J* = 18.4, Ar-*H*), 4.60 (s, 1H, γ-C*H*), 4.56 (m, 1H, OC*H*(Me)Et), 3.79 (sept, 1H, *J* = 6.9, C*H*Me$_2$), 3.77 (sept, 1H, *J* = 7.1, C*H*Me$_2$), 3.10 (sept, 2H, *J* = 6.8, C*H*Me$_2$), 1.64 (s, 3H, NC*Me*), 1.63 (s, 3H, NC*Me*), 1.47 (dd, 6H, J_1 = 6.5, J_2 = 4.8, CH*Me*$_2$), 1.21 (dd, 6H, J_1 = 6.8, J_2 = 1.7, CH*Me*$_2$), 1.15 (d, 6H, *J* = 6.8, CH*Me*$_2$), 1.12 (d, 6H, *J* = 6.8, CH*Me*$_2$), 0.78 (d, 3H, *J* = 6.0, OCH(*Me*)Et), 0.48 (t, 3H, *J* = 7.4, OCH(Me)CH$_2$*Me*). ^{13}C{^{1}H} NMR (C$_6$D$_6$, 303 K): δ 163.4 (N*C*Me), 144.7 (*ipso*-*C*), 142.8 and 141.6 (*o*-*C*), 125.8 (*p*-*C*), 123.4 and 123.3 (*m*-*C*), 99.1 (γ-*C*H), 70.8 (O*C*(Me)Et), 36.3 (OC(*Me*)Et), 27.9 (NC*Me*), 27.8 and 27.7 (*C*HMe$_2$), 26.0, 25.0, 24.2, and 23.7 (CH*Me*$_2$), 24.4 (OC(Me)*C*H$_2$Me), 10.5 (OC(Me)CH$_2$*Me*). ^{207}Pb NMR (400 MHz, C$_6$D$_6$): δ 1542.8. IR (Nujol, ν/cm^{-1}): 3057, 1556 (s), 1516 (s), 1437 (s), 1251, 1171, 1100 (s), 1023 (s), 986, 961, 936, 917, 840, 791 (s), 750. IR (CCl$_4$, ν/cm^{-1}): 3059 (w), 2962, 2927, 2989, 2291 (w), 2004 (w), 1857 (w), 1550 (s), 1463, 1437, 1359, 1320, 1252 (s), 1217 (s), 1172. Anal. Calcd for C$_{33}$H$_{48}$N$_2$O$_3$Pb: C, 56.79; H, 7.22; N, 4.01. Found: C, 56.66; H, 7.08; N, 3.89.

[CH{(CH$_3$)CN-2,6-^{i}Pr$_2$C$_6$H$_3$}$_2$PbO^{t}Bu] (**4c**). Yellow crystals of (BDI)PbO^{t}Bu **4c** can be obtained in a similar manner to **4** in 80% yield. ^{1}H NMR analysis is in agreement with literature data.[78] ^{1}H NMR (400 MHz, C_6D_6, 303 K): δ 7.26 (d, *J* = 7.5, 2H), 7.10 (d, *J* = 7.5, 2H), 7.03 (d, *J* = 7.6, 2H), 4.47 (s, 1H), 3.83 (sept, *J* = 6.8, 2H), 3.12 (sept, *J* = 6.8, 2H), 1.66 (s, 6H), 1.63 (d, *J* = 6.8, 6H), 1.25 (d, *J* = 6.8, 6H), 1.19 (d, *J* = 6.9, 6H), 1.14 (d, *J* = 6.8, 6H), 0.88 (s, 9H).

[CH{(CH$_3$)CN-2,6-^{i}Pr$_2$C$_6$H$_3$}$_2$PbOCO$_2$^{s}Bu] (**7**). (BDI)PbO^{s}Bu **4** (101 mg, 0.145 mmol) was dissolved in toluene (8 mL) in a sealable ampoule. The gas was evacuated, and CO_2 was added (0.220 mmol). The reaction mixture was cooled to −80 °C to give (BDI)PbOCO$_2$^{s}Bu **7** as yellow powder. ^{1}H NMR (C_6D_6, 303 K): δ 7.09 (s, br, 6H, Ar-*H*), 4.78 (s, 1H, γ-C*H*), 4.71 (sept, 1H, *J* = 6.2, OC*H*(Me)Et), 3.30 (br, 4H, C*H*Me$_2$), 1.67 (m, 1H, OCH(CH$_3$)C*H*$_2$Me), 1.62 (s, 6H, NC*Me*), 1.48 (m, 1H, OCH(Me)C*H*$_2$Me), 1.26 (d, 12H, *J* = 6.2, CH*Me*$_2$), 1.18 (d, 3H, *J* = 6.9, OCH(*Me*)Et), 1.11 (d, 12H, CH*Me*$_2$), 0.90 (t, 3H, *J* = 7.4, OCH(Me)CH$_2$*Me*). ^{13}C{^{1}H} NMR (C_6D_6, 303 K): δ 163.7 (N*C*Me), 160.7 (O*C*O$_2$), 142.4 (*ipso*-*C*), 127.7 and 127.5 (*o*-*C*), 126.5 (*p*-*C*), 124.4 and 124.0 (*m*-*C*), 103.2 (γ-C*H*), 73.2 (O*C*H(Me)Et), 29.3 (OCH(*Me*)Et), 27.8 (NC*Me*), 24.2 (*C*HMe$_2$), 24.1 (CH*Me*$_2$), 19.7 (OCH(Me)*C*H$_2$Me), 9.8 (OCH(Me)CH$_2$*Me*). ^{207}Pb NMR (400 MHz, C_6D_6): δ 810.3. IR (Nujol, ν/cm^{-1}): 3027, 2336 (w), 1940 (w), 1855 (w), 1800 (w), 1604, 1549 (s), 1260 (s), 1081 (s, br), 804 (s), 694 (s). IR (CCl_4, ν/cm^{-1}): 3723, 2693, 3621, 3590, 3063 (w), 2963, 2928, 2870, 2337 (s), 2005 (w), 1857 (w), 1645, 1550 (s), 1459, 1437, 1383, 1364, 1319, 1254 (s), 1217 (s), 1174.

[CH{(CH$_3$)CN-2,6-^{i}Pr$_2$C$_6$H$_3$}$_2$PbO(CO)C$_2$H$_2$CO$_2$^{s}Bu] (**8**). A stirring solid mixture of (BDI)PbO^{s}Bu **4** (71 mg, 0.102 mmol) and maleic anhydride (10 mg, 0.102 mmol) was treated with toluene (5 mL) and the resulting red solution was stirred at room temperature for 45 minutes. The volatile were then evacuated and the red residue was dissolved in the minimum amount of hexane (~ 0.5 mL) and stored at -27°C for one week, affording red crystals of (BDI)Pb(ma) **8** (58 mg, 72%) suitable for X-ray crystallography. ^{1}H NMR (500 MHz, C$_6$D$_6$, 303 K): δ 7.08 (s, 6H, Ar-*H*), 6.00 (d, *J* = 11.9 Hz, 1H, COC*H*CHCO$_2$), 5.90 (d, *J* = 11.9 Hz, 1H, COCHC*H*CO$_2$), 4.96 (m, 1H, OC*H*(Me)Et), 4.74 (s, 1H, γ-C*H*), 1.64 (s, 6H, NC*Me*), 1.56 (m, OCH(Me)C*H*$_2$Me), 1.35 (m, 1H, OCH(Me)C*H*$_2$Me), 1.18 (br, 18H, CH*Me*), 1.13 (d, 6H, *J* = 6.3, CH*Me*), 0.84 (d, 3H, *J* = 7.5, OCH(*Me*)Et), 0.76 (t, 3H, *J* = 7.5, OCH(Me)CH$_2$*Me*). ^{13}C{^{1}H} NMR (500 MHz, d$_8$-toluene, 303 K) δ 170.6 (PbO*C*O), 168.8 (*C*O$_2$^{s}Bu), 165.40 (N*C*Me), 147.4 (*ipso-C*), 141.9 (*o-C*), 132.8 (C*H*=CH), 131.5 (CH=C*H*), 130.0 (*p-C*), 108.0 (γ-*C*H), 76.8 (CO$_2$*C*H(Me)Et), 33.7 (OC(*Me*)Et), 32.8 (CH(Me)*C*H$_2$Me), 29.3 (NC*Me*), 29.2 (NC*Me*), 27.7 (*C*HMe), 24.6 (CH*Me*), 24.0 (CH*Me*), 14.5 (OCH(Me)CH$_2$*Me*). ^{207}Pb NMR (400 MHz, C$_6$D$_6$): δ 871.4. IR (Nujol, ν/cm^{-1}): 1734 (s), 1655, 1645, 1576 (s), 1533 (s), 1519 (s), 1439 (s), 1390 (s), 1379 (s), 1335, 1316 (s), 1266, 1253, 1214 (s), 1173 (s), 1101, 1091, 1056, 1023, 982 (w), 962 (w), 935, 914, 877 (w), 844, 844, 796, 760, 684. Anal. Calcd for C$_{37}$H$_{52}$N$_2$O$_4$Pb: C, 55.83; H, 6.58; N, 3.52. Found: C, 56.00; H, 6.71; N, 3.46.

[CH{(CH$_3$)CNH-2,6-^{i}Pr$_2$C$_6$H$_3$}$_2$]OTf (**9**). (BDI)H **1** (560 mg, 1.34 mmol) was dissolved in diethyl ether (20 mL) and treated dropwise with triflic acid (114 μL, 1.34 mmol). The reaction mixture was stirred for 1 hour, after which a white precipitate appeared. The solution was decanted and the residue washed with

hexane several times to yield pure [(BDI)H_2]OTf **9** in 94% yield (762 mg). ^{1}H NMR (400 MHz, $CDCl_3$) δ 9.30 (s, 2H, CN*H*), 7.16 (t, 2H, *J* = 7.8, Ar-*H*), 6.93 (d, 4H, *J* = 7.7, Ar-*H*), 4.30 (s, 1H, γ-C*H*), 2.53 (m, 2H, C*H*Me), 2.48 (s, 6H, NC*Me*), 0.97 (d, 12H, *J* = 6.7, CH*Me*), 0.78 (d, 12H, *J* = 6.8, CH*Me*). ^{13}C{^{1}H} NMR (400 MHz, $CDCl_3$, 303 K): δ 171.5 (N*C*Me) 144.9 (*ipso-C*), 145.0 (*o-C*), 131.4 (*p-C*), 129.2 (*m-C*), 123.8 (*m-C*), 120.3 (SO_3CF_3), 91.7 (γ-*C*H), 31.5, 28.2 (NC*Me*), 24.1 (*C*HMe), 22.4 (CH*Me*), 21.8 (CH*Me*). ^{19}F NMR (400 MHz, $CDCl_3$) δ -78.58. IR (ATR, ν/cm^{-1}): 3221 (br), 3064 (br), 2968, 2870, 1595, 1562 (s), 1538 92), 1461, 1386, 1281 (s), 1238 (s), 1225 (s), 1159 (s), 1032 (s), 794, 749, 634 (s), 574. Calcd HR-ESI-MS for $C_{29}H_{43}N_2^+$: 419.3421. Found: 419.3411 ((BDI)H_2^+).

[CH{(CH$_3$)CN-2,6-^{i}Pr$_2$C$_6$H$_3$}$_2$SnCl] (**10**). (BDI)H **1** (2.00g, 4.8 mmol) was dissolved in diethyl ether (20 mL) and 2.05 M ^{n}BuLi was added dropwise (2.4 mL). The resulting yellow solution was left stirring for 30 minutes and added dropwise to a stirred $SnCl_2$ (0.91 g, 4.8 mmol) suspension in diethyl ether (20 mL). The reaction mixture was left stirring at room temperature overnight. Filtration through celite and removal of the volatiles afforded an orange powder, that was washed several times with cold pentane affording pure (BDI)SnCl **10** as a very pale yellow powder in 78% yield (2.14 g). ^{1}H and ^{13}C NMR spectra are in agreement with literature data.[145] ^{1}H NMR (500 MHz, C_6D_6) δ 7.16–6.98 (m, 6H), 5.03 (s, 1H), 3.92 (sept, 2H, *J* = 6.6), 3.09 (sept, 2H, *J* = 6.7), 1.59 (s, 6H), 1.42 (d, 6H, *J* = 6.5), 1.19 (d, 6H, *J* = 6.7), 1.16 (d, 6H, *J* = 6.9), 1.03 (d, 6H, *J* = 6.7).

[CH{(CH$_3$)CN-2,6-^{i}Pr$_2$C$_6$H$_3$}$_2$SnO^{i}Pr] (**11a**). A suspension of KO^{i}Pr (86 mg, 0.87 mmol) in THF (5 mL) was added to a THF (10 mL) stirred solution of (BDI)SnCl **10**

(86 mg, 0.87 mmol) at room temperature and the reaction mixture was left stirring for 3 days. The volatiles were evacuated and the yellow residue was dissolved in toluene and filtered through celite. The solvents were evacuated and the residue was washed with cold pentane three times. Storage of a concentrated pentane solution for 2 days afforded 0.37 g of yellow crystals of BDI-SnO^{i}Pr **11a** in 78% yield. ^{1}H NMR analysis is in agreement with literature data.[81] ^{1}H NMR (400 MHz, C_6D_6) δ 7.20–7.00 (m, 6H), 4.70 (s, 1H), 4.10 (sept, 1H, *J* = 6.0), 3.82 (sept, 2H, *J* = 6.8), 3.21 (sept, 2H, *J* = 6.8), 1.56 (s, 6H), 1.49 (d, 6H, *J* = 6.8), 1.24 (d, 6H, *J* = 6.9), 1.20 (d, 6H, *J* = 6.9), 1.10 (d, 6H, *J* = 6.8), 0.86 (d, 6H, *J* = 6.0). UV–vis (benzene): λ_{max} (ε, L mol^{-1} cm^{-1}) 366 nm (11000).

[CH{(CH$_3$)CN-2,6-^{i}Pr$_2$C$_6$H$_3$}$_2$SnO^{s}Bu] (**11b**). Yellow crystals of (BDI)SnO^{s}Bu **11b** can be obtained in a way similar to that for **11a** in high yield (80%). ^{1}H NMR (400 MHz, C_6D_6, 303 K): δ 7.22 (d, *J* = 7.6, 2H, Ar-*H*), 7.14 (t, *J* = 7.6, 2H, Ar-*H*), 7.07 (d, *J* = 7.7, 2H, Ar-*H*), 4.71 (s, 1H, γ-C*H*), 3.81 (m, 3H, C*H*Me$_2$ + OC*H*(Me)Et), 3.22 (m, 2H, C*H*Me$_2$), 1.55 (s, 3H, NC*Me*), 1.54 (s, 3H, NC*Me*), 1.50 (d, *J* = 6.1, 3H, CH*Me*), 1.48 (d, *J* = 6.1, 3H, CH*Me*), 1.25 (d, *J* = 6.8, 6H, CH*Me*), 1.19 (d, *J* = 6.9, 6H, CH*Me*), 1.11 (d, *J* = 6.8, 6H, CH*Me*), 0.75 (d, *J* = 6.0, 3H, OCH(*Me*)Et, 0.46 (t, *J* = 7.4, OCH(Me)CH_2*Me*). ^{13}C{^{1}H} NMR (500 MHz, C_6D_6, 303 K): δ 164.6 (N*C*Me), 144.9 (*ipso-C*), 142.6 (*o-C*), 141.1 (*o-C*), 126.2 (*p-C*), 124.3 (*m-C*), 123.8 (*m-C*), 96.3 (γ-*C*H), 70.7 (O*C*H(Me)Et), 34.9 (OCH(Me)*C*H_2Me), 28.2 (NC*Me*), 28.1 (NC*Me*), 26.6 (*C*HMe), 26.0 (*C*HMe), 24.6 (CH*Me*), 24.4 (CH*Me*), 24.3 (CH*Me*), 24.2 (CH*Me*), 23.1 (OCH(*Me*)Et), 10.3 (OCH(Me)CH_2*Me*). ^{119}Sn NMR (400 MHz, C_6D_6, 303 K): δ -181.5. UV–vis (benzene): λ_{max} (ε, L mol^{-1} cm^{-1}) 366 nm (12000). IR (Nujol, ν/cm^{-1}): 1554

(s), 1518 (s), 1260 (s), 1098, 1018 (s), 795 (s). Anal. Calcd for $C_{33}H_{50}N_2OSn$: C, 65.03; H, 8.27; N, 4.60. Found: C, 64.96; H, 8.23; N, 4.57.

[CH{(CH$_3$)CN-2,6-^{i}Pr$_2$C$_6$H$_3$}$_2$SnO^{t}Bu] (**11c**). Yellow crystals of (BDI)SnO^{t}Bu **11c** can be obtained in a way similar to that for **11a** in high yield (76%). ^{1}H NMR (400 MHz, C_6D_6, 303 K): δ 7.18 (d, *J* = 7.6, 2H, Ar-*H*), 7.14–7.06 (m, 2H, Ar-*H*), 7.03 (d, *J* = 7.6, 2H, Ar-*H*), 4.61 (s, 1H, γ-C*H*), 3.89 (m, 2H, C*H*Me$_2$), 3.21 (m, 2H, C*H*Me$_2$), 1.54 (s, 6H, NC*Me*), 1.53 (d, *J* = 6.9, 6H, CH*Me*), 1.28 (d, *J* = 6.8, 6H, CH*Me*), 1.17 (d, *J* = 6.9, 6H, CH*Me*), 1.12 (d, *J* = 6.8, 6H, CH*Me*), 0.86 (s, 9H, OC(*Me*)$_3$). ^{13}C{^{1}H} NMR (400 MHz, C_6D_6, 303 K): δ 169.4 (N*C*Me), 165.0 (N*C*Me), 144.9 (*ipso-C*), 142.6 (*o-C*), 140.9 (*o-C*), 126.1 (*p-C*), 123.9 (*m-C*), 123.8 (*m-C*), 95.5 (γ-*C*H), 69.4 (O*C*(Me)$_3$), 34.9 (OC(*Me*)$_3$), 28.2 (NC*Me*), 28.2 (NC*Me*), 26.1 (*C*HMe), 24.4 (CH*Me*), 24.3 (CH*Me*), 24.2 (CH*Me*), 23.0 (CH*Me*). ^{119}Sn NMR (400 MHz, C_6D_6, 303 K): δ -149.1. UV–vis (benzene): λ_{max} (ε, L mol^{-1} cm^{-1}) 365 nm (13000). IR (Nujol, ν/cm^{-1}): 1555 (s), 1261 (s), 1093, 1018 (s), 939 (s), 796 (s). Anal. Calcd for $C_{33}H_{50}N_2OSn$: C, 65.03; H, 8.27; N, 4.60. Found: C, 64.97; H, 8.32; N, 4.55.

[CH{(CH$_3$)CN-2,6-^{i}Pr$_2$C$_6$H$_3$}$_2$SnOC(CF$_3$)$_3$] (**11d**). A solution of NaO^{t}Bu^F (0.14 g, 0.55 mmol) in THF (5 mL) was added to a solution of (BDI)SnCl **10** (0.31 g, 0.55 mmol) in THF (5 mL) at room temperature, and the reaction mixture was stirred for 3 d. The solvent was removed under vacuum, the yellow crude product was extracted with toluene and the solution was filtered through Celite. The volatiles were removed and the yellow/green solid was washed with pentane. Recrystallisation from THF overnight afforded green crystals of LSnO^{t}Bu^F **11d** (0.29 g, 69%). ^{1}H NMR (400 MHz, C_6D_6, 303 K): δ 7.16 (d, *J* = 7.6, 2H, Ar-*H*), 7.09 (d,

J = 7.7, 2H, Ar-*H*), 7.03 (d, *J* = 7.7, 2H, Ar-*H*), 4.55 (s, 1H, γ-C*H*), 3.80 – 3.34 (m, 2H, C*H*Me$_2$), 3.16 – 2.76 (m, 2H, C*H*Me$_2$), 1.45 (d, *J* = 5.7, 6H, CH*Me*), 1.44 (s, 6H, NC*Me*), 1.23 (d, *J* = 6.8, 6H, CH*Me*), 1.10 (d, *J* = 6.7, 6H, CH*Me*), 1.09 (d, *J* = 6.5, 6H, CH*Me*).^{13}C{^{1}H} NMR (500 MHz, C_6D_6, 303 K): δ 166.0 (N*C*Me), 143.8 (*ipso-C*), 142.2 (*o-C*), 139.7 (*o-C*), 127.5 (*p-C*), 126.8 (*m-C*), 124.3 (*m-C*), 96.4 (γ-*C*H), 67.4 (O*C*(CF$_3$)$_3$), 28.6 (OC(*C*F$_3$)$_3$), 28.3 (NC*Me*), 25.4 (*C*HMe), 24.6 (CH*Me*), 24.3 (CH*Me*), 23.0 (CH*Me*), 23.0 (CH*Me*). ^{19}F NMR (400 MHz, C_6D_6, 303 K): δ -73.0. ^{119}Sn NMR (400 MHz, C_6D_6, 303 K): δ -256.3. UV–vis (benzene): λ_{max} (ε, L mol^{-1} cm^{-1}) 320 nm (22000). IR (Nujol, ν/cm^{-1}): 2024, 1945, 1548, 1518, 1319, 1262 (s), 1233 (s), 1167 (s), 1017, 966 (s), 795. Anal. Calcd for $C_{33}H_{41}F_9N_2OSn$: C, 51.38; H, 5.36; N, 3.63. Found: C, 51.41 ; H, 5.30; N, 3.64.

[CH{(CH$_3$)CN-2,6-^{i}Pr$_2$C$_6$H$_3$}$_2$SnO(CO)C$_2$H$_2$CO$_2$^{i}Pr] (**13**). A solid mixture of (BDI)SnO^{i}Pr **11a** (250 mg, 0.41 mmol) and maleic anhydride (40 mg, 0.41 mmol) was dissolved in toluene (10 mL) and stirred for 2 h, affording a orange solution. After evaporation of the solvent, the residue was dissolved in the minimum amount of hexane. Storage at -32°C for 3 days afforded deep red crystals of (BDI)Sn(Ma) **13** (248 mg, 87%). ^{1}H NMR (400 MHz, C_6D_6, 303 K): δ 7.21 – 6.93 (m, 6H, Ar-*H*), 5.96 (d, *J* = 11.9 Hz, 1H, COC*H*CHCO$_2$), 5.83 (d, *J* = 12.0 Hz, 1H, COCHC*H*CO$_2$), 5.09 (sept, 6.0 Hz, 1H, CO$_2$C*H*Me$_2$), 4.91 (s, 1H, γ-C*H*), 3.62 (sept, *J* = 6.7 Hz, 2H, C*H*Me$_2$), 3.04 (sept, *J* = 6.7 Hz, 2H, C*H*Me$_2$), 1.59 (s, 6H, NC*Me*), 1.37 (d, *J* = 6.6 Hz, 6H, CH*Me$_2$*), 1.27 (d, *J* = 6.7 Hz, 6H, CH*Me$_2$*), 1.12 (d, *J* = 6.8 Hz, 6H, CH*Me$_2$*), 1.07 (d, *J* = 6.2 Hz, 6H, CH*Me$_2$*), 1.04 (d, *J* = 6.8 Hz, 6H, CH*Me$_2$*). ^{13}C{^{1}H} NMR (400 MHz, C_6D_6, 303 K): δ 170.0 (SnO*C*O), 169.3 (*C*O$_2$^{i}Pr), 165.40 (N*C*Me), 145.31 (*ipso-C*), 142.43 (*o-C*), 141.27 (*o-C*), 131.0 (C*H*=CH), 130.0 (CH=C*H*), 127.1 (*p-C*), 124.8

(*m-C*), 123.7 (*m-C*), 99.8 (γ-*C*H), 67.5 (CO_2*C*HMe_2), 28.7 (NC*Me*), 27.7 (NC*Me*), 26.4 (*C*HMe), 24.6 (*C*HMe), 24.1 (CH*Me*), 23.60 (CH*Me*), 21.4 (CH*Me*). ^{119}Sn NMR (400 MHz, C_6D_6, 303 K): δ -374.2. IR (Nujol, ν/cm^{-1}): 1735 (s), 1600, 1552, 1524, 1261 (s), 1211, 1172, 1102 (s), 1019 (s), 797(s). Anal. Calcd for $C_{36}H_{50}N_2O_4Sn$: C, 62.35; H, 7.27; N, 4.04. Found: C, 62.39; H, 7.15; N, 3.94.

[CH{(CH$_3$)CN-2,6-^{i}Pr$_2$C$_6$H$_3$}$_2$SnO(CO$_2$)^{i}Pr] (**14a**). (BDI)SnO^{i}Pr **11a** (8.5 mg, 0.014 mmol) was dissolved in C_6D_6 (400μL) in an NMR tube sealed with a Young's tap. The NMR tube was submerged in a dry ice/ethanol bath, the gas inside the NMR tube was evacuated and CO_2 was introduced at a pressure of 1 atm. A pale yellow solution mixture was observed, and the reaction mixture was kept at room temperature for 48 h and was monitored by ^{1}H NMR spectroscopy. ^{1}H NMR (400 MHz, C_6D_6, 303 K): δ 7.27–6.95 (m, 6H, Ar-*H*), 4.95 (s, 1H, γ-C*H*), 4.89 (sept, *J* = 6.2, 1H, CO_2C*H*Me_2), 3.71 (sept, *J* = 6.7, 2H, C*H*Me_2), 3.07 (sept, 2H, *J* = 6.9, C*H*Me_2), 1.59 (s, 6H, NC*Me*), 1.44 (d, *J* = 6.7, 6H, CH*Me*), 1.22 (d, *J* = 6.8, 6H, CH*Me*), 1.18 (d, *J* = 6.3, 6H, CH*Me*), 1.16 (d, *J* = 7.0, 6H, CH*Me*), 1.06 (d, *J* = 6.8, 6H, CO_2CH*Me*). ^{13}C{^{1}H} NMR (400 MHz, C_6D_6, 303 K): δ 165.2 (N*C*Me), 158.7 (O*C*O_2), 145.4 (*ipso-C*), 142.5 (*o-C*), 141.3 (*o-C*), 127.1 (*p-C*), 124.7 (*m-C*), 123.6 (*m-C*), 99.7 (γ-*C*H), 68.5 (OCO_2*C*HMe_2), 28.7 (OCO_2CH*Me*$_2$), 27.7 (NC*Me*), 26.0 (NC*Me*), 24.5 (*C*HMe), 24.1 (CH*Me*), 23.9 (CH*Me*), 23.5 (CH*Me*), 22.0 (CH*Me*). ^{119}Sn NMR (400 MHz, C_6D_6, 303 K): δ -379.7. UV–vis (benzene): λ_{max} 321 nm. IR (CCl_4, ν/cm^{-1}): 2963 (s), 2927, 2871, 2339 (s), 1718 (w), 1550 (s), 1463, 1437, 1385, 1318, 1254, 1216, 1002.

[CH{(CH$_3$)CN-2,6-^{i}Pr$_2$C$_6$H$_3$}$_2$SnO(CO$_2$)^{s}Bu] (**14b**). LSnO^{s}Bu **11b** (9.5 mg, 0.016 mmol) was dissolved in C_6D_6 (400μL) in an NMR tube sealed with a Young's tap.

The NMR tube was submerged in a dry ice/ethanol bath, the gas inside the NMR tube was evacuated and CO_2 was introduced at a pressure of 1 atm. A pale yellow solution mixture was observed, and the reaction mixture was kept at room temperature for 48 h and was monitored by ^{1}H NMR spectroscopy. ^{1}H NMR (400 MHz, C_6D_6, 303 K): δ 7.27–7.01 (m, 6H, Ar*H*), 4.93 (s, 1H, γ-C*H*), 4.72 (m, 1H, CO_2C*H*(Me)Et), 3.72 (sept, *J* = 6.8, 2H, C*H*Me$_2$), 3.06 (m, 2H, C*H*Me$_2$), 1.59 (s, 3H, NC*Me*), 1.58 (s, 3H, NC*Me*), 1.47 (d, *J* = 6.7, 3H, CH*Me*), 1.45 (d, *J* = 6.7, 3H, CH*Me*), 1.27–1.20 (m, 11H, CO_2CH(Me)C*H*$_2$Me + CO_2CH(*Me*)CH$_2$Me+ CH*Me*), 1.16(d, *J* = 6.9 6H, CH*Me*), 1.06 (d, *J* = 6.8, 6H, CH*Me*), 0.85 (t, *J* = 7.5, 3H, CO_2CH(Me)CH$_2$*Me*). ^{13}C{^{1}H} NMR (400 MHz, C_6D_6, 303 K): δ 167.0 (N*C*Me), 165.2 (N*C*Me), 158.8 (O*C*O$_2$), 145.4 (*ipso-C*), 142.5 (*o-C*), 141.2 (*o-C*), 127.0 (*p-C*), 124.7 (*m-C*), 123.6 (*m-C*), 99.8 (γ-*C*H), 73.3 (OCO$_2$*C*(Me)Et), 29.0 (OCH(Me)*C*H$_2$Me), 28.7 (NC*Me*), 27.6 (NC*Me*), 26.1 (*C*HMe), 24.5 (*C*HMe), 24.0 (CH*Me*), 23.8 (CH*Me*), 23.4 (CH*Me*), 22.9 (CH*Me*), 19.4 (OCH(*Me*)Et), 9.6 (OCH(Me)CH$_2$*Me*). ^{119}Sn NMR (400 MHz, C_6D_6, 303 K): δ -379.1. UV–vis (benzene): λ_{max} 321 nm. IR (CCl_4, ν/cm^{-1}): 2965 (s), 2928, 2869, 2336 (s), 1720 (w), 1551 (s), 1463, 1437, 1385, 1319, 1254, 1216, 1006, 979.

[CH{(CH$_3$)CN-2,6-^{i}Pr$_2$C$_6$H$_3$}$_2$SnO(CO$_2$)^{t}Bu] (**14c**). LSnO^{t}Bu **11c** (10.1 mg, 0.017 mmol) was dissolved in C_6D_6 (400μL) in an NMR tube sealed with a Young's tap. The NMR tube was submerged in a dry ice/ethanol bath, the gas inside the NMR tube was evacuated and CO_2 was introduced at a pressure of 1 atm. A pale yellow solution mixture was observed, and the reaction mixture was kept at room temperature for 48 h and was monitored by ^{1}H NMR spectroscopy. ^{1}H NMR (400 MHz, C_6D_6, 303 K): δ 7.23–7.06 (m, 6H, Ar-*H*), 4.89 (s, 1H, γ-C*H*), 3.68 (sept, *J* = 6.8, 2H, C*H*Me$_2$), 3.05 (sept, 2H, *J* = 6.8, C*H*Me$_2$), 1.44 (d, *J* = 6.7, 6H, CH*Me*), 1.42 (s, 6H,

NC*Me*), 1.18 (d, *J* = 6.8, 6H, CH*Me*), 1.13 (d, *J* = 6.8, 6H, CH*Me*), 1.02 (d, *J* = 7.0, 6H, CH*Me*), 0.87 (s, 9H, OC*Me*$_3$). $^{13}C\{^1H\}$ NMR (400 MHz, C_6D_6, 303 K): δ 167.0 (N*C*Me), 165.3 (N*C*Me), 157.9 (O*C*O$_2$), 145.3 (*ipso-C*), 142.4 (*o-C*), 141.3 (*o-C*), 127.0 (*p-C*), 124.6 (*m-C*), 123.6 (*m-C*), 99.7 (γ-*C*H), 77.1 (O*C*(Me)$_3$), 34.8 (OC*Me*$_3$), 28.7 (NC*Me*), 28.0 (NC*Me*), 27.6 (*C*HMe), 26.3 (*C*HMe), 24.4 (CH*Me*), 24.1 (CH*Me*), 23.8 (CH*Me*), 23.4 (CH*Me*). ^{119}Sn NMR (400 MHz, C_6D_6, 303 K): δ -377.4. UV–vis (benzene): λ_{max} 325 nm. IR (CCl_4, ν/cm^{-1}): 2966, 2928, 2870, 2337 (s), 1717 (w), 1551 (s), 1463, 1438, 1386, 1318, 1254 (s), 1216, 1006.

[GeCl$_2$·(dioxane)].[33] $GeCl_4$ (20 mL, 87.7 mmol) and 1,4-dioxane (15 mL) were dissolved in a 1:1 hexane:Et_2O mixture (100 mL) in a sealable ampoule and treated with ^{n}BuSnH (25mL, 92.9 mmol) in 500 mL sealable ampoule. After stirring at room temperature for 30 minutes a white precipitate appeared. This was filtered off and washed with cold hexane and identified as the pure $GeCl_2$(diox) (2 g). The mother liquor was then transferred back into the ampoule and left at room temperature for 2 days, affording white crystals of $GeCl_2$(diox) (17.0 g) upon standing, for a total combined yield of 84%. *Note: repeated experiments on a smaller scale resulted in a considerably lowered yield (10-18%).*

[CH{(CH$_3$)CN-2,6-^{i}Pr$_2$C$_6$H$_3$}$_2$GeCl]. (BDI)H (2.00g, 4.8 mmol) was dissolved in diethyl ether (20 mL) and 2.05 M ^{n}BuLi was added dropwise (2.4 mL). The resulting yellow solution was left stirring for 30 minutes and added dropwise to a stirred $GeCl_2$(diox) (1.12 g, 4.8 mmol) solution in diethyl ether (20 mL). The reaction mixture was left stirring at room temperature overnight. The volatiles were then removed and the resulting dark red solid residue was treated with

toluene (25 mL) and the slurry was filtered through celite. The solvents were evacuated and the red residue was washed with cold pentane several times affording (BDI)GeCl as a pink powder in 81% yield (2.04 g). ^{1}H NMR analysis is in agreement with literature data.[145] ^{1}H NMR (500 MHz, C_6D_6) δ 7.08 (m, 6H), 5.03 (s, 1H), 3.92 (sept, 2H, *J* = 6.6), 3.09 (sept, 2H, *J* = 6.7), 1.59 (s, 6H), 1.42 (d, 6H, *J* = 6.5), 1.19 (d, 6H, *J* = 6.7), 1.16 (d, 6H, *J* = 6.9), 1.03 (d, 6H, *J* = 6.7).

[CH{(CH$_3$)CN-2,6-^{i}Pr$_2$C$_6$H$_3$}$_2$GeO^{i}Pr] (**15a**). A suspension of KO^{i}Pr (94 mg, 0.95 mmol) in THF (5 mL) was added to a solution of (BDI)GeCl (0.50 g, 0.95 mmol) in THF (5 mL) at room temperature, and the reaction mixture was stirred for 3 d. The solvent was removed under vacuum, the orange crude product was extracted with toluene and the solution was filtered through Celite. Removal of the volatiles and recrystallisation from hexane overnight at -27°C afforded orange crystals of (BDI)GeO^{i}Pr **15a** (0.38 g, 72%). ^{1}H NMR (400 MHz, C_6D_6, 303 K): δ 7.17 – 7.02 (m, 6H, Ar-*H*), 4.64 (s, 1H, γ-C*H*), 3.73 (m, 3H, C*H*Me$_2$+OC*H*Me$_2$), 3.34 (sept, *J* = 6.8, 2H, C*H*Me$_2$), 1.51 (s, 6H, NC*Me*), 1.49 (d, *J* = 6.8, 6H, CH*Me*), 1.17 (d, *J* = 6.9, 6H, CH*Me*), 1.10 (d, *J* = 6.8, 6H, CH*Me*), 0.57 (d, *J* = 6.1, 6H, OCH*Me*). ^{13}C{^{1}H} NMR (400 MHz, $CDCl_3$): δ 163.29 (N*C*Me), 145.04 (*ipso-C*), 139.20 (*o-C*), 126.45 (*p-C*), 124.66 (*m-C*), 123.97 (*m-C*), 94.99 (γ-*C*H), 64.93 (O*C*HMe$_2$), 28.40 (NC*Me*), 27.97 (NC*Me*), 26.31 (*C*HMe),24.45 (*C*HMe), 24.24 (*C*HMe), 22.70 (CH*Me*), 22.31 (CH*Me*), 20.37 (CH*Me*). IR (Nujol, ν/cm^{-1}): 1561, 1521, 1321, 1260, 1174, 1019, 964, 795. Anal. Calcd for $C_{32}H_{48}GeN_2O$: C, 69.96; H, 8.81; N, 5.10. Found: C, 69.84; H, 8.72; N, 4.92.

[CH{(CH$_3$)CN-2,6-^{i}Pr$_2$C$_6$H$_3$}$_2$GeO^{s}Bu] (**15b**). Orange crystals suitable for X-ray crystallography of (BDI)GeO^{s}Bu **15b** can be obtained in a similar way to **15a** in

81% yield. ^{1}H NMR (400 MHz, C_6D_6, 303 K): δ 7.20 – 7.02 (m, 6H, Ar-*H*), 4.66 (s, 1H, γ-C*H*), 3.84 – 3.68 (m, 2H, C*H*Me$_2$), 3.55 – 3.43 (m, 1H, OC*H*(Me)Et), 3.37 (sept, 6.7, 2H, C*H*Me$_2$), 1.51 (s, 3H, NC*Me*), 1.50 (s, 3H, NC*Me*), 1.48 (d, *J* = 7.4, 6H, CH*Me*), 1.34 (d, *J* = 6.3, 6H, CH*Me*), 1.33 (d, *J* = 6.4, 6H, CH*Me*), 1.19 (d, *J* = 6.9, 7H), 1.08 – 0.94 (m, 2H, OC(Me)C*H$_2$*Me), 0.45 (d, *J* = 6.2, 3H, OCH(*Me*)Et), 0.26 (t, *J* = 7.4, 3H, OCH(Me)CH$_2$*Me*). ^{13}C{^{1}H } NMR (400 MHz, C_6D_6): δ 163.24 (N*C*Me), 144.17 (*ipso-C*), 137.03 (*o-C*), 126.59 (*p-C*), 124.13 (*m-C*), 124.02 (*m-C*), 95.20 (γ-*C*H), 70.68 (O*C*(Me)Et), 33.37 (OCH(Me)*C*H$_2$Me), 28.37 (NC*Me*), 28.25 (NC*Me*), 26.24 (*C*HMe), 24.41 (*C*HMe), 23.02 (CH*Me*), 22.34 (CH*Me*), 21.77 (CH*Me*), 20.38 (OCH(*Me*)Et), 10.02 (OCH(Me)CH$_2$*Me*). IR (Nujol, ν/cm^{-1}): 1557, 1522, 1320, 1175, 1018, 918, 795. Anal. Calcd for $C_{33}H_{50}GeN_2O$: C, 70.35; H, 8.95; N, 4.97. Found: C, 70.46; H, 9.01; N 4.87.

[CH{(CH$_3$)CN-2,6-^{i}Pr$_2$C$_6$H$_3$}$_2$GeO^{t}Bu] (**15c**). Orange crystals suitable for X-ray crystallography of (BDI)GeO^{t}Bu **15c** can be obtained in a similar way to **15a** in 76% yield. ^{1}H NMR (400 MHz, C_6D_6, 303 K): δ 7.25 – 6.96 (m, 6H, Ar-*H*), 4.61 (s, 1H, γ-C*H*), 3.82 (sept, *J* = 6.9 Hz, 2H, C*H*Me$_2$), 3.34 (sept, *J* = 6.8 Hz, 2H, C*H*Me$_2$), 1.51 (s, 6H, NC*Me*), 1.50 (d, *J* = 7.2 Hz, 6H, CH*Me*), 1.33 (d, *J* = 6.8 Hz, 6H, CH*Me*), 1.16 (d, *J* = 6.9 Hz, 6H, CH*Me*), 1.10 (d, *J* = 6.8 Hz, 6H, CH*Me*), 0.78 (s, 9H, OC*Me$_3$*). ^{13}C{^{1}H } NMR (400 MHz, $CDCl_3$): δ 163.61 (N*C*Me), 145.16 (*ipso-C*), 139.66 (*o-C*), 126.45 (*p-C*), 124.66 (*m-C*), 123.71 (*m-C*), 96.03 (γ-*C*H), 70.00 (O*C*Me$_3$), 33.21 (OC*Me$_3$*), 28.47 (NC*Me*), 27.08 (NC*Me*), 26.46 (*C*HMe$_2$), 25.82 (*C*HMe$_2$), 24.86 (CH*Me*), 22.44 (CH*Me*). IR (Nujol, ν/cm^{-1}): 1553, 1520, 1322, 1260, 1175, 1100, 1020, 935, 795. Anal. Calcd for $C_{33}H_{50}GeN_2O$: C, 70.35; H, 8.95; N, 4.97. Found: C, 70.49; H, 9.05; N, 4.90.

[CH{(CH$_3$)CN-2,6-^{i}Pr$_2$C$_6$H$_3$}$_2$Ge(Me)O^{t}Bu]I (**17**). MeI (7.8 μL, 0.12 mmol) was added to a toluene stirred solution of (BDI)GeO^{t}Bu **15c** (70 mg, 0.12 mmol). After 1 h a pale precipitate was formed and the solution turned pale yellow. The volatiles were removed and the solid washed with cold pentane affording a pale yellow powder of [(BDI)Ge(Me)O^{t}Bu]I **17** in 90% yield (78 mg). Colourless crystals suitable for X-ray crystallography can be obtained by performing the reaction without stirring and leaving the reaction mixture overnight at room temperature. ^{1}H NMR (500 MHz, CD_2Cl_2): δ 7.51 (t, *J* = 7.8, 2H, Ar-*H*), 7.38 (d, *J* = 7.8, 4H, Ar-*H*), 6.10 (s, 1H, γ-C*H*), 3.14 (sept, *J* = 6.8, 2H, C*H*Me$_2$), 2.92 (sept, *J* = 6.8, 2H, C*H*Me$_2$), 2.18 (s, 6H, NC*Me*), 1.58 (s, 3H, Ge*Me*), 1.43 (d, *J* = 6.8, 6H, CH*Me$_2$*), 1.36 (d, *J* = 6.7, 6H, CH*Me$_2$*), 1.34 (d, *J* = 6.6, 6H, CH*Me$_2$*), 1.14 (d, *J* = 6.8, 6H, CH*Me$_2$*), 0.74 (s, 9H, OC*Me*). ^{13}C{^{1}H } NMR (400 MHz, CD_2Cl_2): δ 173.60 (N*C*Me), 145.31 (*ipso-C*), 130.28 (*o-C*), 125.67 (*p-C*), 125.39 (*m-C)*, 100.75 (γ-*C*H), 75.58 (O*C*Me$_3$), 31.39 (OC*Me$_3$*), 29.14 (NC*Me*), 28.01 (NC*Me*), 25.29 (*C*HMe$_2$), 24.99 (*C*HMe$_2$), 24.51 (CH*Me*), 23.61 (CH*Me*), 6.0 (Ge*Me*). IR (Nujol, ν/cm^{-1}): 3059, 1624, 1553, 1363, 1253, 1176, 1101, 935, 799, 785, 758. Anal. Calcd for $C_{34}H_{53}GeIN_2O$: C, 57.90; H, 7.57; N, 3.97. Found: C, 57.84; H, 7.55; N, 3.91.

[CH{(CH$_3$)CN-2,6-^{i}Pr$_2$C$_6$H$_3$}$_2$Ge(Me)O^{s}Bu]OTf (**18b**). (BDI)GeO^{s}Bu **15b** (230 mg, 0.41 mmol) was dissolved in pentane (5 mL) and treated with methyl triflate (45 μL, 0.41 mmol). The reaction mixture was stirred for 1 hour, after which a pale yellow precipitate was formed. The solution was decanted and the residue washed with pentane. Storage of a saturated THF solution at -27°C for 2 weeks yielded colourless crystals of [(BDI)Ge(Me)O^{t}Bu]OTf **18b** (229 mg, 77 %), suitable for X-

ray crystallography. ^{1}H NMR (399 MHz, $CDCl_3$): δ 7.29 (m, 6H, Ar-*H*), 5.99 (s, 1H, γ-C*H*), 3.28 (m, 1H, OC*H*(Me)Et), 3.12 (m, 2H, C*H*Me$_2$), 3.03 (m, 2H, C*H*Me$_2$), 2.13 (s, 3H, NC*Me*), 2.11 (s, 3H, NC*Me*), 1.44 (s, 3H, Ge*Me*), 1.29 (d, 6H, J = 5.8, CH*Me*), 1.27 (m, 2H, OC(Me)C*H*$_2$Me), 1.14 (d, 6H, J = 6.9, CH*Me*), 1.06 (d, 6H, J = 6.8, CH*Me*), 0.81 (d, 6H, J = 6.8, CH*Me*), 0.32 (d, 3H, J = 6.0, OCH(*Me*)Et), 0.15 (t, 3H, J = 7.5, OCH(Me)CH$_2$*Me*). ^{13}C{^{1}H } NMR (399 MHz, $CDCl_3$): 172.7 (N*C*Me), 145.2 (*ipso-C*), 130.0 (*o-C*), 125.1 (*p-C*), 123.4 (*m-C*), 102.1 (γ-*C*H), 74.8 (O*C*H(Me)Et), 28.7 (NC*Me*), 27.4 (*C*HMe), 24.8 (CH*Me*), 24.4 (OCH(Me)*C*H$_2$Me), 23.8 (CH*Me*), 22.4 (OCH(*Me*)Et), 9.18 (O(Me)CH$_2$*Me*), 0.0 (Ge*Me*). ^{19}F NMR (400 MHz, $CDCl_3$) δ -78.31. IR (Nujol, ν/cm^{-1}): 1549, 1378 (s), 1370 (s), 1323, 1269 (s), 1235, 1150, 1110, 1032 (s), 955, 810, 762, 637. Anal. Calcd for $C_{35}H_{35}F_3N_2O_4GeS$: C, 57.78; H, 7.34; N, 3.85. Found: C, 57.83; H, 7.40; N, 3.76.

[CH{(CH$_3$)CN-2,6-^{i}Pr$_2$C$_6$H$_3$}$_2$Ge(Me)O^{t}Bu]OTf (**18c**). [(BDI)Ge(Me)O^{s}Bu]OTf **18c** can be obtained as a pale yellow powder in a way similar to **18b** in 72% yield. ^{1}H NMR (399 MHz, $CDCl_3$): δ 7.36 (m, 6H, Ar-*H*), 6.04 (s, 1H, γ-C*H*), 3.16 (sept, 2H, J = 6.7, C*H*Me$_2$), 3.06 (sept, 2H, J = 6.6, C*H*Me$_2$), 2.15 (s, 6H, NC*Me*), 1.62 (s, 3H, Ge*Me*), 1.40 (d, 6H, J = 6.8, CH*Me*), 1.32 (d, 6H, J = 6.7, CH*Me*), 1.31 (d, 6H, J = 6.5, CH*Me*), 1.11 (d, 6H, J = 6.9, CH*Me*), 0.71 (s, 9H, OC*Me$_3$*). ^{13}C{^{1}H } NMR (399 MHz, $CDCl_3$): δ 173.6 (N*C*Me), 146.0 (*ipso-C*), 130.0 (*o-C*), 125.6(*p-C*), 124.9(*m-C*), 120.9 (SO$_3$*C*F$_3$), 101.7 (γ-*C*H), 88.5 (O*C*Me$_3$), 31.56 (OC*Me$_3$*), 29.07 (NC*Me*), 27.7 (*C*HMe$_2$), 25.5 (*C*HMe$_2$), 25.1 (CH*Me*), 24.7 (CH*Me*), 24.0 (CH*Me*), 23.8 (CH*Me*), 6.1 (Ge*Me*). ^{19}F NMR (400 MHz, $CDCl_3$) δ -78.19. IR (Nujol, ν/cm^{-1}): 1544, 1377 (s), 1366 (s), 1318, 1266 (s), 1223, 1149, 1106, 1030 (s), 947, 894 (w), 808, 752, 637. Anal.

Calcd for $C_{35}H_{35}F_3N_2O_4GeS$: C, 57.78; H, 7.34; N, 3.85. Found: C, 57.99; H, 7.48; N, 3.73.

[CH{(CH$_3$)CN-2,6-^{i}Pr$_2$C$_6$H$_3$}$_2$Ge(I)O^{t}Bu]I$_3$ (**19**). Iodine (46 mg, 0.24 mmol) was added to a toluene stirred solution of (BDI)GeO^{t}Bu **15c** (52 mg, 0.09 mmol). The reaction mixture was stirred overnight producing a pale precipitate. The solution was decanted and the precipitate was washed several times with pentane, affording [(BDI)Ge(I)O^{t}Bu]I$_3$ **19** a dark orange powder in 92% yield (89 mg). Dark red crystals were obtained by storing a THF/C_6H_5F solution of **19** at -27°C for one week. ^{1}H NMR (400 MHz, $CDCl_3$): δ 7.50 (t, *J* = 7.8, 2H, Ar-*H*), 7.40 (d, *J* = 7.8, 2H, Ar-*H*), 7.34 (d, *J* = 7.8, 2H, ^{m}Ar-*H*), 6.47 (s, 1H, γ-C*H*), 3.24 (sept, *J* = 6.6, 2H, C*H*Me$_2$), 3.11 (sept, *J* = 6.7, 2H, C*H*Me$_2$), 2.33 (s, 6H, NC*Me*), 1.43 (d, *J* = 6.8, 6H, CH*Me$_2$*), 1.40 (d, *J* = 7.5, 6H, CH*Me$_2$*), 1.38 (d, *J* = 7.1, 6H, CH*Me$_2$*), 1.11 (d, *J* = 6.8, 6H, CH*Me$_2$*), 0.90 (s, 9H, OC*Me$_3$*). ^{13}C{^{1}H } NMR (400 MHz, $CDCl_3$): δ 174.75 (N*C*Me), 146.68 (*ipso*-*C*), 130.80 (*o*-*C*), 126.53 (*p*-*C*), 125.04 (*m*-*C*), 102.83 (γ-*C*H), 82.80 (O*C*Me$_3$), 31.57 (OC*Me$_3$*), 29.57 (NC*Me*), 28.94 (NC*Me*), 28.00 (*C*HMe$_2$), 25.54 (*C*HMe$_2$), 25.01 (CH*Me*), 23.56 (CH*Me*). IR (Nujol, ν/cm^{-1}): 1541, 1519, 1317, 1251, 1158, 1024, 933, 810. Anal. Calcd for : C, 37.01 ; H, 4.71; N, 2.62. Found: C, 36.86; H, 4.62; N, 2.49.

[CH{(CH$_3$)CN-2,6-^{i}Pr$_2$C$_6$H$_3$}$_2$Sn(I)$_2$O^{t}Bu] (**20**). (BDI)SnO^{t}Bu **11c** (330 mg, 0.54 mmol) was dissolved in pentane and treated with a 0.5 M solution of iodine in toluene (1.07 mL). The resulting orange mixture was stirred at room temperature for 30 min, after which a pale yellow precipitate appeared. The overstanding solution was decanted and the residue washed with cold pentane and dried under

vacuum. Dissolution in the minimum amount of THF and storage at -27 ˚C for 3 days afforded orange crystals suitable for X-ray crystallography of (BDI)SnI_2O^tBu **20** in 79% yield (352 mg). ^{1}H NMR (400 MHz, d_8-thf, 303 K) δ 7.25 – 7.12 (m, 6H, Ar*H*), 5.54 (s, 1H, γ-C*H*), 3.42 (m, 2H, C*H*Me_2), 3.15 (m, 2H, C*H*Me_2), 1.92 (s, 6H), 1.42 (d, 12H, *J* = 6.4, CH*Me*), 1.26 (d, 6H, *J* = 6.4, CH*Me*), 1.13 (d, 6H, *J* = 5.9, CH*Me*), 0.97 (s, 9H, OC*Me*$_3$). ^{13}C{^{1}H} NMR (400 MHz, C_6D_6, 303 K): 171.9 (N*C*Me), 145.7, 143.6, 142.8, 127.3, 124.6, 123.4 (^{Ar}*C*), 97.9 (γ-*C*H), 76.1, O*C*Me_3, 31.9 (OC*Me*$_3$), 29.5, 28.3, 27.4, 26.7 (*C*HMe_2), 24.7, 24.5, 24.0, 22.7 (CH*Me*). ^{119}Sn NMR (400 MHz, C_6D_6, 303 K): δ -1095. IR (Nujol, ν/cm^{-1}): 1523 (s), 1312, 1250, 1170, 1098, 1019, 931 (s), 843, 794 (s), 758. Anal. Calcd for $C_{33}H_{50}I_2N_2OSn$: C, 45.91; H, 5.84; N, 3.24. Found: C, 46.00; H, 5.75; N, 3.20.

{μ-$(CuI)_2$}[CH{(CH_3)CN-2,6-^{i}Pr$_2C_6H_3$}$_2$GeO^{t}Bu]$_2$ (**21**). THF (5 mL) was added to a stirring solid mixture of CuI (18 mg, 0.09 mmol) and (BDI)GeO^{t}Bu **15c** (52 mg, 0.09 mmol). After stirring for 3 days, volatiles were evacuated and the resulting precipitated was extracted with toluene and filtered through celite. Removal of the volatiles and washing with cold pentane afforded (BDI)Ge(O^{t}Bu)CuI **20** as a bright yellow powder in 61% yield (43 mg). Storage at -27°C for one month of a concentrated toluene solution of **20** afforded pale yellow crystals suitable for X-ray crystallography. ^{1}H NMR (400 MHz, d_8-THF): δ 7.11 (m, 12H, Ar-*H*), 4.91 (s, 2H, γ-C*H*), 3.46 (br, 8H, C*H*Me_2), 1.66 (s, 12H, NC*Me*), 1.34 (d, *J* = 5.9,12H, CH*Me*$_2$), 1.29 (d, *J* = 6.8, 12H, CH*Me*$_2$), 1.17 (d, *J* = 6.7, 12H, CH*Me*$_2$), 1.03 (d, *J* = 6.8, 12H, CH*Me*$_2$), 0.57 (s, 18H, OC*Me*$_3$). ^{13}C{^{1}H} NMR (400 MHz, d_8-THF): δ 165.74 (N*C*Me), 145.11 (*ipso-C*), 135.59 (*o-C*), 123.58 (*p-C*), 122.72 (*m-C*), 99.03 (γ-*C*H), 67.93 (O*C*Me_3), 32.87 (OC*Me*$_3$), 28.61 (NC*Me*), 28.20 (NC*Me*), 24.81 (*C*HMe_2), 23.85 (*C*HMe_2), 22.45

(CH*Me*), 22.21 (CH*Me*). IR (Nujol, ν/cm^{-1}): 2321, 1523, 1261, 1097, 1020, 936, 802. Repeated attempts of obtaining elemental analysis for compound **20** were unsuccessful.

[CH{(CH$_3$)CN-2,6-^{i}Pr$_2$C$_6$H$_3$}$_2$]$_2$Hg (**22**). Lithium diisopropylamide (1.20 mmol, 2M in THF) was added dropwise to a toluene solution of BDI-H (500 mg, 1.20 mmol). The red solution was stirred for 30 min, cooled to –78 °C and added dropwise to a stirring suspension of $HgCl_2$ (163 mg, 0.60 mmol) in toluene at –78 °C. This mixture was stirred overnight, slowly warming up to room temperature. The resulting gray suspension was filtered through celite and the volatiles were evacuated producing a pale green precipitate that was washed several times with pentane affording (BDI)$_2$Hg **22** as a white powder in 34% yield (0.24 mol, 213 mg). Colourless crystals suitable for X-ray diffraction were grown from a concentrated DCM solution stored in an ethylene glycol bath at 8 °C for 3 days and –12 °C for a week. ^{1}H NMR (400 MHz, $CDCl_3$, 303 K): δ 6.93 – 7.17 (m, 6H, Ar-*H*), 4.75 (s, 1H, γ-C*H*), 3.98 (s, 1H, γ-C*H*), 3.71 (s, 1H, γ-C*H*), 3.33 (sept, *J* = 6.4 Hz, 4H, C*H*Me$_2$), 2.97 (sept, *J* = 6.8 Hz, 2H, C*H*Me$_2$), 2.91 (m, 2H, C*H*Me$_2$), 2.81 (sept, *J* = 6.9 Hz, 2H, C*H*Me$_2$), 2.49 (sept, *J* = 6.7 Hz, 2H, C*H*Me$_2$), 1.85 (s, 6H, NC*Me*), 1.72 (s, 6H, NC*Me*), 1.51 (s, 6H, NC*Me*), 1.18 (d, *J* = 6.8 Hz, 12H, CH*Me*), 1.14 (d, *J* = 6.9 Hz, 12H, CH*Me*), 1.11 (d, *J* = 6.8 Hz, 6H, CH*Me*), 1.10 (d, *J* = 6.8 Hz, 12H, CH*Me*), 1.06 (d, *J* = 6.8 Hz, 6H, CH*Me*), δ 0.98 (d, *J* = 6.8 Hz, 12H, CH*Me*), 0.89 (d, *J* = 6.7 Hz, 6H, CH*Me*), 0.85 (d, *J* = 6.9 Hz, 6H, CH*Me*). ^{13}C{^{1}H} NMR (100MHz, $CDCl_3$): δ 171.38 (N*C*Me), 169.97 (N*C*Me), 164.34 (N*C*Me), 146.46 (*o*-*C*), 141.48 (*o*-*C*), 137.03 (*ipso*-*C*), 136.46 (*ipso*-*C*), 123.50 (^{Ar}*C*), 123.21 (^{Ar}*C*), 122.99 (^{Ar}*C*), 122.89 (^{Ar}*C*), 122.76 (^{Ar}*C*), 122.63 (^{Ar}*C*), 121.92 (^{Ar}*C*), 96.23 (g-*C*), 77.72 (g-*C*), 66.69 (g-*C*), 28.51 (*C*HMe), 28.51 (*C*HMe),

28.21 (*C*HMe), 27.78(*C*HMe), 27.69 (CH*Me*), 25.32 (NC*Me*), 24.48 (CH*Me*), 23.75 (CH*Me*), 23.20 (CH*Me*), 22.97 (CH*Me*), 22.49 (CH*Me*), 21.91 (NC*Me*), 21.40 (NC*Me*). ^{199}Hg NMR (71.5 MHz, $CDCl_3$, 303 K) δ -989.7. IR (Nujol, cm^{-1}): 3050, 1921, 1866, 1806, 1720, 1648 (s), 1624 (s), 1589 (s), 1439 (s), 1358 (s),1328 (s), 1245, 1207 (s), 1188 (s), 1163 (s), 1107, 1068, 1059, 1042, 972, 936, 916, 789 (s), 760 (s), 690, 523. IR (CCl_4, cm^{-1}): 3061(w), 2963, 2869, 2990 (br), 2004 (br), 1856 (br), 1635, 1549 (br, s), 1461, 1436, 1409, 1382, 1363, 1322, 1253 (s), 1216 (s), 1165 (w). Anal. Calcd for: C, 67.25; H, 7.98; N, 5.41. Found: C, 67.16; H, 8.07; N, 5.39.

Key Chemical Shifts for 22: ^{1}H NMR (400 MHz, $CDCl_3$, 303 K): δ 3.98 (s, 1H, γ-C*H*), 2.97 (sept, *J* = 6.8 Hz, 2H, C*H*Me_2), 2.81 (sept, *J* = 6.9 Hz, 2H, C*H*Me_2), 1.85 (s, 6H, NC*Me*), 1.11 (d, *J* = 6.8 Hz, 6H, CH*Me*), 1.10 (d, *J* = 6.8 Hz, 12H, CH*Me*), 0.8 (d, *J* = 6.8 Hz, 6H, CH*Me*). ^{13}C{^{1}H } NMR (100 MHz, $CDCl_3$): δ 171.38 (N*C*Me), 146.46 (*o*-*C*), 136.46 (*ipso*-*C*), 77.72 (g -*C*), 28.51 (*C*HMe), 23.20 (CH*Me*), 22.97 (CH*Me*), 21.91 (NC*Me*).

Key Chemical Shifts for 23: *N,N*'-bound ligand: ^{1}H NMR (400 MHz, $CDCl_3$, 303 K): δ 4.75 (s, 1H, γ-C*H*), 3.33 (sept, *J* = 6.4 Hz, 4H, C*H*Me_2), 1.72 (s, 6H, NC*Me*), 1.18 (d, *J* = 6.8 Hz, 12H, CH*Me*), 1.14 (d, *J* = 6.9 Hz, 12H, CH*Me*). ^{13}C{^{1}H } NMR (100 MHz, $CDCl_3$): d 164.34 (N*C*Me), (*ipso*-*C*), 141.48 (*o*-*C*), 141.26 (*o*-*C*), 96.23 (g -*C*), 27.78(*C*HMe), 27.69 (CH*Me*), 25.32 (NC*Me*), 24.48 (CH*Me*). γ-bound ligand: ^{1}H NMR (400 MHz, $CDCl_3$, 303 K): δ 3.71 (s, 1H, γ-C*H*), 2.91 (m, 2H, C*H*Me_2), 2.49 (sept, *J* = 6.7 Hz, 2H, C*H*Me_2), 1.51 (s, 6H, NC*Me*), 0.98 (d, *J* = 6.8 Hz, 12H, CH*Me*), 0.89 (d, *J* = 6.7 Hz, 6H, CH*Me*), 0.85 (d, *J* = 6.9 Hz, 6H, CH*Me*),. ^{13}C{^{1}H } NMR (400 MHz, $CDCl_3$): δ 169.97 (N*C*Me), 137.03 (*ipso*-*C*), 66.69 (γ-*C*), 28.21 (*C*HMe), 28.51 (*C*HMe), 23.75 (CH*Me*), 23.20 (CH*Me*), 22.49 (CH*Me*), 21.40 (NC*Me*).

3.4 Kinetic and thermodynamic measurement procedures

(BDI)SnOR + CO_2 NMR monitored thermodynamic measurement. $1.64 \cdot 10^{-5}$ mol of (BDI)SnOR **11** and $2.68 \cdot 10^{-6}$ mol of ferrocene (as a standard solution in C_6D_6) for a total of 0.45 mL were charged in an NMR tube with a 50 cm^3 headspace sealed with a Young's tap. It was then submerged in a dry ice/ethanol bath, the gas inside the NMR tube was evacuated and CO_2 was introduced at a pressure of 1 atm. The reaction mixture was kept at 313.1 K in a thermostated bath for 72 h and the alkoxide/carbonate **11**/**14** ratio was monitored by comparing the γ-C*H* ^{1}H NMR signal to the internal standard ferrocene. In order to ensure accurate integration, a 10s delay between 30˚ pulses was utilised (number of scans = 4, acquisition time = 4).

(BDI)SnOR + MeOTf $t_{½}$ measurement. An NMR tube sealed with a Young's tap was charged with $1.7 \cdot 10^{-5}$ mol of (BDI)SnOR **11** (as a standard solution in C_6D_6), 1.1 μL of dichloromethane ($1.7 \cdot 10^{-5}$ mol) and 1.9 μL of MeOTf ($1.7 \cdot 10^{-5}$ mol) to give a total volume of 0.25 mL. The NMR tube was then placed in the thermostated probe (298.1 K) of a Varian 400 MHz spectrometer. The conversion was monitored by ^{1}H NMR spectroscopy. NMR spectra were taken in 5 minutes time intervals. In order to ensure accurate integration, a 10s delay between 30˚ pulses was utilised (number of scans = 4, acquisition time = 4). $t_{½}$ was determined by comparing the γ-C*H* signal integration of (BDI)SnOR and LSnOTf, using the DCM peak as standard.

(BDI)SnOR + CO_2 UV monitored kinetic experiment. A custom designed UV cell (Figure 29) was loaded with a 2mm magnetic stirrer bar and (BDI)SnOR **11** ($6.25 \cdot 10^{-8}$ mol from a benzene standard solution, 100 μL) and Young's tap ***A***, ***B*** and ***C*** were sealed. The sidearm was loaded with benzene to the 2.5 mL mark and ***D*** was sealed. The gas reservoir was then evacuated trough ***E*** on a high vacuum line ($3.0 \cdot 10^{-4}$ mbar) and refilled with carbon dioxide (1.05 atm). ***E*** was then sealed and ***D*** opened for 30 seconds at a 5 minutes interval for 5 times in order to let carbon dioxide to diffuse in benzene. The UV cell was placed in a Varian Cary 50 UV-vis spectrometer equipped with a peltier set at 40°C and a magnetic stirrer set at the maximum speed. ***D***, ***C*** and ***B*** were then opened adding 2.5mL of benzene into the UV cell (UV reading started in this moment, spectra were acquired at 15 min time interval). ***D*** and ***B*** were kept closed during the experiment, while ***C*** was opened for a minute every hour to allow a constant 1 atm pressure and reduce solvent evaporation at the same time.

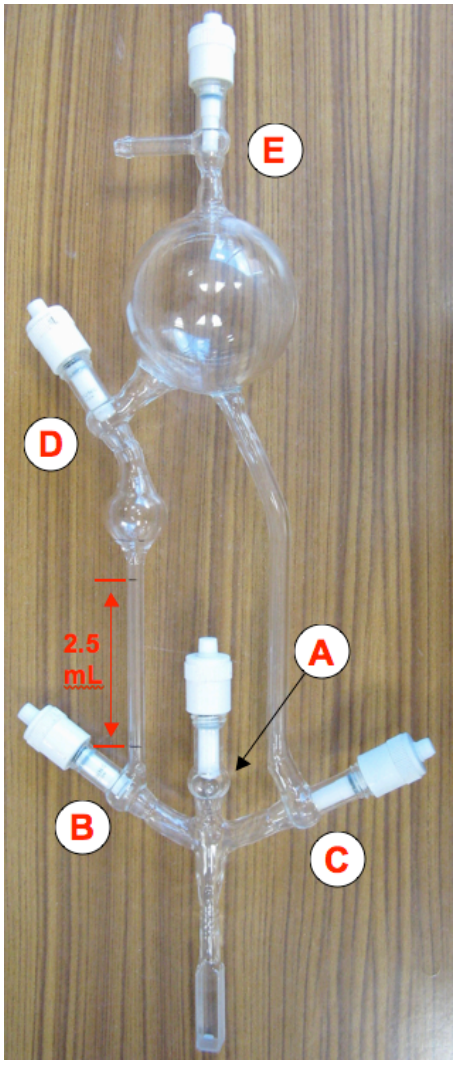

Figure 29 UV kinetic glassware.

4 References

1. Trifonov, D. N.; Trifonov, V. D., *How the Chemical Elements were Discovered*. Education: Moscow, 1980.
2. Winkler, C. A., *Chem. Ber.* **1887,** *20*, 667.
3. Dennis, L. M.; Papish, J., *J. Am. Chem. Soc.* **1921,** *43*, 2131-2143; McCabe, L., *Ind. Eng. Chem.* **1951,** *44*, 113A.
4. Tabern, D. I.; Orndorff, W. R.; Dennis, L. M., *J. Am. Chem. Soc.* **1925,** *47*, 2039-2044; Orndorff, W. R.; Tabern, D. L.; Dennis, L. M., *J. Am. Chem. Soc.* **1927,** *49*, 2512-2516; Geddes, R. L.; Mack, E., *J. Am. Chem. Soc.* **1930,** *52* (11), 4372-4380; Kraus, C. A.; Flood, E. A., *J. Am. Chem. Soc.* **1932,** *54* (4), 1635-1644.
5. Davidson, P. J.; Harris, D. H.; Lappert, M. F., *J. Chem. Soc., Dalton Trans.* **1976,** (21), 2268-2274.
6. Harris, D. H.; Lappert, M. F., *J. Chem. Soc., Chem. Commun.* **1974,** (21), 895-896.
7. Hammett, F. S.; Nowrey, J. E.; Muller, J. H., *J. Exp. Med.* **1922,** *35* (2), 173-180.
8. Tsutsui, M.; Kakimoto, N.; Axtell, D. D.; Oikawa, H.; Asai, K., *J. Am. Chem. Soc.* **1976,** *98* (25), 8287-8289; Saiers, J. H.; Blumenstein, B.; Slavik, M.; Costanzi, J. H.; Crawford, E. D., *Cancer Treat. Rep.* **1987,** *71* (12), 1305-1306; Lukevics, E.; Ignatovich, L.; Shilina, N.; Germane, S., *Appl. Organomet. Chem.* **1992,** *6* (3), 261-266; Kopfmaier, P., *Eur. J. Clin. Pharmacol.* **1994,** *47* (1), 1-16; Aso, H.; Suzuki, F.; Yamaguchi, T.; Hayashi, Y.; Ebina, T.; Ishida, N., *Microbiol. Immunol.* **1985,** *29* (1), 65-74; Kumano, N.; Ishikawa, T.; Koinumaru, S.;

Kikumoto, T.; Suzuki, S.; Nakai, Y.; Konno, K., *Tohoku J. Exp. Med.* **1985,** *146* (1), 97-104.

9. Rice, L. M.; Wheeler, J. W.; Geschickter, C. F., *J. Heterocycl. Chem.* **1974,** *11* (6), 1041-1047; Henry, M. C.; Rosen, E.; Port, C. D.; Levine, B. S., *Cancer Treat. Rep.* **1980,** *64* (12), 1207-1210.

10. Lukevics, Y. A.; Gar, L. M.; Ignatovich, L. M.; Mironov, V. F., *Biological Germanium Compounds*. Zinatne: Riga, 1990; Bulten, E. J.; van der Kerk, G. J. M., *New Uses for Germanium*. Midwest Research Institute: Kansas City, 1974.

11. Razuvaev, G. A.; Gribov, B. G.; Domrachev, G. A.; Salamatin, B. A., *Organometallic Compounds in Electronics*. Science: Moscow, 1972.

12. Gribov, B. G.; Domrachev, G. A.; Zhuk, B. V.; Kaverin, B. S.; Kozyrkin, B. I.; Mel'nikov, V. V.; Suvorova, O. N., *Precipitation of Films and Covers by Decomposition of Metalloorganic Compounds*. Science: Moscow, 1981.

13. Smith, E. F., *J. Chem. Educ.* **1926,** *3* (4), 382.

14. Löwig, C., *Ann. Chem.* **1852,** *84*, 308; Löwig, C., *Chem. Zentr.* **1852**, 575.

15. West, R., *J. Am. Chem. Soc.* **1953,** *75* (23), 6080-6081.

16. Goldberg, D. E.; Harris, D. H.; Lappert, M. F.; Thomas, K. M., *J. Chem. Soc., Chem. Commun.* **1976,** (7), 261-262.

17. Krause, E.; Reissaus, G. G., *Chem. Ber.* **1922,** *55*, 888-902.

18. Arakawa, Y.; Wada, O., *Metal Ions in Biological Systems*. Marcel Dekker: New York, 1993; p 101; Lukevics, E.; Pudova, O., *The Chemistry of Organic Germanium, Tin and Lead Compounds, Vol. 2*. John Wiley & Sons, Ltd: Chichester, 2002; p 1685-1714.

19. Barnes, J. M.; Stoner, H. B., *Pharmacol. Rev.* **1959,** *11* (2), 211-231; Hunt, R., *J. Pharmacol. Exp. Ther.* **1926,** *28* (3), 367-388; Stoner, H. B.; Barnes, J. M.;

Duff, J. I., *British Journal of Pharmacology and Chemotherapy* **1955,** *10* (1), 16-25.

20. Luijten, J. G.; van der Kerk, G. J., Tin, *Investigation in the Field of Organotin Chemistry*. Tin Research Institute: Greenford, 1955.
21. de Bataafsche, N. V.; Maatschappij, P. 1951.
22. McCombie, H.; Saunders, B. C., *Nature* **1947,** *159* (4041), 491-494; Seifter, J., *J. Pharmacol. Exper. Ther.* **1939,** *66*, 32.
23. Ingham, R. K.; Rosenberg, S. D.; Gilman, H., *Chem. Rev.* **1960,** *60* (5), 459-539.
24. Klippel, J., *Z. Prakt. Chem.* **1860,** (81), 287.
25. Browder, A. A.; Joselow, M. M.; Louria, D. B., *Medicine (Baltimore).* **1973,** *52* (2), 121-139.
26. Bolanowska, W.; Wisniewskaknypl, J. M., *Biochem. Pharmacol.* **1972,** *21*, 2018.
27. Saunders, B. C.; Stacey, G. J., *J. Chem. Soc.* **1949,** 919-925; Saunders, B. C.; Stacey, G. J., *J. Chem. Soc.* **1948,** 1773-1779; Saunders, B. C.; Stacey, G. J.; Wild, F.; Wilding, I. G. E., *J. Chem. Soc.* **1948,** 699-703; McCombie, H.; Saunders, B. C., *Nature* **1946,** *158* (4011), 382-385.
28. Thayer, J. S., *J. Organomet. Chem.* **1974,** *76* (3), 265-295.
29. Claudio, E. S.; Godwin, H. A.; Magyar, J. S., Fundamental coordination chemistry, environmental chemistry, and biochemistry of lead(II). In *Progress in Inorganic Chemistry, Vol 51*, John Wiley & Sons Inc: New York, 2003; Vol. 51, pp 1-144.
30. Housecroft, C. E.; Sharpe, A. G., *Inorganic Chemistry*. Pearson Education Ltd: Harlow, 2001; p 284.

31. Goldberg, D. E.; Hitchcock, P. B.; Lappert, M. F.; Thomas, K. M.; Thorne, A. J.; Fjeldberg, T.; Haaland, A.; Schilling, B. E. R., *J. Chem. Soc., Dalton Trans.* **1986,** (11), 2387-2394; Fjeldberg, T.; Hope, H.; Lappert, M. F.; Power, P. P.; Thorne, A. J., *J. Chem. Soc., Chem. Commun.* **1983,** (11), 639-641; Jutzi, P.; Leue, C., *Organometallics* **1994,** *13* (7), 2898-2899; Jutzi, P.; Becker, A.; Stammler, H. G.; Neumann, B., *Organometallics* **1991,** *10* (6), 1647-1648; Jutzi, P.; Schmidt, H.; Neumann, B.; Stammler, H.-G., *Organometallics* **1996,** *15* (2), 741-746; Ossig, G.; Meller, A.; Bronneke, C.; Muller, O.; Schafer, M.; Herbst-Irmer, R., *Organometallics* **1997,** *16* (10), 2116-2120; Herrmann, W. A.; Denk, M.; Behm, J.; Scherer, W.; Klingan, F.-R.; Bock, H.; Solouki, B.; Wagner, M., *Angew. Chem. Int. Ed. Engl.* **1992,** *31* (11), 1485-1488; Wegner, G. L.; Berger, R. J. F.; Schier, A.; Schmidbaur, H., *Organometallics* **2001,** *20* (3), 418-423; Foley, S. R.; Bensimon, C.; Richeson, D. S., *J. Am. Chem. Soc.* **1997,** *119* (43), 10359-10363; Barrau, J.; Rima, G.; El, A., *Organometallics* **1998,** *17* (4), 607-614; Veith, M.; Becker, S.; Huch, V., *Angew. Chem. Int. Ed. Engl.* **1989,** *28* (9), 1237-1238; Karsch, H. H.; Schlüter, P. A.; Reisky, M., *Eur. J. Inorg. Chem.* **1998,** *1998* (4), 433-436.

32. Leung, W.-P.; Kwok, W.-H.; Weng, L.-H.; T. C. Law, L.; Yuan Zhou, Z.; C. W. Mak, T., *J. Chem. Soc., Dalton Trans.* **1997,** (22), 4301-4306.

33. Fjeldberg, T.; Haaland, A.; Schilling, B. E. R.; Lappert, M. F.; Thorne, A. J., *J. Chem. Soc., Dalton Trans.* **1986,** (8), 1551-1556.

34. Klinkhammer, K. W.; Schwarz, W., *Angew. Chem. Int. Ed. Engl.* **1995,** *34* (12), 1334-1336.

35. Krause, E.; Becker, R., *Ber. Dtsch. Chem. Ges.* **1920,** *53* (2), 173-190; Weidenbruch, M.; Schlaefke, J.; Schäfer, A.; Peters, K.; von Schnering, H. G.;

Marsmann, H., *Angew. Chem. Int. Ed. Engl.* **1994,** *33* (18), 1846-1848; Tokitoh, N.; Saito, M.; Okazaki, R., *J. Am. Chem. Soc.* **1993,** *115* (5), 2065-2066; Gruetzmacher, H.; Pritzkow, H.; Edelmann, F. T., *Organometallics* **1991,** *10* (1), 23-25; Masamune, S.; Sita, L. R., *J. Am. Chem. Soc.* **1985,** *107* (22), 6390-6391; Bigwood, M. P.; Corvan, P. J.; Zuckerman, J. J., *J. Am. Chem. Soc.* **1981,** *103* (25), 7643-7646; Saito, M.; Tokitoh, N.; Okazaki, R., *Organometallics* **1996,** *15* (21), 4531-4536; Eaborn, C.; Hill, M. S.; Hitchcock, P. B.; Patel, D.; Smith, J. D.; Zhang, S., *Organometallics* **1999,** *19* (1), 49-53; Engelhardt, L. M.; Jolly, B. S.; Lappert, M. F.; Raston, C. L.; White, A. H., *J. Chem. Soc., Chem. Commun.* **1988,** (5), 336-338; Drost, C.; Hitchcock, P. B.; Lappert, M. F., *Organometallics* **1998,** *17* (18), 3838-3840; J. Cardin, C.; J. Cardin, D.; P. Constantine, S.; G. B. Drew, M.; Rashid, H.; A. Convery, M.; Fenske, D., *J. Chem. Soc., Dalton Trans.* **1998,** (16), 2749-2756; A. Barney, A.; F. Heyduk, A.; G. Nocera, D., *Chem. Commun.* **1999,** (23), 2379-2380; Eaborn, C.; Hitchcock, P. B.; Smith, J. D.; Sozerli, S. E., *Organometallics* **1997,** *16* (26), 5653-5658.

36. Fischer, E. O.; Grubert, H., *Z. Anorg. Allg. Chem.* **1956,** *286* (5-6), 237-242; Gynane, M. J. S.; Harris, D. H.; Lappert, M. F.; Power, P. P.; Riviere, P.; Riviere-Baudet, M., *J. Chem. Soc., Dalton Trans.* **1977,** (20), 2004-2009; Balch, A. L.; Oram, D. E., *Inorg. Chem.* **1987,** *26* (12), 1906-1912; Brooker, S.; Buijink, J. K.; Edelmann, F. T., *Organometallics* **1991,** *10* (1), 25-26; Driess, M.; Janoschek, R.; Pritzkow, H.; Rell, S.; Winkler, U., *Angew. Chem. Int. Ed. Engl.* **1995,** *34* (15), 1614-1616; B. Hitchcock, P.; F. Lappert, M.; Wang, Z.-X., *Chem. Commun.* **1997,** (12), 1113-1114; Drost, C.; B. Hitchcock, P.; F. Lappert, M.; J.-M. Pierssens, L., *Chem. Commun.* **1997,** (12), 1141-1142;

Gehrhus, B.; Hitchcock, P. B.; Lappert, M. F., *Angew. Chem. Int. Ed. Engl.* **1997,** *36* (22), 2514-2516; Klinkhammer, K. W.; Fässler, T. F.; Grützmacher, H., *Angew. Chem. Int. Ed.* **1998,** *37* (1-2), 124-126.

37. Mizuhata, Y.; Sasamori, T.; Tokitoh, N., *Chem. Rev.* **2009,** *109* (8), 3479-3511; Fischer, R. C.; Power, P. P., *Chem. Rev.* **2010,** *110* (7), 3877-3923.

38. Pu, L. H.; Olmstead, M. M.; Power, P. P.; Schiemenz, B., *Organometallics* **1998,** *17* (26), 5602-5606; Simons, R. S.; Pu, L. H.; Olmstead, M. M.; Power, P. P., *Organometallics* **1997,** *16* (9), 1920-1925; Eichler, B. E.; Power, P. P., *Inorg. Chem.* **2000,** *39* (24), 5444-5449; Stender, M.; Pu, L. H.; Power, P. P., *Organometallics* **2001,** *20* (9), 1820-1824; Eichler, B. E.; Pu, L. H.; Stender, M.; Power, P. P., *Polyhedron* **2001,** *20* (6), 551-556; Stanciu, C.; Hino, S. S.; Stender, M.; Richards, A. F.; Olmstead, M. M.; Power, P. P., *Inorg. Chem.* **2005,** *44* (8), 2774-2780.

39. Power, P. P., *Organometallics* **2007,** *26* (18), 4362-4372.

40. Hino, S.; Brynda, M.; Phillips, A. D.; Power, P. P., *Angew. Chem. Int. Ed.* **2004,** *43* (20), 2655-2658.

41. Wang, X.; Zhu, Z.; Peng, Y.; Lei, H.; Fettinger, J. C.; Power, P. P., *J. Am. Chem. Soc.* **2009,** *131* (20), 6912-6913.

42. Peng, Y.; Guo, J.-D.; Ellis, B. D.; Zhu, Z.; Fettinger, J. C.; Nagase, S.; Power, P. P., *J. Am. Chem. Soc.* **2009,** *131* (44), 16272-16282.

43. Merrill, W. A.; Rivard, E.; DeRopp, J. S.; Wang, X.; Ellis, B. D.; Fettinger, J. C.; Wrackmeyer, B.; Power, P. P., *Inorg. Chem.* **2010,** *49* (18), 8481-8486.

44. Rupar, P. A.; Staroverov, V. N.; Ragogna, P. J.; Baines, K. M., *J. Am. Chem. Soc.* **2007,** *129* (49), 15138.

45. Rupar, P. A.; Staroverov, V. N.; Baines, K. M., *Science* **2008,** *322* (5906), 1360-1363.

46. Rupar, P. A.; Bandyopadhyay, R.; Cooper, B. F. T.; Stinchcombe, M. R.; Ragogna, P. J.; Macdonald, C. L. B.; Baines, K. M., *Angew. Chem. Int. Ed.* **2009,** *48* (28), 5155-5158.

47. Thimer, K. C.; Al-Rafia, S. M. I.; Ferguson, M. J.; McDonald, R.; Rivard, E., *Chem. Commun.* **2009,** (46), 7119-7121.

48. Al-Rafia, S. M. I.; Lummis, P. A.; Ferguson, M. J.; McDonald, R.; Rivard, E., *Inorg. Chem.* **2010,** *49* (20), 9709-9717.

49. Sidiropoulos, A.; Jones, C.; Stasch, A.; Klein, S.; Frenking, G., *Angew. Chem. Int. Ed.* **2009,** *48* (51), 9701-9704.

50. Green, S. P.; Jones, C.; Junk, P. C.; Lippert, K.-A.; Stasch, A., *Chem. Commun.* **2006,** (38), 3978-3980.

51. Stasch, A.; Forsyth, C. M.; Jones, C.; Junk, P. C., *New J. Chem.* **2008,** *32* (5), 829-834; Jones, C.; Rose, R. P.; Stasch, A., *Dalton Trans.* **2008,** (21), 2871-2878.

52. Nagendran, S.; Sen, S. S.; Roesky, H. W.; Koley, D.; GrubmuÃàller, H.; Pal, A.; Herbst-Irmer, R., *Organometallics* **2008,** *27* (21), 5459-5463.

53. Breher, F.; Rüegger, H., *Angew. Chem. Int. Ed.* **2005,** *44* (3), 473-477.

54. Eisler, D. J.; Less, R. J.; Naseri, V.; Rawson, J. M.; Wright, D. S., *Dalton Trans.* **2008,** (18), 2382-2384.

55. Izod, K.; Stewart, J.; Clegg, W.; Harrington, R. W., *Organometallics* **2010,** *29* (1), 108-116.

56. Izod, K.; Stewart, J.; Clark, E. R.; Clegg, W.; Harrington, R. W., *Inorg. Chem.* **2010,** *49* (10), 4698-4707.

57. Izod, K.; Wills, C.; Clegg, W.; Harrington, R. W., *Organometallics* **2009,** *28* (7), 2211-2217.

58. Zabula, A. V.; Pape, T.; Hepp, A.; Schappacher, F. M.; Rodewald, U. C.; Pottgen, R.; Hahn, F. E., *J. Am. Chem. Soc.* **2008,** *130* (17), 5648-5649.

59. Kim, W.-K.; Fevola, M. J.; Liable-Sands, L. M.; Rheingold, A. L.; Theopold, K. H., *Organometallics* **1998,** *17* (21), 4541-4543.

60. Dove, A. P.; Gibson, V. C.; Marshall, E. L.; Rzepa, H. S.; White, A. J. P.; Williams, D. J., *J. Am. Chem. Soc.* **2006,** *128* (30), 9834-9843.

61. Bourget-Merle, L.; Lappert, M. F.; Severn, J. R., *Chem. Rev.* **2002,** *102* (9), 3031-3066.

62. Cui, C.; Roesky, H. W.; Schmidt, H.-G.; Noltemeyer, M.; Hao, H.; Cimpoesu, F., *Angew. Chem. Int. Ed.* **2000,** *39* (23), 4274-4276.

63. Hardman, N. J.; Eichler, B. E.; Power, P. P., *Chem. Commun.* **2000,** (20), 1991-1992.

64. Hill, M. S.; Hitchcock, P. B.; Pongtavornpinyo, R., *Science* **2006,** *311* (5769), 1904-1907.

65. Green, S. P.; Jones, C.; Stasch, A., *Science* **2007,** *318* (5857), 1754-1757.

66. Tsai, Y.-C.; Wang, P.-Y.; Chen, S.-A.; Chen, J.-M., *J. Am. Chem. Soc.* **2007,** *129* (26), 8066-8067.

67. Tsai, Y.-C.; Wang, P.-Y.; Lin, K.-M.; Chen, S.-A.; Chen, J.-M., *Chem. Commun.* **2008,** (2), 205-207.

68. Tran, B. L.; Pink, M.; Gao, X.; Park, H.; Mindiola, D. J., *J. Am. Chem. Soc.* **2010,** *132* (5), 1458-1459.

69. Pfirrmann, S.; Limberg, C.; Herwig, C.; Stößer, R.; Ziemer, B., *Angew. Chem. Int. Ed.* **2009,** *48* (18), 3357-3361.

70. Smith, J. M.; Lachicotte, R. J.; Pittard, K. A.; Cundari, T. R.; Lukat-Rodgers, G.; Rodgers, K. R.; Holland, P. L., *J. Am. Chem. Soc.* **2001,** *123* (37), 9222-9223.

71. Akkari, A.; Byrne, J. J.; Saur, I.; Rima, G.; Gornitzka, H.; Barrau, J., *J. Organomet. Chem.* **2001,** *622* (1-2), 190-198.

72. Ayers, A. E.; Klapotke, T. M.; Dias, H. V. R., *Inorg. Chem.* **2001,** *40* (5), 1000-1005.

73. Ding, Y. Q.; Roesky, H. W.; Noltemeyer, M.; Schmidt, H. G.; Power, P. P., *Organometallics* **2001,** *20* (6), 1190-1194.

74. Driess, M.; Yao, S.; Brym, M.; van W√ºllen, C.; Lentz, D., *J. Am. Chem. Soc.* **2006,** *128* (30), 9628-9629.

75. Chen, M.; Fulton, J. R.; Hitchcock, P. B.; Johnstone, N. C.; Lappert, M. F.; Protchenko, A. V., *Dalton Trans.* **2007,** (26), 2770-2778.

76. Jana, A.; Sarish, S. P.; Roesky, H. W.; Schulzke, C.; Doring, A.; John, M., *Organometallics* **2009,** *28* (8), 2563-2567.

77. Jana, A.; Roesky, H. W.; Schulzke, C.; Doring, A.; Back, T.; Pal, A.; Herbst-Irmer, R., *Inorg. Chem.* **2009,** *48* (1), 193-197.

78. Tam, E. C. Y.; Johnstone, N. C.; Ferro, L.; Hitchcock, P. B.; Fulton, J. R., *Inorg. Chem.* **2009,** *48* (18), 8971-8976.

79. Jana, A.; Nekoueishahraki, B.; Roesky, H. W.; Schulzke, C., *Organometallics* **2009,** *28* (13), 3763-3766.

80. Fulton, J. R.; Hitchcock, P. B.; Johnstone, N. C.; Tam, E. C. Y., *Dalton Trans.* **2007,** (31), 3360-3362.

81. Dove, A. P.; Gibson, V. C.; Marshall, E. L.; White, A. J. P.; Williams, D. J., *Chem. Commun.* **2001,** (3), 283-284.

82. Jana, A.; Roesky, H. W.; Schulzke, C.; Samuel, P. P.; Doring, A., *Inorg. Chem.* **2010,** *49* (12), 5554-5559.

83. Yao, S. L.; Brym, M.; Merz, K.; Driess, M., *Organometallics* **2008,** *27* (14), 3601-3607.

84. Yao, S.; Block, S.; Brym, M.; Driess, M., *Chem. Commun.* **2007,** (37), 3844-3846.

85. Pineda, L. W.; Jancik, V.; Starke, K.; Oswald, R. B.; Roesky, H. W., *Angew. Chem. Int. Ed.* **2006,** *45* (16), 2602-2605.

86. Jana, A.; Sen, S. S.; Roesky, H. W.; Schulzke, C.; Dutta, S.; Pati, S. K., *Angew. Chem. Int. Ed.* **2009,** *48* (23), 4246-4248.

87. Jana, A.; Ghoshal, D.; Roesky, H. W.; Objartel, I.; Schwab, G.; Stalke, D., *J. Am. Chem. Soc.* **2009,** *131* (3), 1288-1293.

88. Jana, A.; Roesky, H. W.; Schulzke, C., *Dalton Trans.* **2010,** *39* (1), 132-138.

89. Jana, A.; Roesky, H. W.; Schulzke, C.; Döring, A., *Angew. Chem. Int. Ed.* **2009,** *48* (6), 1106-1109.

90. Pineda, L. W.; Jancik, V.; Roesky, H. W.; Necuali, D.; Neculai, A. M., *Angew. Chem.-Int. Edit.* **2004,** *43* (11), 1419-1421.

91. Jana, A.; Sarish, S. P.; Roesky, H. W.; Schulzke, C.; Samuel, P. P., *Chem. Commun.* **2010,** *46* (5), 707-709.

92. Wang, W.; Yao, S.; van WuÃàllen, C.; Driess, M., *J. Am. Chem. Soc.* **2008,** *130* (30), 9640-9641.

93. Wang, W. Y.; Inoue, S.; Yao, S. L.; Driess, M., *Chem. Commun.* **2009,** (19), 2661-2663.

94. Woodul, W. D.; Richards, A. F.; Stasch, A.; Driess, M.; Jones, C., *Organometallics* **2010,** *29* (16), 3655-3660.

95. Aresta, M.; Dibenedetto, A., *Dalton Trans.* **2007,** (28), 2975-2992; Dell'Amico, D. B.; Calderazzo, F.; Labella, L.; Marchetti, F.; Pampaloni, G., *Chem. Rev.* **2003,** *103* (10), 3857-3897; Sakakura, T.; Choi, J. C.; Yasuda, H., *Chem. Rev.* **2007,** *107* (6), 2365-2387.

96. Tsuda, T.; Saegusa, T., *Inorg. Chem.* **1972,** *11* (10), 2561-2563; Chisholm, M. H.; Cotton, F. A.; Extine, M. W.; Reichert, W. W., *J. Am. Chem. Soc.* **1978,** *100* (6), 1727-1734; Mandal, S. K.; Ho, D. M.; Orchin, M., *Organometallics* **1993,** *12* (5), 1714-1719; Boyd, C. L.; Clot, E.; Guiducci, A. E.; Mountford, P., *Organometallics* **2005,** *24* (10), 2347-2367.

97. Darensbourg, D. J.; Sanchez, K. M.; Reibenspies, J. H.; Rheingold, A. L., *J. Am. Chem. Soc.* **1989,** *111* (18), 7094-7103.

98. Simpson, R. D.; Bergman, R. G., *Organometallics* **1992,** *11* (12), 4306-4315.

99. Choi, J.-C.; Sakakura, T.; Sako, T., *J. Am. Chem. Soc.* **1999,** *121* (15), 3793-3794.

100. Darensbourg, D. J.; Lee, W.-Z.; Phelps, A. L.; Guidry, E., *Organometallics* **2003,** *22* (26), 5585-5588.

101. Brombacher, H.; Vahrenkamp, H., *Inorg. Chem.* **2004,** *43* (19), 6042-6049.

102. Darensbourg, D. J.; Mueller, B. L.; Bischoff, C. J.; Chojnacki, S. S.; Reibenspies, J. H., *Inorg. Chem.* **1991,** *30* (10), 2418-2424.

103. Shriver, D. F.; Atkins, P. W., *Inorganic Chemistry*. OUP: Oxford, 1999.

104. Cox, H.; Stace, A. J., *J. Am. Chem. Soc.* **2004,** *126* (12), 3939-3947.

105. Stender, M.; Wright, R. J.; Eichler, B. E.; Prust, J.; Olmstead, M. M.; Roesky, H. W.; Power, P. P., *J. Chem. Soc., Dalton Trans.* **2001,** (23), 3465-3469.

106. Hill, M. S.; Hitchcock, P. B.; Pongtavornpinyo, R., *Dalton Trans.* **2008,** (21), 2854-2860; Lesikar, L. A.; Richards, A. F., *J. Organomet. Chem.* **2006,** *691* (20), 4250-4256.

107. Reisinger, A.; Trapp, N.; Krossing, I., *Organometallics* **2007,** *26* (8), 2096-2105; Samuels, J. A.; Lobkovsky, E. B.; Streib, W. E.; Folting, K.; Huffman, J. C.; Zwanziger, J. W.; Caulton, K. G., *J. Am. Chem. Soc.* **1993,** *115* (12), 5093-5104.

108. Fogg, P. G. T.; Gerrard, W., *Solubility of Gases in Liquids*. Chichester, England, 1991.

109. Wakamatsu, K.; Orita, A.; Otera, J., *Organometallics* **2010,** *29* (5), 1290-1295.

110. Olmstead, W. N.; Margolin, Z.; Bordwell, F. G., *J. Org. Chem.* **1980,** *45* (16), 3295-3299.

111. Bryndza, H. E.; Fong, L. K.; Paciello, R. A.; Tam, W.; Bercaw, J. E., *J. Am. Chem. Soc.* **1987,** *109* (5), 1444-1456.

112. Arnett, E. M.; Venkatasubramaniam, K. G., *J. Org. Chem.* **1983,** *48* (10), 1569-1578.

113. Bryndza, H. E.; Tam, W., *Chem. Rev.* **1988,** *88* (7), 1163-1188; Park, S.; Rheingold, A. L.; Roundhill, D. M., *Organometallics* **1991,** *10* (3), 615-623.

114. Brauman, J. I.; Blair, L. K., *J. Am. Chem. Soc.* **1970,** *92* (20), 5986-5992.

115. Blanksby, S. J.; Ellison, G. B., *Acc. Chem. Res.* **2003,** *36* (4), 255-263.

116. Ferro, L.; Hitchcock, P. B.; Coles, M. P.; Cox, H.; Fulton, J. R., *Inorg. Chem.* **2011,** *50* (5), 1879-1888.

117. Ding, Y.; Ma, Q.; Roesky, H. W.; Herbst-Irmer, R.; Us√≥n, I.; Noltemeyer, M.; Schmidt, H.-G., *Organometallics* **2002,** *21* (24), 5216-5220.

118. Ding, Y.; Ma, Q.; Uson, I.; Roesky, H. W.; Noltemeyer, M.; Schmidt, H.-G., *J. Am. Chem. Soc.* **2002,** *124* (29), 8542-8543.

119. Rake, A.; Zulch, F.; Ding, Y.; Prust, J.; Roesky, H. W.; Noltemeyer, M.; Schmidt, H. G., *Z. Anorg. Allg. Chem.* **2001,** *627* (5), 836-840.

120. Glockling, F.; Hooton, K. A., *Journal of the Chemical Society (Resumed)* **1962**, 2658-2661; Orlov, N. A.; Bochkarev, L. N.; Nikitinsky, A. V.; Zhiitsov, S. F.; Zakharov, L. N.; Fukin, G. K.; Ya. Khorshev, S., *J. Organomet. Chem.* **1997,** *547* (1), 65-69; Orlov, N. A.; Bochkarev, L. N.; Nikitinsky, A. V.; Kropotova, V. Y.; N. Zakharov, L.; Fukin, G. K.; Khorshev, S. Y., *J. Organomet. Chem.* **1998,** *560* (1-2), 21-25; York, J. T.; Young, V. G.; Tolman, W. B., *Inorg. Chem.* **2006,** *45* (10), 4191-4198.

121. Leung, W.-P.; So, C.-W.; Chong, K.-H.; Kan, K.-W.; Chan, H.-S.; Mak, T. C. W., *Organometallics* **2006,** *25* (11), 2851-2858; Arii, H.; Nakadate, F.; Mochida, K., *Organometallics* **2009,** *28* (17), 4909-4911.

122. Boehme, C.; Frenking, G., *Organometallics* **1998,** *17* (26), 5801-5809.

123. Soloveichik, G. L.; Eisenstein, O.; Poulton, J. T.; Streib, W. E.; Huffman, J. C.; Caulton, K. G., *Inorg. Chem.* **1992,** *31* (15), 3306-3312; Bowmaker, G. A.; Boyd, S. E.; Hanna, J. V.; Hart, R. D.; Healy, P. C.; Skelton, B. W.; White, A. H., *J. Chem. Soc., Dalton Trans.* **2002,** (13), 2722-2730; Oakley, S. H.; Coles, M. P.; Hitchcock, P. B., *Inorg. Chem.* **2004,** *43* (16), 5168-5172; Oakley, S. H.; Soria, D. B.; Coles, M. P.; Hitchcock, P. B., *Dalton Trans.* **2004,** (4), 537-546; Chandrasekaran, P.; Mague, J. T.; Venkateswaran, R.; Balakrishna, M. S., *Eur. J. Inorg. Chem.* **2007,** *2007* (31), 4988-4997; Knishevitsky, A. V.; Korotkikh, N. I.; Cowley, A. H.; Moore, J. A.; Pekhtereva, T. M.; Shvaika, O. P.; Reeske, G., *J. Organomet. Chem.* **2008,** *693* (8-9), 1405-1411.

124. Prust, J.; Hohmeister, H.; Stasch, A.; Roesky, Herbert W.; Magull, J.; Alexopoulos, E.; Usón, I.; Schmidt, H.-G.; Noltemeyer, M., *Eur. J. Inorg. Chem.* **2002,** *2002* (8), 2156-2162.

125. Bel'sky, V. K.; Ishchenko, V. M.; Bulychev, B. M.; Soloveichik, G. L., *Polyhedron* **1984,** *3* (6), 749-752.

126. Hou, H.-W.; Xin, X.-q.; Liu, J.; Chen, M.-q.; Shu, S., *J. Chem. Soc., Dalton Trans.* **1994,** (22), 3211-3214.

127. Bowmaker, G. A.; Hart, R. D.; deSilva, E. N.; Skelton, B. W.; White, A. H., *Aust. J. Chem.* **1997,** *50* (6), 621-626.

128. Clarkson, T. W.; Magos, L., *Crit. Rev. Toxicol.* **2006,** *36* (8), 609-662.

129. Geier, D. A.; Sykes, L. K.; Geier, M. R., *Journal of Toxicology and Environmental Health, Part B: Critical Reviews* **2007,** *10* (8), 575 - 596; Melnick, J. G.; Yurkerwich, K.; Buccella, D.; Sattler, W.; Parkin, G., *Inorg. Chem.* **2008,** *47* (14), 6421-6426.

130. Onyido, I.; Norris, A. R.; Buncel, E., *Chem. Rev.* **2004,** *104* (12), 5911-5930; Mutter, J.; Naumann, J.; Guethlin, C., *Crit. Rev. Toxicol.* **2007,** *37* (6), 537-549; Alessio, L.; Campagna, M.; Lucchini, R., *Am. J. Ind. Med.* **2007,** *50* (11), 779-787.

131. Tai, H.-C.; Lim, C., *The Journal of Physical Chemistry A* **2005,** *110* (2), 452-462.

132. Kaur, P.; Evje, L.; Aschner, M.; Syversen, T., *Toxicology in Vitro* **2009,** *23* (3), 378-385; Magos, L.; Webb, M.; Clarkson, T. W., *Crit. Rev. Toxicol.* **1980,** *8* (1), 1-42; Cuvin-Aralar, M. L. A.; Furness, R. W., *Ecotoxicol. Environ. Saf.* **1991,** *21* (3), 348-364; Gailer, J., *Appl. Organomet. Chem.* **2002,** *16* (12), 701-707; Gailer, J. r., *Coord. Chem. Rev.* **2007,** *251* (1-2), 234-254; Prince, R. C.; Gailer,

J. r.; Gunson, D. E.; Turner, R. J.; George, G. N.; Pickering, I. J., *J. Inorg. Biochem.* **2007,** *101* (11-12), 1891-1893.

133. Kˆhrle, J., *Biochimie* **1999,** *81* (5), 527-533; Reddy, C. C.; Massaro, E. J., *Fundam. Appl. Toxicol. 3* (5), 431-436.

134. Falnoga, I.; Tušek-Žnidarič, M., *Biol. Trace Elem. Res.* **2007,** *119* (3), 212-220; Sasakura, C.; T. Suzuki, K., *J. Inorg. Biochem.* **1998,** *71* (3-4), 159-162.

135. Ralston, N. V. C.; Ralston, C. R.; Blackwell Iii, J. L.; Raymond, L. J., *Neurotoxicology* **2008,** *29* (5), 802-811; Carvalho, C. M. L.; Chew, E.-H.; Hashemy, S. I.; Lu, J.; Holmgren, A., *J. Biol. Chem.* **2008,** *283* (18), 11913-11923.

136. Moore, M. J.; Distefano, M. D.; Zydowsky, L. D.; Cummings, R. T.; Walsh, C. T., *Acc. Chem. Res.* **1990,** *23* (9), 301-308.

137. Farwell, J. D.; Fernandes, M. A.; Hitchcock, P. B.; Lappert, M. F.; Layh, M.; Omondi, B., *Dalton Trans.* **2003,** (9), 1719-1729.

138. Fernandes, M. A.; Layh, M.; Omondi, B., *Trends in Organometallic Chemistry Research*. Lancaster, U.K., 2005.

139. Hadzovic, A.; Janetzko, J.; Song, D., *Dalton Trans.* **2008,** (25), 3279-3281; Kajiwara, T.; Murao, R.; Ito, T., *J. Chem. Soc., Dalton Trans.* **1997,** (15), 2537-2538; Hadzovic, A.; Song, D., *Organometallics* **2008,** *27* (6), 1290-1298; Feldman, J.; McLain, S. J.; Parthasarathy, A.; Marshall, W. J.; Calabrese, J. C.; Arthur, S. D., *Organometallics* **1997,** *16* (8), 1514-1516; Tian, X.; Goddard, R.; P√∂rschke, K.-R., *Organometallics* **2006,** *25* (25), 5854-5862.

140. Grirrane, A.; Resa, I.; del Rio, D.; Rodrigguez, A.; Alvarez, E.; Mereiter, K.; Carmona, E., *Inorg. Chem.* **2007,** *46* (11), 4667-4676; Matkiviccalogovic, D., *Acta Crystallogr., Sect. C: Cryst. Struct. Commun.* **1987,** *43*, 1473.

141. Chisholm, M. H.; Gallucci, J.; Phomphrai, K., *Inorg. Chem.* **2002,** *41* (10), 2785-2794.

142. Levitt, M. H., *Spin Dynamics: Basics of Nuclear Magnetic Resonance*. 2nd ed ed.; 2008.

143. Carey, D. T.; Cope-Eatough, E. K.; Vilaplana-Mafe, E.; Mair, F. S.; Pritchard, R. G.; Warren, J. E.; Woods, R. J., *Dalton Trans.* **2003,** (6), 1083-1093.

144. Allmann, R.; Musso, H.; Flatau, K., *Chem. Ber. Recl.* **1972,** *105* (9), 3067-&.

145. Ding, Y.; Roesky, H. W.; Noltemeyer, M.; Schmidt, H.-G.; Power, P. P., *Organometallics* **2001,** *20* (6), 1190-1194.

146. Gogoi, S.; Bhuyan, R.; Barua, N. C., *Synth. Commun.* **2005,** *35* (21), 2811 - 2818.

147. Armarego W.L.F.; D.D., P., *Purification of Laboratory Chemicals - 4th edition*. Paperback Ed. Oxford: Boston, 1997.

148. Sheldrick, G. M., *SHELXL-97, Program for the Refinement of Crystal Structures*. University of Göttingen: Göttingen, Germany, 1997.

149. Frisch, M. J.; Trucks, G. W.; Schlegel, H. B.; Scuseria, G. E.; Robb, M. A.; Cheeseman, J. R.; Montgomery, J. A.; Vreven, T.; Kudin, K. N.; Burant, J. C.; Millam, J. M.; Iyengar, S. S.; Tomasi, J.; Barone, V.; Mennucci, B.; Cossi, M.; Scalmani, G.; Rega, N.; Petersson, G. A.; Nakatsuji, H.; Hada, M.; Ehara, M.; Toyota, K.; Fukuda, R.; Hasegawa, J.; Ishida, M.; Nakajima, T.; Honda, Y.; Kitao, O.; Nakai, H.; Klene, M.; Li, X.; Knox, J. E.; Hratchian, H. P.; Cross, J. B.; Bakken, V.; Adamo, C.; Jaramillo, J.; Gomperts, R.; Stratmann, R. E.; Yazyev, O.; Austin, A. J.; Cammi, R.; Pomelli, C.; Ochterski, J. W.; Ayala, P. Y.; Morokuma, K.; Voth, G. A.; Salvador, P.; Dannenberg, J. J.; Zakrzewski, V. G.; Dapprich, S.; Daniels, A. D.; Strain, M. C.; Farkas, O.; Malick, D. K.; Rabuck, A.

D.; Raghavachari, K.; Foresman, J. B.; Ortiz, J. V.; Cui, Q.; Baboul, A. G.; Clifford, S.; Cioslowski, J.; Stefanov, B. B.; Liu, G.; Liashenko, A.; Piskorz, P.; Komaromi, I.; Martin, R. L.; Fox, D. J.; Keith, T.; Laham, A.; Peng, C. Y.; Nanayakkara, A.; Challacombe, M.; Gill, P. M. W.; Johnson, B.; Chen, W.; Wong, M. W.; Gonzalez, C.; Pople, J. A., *Gaussian 03, Revision E.01*. Gaussian, Inc.: Wallingford, CT, 2004.

150. Wadt, W. R.; Hay, P. J., *J. Chem. Phys.* **1985,** *82* (1), 284-298.

151. Takagi, N.; Nagase, S., *Organometallics* **2007,** *26* (3), 469-471.

II. Synthesis of Novel Planar Chiral Complexes Based on [2.2]Paracyclophane

1 Introduction

The formation of carbon–heteroatom bonds in an atom economy fashion plays a pivotal role in the synthesis of pharmaceuticals, fine and bulk chemicals.[1,2] Among various reactions, hydroamination, the direct addition of amines to alkenes and alkynes with the formation of new C–N bonds, has seen a sharp increase in interest from the scientific community in the last decade.[1] Despite being thermodynamically feasible, the reaction requires a catalyst to proceed, due to the 2 + 2 cycloaddition of N–H to C=C which is orbital-forbidden under thermal conditions. Enantioselective intramolecular hydroamination of olefins is the conceptually simplest atom-economical approach to the synthesis of enantioenriched α-chiral heterocyclic amines,[3] valuable precursors in the preparation of natural products and biologically active molecules.[4]

1.1 Rare earth metal catalysed hydroamination

In early studies attention was focused mainly on hydroamination reactions promoted by rare-earth metals, actinides and alkaline earth metal-based complexes, predominantly lanthanocenes. This class of complexes proved to be highly efficient catalysts for intramolecular hydroamination of various unsaturated C–C bonds, such as alkenes, alkynes, allenes and dienes. However, reduced rates were observed in intermolecular processes.[5]

The general hydroamination mechanism for rare-earth metal catalised hydroamination is shown in Scheme 24. It involves the initial catalyst activation via protonation of an alkyl or amide substituent by the aminoalkene substrate; the thermoneutral olefin bond insertion into the Ln–N bond is the rate determining step, and this is followed by rapid protonolysis by another amine substrate (ΔH = – 13 kcal mol^{-1}).[5,6,7]

Scheme 24 Proposed σ-bond insertive mechanism for organolanthanide catalysed intramolecular hydroamination.

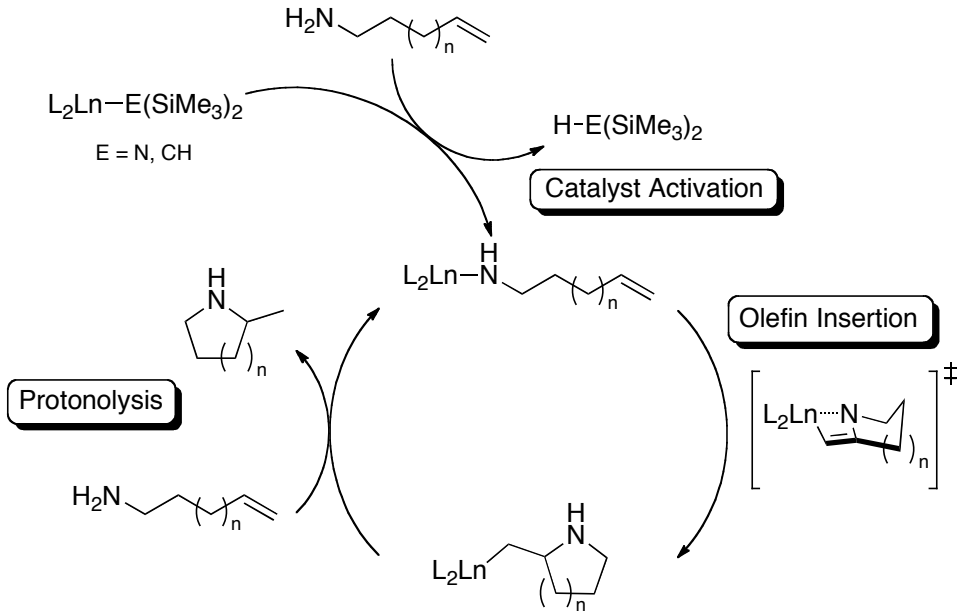

From a kinetic point of view, rare-earth metal catalysed intramolecular hydroamination/cyclisation of aminoalkenes differs significantly from reactions involving aminoalkynes. For instance, catalytic activity increases with increasing ionic radius of the rare-earth metal.[6] Sterically more open, less structurally constrained and electron-donating catalysts cause a further increase of the reaction rate.[8] Hydroamination of aminoalkynes follows the opposite trend: the rate of cyclisation decreases with increasing ionic radius of the metal center and more open coordination sphere around the metal. Generally the rate of cyclisation

decreases with increasing ring size. Furthermore, hydroamination reaction on aminoalkenes commonly proceeds significantly slower than aminoalkynes, and while terminal as well as internal alkynes react with comparable rates, internal double bonds react significantly slower and under much more forcing reactions conditions.[9,10]

Chiral lanthanocenes catalysts were used by Marks and co-workers for initial studies on asymmetric hydroamination in 1989.[5,6,8,11,12] Subsequently non-cyclopentadienyl based catalysts were employed;[13,14,15] however, only the binaphtholate-based complex, **I** (Figure 30, R = Si(3,5-xylyl)$_3$; Ln = Lu), reported by Hultzsch and co-workers in 2006, showed high enantioselectivity.[15] All other complexes have not shown an enantiomeric excess above 90%.

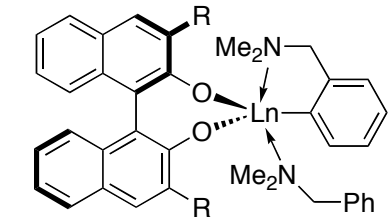

R = $SiPh_3$, $Si(3,5\text{-}Me_2C_6H_3)_3$, $SiPh_2{}^tBu$, $SiPh_2Cy$
Ln = Y, Lu

I

Figure 30 Highly enantioselective binaphtolate-based hydroamination catalyst.

Intermolecular hydroamination of unactivated alkenes with simple amines proved to be a considerably more challenging goal to achive, primarily due to the low binding ability of alkenes compared to amines. This was partially overcome by adjusting reaction conditions for a more efficient catalytic performance using an excess of olefinic substrate; however, this compromised the atom efficiency aspects of the reaction.[15,16,17] Little progress in intermolecular hydroamination has been made in the last 15 years and the Markovnikov addition of *n*-propylamine to

1-pentene mediated by $Me_2Si(Cp)_2NdCH(SiMe_3)$, **II**,[17] reported by Marks and co-workers in 2003 (eq 1), has been the state of art in this field for a long time. In fact, they achieved the addition of unactivated substrates in 90% yield and 0.4 h^{-1} turnover frequency, being the best result until the developments reported by Hultzsch and co-workers in 2010.[18]

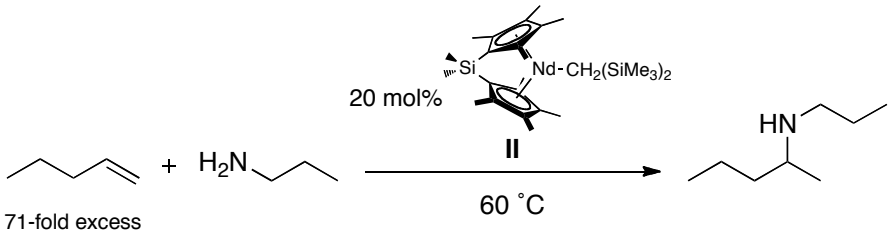

(1)

Following their achievements in enantioselective intramolecular hydroamination,[15] Hultzsch and co-workers reported an efficient asymmetric intermolecular hydroamination system using yttrium and lutetium binaphtholate catalysts **I** (Figure 30). They achieved the addition of a wide range of unactivated amines and alkenes (only 9- to 15-fold excess) in high yields and good *ee*, therefore making good progress in two challenging directions, i.e. intermolecular and asymmetric catalysis.[18] In fact, the binaphtolate ligand proved to be configurationally stable even under very forcing conditions (T = 180 ˚C). This was in contrast to the general issue presented by the common C_1-chiral lantanocene based catalysts, which can undergo epimerization via reversible protolitic cleavage of the metal cyclopentadienyl bond (Scheme 25), therefore compromising the enantioselectivity.[12,19]

Scandium has rarely been used in hydroamination catalysis due to its small ionic-radius, which collocates it at the bottom of the reactivity scale of rare earth metals; however, its very high Lewis acidity compensates for this handicap,

showing good activity in the transformation of aminoalkynes and moderate activity for aminoalkenes.

Scheme 25 Proposed mechanism for the epimerisation of chiral lanthanocene-based complexes.

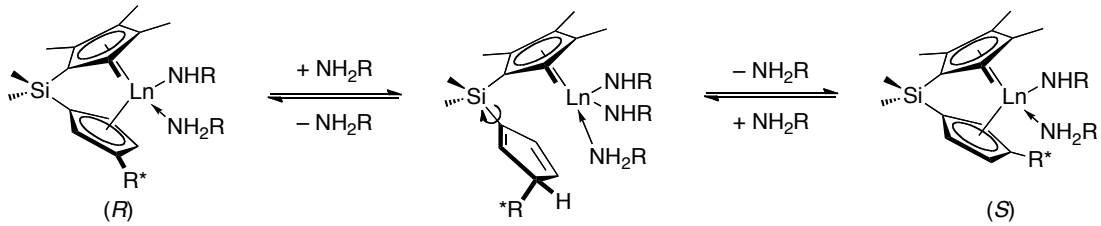

For instance, Schafer and co-workers reported that β-diketiminate complexes (^{tBu}BDI)ScMe$_2$ and [(^{tBu}BDI)ScMe][MeB(C_6F_5)$_3$], **III**, mediate intramolecular hydroamination reactions.[20] The moderately low catalytic activity of the dimethyl derivative, due to the small ionic radius of scandium and the steric bulk imposed by the ligand, was substantially enhanced for the cationic complex. This has to be attributed to the easier accessibility of the substrate to the metal center, resulting in a highly active catalyst for the hydroamination of both aminoalkyne and -alkenes, as long as minimal steric bulk was incorporated near the reactive amine group of the substrate. Stoichiometric reaction of the cationic species with 2,2-diphenylpent-4-en-1-amine led to the isolation of the catalytic intermediate **IV** (Scheme 26).

Scheme 26 Isolation of the amido intermediate **IV** from scandium cationic catalyst **III.**

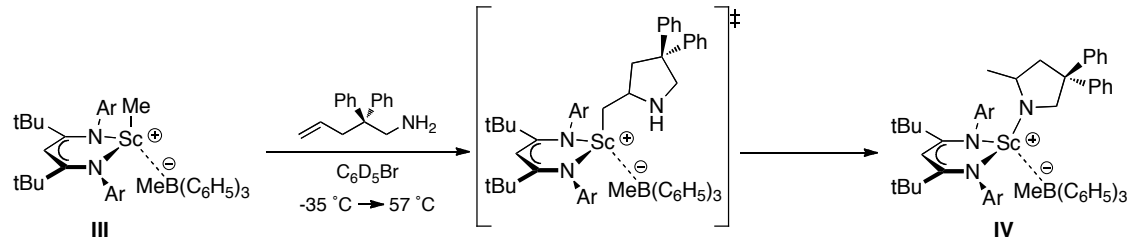

1.2 Group 4 metal catalysed hydroamination

In recent years, due to the lower cost and toxicity, as well as enhanced stability in comparison with rare-earth metal complexes, interest has focused on group 4 complexes mediated hydroamination catalysis, with neutral[21,22,23,24,25-29] and cationic[30,31] zirconium and titanium[24,29,32] systems.

The catalytic mechanism is disputed, due to the vast mechanistic diversity shown by group 4 metal systems. The mechanism for hydroamination of secondary aminoalkenes using cationic zirconium amide systems seems to be analogous to that well established for rare-earth metal systems.[30,31] The observed lack of reactivity towards primary aminoalkenes was attributed to deprotonation of the metal amide to yield a less reactive zirconium imido species.

However, studies on hydroamination of primary amines using neutral group 4 complexes proposed the catalytic cycle to occur via a [2+2] cycloaddition between the unsaturated substrate and a metal–imido bond (Scheme 27),[33,34] analogous to Bergman's hydroamination of alkynes and allenes.[35] Nevertheless, azametallacyles resulting from the stoichiometric [2+2] cycloaddition of group 4 metal–imido complexes and C–C unsaturated bonds have been confirmed through both experimental[33,35,36] and computational[34,37] methods. In a recent contribution, through a very detailed synthetic, thermodynamic and kinetic study, Scott and Fox proposed that the formation of an imido species was the rate determining step. Also, in contrast to rare-earth metal systems, the rate was reported to be in order of increasing steric bulk of the catalyst.[26]

Scheme 27 Proposed [2+2] cycloaddition mechanistic pathway via imido formation for intramolecular alkene/alkyne hydroamination.

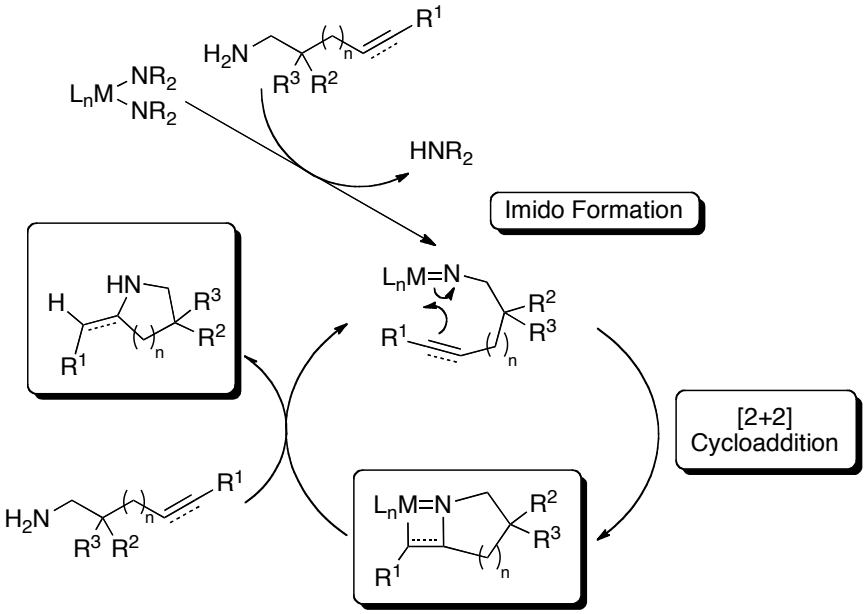

A limited number of Group 4 metal systems (Scheme 28, **V-VIII**) showed the ability in performing hydroamination reactions with both primary and secondary amines.[24,25,27] Valuable progress in this direction was made by Schafer and co-workers, who used a tethered ureate zirconium complex (**VI**) capable of catalysing intra- and intermolecular hydroamination reactions on a vast variety of substrates.[25] Marks and co-workers provided evidence in support of a σ-bond insertion mechanism through a detailed synthetic and kinetic study using the "constrained-geometry" complexes **V**.[27]

Scheme 28 Group 4 metal complexes capable of hydroamination of both primary and secondary amines

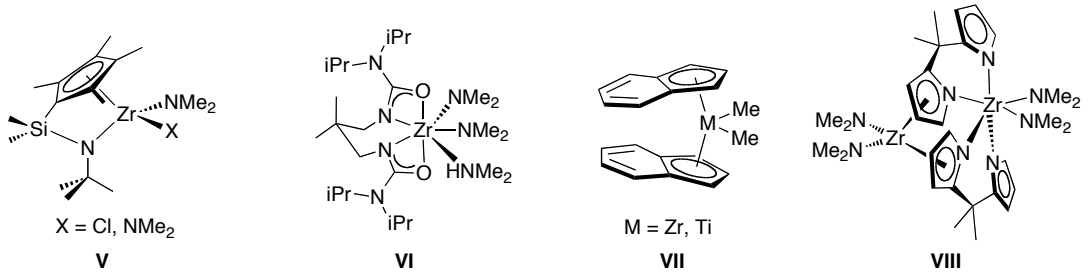

X = Cl, NMe_2 **V** **VI** M = Zr, Ti **VII** **VIII**

The proposed mechanism, shown in Scheme 29, proceeds via the insertion into the M–N σ-bond followed by cyclisation and deprotonation to yield a pyrrolidine, which is an analogous pathway to rare-earth metal-based hydroamination reactions.

Scheme 29 Proposed σ-bond insertive mechanism for Group 4 metal catalysed intramolecular hydroamination.

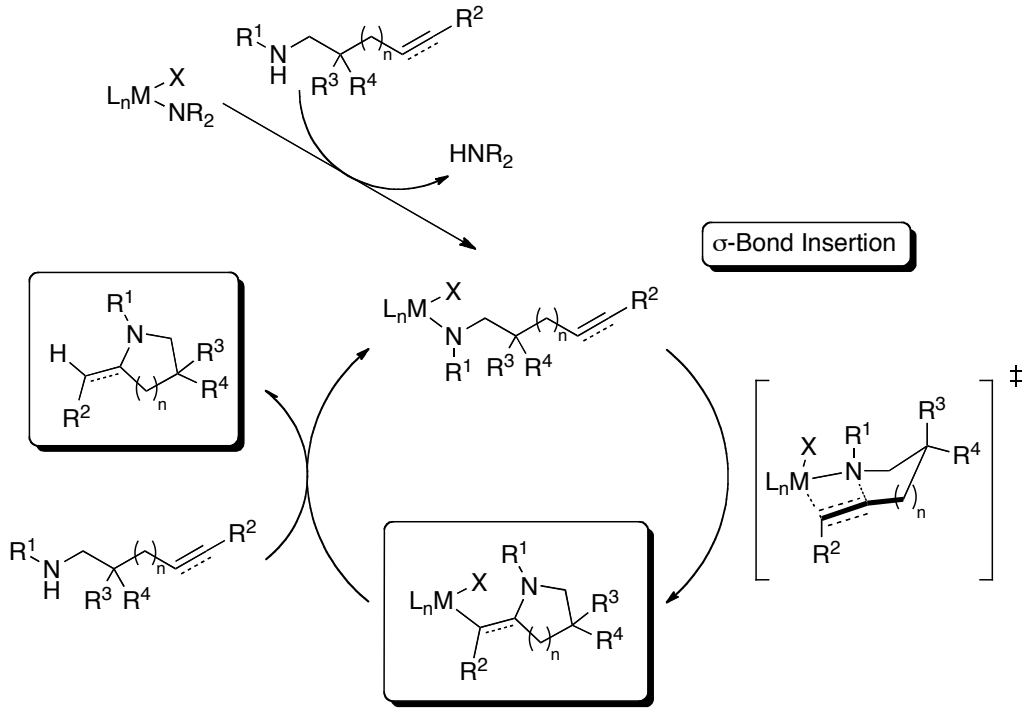

Further support of this mechanism was given by the Bergman and Schafer groups, in the isolation of a vinylamine catalytic intermediate, obtained in the presence of excess olefin (eq 2 and 3).[38]

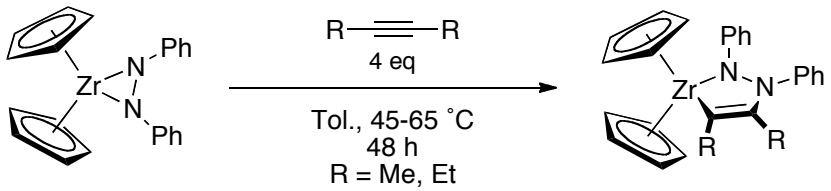

(2)

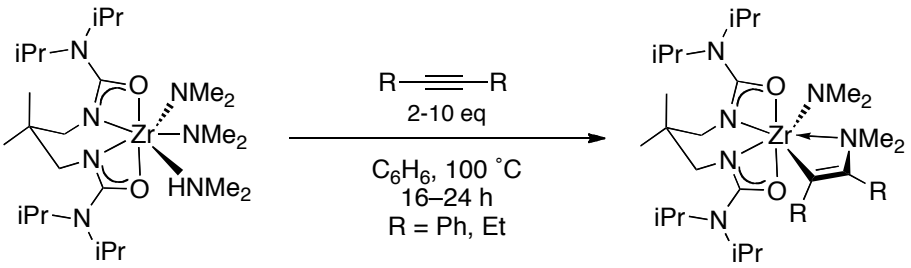

(3)

A limited number of group 4 derived asymmetric catalyst have been reported so far (Scheme 30).[22,23,28,31] Significant advancements in this field were initially made by pioneering studies by Scott and co-workers who developed the chiral cationic zirconium complex **IX**, active towards asymmetric hydroamination of selected secondary aminoalkenes.[31] Schafer and co-workers developed a series of chiral zirconium (bis)amidate complexes (**X**, Ar = Mes, Ind, Ad), which provide good enantioselectivity (*ee* > 90%) for a range of terminal alkenes, but require a geminal dialkyl group to activate the substrates toward cyclization.[23]

Scheme 30 Enantioselective Group 4 metal based hydroamination catalysts.

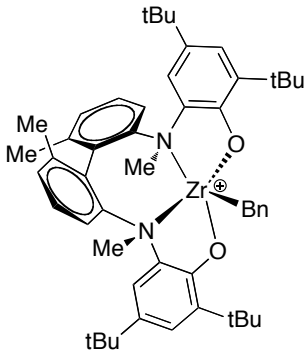

IX

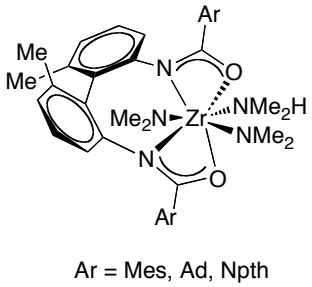

Ar = Mes, Ad, Npth

X

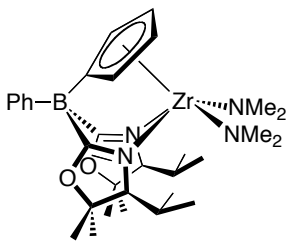

XI

Very recently, Sadow and co-workers reported the preparation of an optically active oxazolynborate based complex (**XI**), which is a highly reactive and non-epimerizable catalyst, that rapidly cyclises a wide range of primary aminoalkenes yielding pyrrolidines with good to excellent enantiomeric excess (*ee*: 89–98 %).[28]

Nevertheless, the development of catalysts for the enantioselective hydroamination of a broad range of aminoalkenes remains a challenging goal.

1.3 Paracyclophane based ligand systems

The use of asymmetric catalysts that do not rely exclusively on tetrahedral chirality is well documented. For instance, such catalysts can possess axial or planar chirality, such as binaphthalene or ferrocene derivatives, respectively. Although the synthesis of [2.2]paracyclophane was firstly reported over 60 years ago,[39] and the introduction of only one substituent is needed to create planar chirality, there are only a few examples of enantioselective catalytic systems based on this compound present in the literature.[40,41,42,43,44] This is despite the fact that these compounds do not undergo racemisation at usual working temperature (< 200 °C),[45] and their cyclophane backbone is chemically stable towards light, temperature, acids, bases and oxidations.[46] The major problem responsible for the non-proliferation of paracyclophane-based catalyst is the lack of fast and effective strategies for the preparation of enantiopure derivatives; the area is, in fact, still dominated by tedious and frequently expensive resolution methods.[47]

[2.2]Paracyclophane chiral derivatives have been used as ligands for asymmetric hydrogenation reactions,[40] enantioselective 1,2- and 1,4-additions of organozinc reagents to aldehydes and imines[42] as well as in palladium catalysed allylic alkylation and aldehydes allylation.[41] Noteworthy are the advancements reported by by Bräse and co-workers with [2.2]Paracyclophane-based *N*,*O*-ligands (Scheme 31, **XII**), and Andrus and co-workers, whith the synthesis of bis-paracyclophane disubstituted *N*-heterocyclic carbenes compounds (Scheme 31,

XIII). Such compounds are very effective in the ruthenium catalyzed asymmetric hydrosilylation of ketones and aryl boron reagents addition to enones in excellent yields and *ee*'s up to 98%.[44]

Scheme 31 Remarkable examples of enantioselective paracyclophane based catalysts.

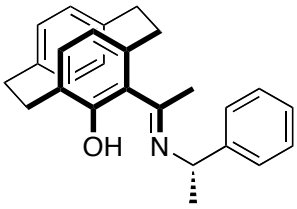

XII

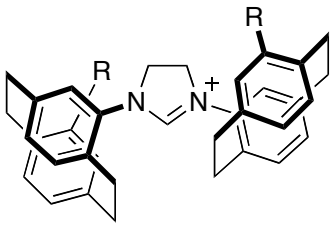

R = H, Ph, Cy, 2-(OMe)C_6H_4

XIII

Despite the popularity of β-diketiminate ligands,[48] little attention has been focused on the design of chiral one. Only one example is to date reported in the literature, which bears a (*S*)-phenylethylamine as the *N*-substituent, **XIV** (Scheme 32). Although firstly obtained by Buch and Harder, in their failed attempts to stabilise benzylcalcium complexes,[49] Schaper and co-workers then proposed an optimised synthesis and also managed to isolate and characterise its copper,[50] zirconium[51] and zinc[52] derivatives. The latter system proved to be catalytically active towards polymerization of *rac*-lactide, producing highly heterotactic polymers; however, no enantioselectivity was observed.[52]

Scheme 32 Bis-(2-phenylethyl)-nacnac (left) and bis-([2.2]paracyclopenyl)-nacnac (right).

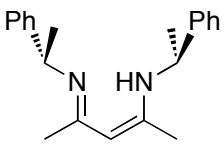

XIV

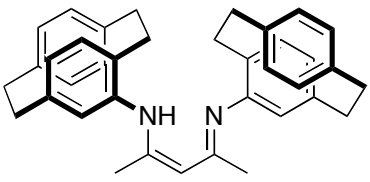

XV

We therefore decided to exploit the planar chirality of monosubstituted [2.2]paracyclophane, attempting the synthesis of a chiral β-diketiminine in which each *N*-substituent is a paracyclophenyl group, **XV** (Scheme 32).

2 Results and Discussion

2.1 Ligand synthesis

2.1.1 (R_p)-amino[2.2]paracyclophane preparation

The syntheses of enantiomerically pure (R_p)-amino[2.2]paracyclophane proposed by Rowlands and Fringuelli were followed and optimised.[53,54] Bromination of [2.2]paracyclophane in presence of iron gave 4-bromo[2.2]paracyclophane, **1**, in 97% yield (Scheme 33). The mechanism of bromination step is consistent with S_EAr mechanism since [2.2]paracyclophane has the same electronic characters as an electron-rich aromatic compound.

Scheme 33 [2.2]Paracyclophane bromination mechanism.

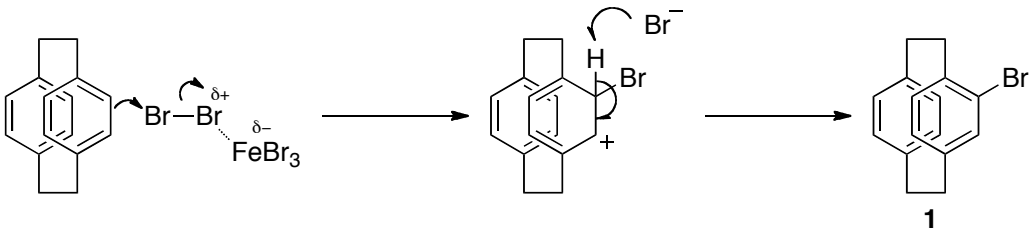

The resulting bromide **1** was lithiatied with ^{n}BuLi and subsequently treated with tosyl azide to give azo[2.2]paracyclophane, **2** (Scheme 34). Reduction of azide with excess $NaBH_4$ (20 eq) in a mixture of THF and water after four days stirring at room temperature produced amino[2.2]paracyclophane, **3**, in 48% yield after purification by column chromatography. Resolution of the racemic amine was achieved by multiple recrystallisations of the diastereoisomeric salts formed by

treatment with stoichiometric amount of (*S*)-(+)-10-camphorsulfonic acid in ethyl acetate, yielding the (R_p) enantiomer **(R_p)-3** in 38% yield and 94% *ee*.

Scheme 34 (*R*)-amino[2.2]paracyclophane synthesis.

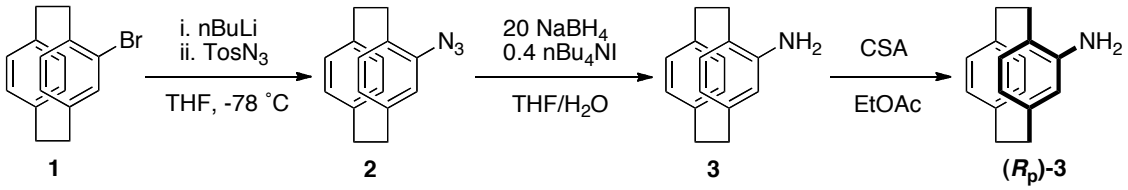

Unfortunately the resolution step takes about a month and a half, so, following the procedure proposed by Ma for the resolution of (±)-4-amino-13-bromo-[2,2]-paracyclophane,[55] we tried to resolve the amine using a chiral auxiliary reagent, (*R*)-(–)-10-camphorsulfonyl chloride ((–)-CSC), converting the amine to a mixture of diasteroisomeric amides in presence of triethylamine (Scheme 35). These could then be separated by flash chromatography. Unfortunately, the very small R_f difference of the two diasteromers makes this procedure not feasible.

Scheme 35 Attempted alternative resolution of amino[2.2]paracyclophane .

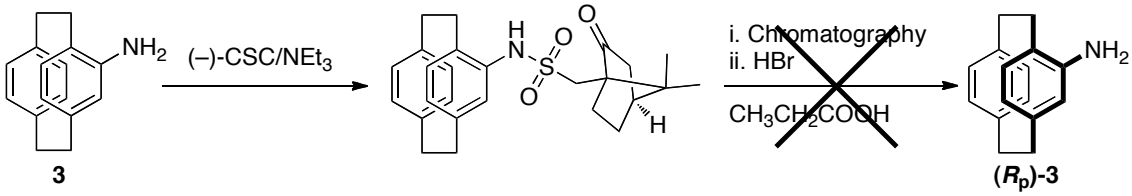

Another synthetic route for the synthesis of amino[2.2]paracyclophane was investigated (Scheme 36). Compound **3** can also be obtained by the reduction of [2.2]nitroparacyclophane (**4**), synthesised by Cram and co-workers in poor yield from [2.2]paracyclophane using a nitrating mixture consisting of fuming nitric acid in acetic acid at 80 °C.[56] Optimised reduction to the amine was proposed by Neugebauer and carried out with H_2 in the presence of Pd-$BaSO_4$.[57] However, low

yields and unfavourable reaction conditions makes preferable a recent new synthetic route proposed by Langer and co-workers,[58] safer and more efficient. They reported the treatment of [2.2]paracyclophane with Nafion® NR-50 superacidic ion exchange resin (H^+ form), previously incubated in 100% nitric acid overnight under inert atmosphere, yielding [2.2]nitroparacyclophane, **4**, in 95% yield. Subsequent treatment with KOH, triirondodecacarbonyl and 18-crown-6 in a biphasic toluene/water solvent system afforded the racemic [2.2]aminoparacyclophane. Under mild condition [$Fe_3(CO)_{12}$)] is converted in situ to the powerful reducing species [$Fe_3(CO)_{11}$)]$^{\cdot-}$. The use of a biphasic system toluene/aqueous KOH and 18-crown-6 acting as phase-transfer catalyst led to a straightforward reaction to the amine.

Scheme 36 Proposed alternative synthetic route for [2.2]aminoparacyclophane.

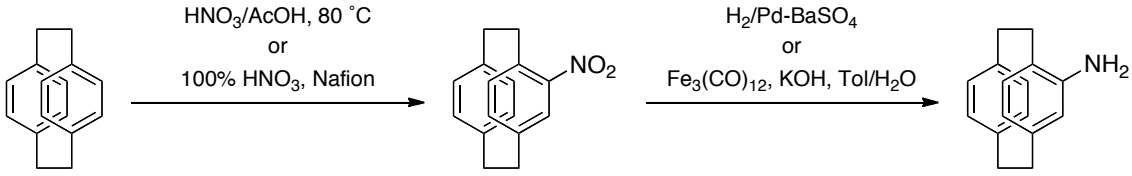

1 **4** **3**

The latter synthetic route was followed, however, despite succeeding in the nitration of [2.2]paracyclophane in good yields (70%), repeated attempts of reduction with KOH, $Fe_3(CO)_{12}$ and 18-crown-6 never resulted in a clean conversion to the amino derivative, which was never detected in the ^{1}H NMR spectrum of the crude reaction mixture.

2.1.2 Ligand synthesis

Synthesis of β-diketiminate ligand via direct double condensation of amino[2.2]paracyclophane (2 eq) with acetylacetone catalysed by hydrochloric acid was previously reported to be unsuccessful.[59] Initial attempts of synthesis via well established synthetic routes for the synthesis of bulky β-diketiminate compounds unfortunately proved to be unsuccessful too, using titanium tetrachloride or the Meerwin reagent $[Et_3O][BF_4]$.[48,60,61]

Following the work done by Barua and co-workers, who reported the iodine-catalysed conversion of β-diketones into β-enaminones with high yield,[62] the amine **(R_p)-3** was treated with acetylacetone in the presence of a catalytic amount of iodine (20%). The corresponding enaminoketone (R_p)-(papo)H (**(R_p)-5**) was obtained in 75% yield after purification by column chromatrography (Scheme 37).

Scheme 37 Synthesis of **(R_p)-5** via iodine catalysed condensation.

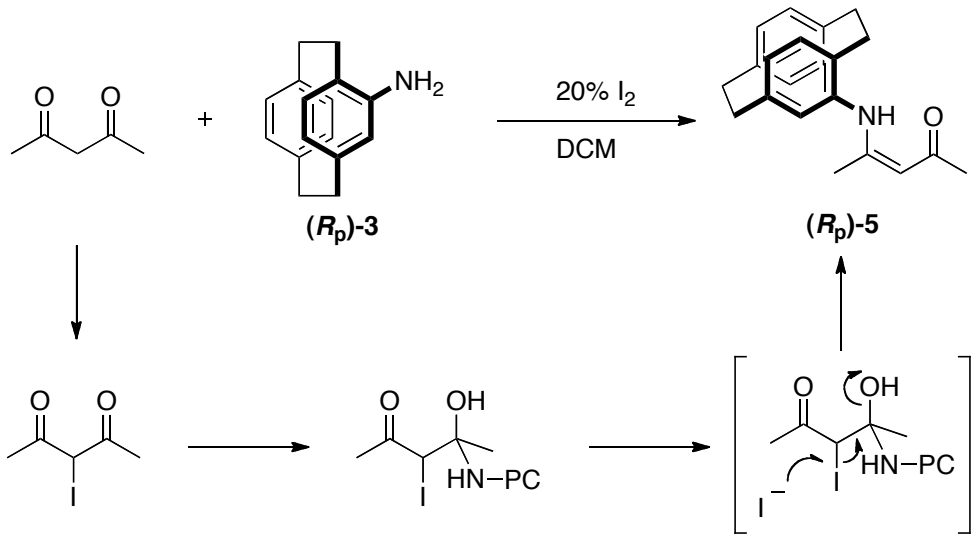

Compound **(R_p)-5** was charachterised by mass spectrometry, X-ray structural analysis, ^1H and ^{13}C NMR and IR spectroscopy. The ^1H NMR spectrum shows the typical paracyclophenyl pattern in the aromatic and alkyl regions. Three

characteristic singlets for compound **(R_p)-5** are observed: the enamine proton (δ 12.33 ppm), the aromatic proton in *ortho* position (δ 6.01 ppm) and the methine proton in the C_3NO backbone (δ 5.20 ppm). Single crystals suitable for an X-ray diffraction study were obtained by cooling a warm saturate ethyl acetate solution to room temperature, followed by overnight evaporation (Figure 31). The hydrogen atom H1 on the nitrogen was located and refined. Although the C–C bond length pattern is in agreement with an enaminoketone structure, all the bond lengths are in between the typical single and double bond lengths (Table 15).

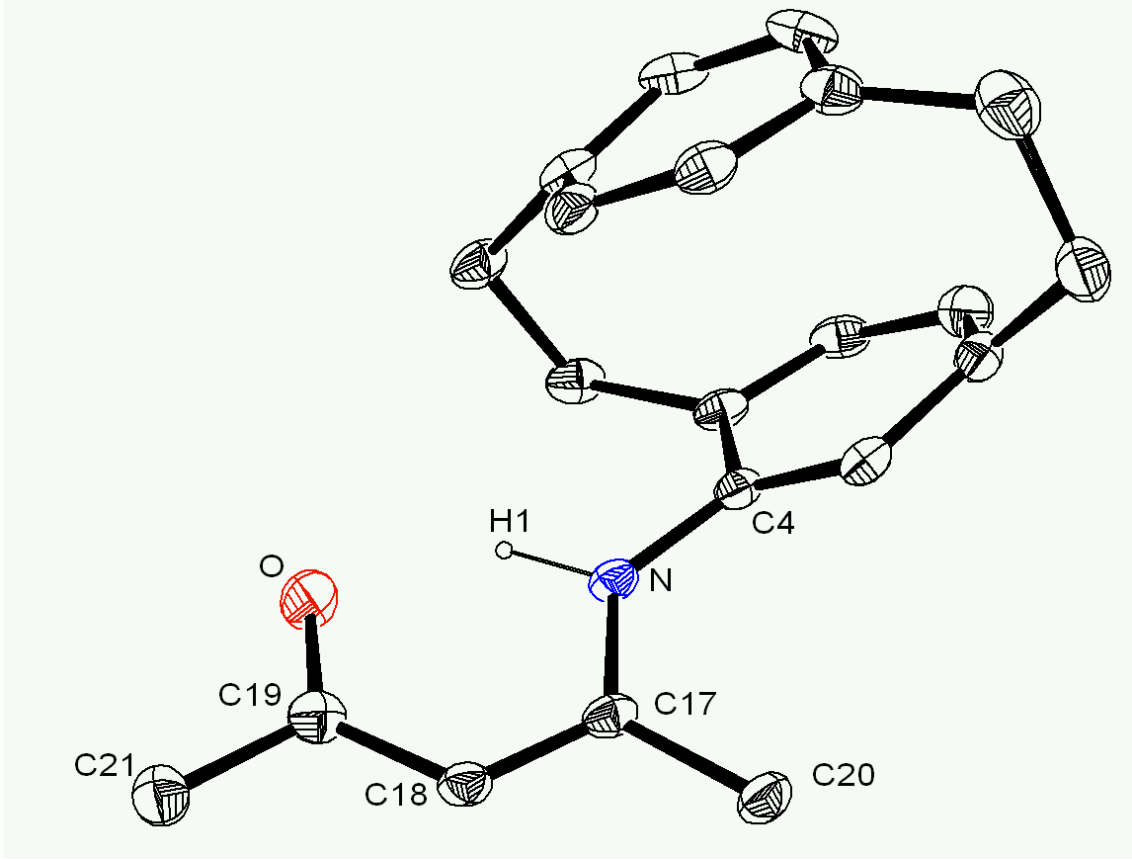

Figure 31 ORTEP diagram of (R_p)-(papo)H, **(R_p)-5**. Only H1 hydrogen atom is shown for clarity. Thermal ellipsoids are shown at 30%.

Table 15 Selected bond lengths (Å) and angles (deg) for compound **(R_p)-5**.

C19–O	1.261(5)	C21–C19–O	118.8(4)
C17–N	1.359(4)	O–C19–C18	123.0(3)
C21–C19	1.502(6)	C21–C19–C18	118.2(3)
C19–C18	1.412(5)	C19–C18–C17	125.0(3)
C18–C17	1.370(5)	C18–C17–C20	120.4(3)
C17–C20	1.503(5)	C18–C17–N	119.5(3)
N–C4	1.414(5)	C20–C17–N	120.1(3)
		C17–N–C4	129.7(3)

For instance, the observed C–O bond length is 1.261(5) Å (C–OH: av. 1.432; $(C)_2C{=}O$: av. 1.210 Å), C–N bond length is 1.359(4) Å (C–N: av. 1.469; C–C=N–C: av. 1.279 Å) and C–C bond lengths are 1.412(5) and 1.370(5) Å (C–C: av. 1.530; $(C)HC_{sp2}{=}\ C_{sp2}(C)2$: av. 1.326 Å).[63] This can be attributed to a partial delocalisation of the π-electrons along the conjugated planar C_3NO backbone. The sum of bond angles around the atoms of the backbone is for all close to 360°. This data are similar to the bulky enaminoketone TbtNHC(Me)CHC(O)Me (Tbt = 2,4,6-$[CH(SiMe_3)_2]_3C_6H_2$)) reported by Tokitoh and co-workers.[61]

Refluxing a toluene solution of **(R_p)-5** with a stoichiometric equivalent of *para*-toluenesulfonic acid, with water removed by azeotropic distillation, led to the desired β-diketimine, (R_p,R_p)-(PacNac)H, **(R_p,R_p)-6**, in 67% yield and 98% *de* after purification by column chromatography (eq 4).

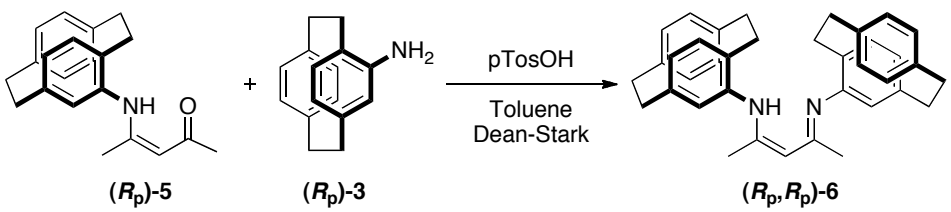

(R_p)-5 (R_p)-3 (R_p,R_p)-6 (4)

Compound **(R_p,R_p)-6** is not soluble in aliphatic polar and non-polar solvents, while moderate solubility was observed in THF, dichloromethane and aromatic

hydrocarbons. It has been charachterised by multinuclear NMR and IR spectroscopy and mass spectrometry. The ^{1}H NMR spectroscopic analysis shows a single resonance for the methyl protons of the ligand backbone (δ = 1.89 ppm), suggesting a symmetric disposition of the molecule. Three characteristic singlet spectral resonances are present at δ 11.96, 6.17 and 4.89 ppm, respectively corresponding to the N*H*, *o*-C*H* and γ-C*H* proton. Unfortunately, it still has not been possible to grow single crystals of **(*R*$_p$,*R*$_p$)-6** suitable for X-ray structural analysis. DFT geometry optimisation at the B3LYP/6-31g(d,p) was performed in order to simulate the molecular structure of the diketimine **(*R*$_p$,*R*$_p$)-6** (Figure 32).

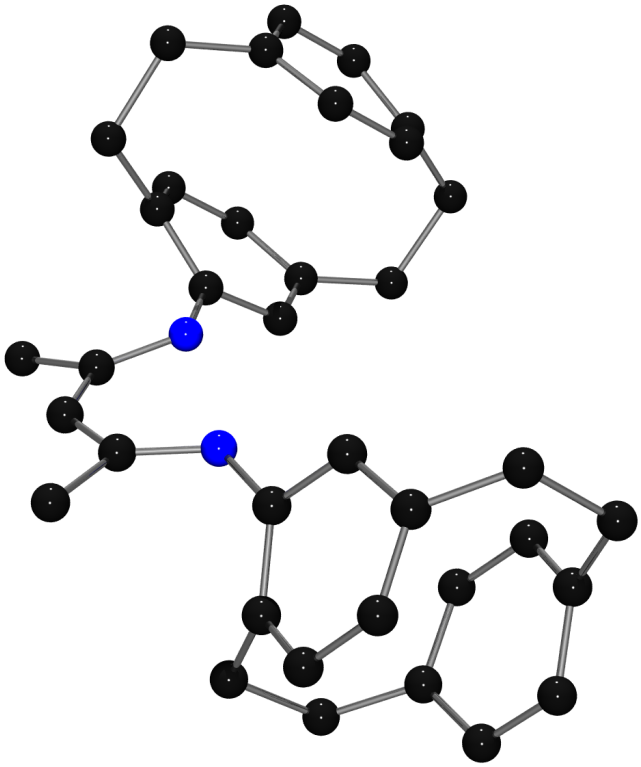

Figure 32 POV-Ray diagram of the DFT optimised structure of (*R*$_p$,*R*$_p$)-(PacNac)H, **(*R*$_p$,*R*$_p$)-6**, at the B3LYP/6-31g(d,p) level of theory.

2.2 PacNac and papo derivated complexes

2.2.1 (PacNac)ScCl$_2$ synthesis

A toluene solution of **(R_p,R_p)-6** was treated with 1eq of ^{n}BuLi at -78 °C and was added to a stirred suspension of $ScCl_3 \cdot (THF)_3$ after 1 h. The resulting mixture was stirred overnight at 60°C, presumably resulting in the formation of the dichloride complex **(R_p,R_p)-7** in 61% yield (eq 5).

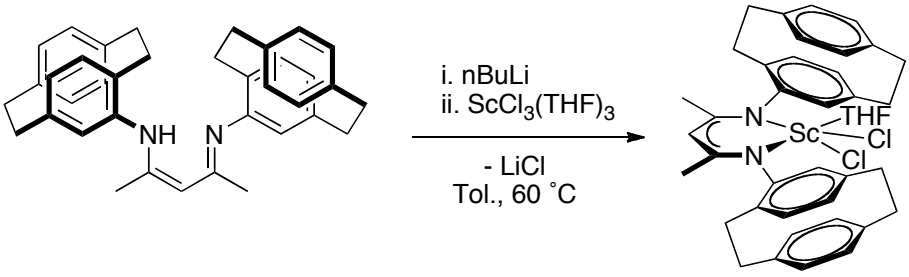

(R_p,R_p)-6 (R_p,R_p)-7 (5)

Running the reaction at room temperature resulted in no conversion to **(R_p,R_p)-7**, while heating the mixture up to 90°C resulted in partial decomposition, producing protonated ligand **(R_p,R_p)-6**. Unfortunately, this synthetic route proved to be not reproducibile. In fact, both the lithiation and the methatesis step sometimes results in the formation of protonated ligand. Moreover, it has not been possible either to crystallise the product or to wash it to get rid of the eventual presence of protonated ligand, as both are soluble in aromatic solvents and THF and nearly completely insoluble in aliphatic polar and non-polar solvents.

Attempts in converting **(R_p,R_p)-7** into the dimethyl or di-methyltrimethylsilyl derivatives **(R_p,R_p)-8–9** (eq 6, Figure 33), in > 50 mg scale, always resulted in the formation of (PacNac)H, despite promising results shown in NMR scale test reactions.

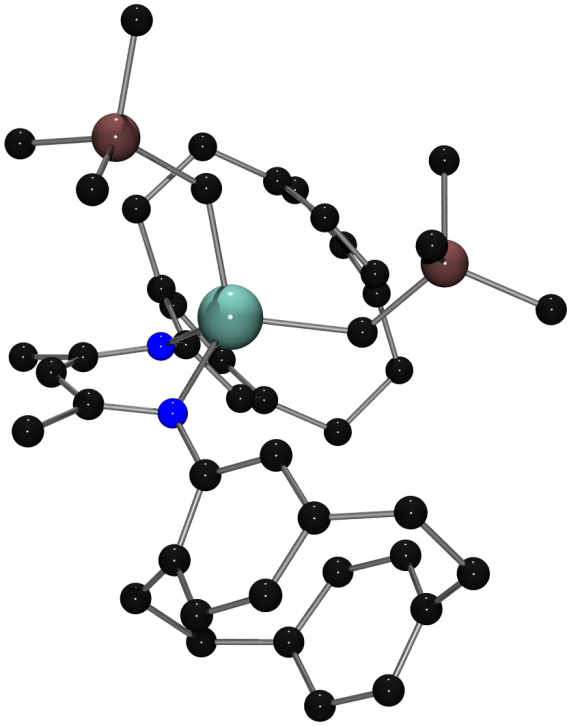

Figure 33 POV-Ray diagram of the DFT optimised geometry of compound **(R_p,R_p)-9** at the B3LYP/LanL2dz/6-31g(d,p) level of theory.

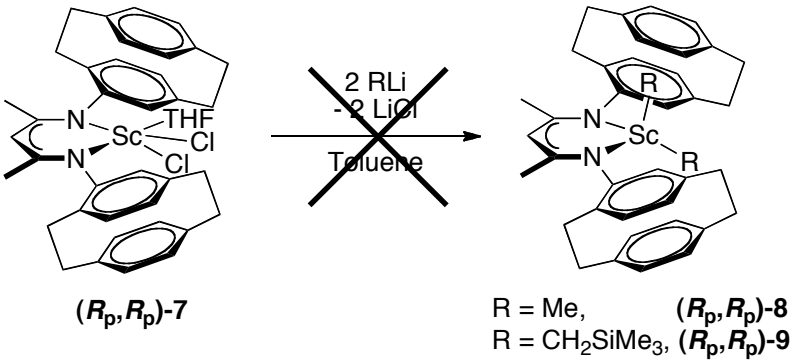

(R_p,R_p)-7

R = Me, (R_p,R_p)-8
R = CH_2SiMe_3, (R_p,R_p)-9

(6)

The alkyl complexes **(R_p,R_p)-8–9** obtained in NMR scale were treated *in situ* with 10 equivalents of 2,2-diphenyl-1-amino-4-pentene and 5-phenyl-4-pentyn-1-amine. However, no activity towards the intramolecular hydroamination of either diphenyl-1-amino-4-pentene or 5-phenyl-4-pentyn-1-amine was observed.

2.2.2 (papo)$_2$Zr(NMe$_2$)$_2$ synthesis

Due to the solubility and crystallisation issues presented by PacNac derivatives, as well as the low availability of amino[2.2]paracyclophane, and encouraged by the good results obtained by Schafer and co-workers in the utilisation of N,O-ligands for zirconium catalysed hydroamination,[25,29] attention turned to the enaminone (papo)H, **(R_p)-5**, as potential ligand for zirconium catalised enantioselective hydroamination.

Treatment of the enaminone **(R_p)-5** (2 eq) with Zr(NMe$_2$)$_4$ in toluene resulted in the heteroleptic (papo)$_2$Zr(NMe$_2$)$_2$ complex, **(R_p)-10** (eq 7). Interestingly, reaction with equimolar amounts of the ligand and Zr(NMe$_2$)$_4$ results in the formation of **(R_p)-10** as well, with a leftover unreacted half equivalent of the zirconium amide.

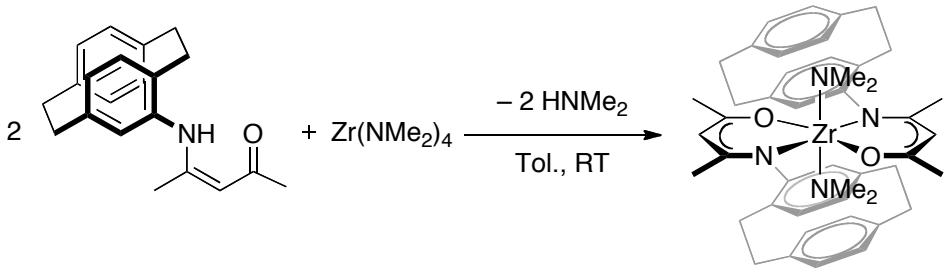

(7)

(R_p)-5 (R_p)-10

Compound **(R_p)-10** was characterised by multinuclear NMR and IR spectroscopy. The ^{1}H NMR spectrum exhibits the typical paracyclophane pattern, with the *o*-C*H* singlet spectral resonance lying at δ 5.60 ppm, while the key signals of the C_5H_7 ligand backbone lie at δ 4.69, 2.70 and 1.72 ppm, corresponding to the methine and two methyl environments. The dimethyl amide substituents resonate at 2.32 ppm, in accordance with similar systems.[25,28] The 1:1 ratio between the integration of the spectral resonances corresponding to the amide substituents

and the *N*,*O*-ligand confirms the presence of two enaminone molecule around the zirconium center.

Although treatment of the enamine proligand **(R_p)-10** with $Zr(NMe_2)_4$, followed by the addition of 10 eq 2,2-diphenyl-1-amino-4-pentene *in situ* and heating to 100 ˚C resulted in the formation of the corresponding pyrrolidine, treatment of isolated crystals of $(papo)_2Zr(NMe_2)_2$ with 10 eq of the aminoalkene showed no catalytic activity whatsoever. This can be attributed to the reported capability of $Zr(NMe_2)_4$ of giving conversion of primary aminoalkenes to the cyclised product,[25] therefore proving a lack of catalytic activity of the proposed system.This lack of activity was also observed with aminoalkynes such as 5-phenyl-4-pentyn-1-amine.

Unfortunately X-ray ray crystallography resulted in the analysis of a minor colourless byproduct $[(Me_2N)_3Zr(\mu\text{-}NMe_2)(\mu\text{-}O)Zr(NMe_2)_2]_2$, **11**, presumably resulting from the reaction of $Zr(NMe_2)_4$ with O_2 with the possible elimination of tetramethylhydrazine (eq 8). A similar reaction was previously reported by Wu and Xue, in which a trinuclear oxo aminoxide complex $Zr_3(NMe_2)_6(\mu\text{-}NMe_2)_3(\mu_3\text{-}O)(\mu_3\text{-}ONMe_2)$ was formed as a result of the treatment of excess $Zr(NMe_2)_4$ with O_2.[64]

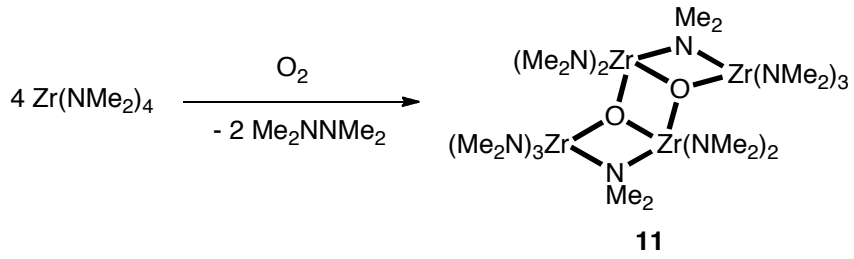

11 (8)

The molecule lies on an inversion center (Figure 34). It consists of three fused four-membered rings: the central $[Zr_2O_2]$ core and two peripheral $[Zr_2NO]$ units. Each oxygen atom is tricoordinate and bridging between peripheral–central (Zr1–

Zr2 and Zr1–Zr2') and central–central (Zr2–Zr2') zirconium atoms. The peripheral zirconium atom (Zr1) is coordinated to three dimethylamide substituents (N1, N2 and N3), plus a fourth amide bridging with the core zirconium atom (Zr1–N4–Zr2). Each central zirconium atom is coordinated to two further amide groups (N5, N6).

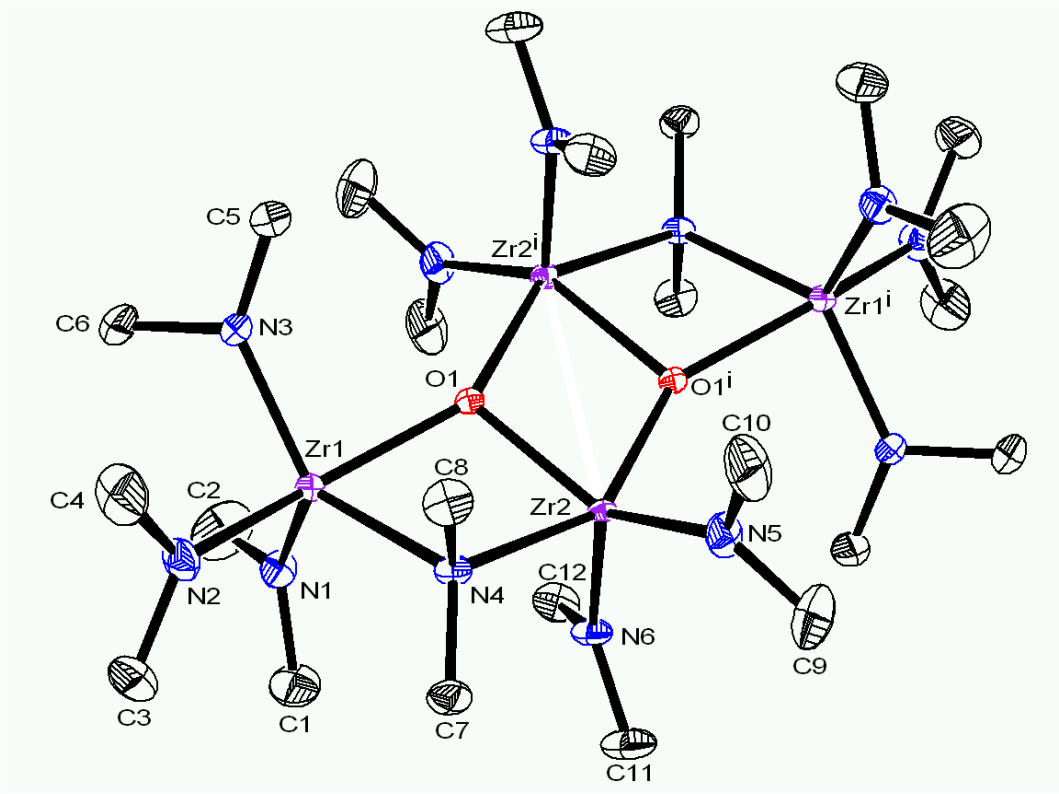

Figure 34 ORTEP diagram of $[Zr_2(NMe_2)_6O]_2$, **11**. Hydrogen atoms are omitted for clarity. Thermal ellipsoids at 30%. Atoms marked with a prime (^{i}) are at equivalent positions (–*x*, –*y*, –*z*).

The Zr–N bond lengths are between 2.0412(2) Å and 2.097(2) Å, with the exception of the bridging amide (2.2818(19) and 2.282(2) Å). The Zr–O bond lengths are 2.0725(15) and 2.0844(15) Å for the central Zr1–O bonds, and longer for the peripheral Zr–O bonds (Zr1–O1 = 2.2013 Å). Interestingly, the ^1H and ^{13}C NMR analyses show only a singlet spectral resonance for the dimethyl amide groups at δ 2.94 and 42.9 ppm respectively, indicating of a fluxional structure in solution. All these observations, regarding bond lengths and spectroscopic data,

are in accordance with the previously reported $Zr_3(NMe_2)_6(\mu\text{-}NMe_2)_3(\mu_3\text{-}O)(\mu_3\text{-}ONMe_2)$ complex.[64] No attempts to make this compound independently were performed.

2.3 Future work

Despite not being fully characterised, preliminary tests showed no activity of the proposed complexes towards hydroamination. Also, the difficulty in the synthesis of the ligand, as well as the tedious and non efficient resolution of [2.2]aminoparacyclophane, make this system unattractive towards further investigations.

Attention should then be focused on more easily synthesisabe planar chiral substituents to be incorporated as the *N*-substituents in β-diketiminate ligands, such as chiral substituted ferrocenyl amine. Preliminary work in this direction holds good promise for the future.

3 Experimental

3.1 General considerations

Chemicals were commercially purchased from Acros, Fisher or Aldrich and used as received, unless otherwise stated. [2,2]Paracyclophane was purchased from Galentis. Nafion® NR 50 1100 EW superacidic resin was purchased from Ion Power. $ScCl_3 \cdot H_2O$ was generously donated by Prof. F.G.N. Cloke. PCBr,[53] PCN_3,[54] $PCNO_2$,[65] $PCNH_2$,[54] (R_p)-$PCNH_2$,[53] $Fe_3(CO)_{12}$,[66] $Sc(CH_2SiMe_3)_3 \cdot 2THF$[67] and $Zr(NMe_2)_4$[68] were prepared accordingly to literature procedures. $ScCl_3(THF)_3$ synthesis[69] was modified under the suggestion of Prof. F. G. N. Cloke. 2,2-Diphenyl-1-amino-4-pentene[14] and 5-phenyl-4-pentyn-1-amine[10] were prepared according to literature procedures and freshly distilled over CaH_2 before use. The ^1H and ^{13}C NMR spectra were recorded on Varian 400 MHz or Varian 500 MHz spectrometers. All the spectrometers were equipped with X{^1H} broadband-observe probes. ^1H and ^{13}C NMR spectroscopy chemical shifts are given relative to residual solvent peaks. The ^1H–^{13}C HSQC and ^1H–^{13}C HMBC spectra were recorded using the Varian ChemPack 4.1 sequences gHSQCAD and gHMBCAD. IR spectrophotometry was carried out on a Perkin-Elmer 1500 FT-IR instrument. Elemental analyses were carried out by London Metropolitan University. The data for X-ray structures were collected at 173 K on a Nonius KappaCCD diffractometer, k(Mo-Kα) = 0.71073 Å and refined using the *SHELXL-97* software package.[70] Enantiomeric excess of **(R_p)-3** and diasteroisomeric excess of **(R_p,R_p)-6** was determined by HPLC analysis on a

25 × 0.46 cm cellulose tris(3,5-dimethylphenylcarbamate) column (Chiracel OD, Diacel) 8:2 hexane:2-propanol as the eluent at 2mL/min flow rate.

3.2 Synthetic procedures

(±)-4-bromo[2,2]paracyclophane (**1**). A solution of bromine (7.8 mL, 0.15 mol) in dichloromethane (1.5 L) was prepared and 150 mL of such solution were added to a flask containing iron turnings (2.42 g, 0.04 mol, 0.3 equiv) under nitrogen and protected from light. Afterwards a solution of [2.2]paracyclophane (30 g, 0.14 mol) in dichloromethane (1.5 L) was added to the reaction flask in one portion, followed by addition of the rest bromine solution. The mixture was stirred under for 0.5 hours. The reaction was poured into saturated ammonium chloride (2 L) and extracted with dichloromethane (3×400 mL). The combined organic phase was washed with sodium thiosulfate (2 L) and dried with $MgSO_4$. After evaporation, PCBr **1** was given with 40 g (97%). ^{1}H NMR (500 MHz, $CDCl_3$) δ 7.17 (d, 1H, J = 7.9), 6.59 – 6.44 (m, 6H), 3.46 (d, 1H), 3.25–2.80 (m, 8H). The ^{1}H spectrum analysis is in agreement with literature data:[53] ^{1}H NMR δ 7.16 (1H, d, J=7.8), 6.58–6.44 (6H, m), 3.47 (1H, d, J=12.4), 3.18–2.80 (8H, m).

(±)-4-azo[2,2]paracyclophane (**2**). A solution of ^{n}BuLi (2.37 M in hexane, 70 mL, 165 mmol) was added dropwise to a solution of PCBr **1** (40 g, 139 mmol) in THF (1.6 L) at -78°C. The yellow solution was stirred for 1 hour and then was added to a solution of tosyl azide (33 g, 167 mmol) in THF (100 mL) in one portion. The reaction mixture was warmed up to room temperature overnight. The reaction

mixture was poured into saturated ammonium chloride solution and extracted with Et_2O (3×400mL). The organic phase was dried with $MgSO_4$ and concentrated. The crude product PCN_3 **2** was identified by ^{1}H-NMR and used for the next step without further purification. ^{1}H NMR (400 MHz, $CDCl_3$): δ 6.87 (d, 1H, J = 7.9), 6.55 – 6.38 (m, 5H), 5.97 (s, 1H), 3.37 – 3.30 (m, 1H), 3.13 – 3.00 (m, 8H), 2.68 – 2.60 (m, 1H). The ^{1}H spectrum analysis is in agreement with literature data:[54] 6.88 (1H, d, *J*=7.8), 6.45-6.48 (6H, m), 3.34 (1H, m), 3.08-3.01 (6H, m), 2.61-2.66 (1H, m).

(±)-4-amino[2,2]paracyclophane (**3**). $NaBH_4$ (27 g, 720 mmol, 10 equiv), PCN_3 **2** (18 g, 72 mmol, 1.0 equiv) and ^{n}Bu_4NI (10.67g, 29 mmol, 0.4 equiv) were all suspended in a solvent mixture of THF (650 mL) and H_2O (530 mL) and the reaction mixture was stirred at room temperature overnight. An additional 10 more equivalents of $NaBH_4$ (27 g, 720 mmol) was then added to the stirring solution and the reaction was stirred for 3 days. The reaction mixture was poured onto H_2O and extracted with Et_2O (3×250mL). The organic phase was dried with $MgSO_4$ and concentrated. The crude residue was purified by chromatography (4:1 petrol (60-80):Et_2O then 2:1 petrol (60-80):Et_2O) to give $PCNH_2$ **3** (6.1 g, 40%). ^{1}H NMR (500 MHz, CDCl3) δ 7.19 (1H, d, *J* = 7.8), 6.61 (1H, d, *J* = 7.8), 6.43 – 6.39 (2H, m), 6.29 (1H, d, *J* = 7.7), 6.15 (1H, d, *J* = 7.7), 5.39 (1H, s), 3.45 (2H, br), 3.18 – 2.93 (6H, m), 3.00 – 2.78 (1H, m), 2.74 – 2.61 (1H, m). The ^{1}H spectrum analysis is in agreement with literature data:[53] ^{1}H NMR δ 7.15 (dd, J = 7.8, 1.8, 1 H), 6.6−6.0 (m, 5 H), 5.36 (d, J = 1.4, 1 H), 3.3 (br s, 2 H), 2.55−3.15 (m, 8 H).

(*R*$_p$)-(−)-4-amino[2,2]paracyclophane (***R*$_p$-3**). (1*S*)-(+)-10-Camphorsulfonic acid (1.92 g, 40 mmol) was added to a solution of racemic 4-amino[2.2]paracyclophane

3 (1.84 g, 40 mmol) in EtOAc (140 mL). The mixture was stirred at 0°C for 48 hours, after which a white precipitate appeared. After filtration, the resulting solid was poured into fresh EtOAc (45 mL) and stirred for 60 hours at room temperature. The last treatment (filtration, addition of EtOAc and stirring for 60 h) was repeated six more times. The resulting salt was then filtered and treated with 0.1 M sodium hydroxide to give (R_p)-$PCNH_2$ ***R_p*-3** (0.58 g, 32%, 94% *ee*). Enantiomeric excess was determined by HPLC analysis. R_t: S_p, 8 min; R_p, 20 min.

(±)-4-nitro[2,2]paracyclophane (**4**). Acidic ion exchange resin (Nafion®) (50 g) was incubated with nitric acid (100 %; 11 mL) under an N_2 atmosphere for 12 h and subsequently rinsed five times with dichloromethane. [2.2]Paracyclophane (840 mg, 4 mmol) was dissolved in dichloromethane (100 mL) and added to a suspension of the superacidic resin in dichloromethane (100 mL). After the mixture had been stirred for 90 min at 0˚ C and 60 min at room temperature, the suspension was quenched with ice water, extracted with diethyl ether, and purified by column chromatography to yield $PCNO_2$ in 95% yield. ^{1}H NMR (500 MHz, $CDCl_3$): δ 7.26 (s, 1H), 6.79 (d, 2H, J = 7.8), 6.62 (d, 2H, J = 7.6), 6.57 (d, 2H, J = 5.9), 6.48 (d, 2H, J = 7.8), 4.03 (s, 1H), 3.48–2.72 (m, 8H). The ^{1}H spectrum analysis is in agreement with literature data:[65] δ 7.23–7.33 (3 H, CH), 6.63–6.95 (4H), 4.10(1H), 3.30–2.88 (8H). *Nafion® beads were recovered and reactivated by washing several times with water, methanol and dichloromethane, followed by drying overnight at 60 ˚C.*

[$CH_3C(O)CHC(CH_3)N$-(R_p)-$C_{16}H_{15}$]H (***R_p*-5**). Iodine (165 mg, 0.65 mmol) was added to a dichloromethane (100 mL) solution of ***R_p*-3** (0.73 g, 3.28 mmol) and

acetylacetone (0.34 mL, 3.28 mmol) at room temperature. After stirring for 1h the solution was extracted with a saturated solution of NaS_2O_3. The combined organics were dried over $MgSO_4$ and purified by column chromatography (eluent dichloromethane:methanol 9:1) affording (papo)H ***R*$_p$-5** in 75% yield (0.75 g). Storage of an ethyl acetate saturated solution at -32 ˚C for 3 days afforded crystals suitable for X-ray crystallography. ^{1}H NMR (500 MHz, $CDCl_3$): δ 12.33 (s, 1H, N-*H*), 7.17 (d, J = 7.8, 1H, Ar*H*), 6.66 – 6.27 (m, 5H, Ar*H*), 6.01 (s, 1H, NCC*H*), 5.20 (s, 1H, γ-C*H*), 3.19 – 2.94 (m, 8H, ArCH_2CH_2Ar), 2.18 (s, 3H, C*Me*), 1.77 (s, 3H, C*Me*). ^{13}C{^{1}H} NMR (500 MHz, $CDCl_3$): δ 195.9 (*C*=O), 160.9 (Me*C*N), 141.0, 138.5, 138.9, 137.4, 135.0, 135.0, 133.5, 132.9, 131.9, 130.5, 128.3 (^{Ar}*C*), 96.95 (γ-*C*), 35.2, 34.8, 33.9, 32.6 (ArC*C*Ar), 29.11 (C*Me*), 19.59 (C*Me*). MS (EI) *m/z* 305, 263, 248, 201, 43.

[CH{(CH$_3$)CN-(*R*$_p$)-C$_{16}$H$_{15}$}$_2$H] (***R*$_p$,*R*$_p$-6**). ***R*$_p$-3** (0.55g , 2.46 mmol), (papo)H ***R*$_p$-5** (0.75 g, 2.46 mmol) and *para*-toluenesulfonic acid monohydrate (0.47g, 2.46 mmol) were combined in a round bottomed flask in 30 mL toluene. A Dean-Stark apparatus was attached and the solution brought to reflux. After the required amount of water had been removed the solution was cooled and reduced under vacuum. The resulted solid was treated with DCM, water and Na_2CO_3 (1.5 equivalents). The mixture was stirred until all solids had been dissolved. The water layer was removed and extracted with DMC. The combined organic layers were dried over $MgSO_4$ and purified by column chromatography (eluent DCM : MeOH 9 : 1) affording (PacNac)H ***R*$_p$,*R*$_p$-6** in 67% yield (0.84 g). ^{1}H NMR (500 MHz, $CDCl_3$): δ 11.96 (br, 1H, N-*H*), 7.35 (d, J = 6.8, 2H, Ar*H*), 6.70 (d, J = 6.4, 4H, Ar*H*), 6.65 (d, J = 6.8, 2H, Ar*H*), 6.47 (d, J = 7.4, 2H, Ar*H*), 6.39 (d, J = 7.1, 2H, Ar*H*), 6.17 (s, 2H, NCC*H*), 4.89 (s, 1H, γ-C*H*), 3.28 – 2.72 (m, 16H, ArCH_2CH_2Ar), 1.82 (s, 6H, NC*Me*). ^{13}C{^{1}H}

NMR (500 MHz, $CDCl_3$): δ 160.0 (N*C*Me), 144.5, 140.7, 140.3, 139.5, 135.4, 133.2, 133.0, 132.9, 132.5, 129.1, 129.0, 128.9 (^{Ar}C), 97.2 (γ-*C*H), 35.5, 35.2, 34.6, 33.2 (ArC*C*Ar), 21.6 (N*C*Me). MS (EI) *m/z* 510, 406, 263, 248, 144, 119.

$ScCl_3(THF)_3$. $ScCl_3 \cdot 6H_2O$ (1.0 g) was suspended in tetrahydrofuran (50 mL) under a N_2 atmosphere. Trimethylsilyl chloride (24 eq) was added dropwise and the solution was refluxed for 6 hours. Filtration and washing with pentane afforded $ScCl_3(THF)_3$ as a white powder in 94% yield.

[CH{(CH_3)CN-(R_p)-$C_{16}H_{15}$}$_2$]$ScCl_3$·THF (R_p,R_p-7). ^{n}BuLi (2.35M, 208 µL, 0.49 mmol) was added dropwise to a stirred solution of PacNac ***R_p,R_p*-6** (250 mg, 0.49 mmol) at -78°C. The solution turned from yellow to red and was warmed up to room temperature and left stirring for 30 min. ^{1}H NMR (399 MHz, C_6D_6): δ 7.19 (d, J = 7.6, 2H, Ar*H*), 6.59 (d, J = 7.6, 2H, Ar*H*), 6.46 (d, J = 7.7, 2H, Ar*H*), 6.34 (d, J = 7.7, 2H, Ar*H*), 6.20 (d, J = 7.5, 2H, Ar*H*), 5.96 (s, 2H, NCC*H*), 4.85 (s, 1H, γ-C*H*), 3.40 – 2.55 (m, 16H, ArC*H*$_2$CH$_2$Ar), 1.98 (s, 6H, NC*Me*). The solution was then added to a stirred suspension of $ScCl_3(THF)_3$ (179 mg, 0.49 mmol) in toluene and warmed up to 60°C and left stirring overnight. The solution was then filtered through celite and dried under vacuum yielding ***R_p,R_p*-7** as a brown powder in 61% yield (342 mg). ^{1}H NMR (399 MHz, C_6D_6): δ 7.20 (d, J = 10.5, 2H, Ar*H*), 6.98 (d, J = 7.6, 2H, Ar*H*), 6.58 (d, J = 7.6, 1H, Ar*H*), 6.32 (d, 1H, Ar*H*), 6.25 (d, J = 7.8, 1H, Ar*H*), 6.19 (d, J = 7.9, 1H), 6.03 (d, J = 7.0, 1H d, J = 7.6), 5.89 (d, J = 8.1, 1H d, J = 7.6), 5.83 (d, J = 7.6, 2H, Ar-*H*), 5.78 (s, 1H, *H*-5), 5.61 (s, 1H, *H*-5), 4.73 (s, 1H, γ-C*H*), 2.64 (m, 16H, *H*-1, *H*-2, *H*-9, *H*-10), 2.30 (s, 3H, NC*Me*), 2.07 (s, 3H, NC*Me*).

$[CH_3C(O)CHC(CH_3)N\text{-}(R_p)\text{-}C_{16}H_{15}]_2Zr(NMe_2)_2 \bullet (Et_2O)$ (***R_p*-10**). (papo)H ***R_p*-5** was dissolved in toluene (5 mL) and treated dropwise with a toluene solution of tetrakis(dimethylamido)zirconium. The solution turned deep red upon addition and was left stirring at room temperature for 1 h. The solvents were removed in vacuo and the oily residue was washed several times with cold pentane. The resulting solid was dissolved in the minimum amount of diethyl ether and stored in the freezer overnight, yielding deep red crystals of $(papo)_2Zr(NMe_2)_2$ ***R_p*-10** in 75% yield. ^{1}H NMR (400 MHz, C_6D_6) δ 7.49 (d, 2H, J = 7.7, Ar*H*), 6.57 (d, 2H, J = 8.7, Ar*H*), 6.49 (d, 2H, J = 6.8, Ar*H*), 6.47 (d, 2H, J = 6.8, Ar*H*), 6.37 (d, 2H, J = 7.6), 6.49 (d, 2H, J = 6.8, Ar*H*), 6.25 (d, 2H, J = 8.0), 6.49 (d, 2H, J = 6.8, Ar*H*), 5.60 (s, 2H, NCC*H*), 4.69 (s, 2H, γ-C*H*), 3.35 (m, 4H, $ArCH_2CH_2Ar$), 3.23 (q, 4H, J = 7.0, $O(CH_2CH_3)_2$), 2.81 (m, 8H, $ArCH_2CH_2Ar$), 2.70 (s, 6H, C*Me*), 2.53 (m, 4H, $ArCH_2CH_2Ar$), 2.32 (s, 12H, NMe_2), 1.72 (s, 6H, C*Me*), 1.07 (t, 4H, J = 7.0 $O(CH_2CH_3)_2$). $^{13}C\{^1H\}$ NMR (400 MHz, C_6D_6) δ 162.3, 150.5 (*C*Me), 140.0, 139.9, 138.8, 134.4, 133.2, 132.5, 132.2, 129.8, 127.5, 126.9, 126.5 (^{Ar}C), 98.0 (γ-*C*), 65.5 (OCH_2CH_3), 38.8 (NMe_2), 35.5, 35.2, 34.3, (ArC*C*Ar), 32.9, 23.5 (C*Me*), 16.3 (OCH_2CH_3). IR (Nujol, ν/cm^{-1}): 2766, 1615, 1536 (s), 1500 (s), 1483 (s), 1436 (s), 1406, 1356 (s), 1240 (s), 1199, 1175, 1155, 1138, 1106, 1031, 993, 937, 900, 851, 792 (s). Repeated attempts of obtaining elemental analysis for compound ***R_p*-10** were unsuccessful.

General procedure for hydroamination reactions

The catalyst (0.4 M in C_6D_6, 100 μL, 0.04 mmol), ferrocene, as internal standard, (0.4 M in C_6D_6, 100 μL, 0.04 mmol), the aminoalkene/aminoalkyne substrate (4 M

in C_6D_6, 100 μL, 0.4 mmol) and 100 μL of C_6D_6 were loaded into a J. Young NMR tube. The reaction was monitored by ^1H NMR spectroscopy.

General procedure for *in situ* [Zr] catalised hydroamination reactions

The proligand papo(H) (0.4 M in C_6D_6, 100 μL, 0.04 mmol) was treated with $Zr(NMe_2)_4$ (0.4 M in C_6D_6, 100 μL, 0.04 mmol). Ferrocene, as internal standard, was added (0.4 M in C_6D_6, 100 μL, 0.04 mmol) followed by the aminoalkene/aminoalkyne substrate (4 M in C_6D_6, 100 μL, 0.4 mmol), the solution was the diluted with further 100 μL of C_6D_6 and transferred to a J. Young NMR tube. The tube was heated to 100 °C and the reaction monitored by ^1H NMR spectroscopy.

4 References

1. Muller, T. E.; Beller, M., *Chem. Rev.* **1998,** *98* (2), 675-704; Togni, A.; Grtzmacher, H.-J., *Catalytic Heterofunctionalization*. Wiley-VCH: New York, 2001; Alonso, F.; Beletskaya, I. P.; Yus, M., *Chem. Rev.* **2004,** *104* (6), 3079-3160; Hartwig, J. F., *Nature* **2008,** *455* (7211), 314-322; MuÃàller, T. E.; Hultzsch, K. C.; Yus, M.; Foubelo, F.; Tada, M., *Chem. Rev.* **2008,** *108* (9), 3795-3892.
2. Kondo, T.; Mitsudo, T.-a., *Chem. Rev.* **2000,** *100* (8), 3205-3220; Delacroix, O. G., A. C., *Curr. Org. Chem.* **2005,** *9*, 1851-1882.
3. Royer, J., *Asymmetric Synthesis of Nitrogen Heterocycles*. Wiley-VCH: Weinheim, 2009.
4. O'Hagan, D., *Nat. Prod. Rep.* **2000,** *17* (5), 435-446; Mitchinson, A.; Nadin, A., *J. Chem. Soc., Perkin Trans.* **2000,** (17), 2862-2892; Glisan King, A.; Meinwald, J., *Chem. Rev.* **1996,** *96* (3), 1105-1122.
5. Hong, S.; Marks, T. J., *Acc. Chem. Res.* **2004,** *37* (9), 673-686.
6. Gagne, M. R.; Marks, T. J., *J. Am. Chem. Soc.* **1989,** *111* (11), 4108-4109; Gagne, M. R.; Stern, C. L.; Marks, T. J., *J. Am. Chem. Soc.* **1992,** *114* (1), 275-294.
7. Motta, A.; Lanza, G.; Fragala, I. L.; Marks, T. J., *Organometallics* **2004,** *23* (17), 4097-4104; Tobisch, S., *J. Am. Chem. Soc.* **2005,** *127* (34), 11979-11988; Tobisch, S., *Chem.–Eur. J.* **2005,** *11* (21), 6372-6385; Motta, A.; Fragala, I. L.; Marks, T. J., *Organometallics* **2006,** *25* (23), 5533-5539; Tobisch, S., *Chem.–Eur. J.* **2006,** *12* (9), 2520-2531.

8. Tian, S.; Arredondo, V. M.; Stern, C. L.; Marks, T. J., *Organometallics* **1999,** *18* (14), 2568-2570.

9. Li, Y.; Fu, P.-F.; Marks, T. J., *Organometallics* **1994,** *13* (2), 439-440.

10. Li, Y.; Marks, T. J., *J. Am. Chem. Soc.* **1996,** *118* (39), 9295-9306.

11. Gagne, M. R.; Nolan, S. P.; Marks, T. J., *Organometallics* **1990,** *9* (6), 1716-1718.

12. Gagne, M. R.; Brard, L.; Conticello, V. P.; Giardello, M. A.; Stern, C. L.; Marks, T. J., *Organometallics* **1992,** *11* (6), 2003-2005.

13. Kim, Y. K.; Livinghouse, T.; Bercaw, J. E., *Tetrahedron Lett.* **2001,** *42* (16), 2933-2935; Collin, J.; Daran, J.-C.; Schulz, E.; Trifonov, A., *Chem. Commun.* **2003,** (24), 3048-3049; Gribkov, D. V.; Hultzsch, K. C.; Hampel, F., *Chem.–Eur. J.* **2003,** *9* (19), 4796-4810; Kim, Y. K.; Livinghouse, T.; Horino, Y., *J. Am. Chem. Soc.* **2003,** *125* (32), 9560-9561; O'Shaughnessy, P. N.; Knight, P. D.; Morton, C.; Gillespie, K. M.; Scott, P., *Chem. Commun.* **2003,** (14), 1770-1771; O'Shaughnessy, P. N.; Scott, P., *Tetrahedron: Asymmetry* **2003,** *14* (14), 1979-1983; O'Shaughnessy, P. N.; Gillespie, K. M.; Knight, P. D.; Munslow, I. J.; Scott, P., *Dalton Trans.* **2004,** (15), 2251-2256; Collin, J.; Daran, J.-C.; Jacquet, O.; Schulz, E.; Trifonov, A., *Chem.–Eur. J.* **2005,** *11* (11), 3455-3462; Kim, J. Y.; Livinghouse, T., *Org. Lett.* **2005,** *7* (9), 1737-1739; Riegert, D.; Collin, J.; Meddour, A.; Schulz, E.; Trifonov, A., *J. Org. Chem.* **2006,** *71* (6), 2514-2517; Aillaud, I.; Collin, J.; Duhayon, C.; Guillot, R.; Lyubov, D.; Schulz, E.; Trifonov, A., *Chem.–Eur. J.* **2008,** *14* (7), 2189-2200.

14. Hong, S.; Tian, S.; Metz, M. V.; Marks, T. J., *J. Am. Chem. Soc.* **2003,** *125* (48), 14768-14783.

15. Gribkov, D. V.; Hultzsch, K. C.; Hampel, F., *J. Am. Chem. Soc.* **2006,** *128* (11), 3748-3759.

16. Li, Y.; Marks, T. J., *Organometallics* **1996,** *15* (18), 3770-3772; Li, Y.; Marks, T. J., *J. Am. Chem. Soc.* **1998,** *120* (8), 1757-1771; Yuen, H. F.; Marks, T. J., *Organometallics* **2009,** *28* (8), 2423-2440.

17. Ryu, J.-S.; Li, G. Y.; Marks, T. J., *J. Am. Chem. Soc.* **2003,** *125* (41), 12584-12605.

18. Reznichenko, A. L.; Nguyen, H. N.; Hultzsch, K. C., *Angew. Chem. Int. Ed.* **2010,** *49* (47), 8984-8987.

19. Giardello, M. A.; Conticello, V. P.; Brard, L.; Gagne, M. R.; Marks, T. J., *J. Am. Chem. Soc.* **1994,** *116* (22), 10241-10254; Giardello, M. A.; Conticello, V. P.; Brard, L.; Sabat, M.; Rheingold, A. L.; Stern, C. L.; Marks, T. J., *J. Am. Chem. Soc.* **1994,** *116* (22), 10212-10240; Douglass, M. R.; Ogasawara, M.; Hong, S.; Metz, M. V.; Marks, T. J., *Organometallics* **2001,** *21* (2), 283-292; Ryu, J.-S.; Marks, T. J.; McDonald, F. E., *J. Org. Chem.* **2004,** *69* (4), 1038-1052.

20. Lauterwasser, F.; Hayes, P. G.; Brase, S.; Piers, W. E.; Schafer, L. L., *Organometallics* **2004,** *23* (10), 2234-2237.

21. Kim, H.; Lee, P. H.; Livinghouse, T., *Chem. Commun.* **2005,** (41), 5205-5207; Kim, H.; Kim, Y. K.; Shim, J. H.; Kim, M.; Han, M.; Livinghouse, T.; Lee, P. H., *Adv. Synth. Catal.* **2006,** *348* (18), 2609-2618; Thomson, R. K.; Bexrud, J. A.; Schafer, L. L., *Organometallics* **2006,** *25* (17), 4069-4071; Gott, A. L.; Clarke, A. J.; Clarkson, G. J.; Scott, P., *Chem. Commun.* **2008,** (12), 1422-1424; Gott, A. L.; Clarkson, G. J.; Deeth, R. J.; Hammond, M. L.; Morton, C.; Scott, P., *Dalton Trans.* **2008,** (22), 2983-2990; Xiang, L.; Song, H.; Zi, G., *Eur. J. Inorg. Chem.* **2008,** *2008* (7), 1135-1140; Zi, G.; Wang, Q.; Xiang, L.; Song, H., *Dalton Trans.*

2008, (43), 5930-5944; Reznichenko, A. L.; Hultzsch, K. C., *Organometallics* **2009,** *29* (1), 24-27.

22. Watson, D. A.; Chiu, M.; Bergman, R. G., *Organometallics* **2006,** *25* (20), 4731-4733; Gott, A. L.; Clarke, A. J.; Clarkson, G. J.; Scott, P., *Organometallics* **2007,** *26* (7), 1729-1737; Zi, G.; Liu, X.; Xiang, L.; Song, H., *Organometallics* **2009,** *28* (4), 1127-1137.

23. Wood, M. C.; Leitch, D. C.; Yeung, C. S.; Kozak, J. A.; Schafer, L. L., *Angew. Chem. Int. Ed.* **2007,** *46* (3), 354-358.

24. Majumder, S.; Odom, A. L., *Organometallics* **2008,** *27* (6), 1174-1177; Müller, C.; Saak, W.; Doye, S., *Eur. J. Org. Chem.* **2008,** *2008* (16), 2731-2739.

25. Leitch, D. C.; Payne, P. R.; Dunbar, C. R.; Schafer, L. L., *J. Am. Chem. Soc.* **2009,** *131* (51), 18246-18247.

26. Allan, L. E. N.; Clarkson, G. J.; Fox, D. J.; Gott, A. L.; Scott, P., *J. Am. Chem. Soc.* **2010,** *132* (43), 15308-15320.

27. Stubbert, B. D.; Marks, T. J., *J. Am. Chem. Soc.* **2007,** *129* (19), 6149-6167.

28. Manna, K.; Xu, S.; Sadow, A. D., *Angew. Chem. Int. Ed.* **2011,** *50* (8), 1865-1868.

29. Lee, A. V.; Schafer, L. L., *Eur. J. Inorg. Chem.* **2007,** *2007* (16), 2245-2255.

30. Gribkov, D. V.; Hultzsch, K. C., *Angew. Chem. Int. Ed.* **2004,** *43* (41), 5542-5546.

31. Knight, P. D.; Munslow, I.; O'Shaughnessy, P. N.; Scott, P., *Chem. Commun.* **2004,** (7), 894-895.

32. Bexrud, J. A.; Beard, J. D.; Leitch, D. C.; Schafer, L. L., *Org. Lett.* **2005,** *7* (10), 1959-1962; Lee, A. V.; Schafer, L. L., *Organometallics* **2006,** *25* (22), 5249-5254; Müller, C.; Loos, C.; Schulenberg, N.; Doye, S., *Eur. J. Org. Chem.* **2006,**

2006 (11), 2499-2503; Bexrud, J. A.; Li, C.; Schafer, L. L., *Organometallics* **2007,** *26* (25), 6366-6372; Müller, C.; Koch, R.; Doye, S., *Chem.–Eur. J.* **2008,** *14* (33), 10430-10436; Lian, B.; Spaniol, T. P.; Horrillo-Martínez, P.; Hultzsch, K. C.; Okuda, J., *Eur. J. Inorg. Chem.* **2009,** *2009* (3), 429-434.

33. Pohlki, F.; Doye, S., *Angew. Chem. Int. Ed.* **2001,** *40* (12), 2305-2308.

34. Straub, B. F.; Bergman, R. G., *Angew. Chem. Int. Ed.* **2001,** *40* (24), 4632-4635.

35. Walsh, P. J.; Baranger, A. M.; Bergman, R. G., *J. Am. Chem. Soc.* **1992,** *114* (5), 1708-1719.

36. Walsh, P. J.; Hollander, F. J.; Bergman, R. G., *Organometallics* **1993,** *12* (9), 3705-3723; Sun Yeoul, L.; Bergman, R. G., *Tetrahedron* **1995,** *51* (15), 4255-4276; Bashall, A.; McPartlin, M.; E. Collier, P.; Mountford, P.; H. Gade, L.; J. M. Trosch, D., *Chem. Commun.* **1998,** (23), 2555-2556; Polse, J. L.; Andersen, R. A.; Bergman, R. G., *J. Am. Chem. Soc.* **1998,** *120* (51), 13405-13414; Ward, B. D.; Maisse-Francois, A.; Mountford, P.; Gade, L. H., *Chem. Commun.* **2004,** (6), 704-705; Selby, J. D.; Schulten, C.; Schwarz, A. D.; Stasch, A.; Clot, E.; Jones, C.; Mountford, P., *Chem. Commun.* **2008,** (41), 5101-5103.

37. Tobisch, S., *Dalton Trans.* **2006,** (35), 4277-4285; Tobisch, S., *Chem.–Eur. J.* **2007,** *13* (17), 4884-4894.

38. Leitch, D. C.; Turner, C. S.; Schafer, L. L., *Angew. Chem. Int. Ed.* **2010,** *49* (36), 6382-6386; Walsh, P. J.; Hollander, F. J.; Bergman, R. G., *J. Am. Chem. Soc.* **1990,** *112* (2), 894-896.

39. Brown, C. J.; Farthing, A. C., *Nature* **1949,** *164* (4178), 915-916.

40. Pye, P. J.; Rossen, K.; Reamer, R. A.; Tsou, N. N.; Volante, R. P.; Reider, P. J., *J. Am. Chem. Soc.* **1997,** *119* (26), 6207-6208; Zanotti-Gerosa, A.; Malan, C.;

Herzberg, D., *Org. Lett.* **2001,** *3* (23), 3687-3690; Focken, T.; Raabe, G.; Bolm, C., *Tetrahedron: Asymmetry* **2004,** *15* (11), 1693-1706.

41. Hou, X.-L.; Wu, X.-W.; Dai, L.-X.; Cao, B.-X.; Sun, J., *Chem. Commun.* **2000,** (13), 1195-1196; Whelligan, D. K.; Bolm, C., *J. Org. Chem.* **2006,** *71* (12), 4609-4618; Zhang, T.-Z.; Dai, L.-X.; Hou, X.-L., *Tetrahedron: Asymmetry* **2007,** *18* (2), 251-259.

42. Tanji, S.; Ohno, A.; Sato, I.; Soai, K., *Org. Lett.* **2001,** *3* (2), 287-289; Dahmen, S.; Brase, S., *Chem. Commun.* **2002,** (1), 26-27; Dahmen, S.; Bräse, S., *J. Am. Chem. Soc.* **2002,** *124* (21), 5940-5941; Danilova, T. I.; Rozenberg, V. I.; Sergeeva, E. V.; Starikova, Z. A.; Brase, S., *Tetrahedron: Asymmetry* **2003,** *14* (14), 2013-2019; Dahmen, S., *Org. Lett.* **2004,** *6* (13), 2113-2116; Bräse, S.; Höfener, S., *Angew. Chem. Int. Ed.* **2005,** *44* (48), 7879-7881; Lauterwasser, F.; Nieger, M.; Mansikkamäki, H.; Nättinen, K.; Bräse, S., *Chem.–Eur. J.* **2005,** *11* (15), 4509-4525; Lauterwasser, F.; Gall, J.; Höfener, S.; Bräse, S., *Adv. Synth. Catal.* **2006,** *348* (15), 2068-2074.

43. Gibson, S. E.; Knight, J. D., *Organic & Biomolecular Chemistry* **2003,** *1* (8), 1256-1269; Bräse, S.; Dahmen, S.; Höfener, S.; Lauterwasser, F.; Kreis, M.; Ziegert, R. E., *Synlett* **2004,** *2004* (15), 2647,2669.

44. Ma, Y.; Song, C.; Ma, C.; Sun, Z.; Chai, Q.; Andrus, M. B., *Angew. Chem. Int. Ed.* **2003,** *42* (47), 5871-5874; Song, C.; Ma, C.; Ma, Y.; Feng, W.; Ma, S.; Chai, Q.; Andrus, M. B., *Tetrahedron Lett.* **2005,** *46* (18), 3241-3244.

45. Reich, H. J.; Cram, D. J., *J. Am. Chem. Soc.* **1969,** *91* (13), 3517-3526.

46. Rozenberg, V.; Kharitonov, V.; Antonov, D.; Sergeeva, E.; Aleshkin, A.; Ikonnikov, N.; Orlova, S.; Belokon, Y., *Angew. Chem. Int. Ed. Engl.* **1994,** *33* (1), 91-92.

47. Rowlands, G. J., *Organic & Biomolecular Chemistry* **2008,** *6* (9), 1527-1534.

48. Bourget-Merle, L.; Lappert, M. F.; Severn, J. R., *Chem. Rev.* **2002,** *102* (9), 3031-3066.

49. Buch, F.; Harder, S., *Z.Naturforsch.(B)* **2008,** *63* (2), 169-177.

50. Oguadinma, P. O.; Schaper, F., *Organometallics* **2009,** *28* (14), 4089-4097.

51. El-Zoghbi, I.; Latreche, S.; Schaper, F., *Organometallics* **2010,** *29* (7), 1551-1559.

52. Drouin, F.; Oguadinma, P. O.; Whitehorne, T. J. J.; Prudhomme, R. E.; Schaper, F., *Organometallics* **2010,** *29* (9), 2139-2147.

53. Cipiciani, A.; Fringuelli, F.; Mancini, V.; Piermatti, O.; Pizzo, F.; Ruzziconi, R., *J. Org. Chem.* **1997,** *62* (11), 3744-3747.

54. Hitchcock, P. B.; Rowlands, G. J.; Parmar, R., *Chem. Commun.* **2005,** (33), 4219-4221.

55. Duan, W.; Ma, Y.; Xia, H.; Liu, X.; Ma, Q.; Sun, J., *J. Org. Chem.* **2008,** *73* (11), 4330-4333.

56. Reich, H. J.; Cram, D. J., *J. Am. Chem. Soc.* **1969,** *91* (13), 3505-3516.

57. Neugebauer, F. A.; Fischer, H., *J. Chem. Soc., Perkin Trans. 2* **1981,** (6), 896-900.

58. Lahann, J.; Höcker, H.; Langer, R., *Angew. Chem. Int. Ed.* **2001,** *40* (4), 726-728.

59. L. Kamara PhD Thesis, 2010, University of Sussex.

60. Vitanova, D. V.; Hampel, F.; Hultzsch, K. C., *Dalton Trans.* **2005,** (9), 1565-1566.

61. Hamaki, H.; Takeda, N.; Yamasaki, T.; Sasamori, T.; Tokitoh, N., *J. Organomet. Chem.* **2007,** *692* (1-3), 44-54.

62. Gogoi, S.; Bhuyan, R.; Barua, N. C., *Synth. Commun.* **2005,** *35* (21), 2811-2818.

63. Allen, F. H.; Kennard, O.; Watson, D. G.; Brammer, L.; Orpen, A. G.; Taylor, R., *J. Chem. Soc. Perkin Trans. 2* **1987,** (12), S1-S19.

64. Wang, R.; Zhang, X. H.; Chen, S. J.; Yu, X. H.; Wang, C. S.; Beach, D. B.; Wu, Y. D.; Xue, Z. L., *J. Am. Chem. Soc.* **2005,** *127* (14), 5204-5211.

65. Lahann, J.; Hocker, H.; Langer, R., *Angew. Chem. Int. Ed.* **2001,** *40* (4), 726-728.

66. McFarlane, W.; Wilkinson, G.; Hübel, W., *Triiron Dodecacarbonyl*. John Wiley & Sons, Inc.: 2007; p 181-183.

67. Lappert, M. F.; Pearce, R., *J. Chem. Soc.-Chem. Commun.* **1973,** (4), 126-126.

68. Chisholm, M. H.; Hammond, C. E.; Huffman, J. C., *Polyhedron* **1988,** *7* (24), 2515-2520.

69. Manzer, L. E., *Inorg. Synth.* **1982,** *21*, 135-140.

70. Sheldrick, G. M., *SHELXL-97, Program for the Refinement of Crystal Structures*. University of Göttingen: Göttingen, Germany, 1997.

Appendix A – Publications

Inorganic Chemistry
Article

Inorg. Chem. **2009**, *48*, 8971–8976 **8971**
DOI: 10.1021/ic900134f

Carbon Dioxide Activation by "Non-nucleophilic" Lead Alkoxides

Eric C. Y. Tam, Nick C. Johnstone, Lorenzo Ferro, Peter B. Hitchcock, and J. Robin Fulton*

Department of Chemistry, University of Sussex, Falmer, Brighton BN1 9QJ, U.K.

Received January 21, 2009

A series of terminal lead alkoxides have been synthesized utilizing the bulky β-diketiminate ligand [{N(2,6-^{i}Pr$_2$C$_6$H$_3$)-C(Me)}$_2$CH]$^-$ (BDI). The nucleophilicities of these alkoxides have been examined, and unexpected trends were observed. For instance, (BDI)PbOR reacts with methyl iodide only under forcing conditions yet reacts readily, but reversibly, with carbon dioxide. The degree of reversibility is strongly dependent upon minor changes in the R group. For instance, when R = isopropyl, the reversibility is only observed when the resulting alkyl carbonate is treated with other heterocumulenes; however, when R = *tert*-butyl, the reversibility is apparent upon any application of reduced pressure to the corresponding alkyl carbonate. The differences in the reversibility of carbon dioxide insertion are attributed to the ground-state energy differences of lead alkoxides. The mechanism of carbon dioxide insertion is discussed.

Introduction

In contrast to the well-documented reactivity of transition-metal alkoxides,[1−3] the chemistry of lead alkoxides has largely been ignored outside of gas-phase and theoretical studies.[4−6] Divalent lead has an aqueous acidity of 7.2, much smaller than that predicted based upon electrostatic parameters.[7] This acidity has been attributed to a more covalent Pb−O bond, in contrast to the highly polarized transition metal−oxygen bonds. In addition, lead's aqueous acidity has been used to justify its enhanced ability to cleave RNA. At biologically relevant pHs, there will be a sufficient amount of divalent lead hydroxide present to act as a base, deprotonating the 2′-hydroxyl proton of the RNA backbone, and a nucleophile in the cleavage of the resultant cyclic phosphate intermediate.[8,9] This implies that the Pb−O bond has some degree of polarity to be able to act as both a base and a nucleophile. However, no complementary chemical studies have been performed to back this hypothesis. As such, we set out to investigate the nature of the Pb−O bond in order to understand the degree of polarization of the bond. Herein, the results of such studies are reported, and our findings suggest that, although nucleophilic behavior with methyl iodide is not observed, lead alkoxides readily insert carbon dioxide into the Pb−O bond.

We have recently synthesized a series of monomeric divalent lead halides utilizing the bulky β-diketiminate anion [{N(2,6-^{i}Pr$_2$C$_6$H$_3$)C(Me)}$_2$CH]$^-$ (BDI) to stabilize the resulting three-coordinate lead complexes.[10] The chloride complex (BDI)PbCl (**1**) was used to synthesize monomeric lead aryloxide complexes in good yield.[11] Because metal aryloxide complexes are generally not as reactive as their alkoxide counterparts, for our reactivity studies, we turned our attention toward the synthesis of monomeric, terminal lead alkoxide complexes.

Results and Discussion

The treatment of a toluene solution of chloride **1** with KO^{i}Pr or KO^{t}Bu affords lead alkoxides (BDI)PbO^{i}Pr (**2**) and (BDI)PbO^{t}Bu (**3**), respectively (eq 1). Although these lead alkoxide complexes form a stable solid, they will slowly decompose in solution at ambient temperatures. The X-ray crystal structures were determined for both **2** and **3**, showing the expected pyramidal geometry of the ligands around the lead center (Figure 1).[10,11] Selected bond lengths and angles for alkoxides **2** and **3** are listed in Table 1, and data collection parameters are given in Table 2. Both alkyl groups of complexes **2** and **3** lie away from the BDI−Pb core; this is

*To whom correspondence should be addressed. E-mail: j.r.fulton@sussex.ac.uk.

(1) Bryndza, H. E.; Fong, L. K.; Paciello, R. A.; Tam, W.; Bercaw, J. E. *J. Am. Chem. Soc.* **1987**, *109*, 1444.
(2) Bryndza, H. E.; Tam, W. *Chem. Rev.* **1988**, *88*, 1163.
(3) Fulton, J. R.; Holland, A. W.; Fox, D. J.; Bergman, R. G. *Acc. Chem. Res.* **2002**, *35*, 44.
(4) Akibo-Betts, G.; Barran, P. E.; Puskar, L.; Duncombe, B.; Cox, H.; Stace, A. J. *J. Am. Chem. Soc.* **2002**, *124*, 9257.
(5) Cox, H.; Stace, A. J. *J. Am. Chem. Soc.* **2004**, *126*, 3939.
(6) Stace, A. J. *J. Phys. Chem. A* **2002**, *106*, 7993.
(7) Burgess, J. *Metal Ions in Solution*; Ellis Horwood Ltd.: Chichester, U.K., 1978.
(8) Barciszewska, M. Z.; Szymanski, M.; Wyszko, E.; Pas, J.; Rychlewski, L.; Barciszewski, J. *Mutat. Res.* **2005**, *589*, 103.
(9) Winter, D.; Polacek, N.; Halama, E.; Streicher, B.; Barta, A. *Nucleic Acids Res.* **1997**, *25*, 1817.
(10) Chen, M.; Fulton, J. R.; Hitchcock, P. B.; Johnstone, N. C.; Lappert, M. F.; Protchenko, A. V. *Dalton Trans.* **2007**, 2770.
(11) Fulton, J. R.; Hitchcock, P. B.; Johnstone, N. C.; Tam, E. C. Y. *Dalton Trans.* **2007**, 3360.

Published on Web 08/21/2009

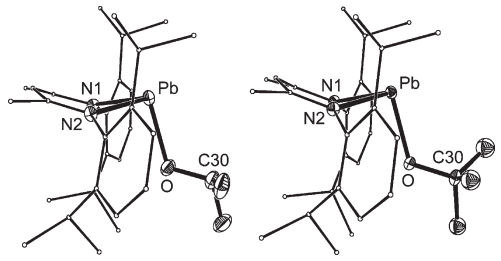

Figure 1. ORTEP diagram of lead isopropoxide **2** (left) and lead *tert*-butoxide **3** (right), with H atoms omitted and BDI C atoms minimized for clarity. The ellipsoid probability is shown at 30%.

Table 1. Selected Bond Lengths and Angles for Compounds **2** and **3**

	LPbO^{i}Pr (**2**)	LPbO^{t}Bu (**3**)
Pb−O	2.135(3)	2.126(3)
Pb−N1	2.307(3)	2.317(3)
Pb−N2	2.311(3)	2.299(3)
O−C30	1.413(5)	1.415(4)
N1−Pb−N2	80.56(9)	81.04(10)
N1−Pb−O	94.94(10)	92.74(10)
N2−Pb−O	93.49(10)	92.26(10)
Pb−O−C30	118.0(2)	121.4(2)
sum of the angles around Pb	268.99	266.04
DOP[a] (%)	101	104

[a] Degree of pyramidalization (DOP) = [360 − (sum of the angles)/0.9].[20]

in contrast to the isostructural tin system, in which the alkyl group lies below the plane consisting of N1−Pb−N2.[12]

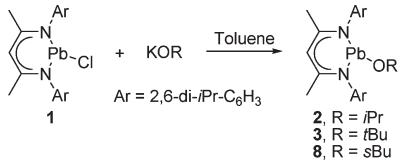

(1)

Two different types of lead alkoxide reactivities were investigated: basicity and nucleophilicity. The treatment of alkoxides **2** or **3** with 2,4-di-*tert*-butylphenol results in alcohol exchange reactions to form the known (BDI)Pb−OAr (Ar = 2,4-^{t}Bu$_2$C$_6$H$_3$) complex **4** with elimination of the corresponding aliphatic alcohols. This reactivity is similar to that observed in late-transition-metal alkoxide systems. However, the presence of free alcohol results in decomposition of aryloxide **4** to an insoluble white precipitate and protonated BDI. Potentially because of their higher pK_a, carbo acids are not reactive toward **2** and **3**; the treatment of isopropoxide **2** with fluorene did not yield the fluorenide anion, and the addition of 1,4-cyclohexadiene did not result in dimerization to an equilibrium mixture of 1,4- and 1,2-cyclohexadiene.

Both lead alkoxides **2** and **3** display seemingly contradictory reactivities toward electrophiles. For instance, neither reacts with benzyl bromide. When methyl iodide was added to either **2** or **3**, the formation of lead iodide was only observed after 2 days at 60 °C.[10] In sharp contrast, both alkoxides react readily with CO_2 (eq 2). The treatment of isopropoxide **2** with 1 equiv of CO_2 results in the clean and quantitative conversion to lead alkyl carbonate **5** after 30 min at room temperature. The IR spectrum shows a stretch at 1695 cm^{-1} (CCl_4), indicative of a carbonate carbonyl functionality; this is further supported by a

(12) Dove, A. P.; Gibson, V. C.; Marshall, E. L.; Rzepa, H. S.; White, A. J. P.; Williams, D. J. *J. Am. Chem. Soc.* **2006**, *128*, 9834.

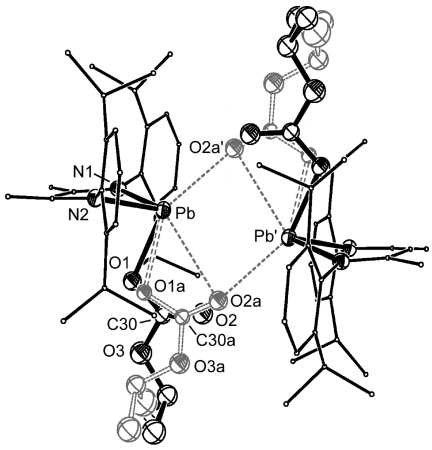

Figure 2. ORTEP diagram of lead carbonate **5** showing both components of the unit cell (major = black; minor = gray). H atoms are omitted and BDI C atoms minimized for clarity. Atoms with a prime are at equivalent positions (−*x*, −*y*, −*z*).

^{13}C NMR spectral resonance at 160.9 ppm. Crystals suitable for an X-ray diffraction study were grown at −30 °C in toluene. Two different binding modes for lead carbonate were observed in the solid state (Figure 2; see Table 3 for selected bond lengths and angles). In the major component, the carbonate is bound in an η^1 fashion and there is weak, long-distance interaction between O2 and Pb′. In the minor component, the carbonate is bound in an η^2 fashion and there is a shorter distance between O2a and Pb′, indicative of a stronger interaction between the two lead carbonate molecules.

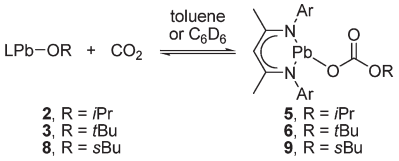

(2)

Because insertion of CO_2 into transition-metal alkoxides can be reversible,[13] we investigated whether the same was true for carbonate **5**. Although the formation of isopropoxide **2** is not observed when **5** is subjected to reduced pressure, the addition of $^{13}CO_2$ to the carbonate does result in ^{13}C incorporation into **5**.

Lead *tert*-butoxide **3** also reacts readily with CO_2 to form lead carbonate **6** (IR: 1699 cm^{-1}, CCl_4). In contrast to the isopropoxide system, the reaction is markedly reversible: the application of reduced pressure results in the almost quantitative formation of alkoxide **3**, thwarting attempts to characterize **6** in the solid state.

Pronounced differences in the reactivity of isopropoxide **2** and *tert*-butoxide **3** were observed upon treatment with phenyl isocyanate. With the former, insertion into the Pb−O bond to generate lead carbamate **7** is observed after 1 day at room temperature (eq 3). X-ray crystallography confirmed the presence of a Pb−N carbamate bond (Figure 3), with the *N*-phenyl group lying perpendicular to and below the plane consisting of N1−Pb−N2. Selected bond lengths and angles are listed in Table 4. In contrast, with *tert*-butoxide **3**, an

(13) For example, see: Tsuda, T.; Saegusa, T. *Inorg. Chem.* **1972**, *11*, 2561. Simpson, R. D.; Bergman, R. G. *Organometallics* **1992**, *11*, 4306. Mandal, S. K.; Ho, D. M.; Orchin, M. *Organometallics* **1993**, *12*, 1714.

Table 2. Crystallographic Data for Compounds **2**, **3**, **5**, and **7**

	LPbO^{i}Pr (**2**)	LPbO^{t}Bu (**3**)	LPbOCO$_2{}^i$Pr (**5**)[a]	LPb[N(Ph)C(O)O^{i}Pr (**7**)[b]
chemical formula	$C_{32}H_{48}N_2OPb$	$C_{33}H_{50}N_2OPb$	$C_{33}H_{48}N_2O_3Pb\cdot0.5(C_7H_8)$	$C_{44}H_{65}N_3O_2Pb$
fw	683.91	697.94	773.99	875.18
temperature (K)	172(2)	173(2)	173(2)	173(2)
wavelength (Å)	0.710 73	0.710 70	0.710 73	0.710 73
cryst size (mm^3)	0.20 × 0.20 × 0.15	0.25 × 0.20 × 0.10	0.15 × 0.10 × 0.05	0.15 × 0.15 × 0.1
cryst syst	triclinic	monoclinic	triclinic	triclinic
space group	$P\bar{1}$ (No. 2)	$P2_1/n$ (No. 14)	$P\bar{1}$ (No. 2)	$P\bar{1}$ (No. 2)
a (Å)	8.6979(2)	13.3743(1)	11.9673(4)	11.5616(3)
b (Å)	12.1195(3)	16.8363(2)	13.2339(5)	11.6261(3)
c (Å)	15.1146(3)	15.2434(2)	13.5828(3)	18.2619(4)
α (deg)	92.885(1)	90	99.649(2)	102.146(1)
β (deg)	98.639(1)	108.168(1)	106.996(2)	95.723(2)
γ (deg)	97.444(1)	90	113.105(1)	112.814(1)
V (Å^3)	1559.71(6)	3261.29(6)	1792.09(10)	2166.78(9)
Z	2	4	2	2
p_c (Mg m^{-3})	1.46	1.42	1.43	1.34
abs coeff (mm^{-1})	5.43	5.20	4.74	3.93
θ range for data collection (deg)	3.40−26.02	3.43−25.82	3.47−26.02	3.44−26.01
measd/indep reflns/R(int)	23 519/6112/0.044	41 847/6251/0.061	26 307/7017/0.066	23 224/8472/ 0.054
reflns with $I > 2\sigma(I)$	5783	5497	5851	7159
data/restraints/param	6112/0/337	6251/30/334	7017/34/380	8472/7/438
GOF on F^2	0.826	1.051	0.962	1.027
final R indices [$I > 2\sigma(I)$]	R1 = 0.023, wR2 = 0.059	R1 = 0.027, wR2 = 0.064	R1 = 0.047, wR2 = 0.107	R1 = 0.041, wR2 = 0.083
R indices (all data)	R1 = 0.026, wR2 = 0.061	R1 = 0.033, wR2 = 0.067	R1 = 0.0631, wR2 = 0.11571	R1 = 0.057, wR2 = 0.090
largst diff peak and hole (e Å^3)	0.78 and −1.37	1.37 and −1.40 (near Pb)	2.45 and −0.72 (close to Pb)	0.96 and 1.40

[a] The OC(O)O^{i}Pr group is disordered unequally over two arrangements with only some of the atoms resolved. The positions for the major component could be located, and for the minor component, approximate starting positions were estimated. The two orientations were then restrained to have similar geometry by use of the *same* instruction. This refinement converged successfully. There is a molecule of toluene solvate disordered about an inversion center for which the H atoms were omitted. All disordered atoms were left isotropic. [b] The poorly defined pentane solvate was included with isotropic C atoms and restrained geometry.

intractable reaction mixture is found. Even though the reaction between isopropoxide **2** and CO_2 is much faster than the reaction between **2** and phenyl isocyanate, there is a thermodynamic preference for the latter; the treatment of alkyl carbonate **5** with phenyl isocyanate results in an exclusive conversion to carbamate **7**. Neither alkoxide reacts with dicyclohexylcarbodiimide, even at elevated temperatures. Both alkoxides **2** and **3**, and their corresponding alkyl carbonates **5** and **6**, react with CS_2 to give intractable reaction mixtures.

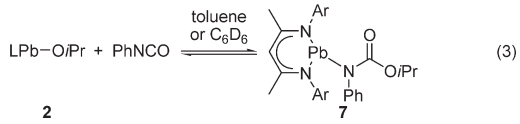

2 **7** (3)

To further understand the differences observed in the reactivity between isopropoxide **2** and *tert*-butoxide **3**, we synthesized the *sec*-butoxide complex **8**. The treatment of *sec*-butoxide **8** with CO_2 resulted in the expected formation of the corresponding carbonate **9** (IR: 1645 cm^{-1}, CCl_4). The degree of reversibility of this reaction is intermediate between the isopropoxide and *tert*-butoxide systems. For instance, when a vacuum is applied for 10 min to an NMR-scale solution of *tert*-butoxide carbonate **6**, almost complete reversion to alkoxide **3** is observed; however, when a similar procedure is repeated for a solution of *sec*-butoxide carbonate **9**, only 20% reversion to alkoxide **8** is observed. Unfortunately, as in the *tert*-butoxide case, this reversibility has prevented solid-state characterization of *sec*-butoxide carbonate **9**. Interestingly, solutions of both the isopropoxide carbonate **4** and *sec*-butoxide carbonate **9** are thermally stable to 60 °C, whereas the *tert*-butoxide carbonate **5** decomposes after standing at room temperature overnight.

The noticeable difference in reactivity with respect to deinsertion of CO_2 from carbonates **5**, **6**, and **9** can be attributed to the ground-state energy differences of the alkoxides. The stability of transition-metal alkoxides correlates to the pK_a of the corresponding alcohol; that is, the higher the pK_a, the more stable the metal alkoxide.[1] If a similar trend is assumed for lead alkoxides, then the lead isopropoxide **2** is less stable than the lead *tert*-butoxide **3** (pK_a of isopropyl alcohol is 30.2, whereas the pK_a of *tert*-butanol is 2 pK_a units higher).[14] The alkyl group will have a much smaller effect on the pK_a of the corresponding alkyl carbonates. An attempt was made to determine the rate of $^{13}CO_2$ exchange with each of the carbonates using ^{13}C NMR spectroscopy. Although exchange was observed, we were unable to obtain reproducible rate data. As such, we investigated the relative ground-state differences between the reactants and products using the B3LYP density functional theory and LanL2DZ pseudopotentials (and basis set) implemented in *Gaussian 03*.[15] The $\Delta H°$ value for the insertion of CO_2 into lead isopropoxide **2** was slightly greater than the analogous reaction for both the lead *sec*-butoxide **8** and

(14) Olmstead, W. M.; Margolin, Z.; Bordwell, F. G. *J. Org. Chem.* **1980**, *45*, 3295.

(15) Frisch, M. J.; Trucks, G. W.; Schlegel, H. B.; Scuseria, G. E.; Robb, M. A.; Cheeseman, J. R.; Montgomery, J. A., Jr.; Vreven, T.; Kudin, K. N.; Burant, J. C.; Millam, J. M.; Iyengar, S. S.; Tomasi, J.; Barone, V.; Mennucci, B.; Cossi, M.; Scalmani, G.; Rega, N.; Petersson, G. A.; Nakatsuji, H.; Hada, M.; Ehara, M.; Toyota, K.; Fukuda, R.; Hasegawa, J.; Ishida, M.; Nakajima, T.; honda, Y.; Kitao, O.; Nakai, H.; Klene, M.; Li, X.; Knox, J. E.; Hratchian, H. P.; Cross, J. B.; Adamo, C.; Jaramillo, J.; Gomperts, R.; Stratmann, R. E.; Yazyev, O.; Austin, A. J.; Cammi, R.; Pomelli, C.; Ochterski, J. W.; Ayala, P. Y.; Morokuma, K.; Voth, G. A.; Salvador, P.; Dannenberg, J. J.; Zakrzewski, V. G.; Dapprich, S.; Daniels, A. D.; Strain, M. C.; Farkas, O.; Malick, D. K.; Rabuck, A. D.; Raghavachari, K.; Foresman, J. B.; Ortiz, J. V.; Cuiq, Q.; Baboul, A. G.; Clifford, S.; Cioslowski, J.; Stefanov, B. B.; Liu, G.; Liashenko, A.; Piskorz, P.; Komaromi, I.; Martin, R. L.; Fox, D. J.; Keith, T.; Al-Laham, M. A.; Peng, C. Y.; Nanayakkara, A.; Challacombe, M.; Pople, J. A. *Gaussian 03*, revision C.02; Gaussian Inc.: Wallingford, CT, **2004**.

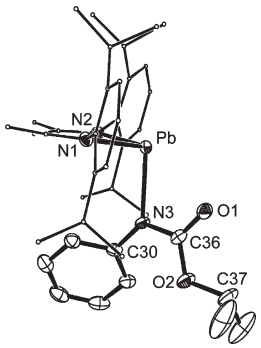

Figure 3. ORTEP diagram of lead carbamate **7** with H atoms omitted and BDI C atoms minimized for clarity. The ellipsoid probability is shown at 30%.

Table 3. Selected Bond Lengths and Angles for Compound **5**

Pb−O1	2.217(10)	N1−Pb−N2	83.23(18)
Pb−N1	2.292(5)	N1−Pb−O1	83.5(3)
Pb−N2	2.291(5)	N2−Pb−O1	82.2(3)
Pb−O1A	2.399(13)	N1−Pb−O1A	91.7(3)
Pb−O2A′	2.777(13)	N2−Pb−O1A	90.2(3)
Pb···Pb′	3.7842(5)	O1−Pb−O2A′	145.7(4)
O1−C30	1.309(16)	N1−Pb−O2A′	130.5(3)
O2−C30	1.188(17)	N2−Pb−O2A′	96.3(3)
O3−C30	1.372(14)	O1A−Pb−O2A′	137.8(4)
O3−C31	1.451(15)	Pb−O1−C30	113.5(8)
O1A−C30A	1.314(18)	O1−C30−O2	127.9(12)
O2A−C30A	1.18(2)	O1−C30−O3	107.9(12)
O3A−C30A	1.355(15)	O2−C30−O3	124.1(13)
O3A−C31A	1.453(16)	Pb−O1A−C30A	106.2(9)
		Pb′−O2A−C30A	148.4(11)
		O1A−C30−O2A	125.1(13)
sum of the angles around Pb	266.04	O1A−C30−O3A	114.9(16)
DOP[a] (%)	104	O2A−C30−O3A	119.8(16)

[a] Degree of pyramidalization (DOP) = [360 − (sum of the angles)/0.9].[20]

Table 4. Selected Bond Lengths and Angles for Compound **7**

Pb−N1	2.335(4)	N1−Pb−N2	82.47(14)
Pb−N2	2.321(4)	N1−Pb−N3	95.94(14)
Pb−N3	2.340(4)	N2−Pb−N3	96.84(14)
N3−C30	1.420(6)	Pb−N3−C30	132.5(3)
N3−C36	1.340(6)	Pb−N3−C36	103.2(3)
C36−O1	1.236(6)	N3−C36−O1	121.8(5)
C36−O2	1.348(6)	N3−C36−O2	116.4(5)
O2−C37	1.466(7)	O1−C36−O2	121.7(5)
		C36−O2−C37	116.9(4)
		sum of the angles around Pb	275.25
		DOP[a]	94%

[a] Degree of pyramidalization (DOP) = [360 − (sum of the angles)/0.9].[20]

tert-butoxide **3** cases (−9.4 kcal mol^{-1} vs −8.9 and −8.4 kcal mol^{-1}, respectively). Although these are gas-phase calculations, it is reassuring that the trends observed are similar to our experimental results.

The slow to nonexistent reactivity of our lead alkoxides with aliphatic electrophiles is in sharp contrast to the reactivity observed with transition-metal alkoxides. The most striking difference is with Vahrenkamp's pyrazolborate−zinc methoxide complex ($Tp^{Ph,Me}$Zn-OMe),[16] which reacts readily with methyl iodide to generate the corresponding dimethyl ether and pyrazolborate−zinc iodide complex, yet only reacts with CO_2 under forced conditions and not at all with phenyl isocyanate. This implies that the lead alkoxides lack nucleophilic characteristics. Space-filling models of alkoxide **2** reveal that the O atom lies inside a pocket surrounded by the BDI isopropyl groups and the alkyl group on the O atom. Thus, we cannot conclusively state that our lead alkoxides are non-nucleophilic because of potential steric arguments. However, we can conclude that a nucleophilic O atom is *not available* for reactivity.

The mechanism of CO_2 insertion into transition-metal alkoxides is generally thought to proceed via a concerted process in which the new carbon−oxygen and metal−carbonate bonds form at the same time as the cleavage of the metal−alkoxide bond.[17] The symmetry of this transition state must vary depending upon the nucleophilicity of the O atom and the propensity for CO_2 to bind to the metal center. In our examples, the lack of an available nucleophilic O atom implies that coordination of CO_2 to the metal center is key, and it must be this coordination that induces the alkoxide to react with CO_2. This can occur either by changing the steric environment around the alkoxide or by shifting the electron density such that the alkoxide ligand becomes more nucleophilic and CO_2 becomes more electrophilic. However, we have been unable to observe the binding of additional ligands to the metal center, nor can we gain evidence for binding using computational analysis. The addition of extraneous ligands such as CH_3CN, THF, TMEDA, and N-heterocyclic carbenes as well as softer ligands such as trimethyl- and triphenylphosphine did not result in either measurable inhibition of CO_2 insertion or strong evidence of coordination. Indeed, crystals of the alkoxides **2**, **3**, or **8** grown in a 50:50 mixture of CH_3CN and hexane did not result in coordinated CH_3CN in the solid state.

The differing reactivity between our lead alkoxides and transition-metal alkoxides is intriguing both from a fundamental viewpoint and from implications in the mechanism of lead-mediated RNA cleavage, and we are testing whether our apparent non-nucleophilic behavior can be reproduced with less sterically hindered lead alkoxides. In addition, we are currently investigating the mechanism of CO_2 insertion using kinetic studies on the slower isostructural tin system.[12]

Experimental Section

All manipulations were carried out in an atmosphere of dry nitrogen or argon using standard Schlenk techniques or in an inert-atmosphere glovebox. Solvents were dried from the appropriate drying agent, distilled, degassed, and stored over 4 Å sieves. (BDI)PbCl (**1**) was prepared according to the literature.[10] Potassium alkoxide salts were prepared by the slow addition of the relevant alcohol (dried and distilled) to a suspension of potassium hydride. Phenyl isocyanate and carbon disulfide were freshly dried and distilled before use. Carbon dioxide was used as received (Union Carbide, 99.999%), and $^{13}CO_2$ was 99 atom %. The ^{1}H and ^{13}C NMR spectra were recorded on a Bruker DPX 300 MHz spectrometer, a Varian 400 MHz spectrometer, or a Varian 500 MHz spectrometer. The ^{1}H and ^{13}C NMR spectroscopy chemical shifts are given relative to residual solvent peaks,

(16) Brombacher, H.; Vahrenkamp, H. *Inorg. Chem.* **2004**, *43*, 6042.

(17) For a few examples, see ref 15 as well as the following: Chisholm, M. H.; Cotton, F. A.; Extine, M. W.; Reichert, W. W. *J. Am. Chem. Soc.* **1978**, *100*, 1727. Darensbourg, D. J.; Sanchez, K. M.; Rheingold, A. L. *J. Am. Chem. Soc.* **1987**, *109*, 290. Campora, J.; Matas, I.; Palma, P.; Alvarez, E.; Graiff, C.; Tiripicchio, A. *Organometallics* **2007**, *26*, 3840.

and the ^{207}Pb elements were externally referenced to $PbMe_4$. The data for the X-ray structures were collected at 173 K on a Nonius Kappa CCD diffractometer, k(Mo Kα) = 0.710 73 Å and refined using the *SHELXL-97* software package.[18]

[CH{(CH$_3$)$_2$CN-2,6-^{i}Pr$_2$C$_6$H$_3$}$_2$PbO^{i}Pr] (2). 1 (1.08 g, 1.64 mmol) was added to a stirred suspension of KO^{i}Pr (0.127 g, 1.64 mmol) in 10 mL of toluene at room temperature. The reaction vessel was wrapped in foil, and the mixture was stirred overnight. The mixture was filtered through a pad of Celite, and the solvent was removed in a vacuum. The resulting brown oil was dissolved in a minimum of pentane and **2** crystallized upon standing at −30 °C overnight (0.686 g, 62%). ^{1}H NMR (C_6D_6, 293 K): δ 7.26 (d, 2H, J = 7.5 Hz, *m*-H), 7.20 (t, 2H, J = 7.5 Hz, *p*-H), 7.09 (d, 2H, J = 7.5 Hz, *m*-H), 4.96 (septet, 1H, J = 6.8 Hz, C*H*Me$_2$), 4.71 (s, 1H, middle CH), 3.95 (septet, 2H, J = 6.8 Hz, C*H*Me$_2$), 3.18 (septet, 2H, J = 6.8 Hz, C*H*Me$_2$), 1.69 (s, 6H, NC*Me*), 1.57 (d, 6H, J = 6.7 Hz, CH*Me*$_2$), 1.29 (d, 6H, J = 6.8 Hz, CH*Me*$_2$), 1.20 (d, 6H, J = 6.9 Hz, CH*Me*$_2$), 1.17 (d, 6H, J = 6.8 Hz, CH*Me*$_2$), 1.07 (d, 6H, J = 5.9 Hz, CH*Me*$_2$). ^{13}C{^{1}H} NMR (C_6D_6, 293 K): δ 163.9 (N*C*Me), 145.1 and 143.3 (*ipso*- and *o*-C of Ar), 126.4, 124.8, and 123.9 (*m*- and *p*-CH of Ar), 100.2 (middle CH), 66.0 (O*C*HMe$_2$), 30.6 (NC*Me*), 28.2 (OCH*Me*$_2$), 26.3, 25.7, 24.9, and 24.6 (CH*Me*$_2$). IR (Nujol, ν/cm^{-1}): 1553 (s), 1512 (s), 1317 (s), 1265 (s), 1172 (s), 1117 (s), 1012 (s), 960 (s),790 (s), 752 (s), 722 (s). Anal. Calcd for $C_{32}H_{48}ON_2Pb$: C, 56.20; H, 7.07; N, 4.10. Found: C, 56.30; H, 7.17; N, 4.13.

[CH{(CH$_3$)$_2$CN-2,6-^{i}Pr$_2$C$_6$H$_3$}$_2$PbO^{t}Bu] (3). 1 (0.908 g, 1.38 mmol) was added to a stirred suspension of KO^{t}Bu (0.154 g, 1.38 mmol) in toluene (15 mL) at room temperature, and the mixture was stirred overnight. The reaction mixture was filtered through Celite. The solvent was removed under vacuum, producing an orange solid as the crude product. The crude product was washed with pentane and recrystallized from toluene overnight, yielding yellow light-sensitive crystals of **3** (0.720 g, 75%). ^{1}H NMR (300 MHz, C_6D_6, 293 K): δ 7.26 (dd, 2H, J = 7.5 Hz, Ar*H*), 7.10 (d, 2H, J = 7.5 Hz, Ar*H*), 7.04 (dd, 2H, J = 7.5 Hz, Ar*H*), 4.57 (s, 1H, middle C*H*), 3.83 (septet, 2H, J = 6.8 Hz, C*H*Me$_2$), 3.12 (septet, 2H, J = 6.8 Hz, C*H*Me$_2$), 1.65 (s, 6H, CC*H*$_3$), 1.63 (d, 6H, J = 6.8 Hz, C(C*H*$_3$)$_2$), 1.25 (d, 6H, J = 6.9 Hz, C(C*H*$_3$)$_2$), 1.19 (d, 6H, J = 6.9 Hz, C(C*H*$_3$)$_2$), 1.14 (d, 6H, J = 6.8 Hz, C(C*H*$_3$)$_2$), 0.88 (s, 9H, C(C*H*$_3$)$_3$). ^{13}C{^{1}H} NMR (300 MHz, C_6D_6, 293 K): 164.0 (N*C*Me), 145.1 (*ipso*-*C*), 142.8 (*o*-*C*), 141.5 (*o*-*C*), 126.0 (*p*-*C*), 123.7 (*m*-*C*), 123.6 (*m*-*C*), 98.0 (middle *C*H), 69.1 (O*C*Me$_3$), 36.7 (OC(*C*H$_3$)$_3$), 28.4 (*C*HMe$_2$), 28.0 (*C*HMe$_2$), 26.1 (NC*C*H$_3$), 25.2 (C(*C*H$_3$)$_2$), 24.8 (C(*C*H$_3$)$_2$), 24.6 (C(*C*H$_3$)$_2$), 23.9 (C(*C*H$_3$)$_2$). IR (Nujol, ν/cm^{-1}): 1556 (s), 1511 (s), 1318 (s), 1262 (s), 1227 (s), 1015 (s), 941 (s), 838 (s), 791 (s), 751 (s). Anal. Calcd for $C_{33}H_{50}N_2OPb$: C, 56.79; H, 7.22; N, 4.01. Found: C, 56.70; H, 7.15; N, 3.97.

[CH{(CH$_3$)$_2$CN-2,6-^{i}Pr$_2$C$_6$H$_3$}$_2$Pb(CO$_2$)O^{i}Pr] (5). 2 was dissolved in toluene (2 mL) and loaded into an ampule wrapped in aluminum foil. The reaction vessel was connected to a Schlenk line and a cylinder of high-purity CO_2. The vessel was submerged in a dry ice/acetone bath, and after three pump/refill cycles, CO_2 was introduced at a pressure of 1.5 bar. Thawing followed by removal of the solvent gave **5** as a yellow solid in quantitative yield. ^{1}H NMR (C_6D_6, 300 K): δ 7.19 (s, 6H, Ar*H*), 4.97 (septet, 1H, J = 6.3 Hz, OC*H*Me$_2$), 4.86 (s, 1H, middle CH), 3.39−3.32 (br multiplet, 4H), 3.02 (septet, 2H, J = 6.9 Hz, C*H*Me$_2$), 1.69 (s, 6H, NC*Me*), 1.30 (d, 12H, J = 6.3 Hz, CH*Me*$_2$), 1.20 (d, 12H, J = 6.3 Hz, CH*Me*$_2$), 1.24 (d, 6H, J = 6.8 Hz, OCH*Me*$_2$). ^{13}C{^{1}H} NMR (500 MHz, toluene-d_8, 303 K): δ 164.1 (N*C*Me), 160.9 (O*C*═O), 142.8 (*ipso*-*C*), 129.2 (*o*-*C*), 128.3 (*o*-*C*), 127.0 (*p*-*C*), 125.4 (*m*-*C*), 124.5 (*m*-*C*), 103.6 (middle *C*H), 68.7 (O*C*(CH$_3$)$_2$), 34.6 (OC(*C*H$_3$)$_2$), 28.3 (*C*HMe$_2$), 26.0 (*C*HMe$_2$), 24.7 (NC*C*H$_3$), 24.5 (CH(*C*H$_3$)$_2$), 22.8 (CH(*C*H$_3$)$_2$), 22.7 (CH(*C*H$_3$)$_2$), 14.3 (CH(*C*H$_3$)$_2$). ^{207}Pb NMR (400 MHz, toluene-d_8, 303 K): δ 808.7. IR (Nujol, ν/cm^{-1}): 3056 (s), 1611 (s), 1583 (s), 1551 (s), 1519 (s), 1317 (s), 1294 (s), 1171 (s), 1108 (s), 1055 (s), 1020 (s). IR (CCl_4, ν/cm^{-1}): 3060 (s), 2963(s), 2928 (s), 2871 (s), 2335 (br), 1699 (s), 1463 (s), 1438 (s), 1387 (br), 1319 (s), 1292 (s), 1173 (s), 1115 (s). Anal. Calcd for $C_{33}H_{48}N_2O_3Pb$: C, 54.45; H, 6.65; N, 3.85. Found: C, 54.49; H, 6.71; N, 3.75.

[CH{(CH$_3$)$_2$CN-2,6-^{i}Pr$_2$C$_6$H$_3$}$_2$Pb(CO$_2$)O^{t}Bu] (6). 3 (0.050 g, 0.072 mmol) was dissolved in toluene-d_8 in an NMR tube sealed with a Young's tap. The gas inside the NMR tube was evacuated. CO_2 (0.0047 mg, 0.109 mmol) was then added. A yellow solution mixture was observed, and the reaction mixture was kept at room temperature for 24 h and was monitored by ^{1}H NMR spectroscopy. ^{1}H NMR (400 MHz, toluene-d_8, 203 K): δ 7.15 (s, 2H, Ar*H*), 7.07 (d, 2H, J = 4 Hz, Ar*H*), 6.95 (d, 2H, J = 8 Hz, Ar*H*), 4.79 (s, 1H, middle C*H*), 3.64 (m, 2H, C*H*Me$_2$), 2.94 (m, 2H, C*H*Me$_2$), 1.62 (s, 6H, CC*H*$_3$), 1.58 (br, 6H, J = 4 Hz, C(C*H*$_3$)$_2$), 1.50 (d, 6H, J = 4 Hz, C(C*H*$_3$)$_2$), 1.17 (d, 6H, J = 4 Hz, C(C*H*$_3$)$_2$), 1.08 (s, 9H, C(C*H*$_3$)$_3$). ^{13}C{^{1}H} NMR (400 MHz, toluene-d_8, 203 K): δ 163.5 (N*C*Me), 160.3 (O*C*O), 144.2 (*ipso*-*C*), 142.3 (*o*-*C*), 141.6 (*o*-*C*), 103.5 (middle *C*H), 76.6 (O*C*HMe$_2$), 28.5 (OCH(*C*H$_3$)$_2$), 28.1 (NC*C*H$_3$), 27.6 (*C*HMe$_2$), 27.4 (*C*HMe$_2$), 26.8 (*C*HMe$_2$), 26.5 (*C*HMe$_2$), 25.0 (C(*C*H$_3$)$_2$), 24.7 (C(*C*H$_3$)$_2$), 24.3 (C(*C*H$_3$)$_2$), 24.1 (C(*C*H$_3$)$_2$). ^{207}Pb NMR (400 MHz, toluene-d_8, 303 K): δ 817.4. IR (CCl_4, ν/cm^{-1}): 3060 (s), 2965 (s), 2928 (s), 2869 (s), 1699 (s), 1463 (s), 1438 (s), 1389 (b), 1366 (b), 1172 (s), 1102 (s).

[CH{(CH$_3$)$_2$CN-2,6-^{i}Pr$_2$C$_6$H$_3$}$_2$Pb(N(Ph)CO)O^{i}Pr] (7).[19] Phenyl isocyanate (0.032 mL, 0.294 mmol) was added to a solution of **2** (0.196 g, 0.287 mmol) in toluene (3 mL). The reaction vessel was wrapped in foil and stirred at room temperature for 3 h. The volatiles were removed, and the resulting orange residue was dissolved in a minimum of pentane. **7** crystallized upon standing at −30 °C overnight (0.100 g, 44%). ^{1}H NMR (500 MHz, toluene-d_8, 303 K): δ 7.59 (br, 2H, ArH), 7.27 (t, 2H, J = 15 Hz, ArH), 6.85 (t, 1H, J = 15 Hz, ArH), 5.03 (s, 1H, middle C*H*), 4.91 (br, 1H, OC*H*Me$_2$), 3.13 (br, 4H, C*H*Me$_2$), 1.67 (s, 6H, CC*H*$_3$), 1.28 (d, 1H, J = 5 Hz, C(C*H*$_3$)$_2$), 1.25 (d, 1H, J = 5 Hz, C(C*H*$_3$)$_2$), 1.15 (2H, br d, J = 10 Hz, C(C*H*$_3$)$_2$), 0.98 (6H, br, C(C*H*$_3$)$_2$), 0.88 (d, 2H, J = 10 Hz, C(C*H*$_3$)$_2$), 0.87 (d, 2H, J = 5 Hz, OC(C*H*$_3$)$_2$). ^{13}C{^{1}H} NMR (500 MHz, toluene-d_8, 303 K): δ 165.0, 143.3, 129.2, 128.3, 127.9, 126.8, 126.0, 121.7, 103.2, 67.2, 34.6, 28.2, 25.5, 25.2, 24.6, 22.8, 22.4, 14.3. ^{13}C{^{1}H} NMR (400 MHz, toluene-d_8, 198 K): δ 164.7, 164.0, 163.7, 161.4, 158.9, 147.7, 146.6, 144.6, 144.1, 142.9, 142.4, 141.7, 141.4, 129.7, 127.3, 126.5, 126.0, 125.4, 68.0, 67.1, 66.8, 66.4, 65.8, 65.3, 34.5, 27.2, 26.7, 25.8, 25.0, 24.9, 24.4, 24.3, 24.2, 23.1, 22.3, 22.2, 21.9, 14.6. IR (Nujol, ν/cm^{-1}): 1745 (s), 1688 (s), 1578 (s), 1546 (s), 1515 (s), 1483 (s), 1315 (s), 1231 (s), 1168 (s), 1109 (s), 1054 (s), 1035 (s), 1021 (s). Anal. Calcd for $C_{39}H_{53}N_3O_2Pb$: C, 58.31; H, 6.66; N, 5.23. Found: C, 58.39; H, 6.54; N, 5.24.

[CH{(CH$_3$)$_2$CN-2,6-^{i}Pr$_2$C$_6$H$_3$}$_2$PbO^{s}Bu]. A suspension of KO^{s}Bu (0.085 g, 757 mmol in 3 mL of toluene) was added dropwise to a stirred solution of **1** (0.500 g, 757 mmol) in toluene (10 mL) at room temperature. The reaction mixture was stirred overnight. The deep-yellow solution was filtered through Celite, and the solvent was removed under vacuum. The resulting yellow solid was dissolved in the minimum amount of pentane (∼7 mL) and stored at −30 °C overnight, yielding yellow crystals of (BDI)PbOsBu (0.441 g, 83%). ^{1}H NMR (toluene-d_8, 303 K): δ 7.17 (d, 2H, J = 7.5 Hz, *m*-*H*), 7.03 (t, 2H, J = 16.9 Hz, *p*-*H*),

(18) Sheldrick, G. M. *SHELXL-97, Program for the Refinement of Crystal Structures*; University of Göttingen: Göttingen, Germany, **1997**.

(19) The solution-phase chemistry of this compound is complex and is undergoing further studies to understand the variable-temperature NMR spectroscopic behavior.

(20) Maksic, Z. B.; Kovacevic, B. *J. Chem. Soc., Perkin Trans. 2* **1999**, 2623.

7.02 (d, 2H, J = 18.4 Hz, *m-H*), 4.60 (s, 1H, middle C*H*), 4.56 (m, 1H, OC*H*(CH_3)CH_2CH_3), 3.79 (hept, 1H, J = 6.9 Hz, C*H*Me_2), 3.77 (hept, 1H, J = 7.1 Hz, C*H*Me_2), 3.10 (septet, 2H, J = 6.8 Hz, C*H*Me_2), 1.64 (s, 3H, NC*Me*), 1.63 (s, 3H, NC*Me*), 1.47 (dd, 6H, J_1 = 6.5 Hz, J_2 = 4.8 Hz, CH*Me*$_2$), 1.21 (dd, 6H, J_1 = 6.8 Hz, J_2 = 1.7 Hz, CH*Me*$_2$), 1.15 (d, 6H, J = 6.8 Hz, CH*Me*$_2$), 1.12 (d, 6H, J = 6.8 Hz, CH*Me*$_2$), 0.78 (d, 3H, J = 6.0 Hz, OCH(C*H*$_3$)CH_2CH_3), 0.48 (t, 3H, J = 7.4 Hz, OCH(CH_3)CH_2C*H*$_3$). $^{13}C\{^1H\}$ NMR (C_6D_6, 303 K): δ 163.4 (N*C*Me), 144.7 (*ipso-C*), 142.8 and 141.6 (*o-C*), 125.8 (*p-C*), 123.4 and 123.3 (*m-C*), 99.1 (middle *C*H), 70.8 (O*C*(CH_3)CH_2-CH_3), 36.3 (OC(*C*H_3)CH_2CH_3), 27.9 (NC*Me*), 27.8 and 27.7 (*C*HMe_2), 26.0, 25.0, 24.2, and 23.7 (CH*Me*$_2$), 24.4 (OC(CH_3)-*C*H_2CH_3), 10.5 (OC(CH_3)CH_2*C*H_3). ^{207}Pb NMR (400 MHz, C_6D_6): δ 1542.8. IR (Nujol, ν/cm^{-1}): 3057, 1556 (s), 1516 (s), 1437 (s), 1251, 1171, 1100 (s), 1023 (s), 986, 961, 936, 917, 840, 791 (s), 750. IR (CCl_4, ν/cm^{-1}): 3059 (w), 2962, 2927, 2989, 2291 (w), 2004 (w), 1857 (w), 1550 (s), 1463, 1437, 1359, 1320, 1252 (s), 1217 (s), 1172. Anal. Calcd for $C_{33}H_{48}N_2O_3Pb$: C, 56.79; H, 7.22; N, 4.01. Found: C, 56.66; H, 7.08; N, 3.89.

[CH{(CH$_3$)$_2$CN-2,6-^{i}Pr$_2$C$_6$H$_3$}$_2$Pb(CO$_2$)O^{s}Pr] (9). 8 (101 mg, 0.145 mmol) was dissolved in toluene (8 mL) in a sealable ampule. The gas was evacuated, and CO_2 was added (0.220 mmol). The reaction mixture was cooled to −80 °C to give a yellow powder. ^{1}H NMR (C_6D_6, 303 K): δ 7.09 (s, br, 6H, Ar*H*), 4.78 (s, 1H, middle C*H*), 4.71 (sext, 1H, J = 6.21 Hz, OC*H*-(CH_3)CH_2CH_3), 3.30 (br, 4H, C*H*Me_2), 1.67 (m, 1H, OCH-(CH_3)C*H*$_2CH_3$), 1.62 (s, 6H, NC*Me*), 1.48 (m, 1H, OCH-(CH_3)C*H*$_2CH_3$), 1.26 (d, 12H, J_1 = 6.2 Hz, CH*Me*$_2$), 1.18 (d, 3H, J = 6.9 Hz, OCH(C*H*$_3$)CH_2CH_3), 1.11 (d, 12H, CH*Me*$_2$), 0.90 (t, 3H, J = 7.4 Hz, OCH(CH_3)CH_2C*H*$_3$). $^{13}C\{^1H\}$ NMR (C_6D_6, 303 K): δ 163.7 (N*C*Me), 160.7 (O*C*O$_2$), 142.4 (*ipso-C*), 127.7 and 127.5 (*o-C*), 126.5 (*p-C*), 124.4 and 124.0 (*m-C*), 103.2 (middle *C*H), 73.2 (O*C*(CH_3)CH_2CH_3), 29.3 (OC(*C*H_3)CH_2-CH_3), 27.8 (NC*Me*), 24.2 (*C*HMe_2), 24.1 (CH*Me*$_2$), 19.7 (OC(CH_3)*C*H_2CH_3), 9.8 (OC(CH_3)CH_2*C*H_3). ^{207}Pb NMR (400 MHz, C_6D_6): δ 810.3. IR (Nujol, ν/cm^{-1}): 3027, 2336 (w), 1940 (w), 1855 (w), 1800 (w), 1604, 1549 (s), 1260 (s), 1081 (s, br), 804 (s), 694 (s). IR (CCl_4, ν/cm^{-1}): 3723, 2693, 3621, 3590, 3063 (w), 2963, 2928, 2870, 2337 (s), 2005 (w), 1857 (w), 1645, 1550 (s), 1459, 1437, 1383, 1364, 1319, 1254 (s), 1217 (s), 1174. Note: traces of **8** were found in isolated solid-state samples of **9** (even crystallized samples), preventing acceptable elemental analysis.

Computational Details. All calculations were performed using the *Gaussian 03*, revision C.02, suite of programs using the B3LYP density functional theory and LanL2DZ pseudopotentials (and basis set).[15]

Acknowledgment. The authors are grateful for financial support from the EPSRC (Grant EP/E032575/1 to L.F.) and the University of Sussex.

Supporting Information Available: ORTEP diagram, crystallographic data, and selected bond lengths and angles for complex **8** and crystallographic data in CIF format for complexes **2**, **3**, **5**, **7**, and **8**. This material is available free of charge via the Internet at http://pubs.acs.org.

ORGANOMETALLICS
Article

Organometallics **2010,** *29,* 2911–2915 2911
DOI: 10.1021/om100167e

Taking Advantage of Hg−C Bonds: Synthesis of the First Homoleptic Bis-β-diketiminate Complex Bound through the γ-Carbons

Lorenzo Ferro, Martyn P. Coles, Iain J. Day, and J. Robin Fulton*

Department of Chemistry, University of Sussex, Falmer, Brighton BN1 9QJ, U.K.

Received March 2, 2010

The most common β-diketiminate ligand, [{N(2,6-^{i}Pr$_2$C$_6$H$_3$)C(Me)}$_2$CH]$^-$ (BDI), was used to synthesize a new mercury complex in which two BDI ligands are bound to the metal through the γ-carbons in the solid state. In solution, one of the BDI ligands switches to an N,N′-binding mode; this complex is in equilibrium with the homoleptic species. The thermodynamic parameters, $\Delta H°$ (−2.52 kcal mol^{-1}), $\Delta S°$ (−9.24 cal mol^{-1} K^{-1}), and $\Delta G°_{298}$ (0.23 kcal mol^{-1}), were measured using variable-temperature ^{1}H NMR spectroscopy.

The β-diketiminate ligand has seen an explosion in popularity over the past decade.[1] It has been deemed a "Cp" replacement due to its monoanionic nature and the wide range of easily accessible variants along the β-diketiminate backbone (R^1, R^2, R^3, R^4, and R^5; Figure 1), thus influencing both the steric and electronic nature of the ligand. Two common nicknames for this ligand class are found: $(R^1)_2$-nacnac, which generally refers to the ligand in which R^3 = H, R^2, R^4 = Me,[2] and R^1 = R^5, and BDI, which generally refers to the most popular β-diketiminate ligand, [{N(2,6-^{i}Pr$_2$C$_6$H$_3$)-C(Me)}$_2$CH]$^-$.[3,4] The β-diketiminate ligand has a remarkable ability to stabilize low-valent complexes in some rather unusual oxidation states. For instance, Jones and co-workers were able to reduce BDI−MgI to a Mg(I) dimer complex that possesses a Mg−Mg bond.[5] Holland and co-workers utilized this ligand to synthesize a rare three-coordinate transition-metal dinitrogen complex, as well as 12-electron complexes of iron(II).[6,7] Hill took advantage of the steric variants along the β-diketiminate backbone and generated a series of In(I) complexes ranging from a mononuclear complex when a bulky N-aryl substituent was used (BDI), a dimer when methyl groups were placed in the 2-, 4-, and 6-positions of the N-aryl substituent (R^1 and R^5), to a hexaindium chain when methyl groups were placed in the least obstrusive 3- and 5-positions of the N-aryl substituent (R^1 and R^5).[8]

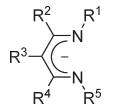

Figure 1. Basic skeleton of the β-diketiminate ligand.

By far the most widely used β-diketiminate ligand is [{N-(2,6-^{i}Pr$_2$C$_6$H$_3$)C(Me)}$_2$CH]$^-$ (BDI or Dipp$_2$nacnac),[9] with over 700 crystal structures reported in the Cambridge Structural Database. With regard to group 12 metals, only the Zn and Cd complexes of this ligand are known.[10−13] Layh and co-workers have synthesized a β-diketiminate−Hg complex (L^1HgCl) in which the N-aryl substituent (R^1 and R^5) possesses tBu groups in the 2- and 5-positions: R^2, R^4 = SiMe$_3$ and R^3 = H. In this system, the β-diketiminate ligand is bound through the γ-carbon.[14] Attempts to place more than one β-diketiminate ligand on Hg were not successful. Lappert and co-workers synthesized a sila-β-diketiminate ligand, [{N(2,6-^{i}Pr$_2$C$_6$H$_3$)C(Me)}$_2$Si(SiMe$_3$)]$^-$ (L^2), in which the methine (CH) group is replaced with a Si(SiMe$_3$).[15] The researchers were able to generate a $(L^2)_2$Hg complex via a disproportionation reaction with Hg_2Cl_2 and Li−L.[2] Similar to the case for L^1HgCl, both ligands were bound to the metal center via the Si backbone.

*To whom correspondence should be addressed, E-mail: j.r.fulton@sussex.ac.uk.

(1) Bourget-Merle, L.; Lappert, M. F.; Severn, J. R. *Chem. Rev.* **2002**, *102*, 3031.
(2) Kim, W. K.; Fevola, M. J.; Liable-Sands, L. M.; Rheingold, A. L.; Theopold, K. H. *Organometallics* **1998**, *17*, 4541.
(3) Aboulkacem, S.; Tyrra, W.; Pantenburg, I. *Z. Anorg. Allg. Chem.* **2003**, *629*, 1569.
(4) This abbreviation has also been used to encompass a variety of different varieties of β-diketiminate ligands; for instance, see: Dove, A. P.; Gibson, V. C.; Marshall, E. L.; Rzepa, H. S.; White, A. J. P.; Williams, D. J. *J. Am. Chem. Soc.* **2006**, *128*, 9834.
(5) Green, S. P.; Jones, C.; Stasch, A. *Science* **2007**, *318*, 1754.
(6) Smith, J. M.; Lachicotte, R. J.; Pittard, K. A.; Cundari, T. R.; Lukat-Rodgers, G.; Rodgers, K. R.; Holland, P. L. *J. Am. Chem. Soc.* **2001**, *123*, 9222.
(7) Smith, J. M.; Lachicotte, R. J.; Holland, P. L. *Organometallics* **2002**, *21*, 4808.
(8) Hill, M. S.; Hitchcock, P. B.; Pongtavornpinyo, R. *Science* **2006**, *311*, 1904.
(9) Feldman, J.; McLain, S. J.; Parthasarathy, A.; Marshall, W. J.; Calabrese, J. C.; Arthur, S. D. *Organometallics* **1997**, *16*, 1514.
(10) Prust, J.; Stasch, A.; Zheng, W. J.; Roesky, H. W.; Alexopoulos, E.; Uson, I.; Bohler, D.; Schuchardt, T. *Organometallics* **2001**, *20*, 3825.
(11) Prust, J.; Most, K.; Muller, I.; Stasch, A.; Roesky, H. W.; Uson, I. *Eur. J. Inorg. Chem.* **2001**, 1613.
(12) Chisholm, M. H.; Gallucci, J.; Phomphrai, K. *Inorg. Chem.* **2002**, *41*, 2785.
(13) Cheng, M.; Moore, D. R.; Reczek, J. J.; Chamberlain, B. M.; Lobkovsky, E. B.; Coates, G. W. *J. Am. Chem. Soc.* **2001**, *123*, 8738.
(14) Fernandes, M. A.; Layh, M.; Omondi, B. In *Trends in Organometallic Chemistry Research*; Cato, M. A., Ed.; Gazelle Book Services: Lancaster, U.K., 2005; p 107.
(15) Farwell, J. D.; Fernandes, M. A.; Hitchcock, P. B.; Lappert, M. F.; Layh, M.; Omondi, B. *Dalton Trans.* **2003**, 1719.

Published on Web 06/15/2010

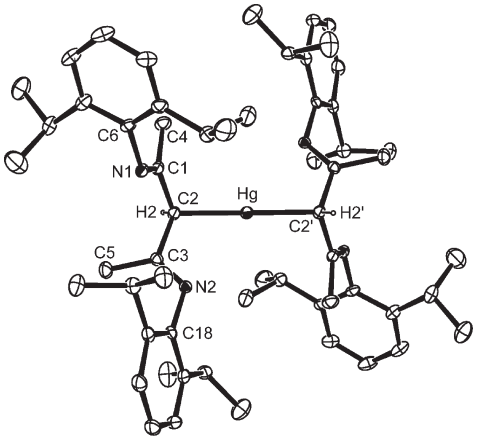

Figure 2. ORTEP diagram of the dialkylmercury species **1** with ellipsoids at the 30% probability level. H atoms, except for H2, are omitted for clarity. Atoms marked with a prime (′) are at equivalent positions ($-x$, $-y$, $-z$).

We have recently synthesized a series of BDI lead aryloxides and alkoxides. The latter complexes show facile reactivity toward heterocumulenes such as carbon dioxide but only sluggish reactivity toward aliphatic electrophiles such as methyl iodide.[16−18] As this is in sharp contrast to the reactivity of late-transition-metal alkoxides,[19] we wanted to explore the other divalent heavy-metal terminal alkoxides in order to ascertain any reactivity trends. Thus, our attention turned to mercury and an attempted synthesis of the BDI−HgCl complex as a precursor to terminal mercury alkoxide and amido complexes. Addition of LiN^iPr_2 to BDI-H, followed by treatment with a suspension of $HgCl_2$ (0.5 equiv) results in the formation of colorless crystals in 34% yield (eq 1).[20] Crystals suitable for an X-ray diffraction study were grown by slowly cooling a saturated CH_2Cl_2 solution (Figure 2). The molecule lies on an inversion center with the BDI ligand bound through the γ-carbon, or the "backbone" of the BDI ligand. Selected bond lengths and angles are shown in Table 1, and data collection parameters are given in Table 2. Although there are a handful of examples of other C-bound β-diketiminate ligands,[14,21−23] including BDI complexes,[9,24−26] this is the first crystallographically characterized compound in which two β-diketiminate ligands are C-bound to a single metal center. Although the geometry of the ligands around Hg is linear, the ligands are in a staggered conformation to each other, which is similar to the case for the sila analogue.[15] The Hg−C bond length of 2.127(3) Å is significantly shorter than that reported for L^1HgCl (2.337(2) Å) but similar to other dialkylmercury complexes.[27,28] The C−C bond lengths of 1.500(5)−1.501(4) Å are similar to those of other sp^2−sp^3 C−C single bonds.[29] A long-range intramolecular nitrogen−mercury interaction is observed, with a Hg···N2 distance of 2.994 Å, slightly shorter than their combined van der Waals radii of 3.10 Å. This type of interaction is observed with both Layh's mercury complex L^1HgCl as well as Lappert's bis-sila-β-diketiminate mercury complex $(L^2)_2Hg$.[14,15]

Table 1. Selected Bond Lengths (Å) and Angles (deg) for Compound 1

Hg−C(2)	2.128(3)	C(1)−N(1)	1.277(3)
C(2)−C(1)	1.500(4)	N(1)−C(6)	1.428(3)
C(2)−C(3)	1.501(4)	C(3)−N(2)	1.272(3)
C(1)−C(4)	1.505(4)	N(2)−C(18)	1.430(3)
C(3)−C(5)	1.510(4)		
C(2)−Hg−C(2′)	180.00(10)	C(2)−C(1)−C(4)	115.6(2)
Hg−C(2)−C(1)	107.75(18)	N(1)−C(1)−C(4)	126.1(3)
Hg−C(2)−C(3)	109.81(18)	C(2)−C(3)−N(2)	119.0(2)
C(1)−C(2)−C(3)	114.2(2)	C(3)−N(2)−C(18)	122.2(2)
C(2)−C(1)−N(1)	118.2(2)	C(2)−C(3)−C(5)	115.9(2)
C(1)−N(1)−C(6)	120.2(2)	N(2)−C(3)−C(5)	125.0(3)

Table 2. Crystallographic Data for Compound 1[a]

chem formula	$C_{58}H_{82}HgN_4 \cdot 0.33CH_2Cl_2$
formula wt	1064.03
temp (K)	173(2)
wavelength (Å)	0.710 73
cryst size (mm^3)	0.19 × 0.16 × 0.16
cryst syst	trigonal
space group	$R\bar{3}$ (No. 148)
a (Å)	33.4216(10)
b (Å)	33.4216(10)
c (Å)	12.6432(3)
α (deg)	90
β (deg)	90
γ (deg)	120
V ($Å^3$)	12 230.4(6)
Z	9
ρ_c ($Mg\ m^{-3}$)	1.37
abs coeff (mm^{-1})	2.97
θ range for data collecn (deg)	3.47−26.72
no. of measd/indep rflns, R(int)	17 578/5739, 0.047
no. of rflns with $I > 2\sigma(I)$	5104
no. of data/restraints/params	5739/0/288
goodness of fit on F^2	1.032
final R indices ($I > 2\sigma(I)$)	R1 = 0.033, wR2 = 0.060
R indices (all data)	R1 = 0.042, wR2 = 0.062
largest diff peak and hole (e $Å^{-3}$)	0.60 and −0.50

[a] This molecule sits on an inversion center. The unit cell contains poorly defined CH_2Cl_2 disordered about a special position which has been treated as a diffuse contribution to the overall scattering without specific atom positions by SQUEEZE/PLATON.

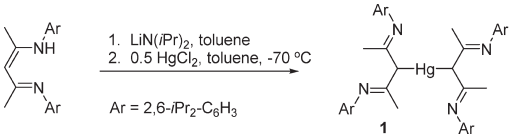

(1)

(16) Chen, M.; Fulton, J. R.; Hitchcock, P. B.; Johnstone, N. C.; Lappert, M. F.; Protchenko, A. V. *Dalton Trans.* **2007**, 2770.
(17) Fulton, J. R.; Hitchcock, P. B.; Johnstone, N. C.; Tam, E. C. Y. *Dalton Trans.* **2007**, 3360.
(18) Tam, E. C. Y.; Johnstone, N. C.; Ferro, L.; Hitchcock, P. B.; Fulton, J. R. *Inorg. Chem.* **2009**, *48*, 8971.
(19) Fulton, J. R.; Holland, A. W.; Fox, D. J.; Bergman, R. G. *Acc. Chem. Res.* **2002**, *35*, 44.
(20) Simple salt metathesis between lithiated β-diketiminate (BDI-Li) and $HgCl_2$ resulted in the formation of an intractable mixture of products; when $LiN(TMS)_2$ was used instead of $LiNiPr_2$, the only isolated BDI-containing product was BDI-Li.
(21) Hadzovic, A.; Janetzko, J.; Song, D. T. *Dalton Trans.* **2008**, 3279.
(22) Kajiwara, T.; Murao, R.; Ito, T. *J. Chem. Soc., Dalton Trans.* **1997**, 2537.
(23) Hadzovic, A.; Song, D. *Organometallics* **2008**, *27*, 1290.
(24) Prust, J.; Hohmeister, H.; Stasch, A.; Roesky, H. W.; Magull, J.; Alexopoulos, E.; Uson, I.; Schmidt, H. G.; Noltemeyer, M. *Eur. J. Inorg. Chem.* **2002**, 2156.
(25) Tian, X.; Goddard, R.; Porschke, K. R. *Organometallics* **2006**, *25*, 5854.
(26) Rake, A.; Zulch, F.; Ding, Y.; Prust, J.; Roesky, H. W.; Noltemeyer, M.; Schmidt, H. G. *Z. Anorg. Allg. Chem.* **2001**, *627*, 836.
(27) Grirrane, A.; Resa, I.; del Rio, D.; Rodriguez, A.; Alvarez, E.; Mereiter, K.; Carmona, E. *Inorg. Chem.* **2007**, *46*, 4667.
(28) Matkoviccalogovic, D. *Acta Crystallogr., Sect. C: Cryst. Struct. Commun.* **1987**, *43*, 1473.
(29) Lide, D. R. *Tetrahedron* **1962**, *17*, 125.

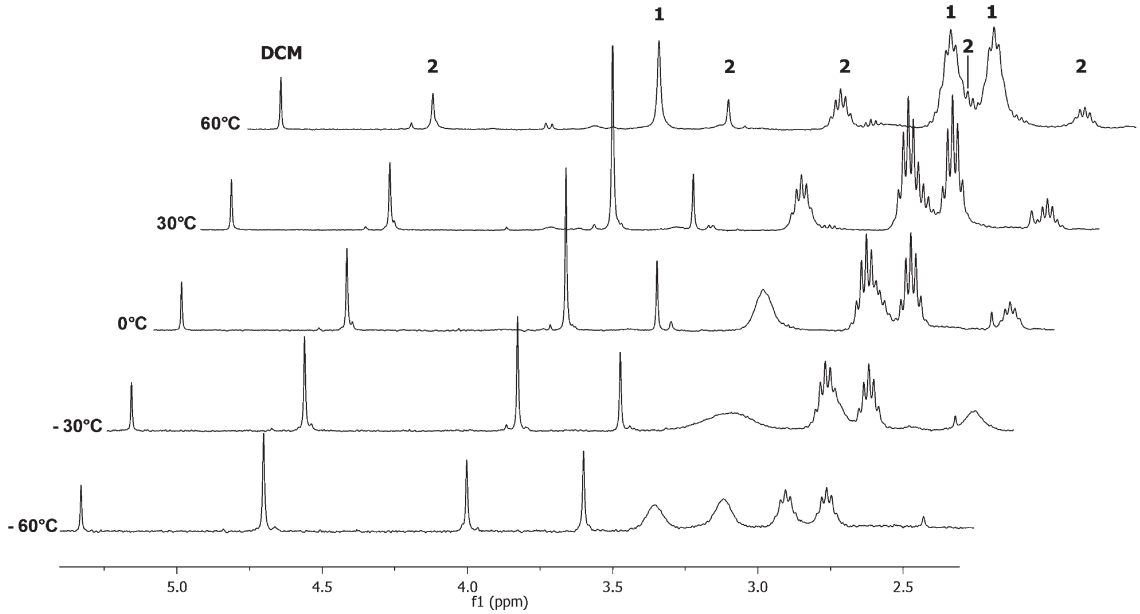

Figure 3. Variable-temperature ^{1}H NMR spectra of **1** and **2** in CD_2Cl_2.

The room-temperature ^{1}H NMR spectrum of **1** reveals the presence of two different compounds in a 3:2 ratio. The major compound can be assigned to the dialkyl species, with a γ-C*H* resonance at δ 3.98 ppm, similar to that reported for L^{1}HgCl. The one-bond ^{1}H$-^{13}$C correlation experiment showed correlation between this proton and a carbon found at δ 77.7 ppm. The resonances corresponding to the minor compound are reminiscent of an N,N′-bound β-diketiminate ligand, with a backbone γ-C*H* resonance at δ 4.75 ppm. Integrating in an approximately 1:1 ratio with this resonance is a peak at δ 3.71 ppm. The ^{1}H$-^{13}$C HSQC experiment revealed that the former proton correlates with a carbon at δ 96.2 ppm, which is in the same range as for other N,N′-bound β-diketiminate compounds,[12,18,30] and the latter proton correlates with a carbon at δ 66.7 ppm, a chemical shift similar to that of the major isomer. No proton−mercury (^{1}H$-^{199}$Hg) or carbon−mercury (^{13}C$-^{199}$Hg) coupling was observed. The ^{199}Hg{^{1}H} NMR spectrum shows a single resonance at both room temperature (−990 ppm) and −60 °C (−1086 ppm). The corresponding resonance line widths at half-height are 144 and 236 Hz, respectively (the data were processed with 75 Hz exponential line broadening prior to Fourier transformation). The observed broad line width can be attributed to the close proximity of the (broad) resonances for the two species (**1** and **2**), leading to the appearance of a single signal, as well as fast relaxation caused by the chemical shift anisotropy of the ^{199}Hg.[31] The latter contribution can be confirmed by the observation that the ^{199}Hg line width at half-height is ∼30% larger at 14.1 T than at 9.4 T (190 Hz, with identical processing parameters). As the line width for this system is larger than the expected magnitude of the coupling constant, no mercury−proton or mercury−carbon coupling could be observed at either temperature. The solid-state IR spectrum (Nujol) revealed three strong bands at 1648, 1624, and 1589 cm^{-1}; although these bands are similar to those for other β-diimine compounds,[15,32] these data are not conclusive for either isomer, as N,N′-bound β-diketiminate complexes have a wide range of stretching frequencies in the same region.[16,18,26] The solution-phase IR spectrum was equally inconclusive.

These data are consistent with an equilibrium mixture of two different mercury species in solution: the major isomer in which both β-diketiminate ligands are bound through the γ-carbon (**1**) and a minor isomer that is still bound to two different β-diketiminate ligands, but one ligand is bound through the N-substituents and the other is bound through the γ-carbon (**2**; eq 2). Variable-temperature ^{1}H NMR spectroscopy revealed that **2** is favored at lower temperatures (Figure 3). From these data, we were able to calculate $\Delta H°$ (−2.52 ± 0.06 kcal mol^{-1}), $\Delta S°$ (−9.24 ± 0.21 cal mol^{-1} K^{-1}), and $\Delta G°_{298}$ (0.23 ± 0.09 kcal mol^{-1}) for the interconversion between the two isomers. This equilibria is similar to a bis(2,2,6,6-tetramethylheptane-3,5-dione)−Hg complex in which an equilibrium is established between a dialkylmercury species and a mercury complex that is bound to one ligand through the γ-carbon and the other ligand through an oxygen atom.[33] Interestingly, the researchers were only able to observe proton−mercury coupling at −40 °C; however, a lower field NMR spectrometer was used, thus significantly decreasing the line width contributions of relaxation due to chemical shift anisotropy.

(30) Dove, A. P.; Gibson, V. C.; Marshall, E. L.; Rzepa, H. S.; White, A. J. P.; Williams, D. J. *J. Am. Chem. Soc.* **2006**, *128*, 9834.
(31) Levitt, M. H. *Spin Dynamics: Basics of Nuclear Magnetic Resonance*, 2nd ed.; WileyBlackwell: 2008.
(32) Carey, D. T.; Cope-Eatough, E. K.; Vilaplana-Mafe, E.; Mair, F. S.; Pritchard, R. G.; Warren, J. E.; Woods, R. J. *Dalton Trans.* **2003**, 1083.
(33) Allmann, R.; Musso, H.; Flatau, K. *Chem. Ber.* **1972**, *105*, 3067.

The thermodynamic parameters were not reported for this latter system.

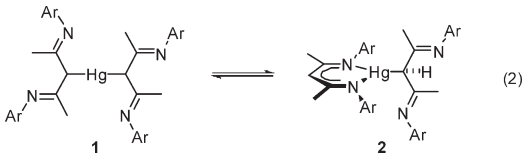

(2)

The variable-temperature ^{1}H NMR spectroscopy experiment also revealed that compound **2** exhibits fluxional behavior on the NMR time scale. At 60 °C, three different resonances corresponding to the isopropyl methine resonances of **2** are observed at δ 3.33, 2.91, and 2.49 ppm integrating to four, two, and two protons each, respectively. The downfield resonance is from the N,N′-bound ligand, and the upfield resonances are from the γ-bound ligand of **2**. At −60 °C, the isopropyl methine resonance on the N,N′-bound ligand of **2** appears as two separate broad resonances, indicating two different environments for the four isopropyl methine protons of this N,N′-bound ligand. This is presumably due to the asymmetry with respect to the γ-bound ligand. At this lower temperature, the bulkiness of the N-aryl groups of both ligands prevent facile rotation around the Hg−C bond. Thus, one aryl group of the N,N′-bound ligand is closer to the methine proton of the γ-carbon of the γ-bound ligand than the other aryl group. Using density functional theory (DFT), we calculated an optimized geometry for compound **2** (Figure 4), which supports this hypothesis. From these variable-temperature studies, the $\Delta G^{\ddagger}$ value for Hg−C bond rotation was determined to be 11 kcal mol^{-1}. Interestingly, the isopropyl methine protons for the γ-bound ligand of **2** appear as septets above 0 °C and as broad resonances at −30 °C and are not observed at −60 °C. Due to the decreasing solubility of **1** and **2**, we were unable to obtain a reliable ^{1}H NMR spectrum below −60 °C to determine the fate of these disappearing signals at lower temperatures. However, it can be assumed that there is further loss of symmetry of the γ-bound ligand due to restricted rotation around the N−aryl bond; as such, we would expect four individual signals for each of the isopropyl methine protons for the γ-bound ligand at temperatures below −60 °C. Interestingly, only two resonances corresponding to the back-bone methyl groups (N−C(Me)−C−C(Me)−N) are observed for compound **2**, even at −60 °C. Although the aliphatic and aromatic regions of the ^{1}H NMR spectrum varied with temperature, due to the overlapping signals, we were unable to gain any further information from this data.

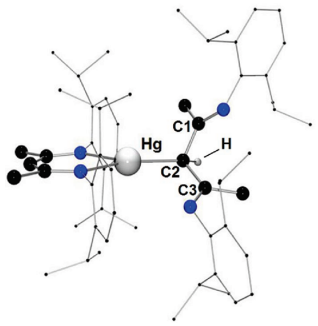

Figure 4. Optimized geometry of **2**.

DFT was also used to calculate the ground-state energies for compounds **1** and **2**. From these data, we were able to calculate $\Delta H°$ (−2.52 ± 0.06 kcal mol^{-1}), $\Delta S°$ (−9.24 ± 0.21 cal mol^{-1} K^{-1}), and $\Delta G°_{298}$ (0.23 ± 0.09 kcal mol^{-1}) for the interconversion between the two isomers. Because of the low level of theory applied, the calculated $\Delta H°$ value (0.60 kcal mol^{-1}) was higher than our measured value and the magnitude of the calculated $\Delta S°$ value (−14 cal mol^{-1} K^{-1}) was greater (although still negative). Due to these discrepancies, the $\Delta G°_{298}$ value (4.9 kcal mol^{-1}) was significantly higher than our experimental results. However, we were able to utilize these calculations in order to predict ^{1}H NMR chemical shifts, and reassuringly, γ-C*H* for isomer **1** was calculated to resonate at δ 4.21 ppm, whereas the Hg-bound γ-C*H* of isomer **2** was calculated to resonate at δ 3.72 ppm and γ-C*H* of the N,N′-bound β-diketiminate ligand of isomer **2** was calculated to resonate at δ 4.48 ppm.

Isolated crystals of compound **1** are relatively air stable, but this compound undergoes thermal decomposition after 48 h at room temperature in solution. Attempts at selectively protonating one of the BDI ligands to form mercury alkoxide or sulfide complexes were not successful. Addition of isopropyl alcohol to **1** led to an intractable mixture of products. Treatment of **1** with 4-methylbenzenethiol gave BDI-H as the only BDI-containing compound.

Experimental Section

All manipulations were carried out under an atmosphere of dry nitrogen or argon using standard Schlenk techniques or in an inert-atmosphere glovebox. Solvents were dried from the appropriate drying agent, distilled, degassed, and stored over 4 Å sieves. The ^{1}H, ^{13}C, and ^{199}Hg NMR spectra were recorded on a Varian 400 MHz spectrometer or a Varian 600 MHz spectrometer. Both spectrometers were equipped with X{^{1}H} broadband-observe probes. The ^{1}H and ^{13}C NMR chemical shifts are given relative to residual solvent peaks, and the ^{199}Hg chemical shifts were determined from the deuterium lock signal and quoted relative to $HgMe_2$ at 0 ppm.[34] The ^{1}H−^{13}C HSQC and ^{1}H−^{13}C HMBC spectra were recorded using the Varian ChemPack 4.1 sequences gHSQCAD and gHMBCAD. The data for the X-ray structure were collected at 173 K on a Nonius Kappa CCD diffractometer (λ(Mo Kα) = 0.710 73 Å) and refined using the SHELXL-97 software package.[35]

[CH{(CH$_3$)$_2$CN-2,6-iPr$_2$C$_6$H$_3$}$_2$]Hg (1). Lithium diisopropylamide (1.20 mmol, 2 M in THF) was added dropwise to a toluene solution of BDI-H (500 mg, 1.20 mmol). The red solution was stirred for 30 min, cooled to −78 °C, and added dropwise to a stirred suspension of $HgCl_2$ (163 mg, 0.60 mmol) in toluene at −78 °C. This mixture was stirred overnight and slowly warmed to room temperature. The resulting gray suspension was filtered through Celite, and the volatiles were evacuated, producing a pale green precipitate that was washed several times with pentane to afford a white powder in 34% yield (0.24 mol, 213 mg). Colorless crystals suitable for X-ray diffraction were grown from a concentrated DCM solution stored in an ethylene glycol bath at 8 °C for 3 days and −12 °C for 1 week. ^{1}H NMR (399 MHz, $CDCl_3$, 303 K): δ 6.93−7.17 (m, 6H, ^{Ar}C*H*), 4.75 (s, 1H, γ-C*H*), 3.98 (s, 1H, γ-C*H*), 3.71 (s, 1H, γ-C*H*), 3.33 (sept, J = 6.4 Hz, 4H, C*H*Me$_2$), 2.97 (sept, J = 6.8 Hz, 2H, C*H*Me$_2$), 2.91 (m, 2H, C*H*Me$_2$), 2.81 (sept, J = 6.9 Hz, 2H,

(34) Harris, R. K.; Becker, E. D.; De Menezes, S. M. C.; Goodfellow, R.; Granger, P. *Pure Appl. Chem.* **2001**, *73*, 1795.
(35) Sheldrick, G. M. In *SHELXL-97, Program for the Refinement of Crystal Structures*; University of Göttingen, Göttingen, Germany, 1997.

C*H*Me$_2$), 2.49 (sept, J = 6.7 Hz, 2H, C*H*Me$_2$), 1.85 (s, 6H, NC*Me*),1.72 (s, 6H, NC*Me*), 1.51 (s, 6H, NC*Me*), 1.18 (d, J = 6.8 Hz, 12H, CH*Me*), 1.14 (d, J = 6.9 Hz, 12H, CH*Me*), 1.11 (d, J = 6.8 Hz, 6H, CH*Me*), 1.10 (d, J = 6.8 Hz, 12H, CH*Me*), 1.06 (d, J = 6.8 Hz, 6H, CH*Me*), δ 0.98 (d, J = 6.8 Hz, 12H, CH*Me*), 0.89 (d, J = 6.7 Hz, 6H, CH*Me*), 0.85 (d, J = 6.9 Hz, 6H, CH*Me*). ^{13}C{^{1}H} NMR (100 MHz, $CDCl_3$): δ 171.38 (N*C*Me), 169.97 (N*C*Me), 164.34 (N*C*Me), 146.46 (*o-C*), 141.48 (*o-C*), 137.03 (*ipso-C*), 136.46 (*ipso-C*), 123.50 (^{Ar}*C*), 123.21 (^{Ar}*C*), 122.99 (^{Ar}*C*), 122.89 (^{Ar}*C*), 122.76 (^{Ar}*C*), 122.63 (^{Ar}*C*), 121.92 (^{Ar}*C*), 96.23 (γ-*C*), 77.72 (γ-*C*), 66.69 (γ-*C*), 28.51 (*C*HMe), 28.51 (*C*HMe), 28.21 (*C*HMe), 27.78 (*C*HMe), 27.69 (CH*Me*), 25.32 (NC*Me*), 24.48 (CH*Me*), 23.75 (CH*Me*), 23.20 (CH*Me*), 22.97 (CH*Me*), 22.49 (CH*Me*), 21.91 (NC*Me*), 21.40 (NC*Me*). ^{199}Hg NMR (71.5 MHz, $CDCl_3$, 303 K): δ −989.7. IR (Nujol, cm^{-1}): 3050, 1921, 1866, 1806, 1720, 1648 (s), 1624 (s), 1589 (s), 1439 (s), 1358 (s),1328 (s), 1245, 1207 (s), 1188 (s), 1163 (s), 1107, 1068, 1059, 1042, 972, 936, 916, 789 (s), 760 (s), 690, 523. IR (CCl_4, cm^{-1}): 3061 (w), 2963, 2869, 2990 (br), 2004 (br), 1856 (br), 1635, 1549 (br, s), 1461, 1436, 1409, 1382, 1363, 1322, 1253 (s), 1216 (s), 1165 (w). Anal. Calcd: C, 67.25; H, 7.98; N, 5.41. Found: C, 67.16; H, 8.07; N, 5.39.

Key Chemical Shifts for 1. ^{1}H NMR (399 MHz, $CDCl_3$, 303 K): δ 3.98 (s, 1H, γ-C*H*), 2.97 (sept, J = 6.8 Hz, 2H, C*H*Me$_2$), 2.81 (sept, J = 6.9 Hz, 2H, C*H*Me$_2$), 1.85 (s, 6H, NC*Me*), 1.11 (d, J = 6.8 Hz, 6H, CH*Me*), 1.10 (d, J = 6.8 Hz, 12H, CH*Me*), 0.8 (d, J = 6.8 Hz, 6H, CH*Me*). ^{13}C{^{1}H} NMR (100 MHz, $CDCl_3$): δ 171.38 (N*C*Me), 146.46 (*o-C*), 136.46 (*ipso-C*), 77.72 (γ -*C*), 28.51 (*C*HMe), 23.20 (CH*Me*), 22.97 (CH*Me*), 21.91 (NC*Me*).

Key Chemical Shifts for 2. N,N′-bound ligand: ^{1}H NMR (399 MHz, $CDCl_3$, 303 K) δ 4.75 (s, 1H, γ-C*H*), 3.33 (sept, J = 6.4 Hz, 4H, C*H*Me$_2$), 1.72 (s, 6H, NC*Me*), 1.18 (d, J = 6.8 Hz, 12H, CH*Me*), 1.14 (d, J = 6.9 Hz, 12H, CH*Me*);^{13}C{^{1}H} NMR (100 MHz, $CDCl_3$) 164.34 (N*C*Me), (*ipso-C*), 141.48 (*o-C*), 141.26 (*o-C*), 96.23 (γ-*C*), 27.78 (*C*HMe), 27.69 (CH*Me*), 25.32 (NC*Me*), 24.48 (CH*Me*). γ-bound ligand: ^{1}H NMR (399 MHz, $CDCl_3$, 303 K) δ 3.71 (s, 1H, γ-C*H*), 2.91 (m, 2H, C*H*Me$_2$), 2.49 (sept, J = 6.7 Hz, 2H, C*H*Me$_2$), 1.51 (s, 6H, NC*Me*), 0.98 (d, J = 6.8 Hz, 12H, CH*Me*), 0.89 (d, J = 6.7 Hz, 6H, CH*Me*), 0.85 (d, J = 6.9 Hz, 6H, CH*Me*); ^{13}C{^{1}H} NMR (399 MHz, $CDCl_3$) δ 169.97 (N*C*Me), 137.03 (*ipso-C*), 66.69 (γ-*C*), 28.21 (*C*HMe), 28.51 (*C*HMe), 23.75 (CH*Me*), 23.20 (CH*Me*), 22.49 (CH*Me*), 21.40 (NC*Me*).

Computational Details. All calculations were performed using the density function theory in the Gaussian 03 program. The geometry optimization was performed at the B3LYP level by using a double-ζ basis set (LanL2DZ) along with the effective core potential (LanL2ECP) for the Hg atom and the 3-21G basis set for all other atoms. Zero-point vibrational energy corrections were also included.[36,37] ^{1}H NMR spectra were estimated with the gauge invariant atomic orbital DFT (GIAO-DFT) calculations at the B3LYP/LanL2DZ/3-21G level.

Acknowledgment. We are grateful for financial support from the EPSRC (LF, Grant No. EP/E032575/1).

Supporting Information Available: Figures giving a van't Hoff plot of the equilibria between **1** and **2**, variable-temperature ^{1}H NMR spectra showing resonances between δ 8 and 0 ppm, and ^{1}H−^{13}C gHSQCAD and ^{1}H−^{13}C gHMBCAD spectra, a table giving Cartesian coordinates of the optimized structures of **1** and **2**, text giving the complete ref 31, and a CIF file giving crystallographic data for complex **1**. This material is available free of charge via the Internet at http://pubs.acs.org.

(36) Frisch, M. J. et al. In *Gaussian 03, Revision E.01*; Gaussian, Inc., Wallingford, CT, 2004.
(37) Wadt, W. R.; Hay, P. J. *J. Chem. Phys.* **1985**, *82*, 284.

Inorganic Chemistry
Article

Inorg. Chem. **2011**, *50*, 1879–1888 **1879**
DOI: 10.1021/ic102273n

Activation of Carbon Dioxide by Divalent Tin Alkoxides Complexes

Lorenzo Ferro, Peter B. Hitchcock, Martyn P. Coles, Hazel Cox, and J. Robin Fulton*

Department of Chemistry, University of Sussex, Falmer, Brighton BN1 9QJ, U.K.

Received November 12, 2010

A series of terminal tin(II) alkoxides have been synthesized utilizing the bulky β-diketiminate ligand [{N(2,6-^{i}Pr$_2$C$_6$H$_3$)-C(Me)}$_2$CH] (BDI). The nucleophilicities of these alkoxides have been examined, and unexpected trends were observed. For instance, (BDI)SnOR only reacts with highly activated aliphatic electrophiles such as methyl triflate, but reacts reversibly with carbon dioxide. Both the rate of reaction and the degree of reversibility is dependent upon minor changes in the alkoxide ligand, with the bulkier *tert*-butoxide ligand displaying slower reactivity than the corresponding isopropyl ligand, although the latter system is a more exergonic reaction. Density Function Theory (DFT) calculations show that the differences in the reversibility of carbon dioxide insertion can be attributed to the ground-state energy differences of tin alkoxides while the rate of reaction is attributed to relative bond strengths of the Sn−O bonds. The mechanism of carbon dioxide insertion is discussed.

Introduction

The activation of carbon dioxide by metal complexes has recently received fresh attention because of the obvious implication for carbon dioxide sequestering or converting carbon dioxide into a useful carbon feedstock. Metal complexes used in carbon dioxide activation generally possess nucleophilic ligands such as alkoxides and amides; in these systems, carbon dioxide is inserted into the M−O or M−N bond to form a metallo-alkylcarbonate (or -alkylcarbamate) complex.[1−11] In general, most metal alkoxide complexes react reversibly with carbon dioxide,[1,3−9] presumably because of similar M−O bond strengths of the metal alkoxide and metallo-alkylcarbonate. Metal amide complexes exhibit both reversible[12] and irreversible reactivity with carbon dioxide.[1,10] The mechanism for carbon dioxide insertion into M−O or M−N bonds has been postulated to occur via a four-membered transition state in which the alkoxide or amide ligand acts as a nucleophile onto the electrophilic carbon atom concurrent with coordination of one of the carbon dioxide oxygen atoms to the metal center and a weakening of the M−O and the C═O bonds (Scheme 1). An open coordination site is unnecessary for this nucleophilic insertion reaction[13] and the driving force for this reaction is generally thought to be the strong nucleophilicity of the alkoxide or amide ligand.[1,9,11]

Although tin(IV) alkoxides complexes are known to react with carbon dioxide,[7,14] the reactivity of the less Lewis acidic tin(II) alkoxides has not been explored outside of lactide polymerization studies.[15,16] Divalent tin has one of the lowest aqueous acidities of any metal species (pK_a = 2),[17,18] significantly lower than what is predicted based upon electrostatic parameters. As such, the resultant tin hydroxide species is very weakly basic and should not exhibit nucleophilic behavior. As the reactivity of alkoxides is similar to that of hydroxides, divalent tin alkoxides should also be very weakly basic and non-nucleophilic.

We have recently synthesized a series of monomeric divalent lead alkoxides complexes utilizing the bulky β-diketiminate monoanionic ligand [{N(2,6-^{i}Pr$_2$C$_6$H$_3$)C(Me)}$_2$CH]$^-$ (BDI) to stabilize the low-coordinate complexes.[4,19] As with divalent

*To whom correspondence should be addressed. E-mail: j.r.fulton@sussex.ac.uk.

(1) Simpson, R. D.; Bergman, R. G. *Organometallics* **1992**, *11*, 4306.
(2) Darensbourg, D. J.; Sanchez, K. M.; Rheingold, A. L. *J. Am. Chem. Soc.* **1987**, *109*, 290.
(3) Darensbourg, D. J.; Sanchez, K. M.; Reibenspies, J. H.; Rheingold, A. L. *J. Am. Chem. Soc.* **1989**, *111*, 7094.
(4) Tam, E. C. Y.; Johnstone, N. C.; Ferro, L.; Hitchcock, P. B.; Fulton, J. R. *Inorg. Chem.* **2009**, *48*, 8971.
(5) Tsuda, T.; Saegusa, T. *Inorg. Chem.* **1972**, *11*, 2561.
(6) Chisholm, M. H.; Cotton, F. A.; Extine, M. W.; Reichert, W. W. *J. Am. Chem. Soc.* **1978**, *100*, 1727.
(7) Choi, J.-C.; Sakakura, T.; Sako, T. *J. Am. Chem. Soc.* **1999**, *121*, 3793.
(8) Mandal, S. K.; Ho, D. M.; Orchin, M. *Organometallics* **1993**, *12*, 1714.
(9) Darensbourg, D. J.; Lee, W. Z.; Phelps, A. L.; Guidry, E. *Organometallics* **2003**, *22*, 5585.
(10) Boyd, C. L.; Clot, E.; Guiducci, A. E.; Mountford, P. *Organometallics* **2005**, *24*, 2347.
(11) Brombacher, H.; Vahrenkamp, H. *Inorg. Chem.* **2004**, *43*, 6042.
(12) McCowan, C. S.; Groy, T. L.; Caudle, M. T. *Inorg. Chem.* **2002**, *41*, 1120.
(13) Darensbourg, D. J.; Mueller, B. L.; Bischoff, C. J.; Chojnacki, S. S.; Reibenspies, J. H. *Inorg. Chem.* **1991**, *30*, 2418.
(14) Kizlink, J. *Collect. Czech. Chem. Commun.* **1993**, *58*, 1399.
(15) Dove, A. P.; Gibson, V. C.; Marshall, E. L.; White, A. J. P.; Williams, D. J. *Chem. Commun.* **2001**, 283.
(16) Dove, A. P.; Gibson, V. C.; Marshall, E. L.; Rzepa, H. S.; White, A. J. P.; Williams, D. J. *J. Am. Chem. Soc.* **2006**, *128*, 9834.
(17) Burgess, J. *Metal Ions in Solution*; Ellis Horwood Ltd: Chichester, U.K., 1978.
(18) Cox, H.; Stace, A. J. *J. Am. Chem. Soc.* **2004**, *126*, 3939.
(19) Fulton, J. R.; Hitchcock, P. B.; Johnstone, N. C.; Tam, E. C. Y. *Dalton Trans.* **2007**, 3360.

Published on Web 01/13/2011

Scheme 1. Insertion of Carbon Dioxide into a M−O Bond via a Four-Membered Transition State. R is Either an Aliphatic or Aromatic Group

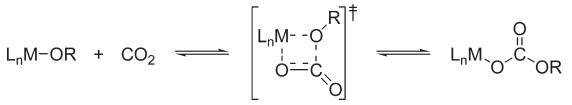

tin, divalent lead has a low aqueous acidity of 7.2.[17] As such, lead hydroxides, and by analogy, lead alkoxides, should only be weakly nucleophilic. Our (BDI)PbOR (R = *i*Pr, *s*Bu, and *t*Bu) complexes displayed only sluggish reactivity with methyl iodide, suggesting that the lead alkoxides are non-nucleophilic. However, these lead alkoxide complexes do react readily and reversibly with carbon dioxide to form lead-alkylcarbonate complexes. Both the rate of reaction as well as the degree of reversibility was found to be dependent upon the alkoxide substituent. For instance, when (BDI)PbO^{i}Pr was treated with carbon dioxide, quantitative formation of the corresponding carbonate was observed. In contrast, when the alkoxide substituent was *tert*-butoxide, (BDI)PbO^{t}Bu, the carbonate was only observed in solution and application of reduced pressure resulted in the reformation of the alkoxide. Although our investigations of the lead system allowed for a qualitative study on these observations, a more quantitative examination was thwarted by decomposition of the *tert*-butyl carbonate, preventing accurate equilibrium measurements. Fortunately, the isostructural tin system has similar, but slower, reactivity patterns to that of the lead alkoxides; as such, we report the results of the thermodynamic and computational studies for the insertion of carbon dioxide into a Sn(II)−O bond, as well as factors behind the apparent non-nucleophilicity of these group 14 alkoxide complexes.

Results

Synthesis and Reactivity. The synthesis of tin isopropoxide (BDI)SnO^{i}Pr (**2a**) has been reported elsewhere.[15] Treatment of a THF solution of (BDI)SnCl(**1**) with KO^{s}Bu and KO^{t}Bu affords tin alkoxides (BDI)SnO^{s}Bu (**2b**) and (BDI)SnO^{t}Bu (**2c**), respectively, after three days at room temperature (eq 1). The X-ray crystal structures were determined for **2b** and **2c**; Figure 1 shows the ORTEP diagrams of *sec*-butoxide **2b** and *tert*-butoxide **2c**. Selected bond lengths and angles for **2a**, **2b**, and **2c** are reported in Table 1 and data collection parameters for **2b** and **2c** are given in Table 2. Analogous to the solid-state structures reported for **2a**, as well as the isostructural lead compounds, a pyramidal ligand arrangement is observed around the tin metal center. This geometry is presumably a result of the relativistic contraction of the 5*s* tin orbital, resulting in minimal hybridization of the *s* and *p* orbitals, thus producing a stereochemically active lone pair.[20,21] The alkoxy group in the solid state structure of **2a**, **2b**, and **2c** points away from the BDI-Sn core and, in contrast to the (BDI)-SnCl precursor, the Sn and alkoxide ligand lie on opposite sides of the BDI backbone N_2C_3 plane. Only minor variations are observed between the tin alkoxide complexes, such as an increase in the Sn−O bond length with the increasing bulk of the alkoxy ligand, and a very slight increase of pyramidalization around the tin metal center with increasing bulk of the alkoxy ligand.

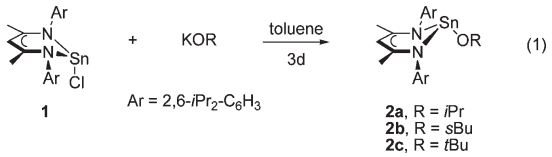

The reactivity of tin alkoxides **2a**, **2b**, and **2c** with aliphatic electrophiles was examined. No reactivity was observed between the tin alkoxides and methyl iodide, even at elevated temperatures. This is in contrast to the apparent nucleophilic reactivity observed with the isostructural lead alkoxides complexes; formation of (BDI)-PbI and the corresponding methyl ether was observed upon heating a solution of (BDI)PbOR with methyl iodide.[4] In addition, this lack of reactivity is also in contrast to transition metal alkoxide complexes in which facile reactivity with aliphatic electrophiles is observed.[11,22] Addition of a more reactive electrophile, methyl triflate, to **2a**, **2b**, and **2c** does result in apparent nucleophilic behavior of the alkoxides as the known (BDI)SnOTf complex (**3**) is formed along with the corresponding methyl ether (eq 2).[23] Interestingly, the half-life for this reaction is dependent upon the alkoxide group, with the tin isopropoxide **2a** proving to be the most reactive ($t_{1/2}$ = 8 min), tin *sec*-butoxide **2b** to be slightly slower ($t_{1/2}$ = 15 min) and the tin *tert*-butoxide **2c** to be the most sluggish ($t_{1/2}$ = 150 min).

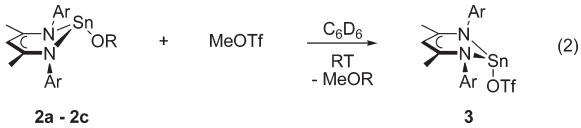

In contrast to aliphatic electrophiles, compounds **2a**, **2b**, and **2c** readily react with unsaturated electrophiles. Although addition of CS_2 and phenylisocyanate to the tin alkoxide complexes gave intractable product mixtures, treatment of isopropoxide **2a** with maleic anhydride results in ring opened product (BDI)SnO$_2$CCHCHCO$_2{}^{i}$Pr **4** in 87% yield (eq 3). The X-ray crystal structure was determined (Figure 2); the bond lengths and bond angles are listed in Table 3 and data collection parameters are listed in Table 2. Although this reactivity is known for transition metal alkoxides this is a rare example a structurally characterized terminal metal maleate complex.[24,25] The unit cell consists of two independent molecules that differ in the conformation of the maleate ligand. In both molecules, the metal center and the maleate ligand lie on the same side of the N_2C_3 backbone plane and the ligand bond angles around the metal center are more acute than in the alkoxide examples. The Sn−O bond length is longer than the alkoxide analogues, potentially due to a stabilizing Sn···O2 interaction

(20) Chen, M.; Fulton, J. R.; Hitchcock, P. B.; Johnstone, N. C.; Lappert, M. F.; Protchenko, A. V. *Dalton Trans.* **2007**, 2770.
(21) For a good description of this hybridization, see reference 16.
(22) Fulton, J. R.; Holland, A. W.; Fox, D. J.; Bergman, R. G. *Acc. Chem. Res.* **2002**, *35*, 44.
(23) Ding, Y.; Roesky, H. W.; Noltemeyer, M.; Schmidt, H.-G.; Power, P. P. *Organometallics* **2001**, *20*, 1190.
(24) Cuesta, L.; Hevia, E.; Morales, D.; Perez, J.; Riera, L.; Miguel, D. *Organometallics* **2006**, *25*, 1717.
(25) Fulton, J. R.; Sklenak, S.; Bouwkamp, M. W.; Bergman, R. G. *J. Am. Chem. Soc.* **2002**, *124*, 4722.

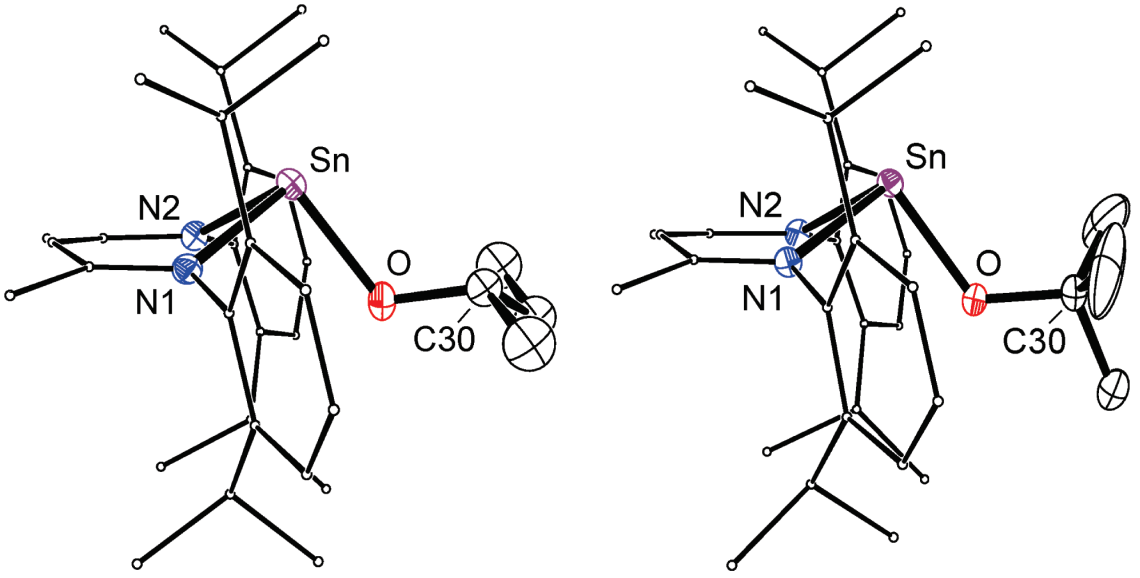

Figure 1. ORTEP diagrams of (BDI)SnO^{t}Bu **2b** (left) and (BDI)SnO^{t}Bu **2c** (right) with H atoms omitted and BDI aryl groups C atoms minimized for clarity; ellipsoid probability shown at 30%.

Table 1. Selected Bond Lengths (Å) and Angles (deg) for Compounds **2a**, **2b**, **2c**, and **2d**

	(BDI)SnO^{i}Pr (**2a**)[a]	(BDI)SnO^{s}Bu (**2b**)	(BDI)SnO^{t}Bu (**2c**)	(BDI)SnO^{t}Bu^F (**2d**)
Sn−O	2.000(5)	2.013(3)	2.0179(16)	2.110(2)
Sn−N(1)	2.206(4)	2.202(3)	2.2015(19)	2.1837(16)
Sn−N(2)	2.208(4)	2.202(3)	2.2100(19)	2.1837(16)
O−C(30)	1.418	1.442(7)	1.419(3)	1.360(3)
N(1)−Sn−N(2)	83.6(2)	82.79(11)	83.02(7)	83.53(8)
N(1)−Sn−O(1)	94.1(2)	94.08(12)	92.66(7)	93.65(6)
N(2)−Sn−O(1)	95.2(2)	94.29(12)	93.89(7)	93.65(6)
Sn−O−C(30)[c]	118.58	118.1(3)	122.40(16)	128.97(18)
Sn−NCCCN plane	0.938	0.974	0.990	1.056
sum of angles around Sn	272.9	271.16	269.57	270.83
DP (%)[b]	97	99	100	99

[a] See ref 14. [b] Degree of pyramidalization, DP (%) = (360 − [sum of angles])/0.9. [c] C(16) for **2d**

of 2.954 Å (molecule A) and 2.898 Å (molecule B), which are inside the combined Sn−O van der Waals radii of 3.69 Å.

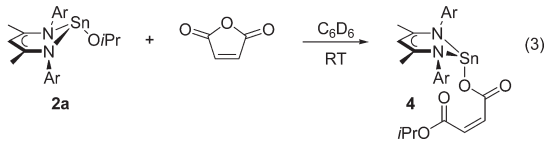

All three tin alkoxides react with carbon dioxide to give the carbonate insertion product (BDI)SnOCO$_2$R (**5a**−**5c**) (Scheme 2). Although the facile reversibility of this reaction has prevented any solid-state characterization of the tin alkylcarbonates **5**, IR spectroscopy (CCl_4) showed the characteristic solution phase carbonyl stretching frequencies at 1621 cm^{-1}. In addition, the ^{13}C NMR spectrum of all three products reveals a resonance at δ 158.7 (**5a**), 158.8 (**5b**), and 158.9 (**5c**) ppm, indicative of a carbonate carbon.[4,8,26] Addition of $^{13}CO_2$ to all of the alkyl carbonates results in an increase of the ^{13}C NMR carbonate resonance. Further conformation of the nature of the product was given by treatment of tin chloride **1** with the potassium salt of monoalkyl carbonate (KO_2COR, R = ^{s}Bu, ^{t}Bu), which produced a mixture of tin alkoxide **2** and tin carbonate **5**. Although KO_2COR does revert to KOR and CO_2, this latter reaction only happens at elevated temperatures.

Interestingly, and similar to the lead alkoxide system, the rate of reaction between **2** and CO_2, as well as the observed equilibria between alkoxide **2**, CO_2 and metallo-alkylcarbonate **5** is dependent upon the nature of the alkyl group on the alkoxide ligand. For instance, the $t_{1/2}$ for the reaction between isopropoxide **2a** or *sec*-butoxide **2b** with 1 atm of CO_2 is < 10 min, and complete conversion to the metallo-alkylcarbonates was observed, but the reaction between *tert*-butoxide **2c** with 1 atm of CO_2 is significantly slower and only goes to 74% completion after one week at room temperature.

Equilibrium Studies. To further understand the influence of the alkyl group on the reaction, we investigated both the equilibria formed between the reactants (**2** and CO_2) and products (**5**), as well as the rate of reaction between the alkoxides and carbon dioxide. These studies

(26) Campora, J.; Matas, I.; Palma, P.; Alvarez, E.; Graiff, C.; Tiripicchio, A. *Organometallics* **2007**, *26*, 3840.

Table 2. Crystallographic Data for Compounds **2b**, **2c**, **2d**, and **4**

	(BDI)SnO^{s}Bu (**2b**)	(BDI)SnO^{t}Bu (**2c**)[a]	(BDI)SnO^{t}Bu^F (**2d**)[b]	(BDI)Sn(Ma)O^{i}Pr (**4**)[c]
chemical formula	$C_{33}H_{50}N_2OSn$	$C_{33}H_{50}N_2OSn$	$C_{33}H_{41}F_9N_2OSn$	$C_{36}H_{50}N_2O_4Sn$
formula weight	609.44	609.44	771.37	693.47
temp (K)	173(2)	173(2)	173(2)	173(2)
wavelength (Å)	0.71073	0.71073	0.71073	0.71073
cryst size (mm^3)	0.4 × 0.3 × 0.3	0.15 × 0.10 × 0.10	0.16 × 0.08 × 0.06	0.23 × 0.20 × 0.10
cryst syst	triclinic	monoclinic	monoclinic	triclinic
space group	$P\bar{1}$ (No.2)	$P2_1/n$ (No. 14)	$P2_1/m$ (No. 11)	$P\bar{1}$ (No.2)
a (Å)	8.7788(2)	13.3880(2)	8.9128(2)	14.7295(3)
b (Å)	9.8810(2)	16.7487(3)	19.8833(5)	16.2188(2)
c (Å)	20.5060(4)	15.2140(2)	10.4482(2)	17.6171(2)
α (deg)	92.884(2)	90	90	110.624(1)
β (deg)	90.071(1)	107.654(1)	113.394(1)	99.628(1)
γ (deg)	113.948(1)	90	90	108.961(1)
V (Å^3)	1623.12(6)	3250.80(9)	1699.96(7)	3531.49(9)
Z	2	4	2	4
p_c (Mg m^{-3})	1.25	1.25	1.51	1.30
abs coeff (mm^{-1})	0.81	0.81	0.83	0.76
θ range for data collection (deg)	3.64−26.06	3.42−26.01	3.74−27.11	3.40−27.10
measured/indep rflns/R(int)	23390/6364/0.043	45959/6387/0.051	27173/3861/0.063	56849/15530/0.058
rflns with $I > 2\sigma$(I)	5816	5479	3446	12240
data/restraints/params	6364/0/331	6387/0/347	3861/0/263	15530/0/779
GOF on F^2	1.110	1.057	1.023	1.011
final R indices [$I > 2\sigma(I)$]	R_1 = 0.045, R_2 = 0.117	R_1 = 0.029, R_2 = 0.067	R_1 = 0.028, R_2 = 00.059	R_1 = 0.033, R_2 = 0.070
R indices (all data)	R_1 = 0.050, R_2 = 0.121	R_1 = 0.037, R_2 = 0.071	R_1 = 0.035, R_2 = 0.062	R_1 = 0.051, R_2 = 0.076
largest diff. peak and hole (e Å^3)	2.63 and −1.13	0.56 and −0.50	0.36 and −0.35	0.44 and −1.10

[a] The isobutyl group attached to O is disordered over two partially overlapping orientations with the C30 and C31 alternative positions resolved, and was included with isotropic C atoms. [b] The molecule lies on a mirror plane with the alkoxide group disordered over two positions. [c] There are two independent molecules in the unit cell that differ in the conformation of the maleate ligand.

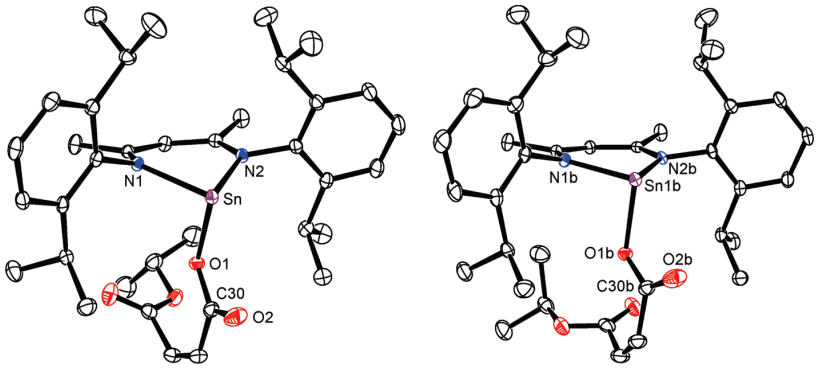

Figure 2. ORTEP diagrams of **4** showing molecule A (left) and molecule B (right) with H atoms omitted for clarity; ellipsoid probability shown at 30%.

Table 3. Selected Bond Lengths and Angles for Compound **4**

molecule A		molecule B	
Sn−O(1)	2.1489(16)	Sn(1b)−O(1b)	2.1534(16)
Sn−N(1)	2.1812(17)	Sn(1b)−N(1b)	2.1866(17)
Sn−N(2)	2.1784(18)	Sn(1b)−N(2b)	2.1851(18)
Sn−O(2)	2.898	Sn(1b)−O(2b)	2.954
N(1)−Sn−N(2)	84.88(7)	N(1b)−Sn(1b)−N(2b)	86.09(7)
O(1)−Sn−N(1)	87.32(7)	O(1b)−Sn(1b)−N(1b)	88.78(6)
O(1)−Sn−N(2)	87.90(7)	O(1b)−Sn(1b)−N(2b)	86.09(7)
sum of angles	260.1	sum of angles	260.96
DP (%)[a]	111	DP (%)[a]	110

[a] Degree of pyramidalization, DP (%) = (360 − [sum of angles]/0.9).

are complicated by an additional equilibria between gas phase and solution phase CO_2, which was partially overcome by flooding the reaction with carbon dioxide (1 atm), allowing us to maintain a steady CO_2 concentration and calculate the mole fraction (χ_{CO2}) solubility corrected to a partial pressure of 1.013 bar.[27]

At 298 K and 1 atm of CO_2, the ^{1}H NMR spectrum shows that the tin isopropoxide **2a** is completely converted to the corresponding carbonate **5a**. However, at 313 K, the conversion is only 92%. As such, we used this temperature to perform our comparative equilibrium measurements. Table 4 shows the ratio of **2** and **5** at 313 K, and the calculated K_{eq} and $\Delta G°$ for each system. Although the apparent equilibrium favors the reactants at elevated temperatures, we are unfortunately limited as to a "usable" temperature range due to lack of carbon dioxide solubility data outside of the 283 − 313 K temperature range at barometric pressures.[27] The equilibria between *tert*-butoxide **2c** and metallo-alkylcarbonate **5c** was measured at four different temperatures and the $\Delta H°$ (−13.8 kcal mol^{-1}), $\Delta S°$ (−39.6 cal mol^{-1} K^{-1}), and $\Delta G°_{298}$ (−2.0 kcal mol^{-1}) were calculated for the insertion of CO_2 into the Sn−O*t*Bu bond. As there was no measurable amount of isopropoxide

(27) Fogg, P. G. T.; Gerrard, W. In *Solubility of Gases in Liquids*; John Wiley & Sons: Chichester, England, 1991, p 249.

Scheme 2. Reaction of Alkoxides **2a**−**2c** with CO_2 to Form Carbonates **5a**−**5c** and the Various Equilibria Involved

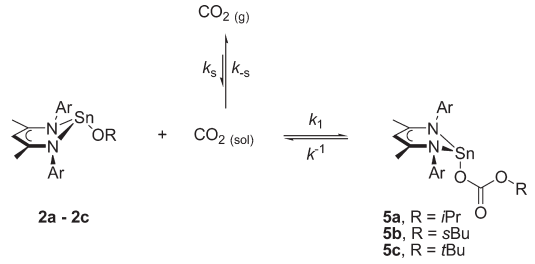

Table 4. Ratio of Alkoxide **2** to Carbonate **5**, K_{eq} $\Delta G°_{313}$ (kcal mol^{-1}), and Relative Time to Equilibrium (t_{equil}) for the Equilibrium between **2**/CO_2 and **5**[a]

	2: **5**	K_{eq}	$\Delta G°_{313}$	(t_{equil})
^{i}Pr (**2a**/**5a**)	7.6:92.4	191	−3.27	3 h
^{s}Bu (**2b**/**5b**)	11.1:88.9	178	−3.22	1 d
^{t}Bu (**2c**/**5c**)	45.4:54.6	20	−1.88	3 d

[a] All measurements were performed in C_6D_6 at 313 K using 36.4 mM alkoxide in a sealed NMR tube with a 50 cm^3 head-space (to maintain a steady CO_2 concentration). The calculated CO_2 concentration at this temperature is 0.091 M.

or *sec*-butoxide at room temperature, the $\Delta H°$ and $\Delta S°$ was not determined for these latter systems.

Although we were able to flood with carbon dioxide to obtain accurate equilibrium measurements, determination of the reaction rate using NMR spectroscopy was impossible because of limited ability to mix the solution, resulting in diffusion of carbon dioxide to be rate influencing. We were able to qualitatively gauge the reaction rate; for the isopropoxide system, equilibrium was established after 3 h at 313K, for the *sec*-butoxide system, equilibrium was established after 1 d at 313 K, and for the *tert*-butoxide system, equilibria was established after 3 d at 313K; however, all reactions proceeded faster when the NMR tube was shaken. Unfortunately, UV−vis spectroscopic measurements gave unreliable results, thus thwarting our attempts to examine the relative rates in greater detail.

Nonafluoro-*tert*-butoxide Tin Complex. The nonafluoro-*tert*-butoxide tin complex **2d** was synthesized in order to gauge the role of steric and electronic factors in the reactivity trends of the tin alkoxides **2a**−**2c**. The X-ray crystal structure was determined for **2d**, and revealed a significantly shorter O−C31 bond length when compared to the per-protio *tert*-butoxide analogue **2c**, presumably due to the electronic withdrawing nature of the fluoroalkyl groups (Figure 3). The Sn−O bond length of 2.110(2) Å is significantly longer than **2c** (2.0179(16) Å). This can be attributed to the increased ionic nature of the Sn−O bond, which is also reflected in the shortened Sn−N bond lengths (average 2.1837 Å for **2d** versus average 2.2058 Å for **2c**). Potential long-range Sn···F interaction is observed between Sn and F1 (3.204 Å), F2 (3.353 Å) and F9 (3.433 Å) as all of these distances are shorter than the sum of the Sn−F radii of 3.64 Å, consistent with other fluoroalkoxide complexes.[28,29]

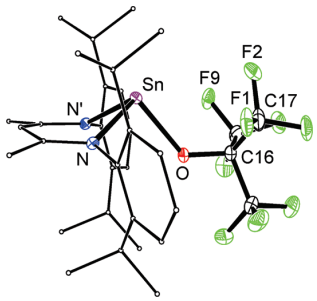

Figure 3. ORTEP diagram of (BDI)SnO^{t}Bu^{F} **2d** (fluorine atoms in green) with H atom omitted and BDI aryl groups C atoms minimized for clarity; ellipsoid probability shown at 30%.

Treatment of (BDI)SnO^{t}Bu^{F} **2d** with methyl triflate produces an intractable mixture of products; no evidence for either (BDI)Sn-OTf or $MeOC(CF_3)_3$ was found. Addition of maleic anhydride to **2d** leads to the protonated ligand LH and no isolable tin containing species. In sharp contrast to the perprotonated alkoxides **2a**−**2c**, perfluoro **2d** does not react with carbon dioxide.

Computational Studies. Density Functional Theory (DFT) studies were performed to further understand the influence of the alkyl group on both the thermodynamics and kinetics for the formation of tin alkylcarbonates from the reaction of tin alkoxides with carbon dioxide. Geometry optimization and single point energy calculations were performed on tin alkoxides **2a**, **2b**, **2c**, and **2d** and the corresponding alkylcarbonates **5a**, **5b**, **5c**, and **5d** using a B3LYP/Lanl2dz/3-21 g level of theory for the geometry optimization of the entire molecule followed by a single point energy calculation using a larger basis set (see Experimental Section).[30] The geometry optimization for the alkoxide complexes (**2a**, **2b**, **2c**, and **2d**) are in good agreement with the experimental results, although the N−Sn−O bond angles are overestimated by 5 − 7% for the nonfluorinated alkoxide complexes **2a**−**2c** (see Supporting Information). The $\Delta G°_{298}$ for the insertion of carbon dioxide into the tin alkoxide was calculated to be closer to neutrality than our experimental results, with a positive $\Delta G°_{298}$ for the *sec*-butyl and *tert*-butyl systems and a negative $\Delta G°_{298}$ for the isopropyl system. However, the trends in reactivity of the different alkyl groups correspond to what we observe; that is, the $\Delta G°_{298}$ was more positive for the *tert*-butoxide system and the least positive for the isopropoxide system.

An abbreviated molecule in which the *N*-aryl groups, as well as the backbone methyl groups, are replaced with protons, $[CH\{CHCNH\}_2]^-$ (L*) was used to give further mechanistic insight into the insertion of carbon dioxide into the tin−oxygen bond.[31] This smaller ligand was utilized in looking for transition states in the reaction pathway and, because of the minimal steric influence of this ligand, providing information about the different electronic contributions from each of the different alkoxide substituents. The reaction profile for the conversion of L*SnO^{i}Pr to the corresponding metallo-alkylcarbonate

(28) Reisinger, A.; Trapp, N.; Krossing, I.; et al. *Organometallics* **2007**, *26*, 2096.
(29) Samuels, J. A.; Lobkovsky, E. B.; Streib, W. E.; Folting, K.; Huffman, J. C.; Zwanziger, J. W.; Caulton, K. G. *J. Am. Chem. Soc.* **1993**, *115*, 5093.
(30) Frisch, M. J. et al. et. al. *Gaussian 03*, revision C.02; Gaussian, Inc.: Wallingford, CT, 2004.
(31) Liu, C.; Munjanja, L.; Cundari, T. R.; Wilson, A. K. *J. Phys. Chem. A* **2010**, *114*, 6207.

Table 5. Calculated Thermodynamic (kcal mol^{-1}) and Kinetic (s^{-1}) Parameters at the B3LYP/[4333111/433111/43]/6-31g(d,p) Level of Theory, for the Transformation of (BDI)SnOR to (BDI)SnO(CO_2)R and L*SnOR to L*SnO(CO_2)R

	L = BDI			L* = [CH {CHCNH}$_2$]					
	$\Delta G°$	$\Delta H°$	$\Delta E°$	$\Delta G°$	$\Delta H°$	$\Delta E°$	$\Delta G^{‡}$	$\Delta H^{‡}$	$\Delta E^{‡}$
^{i}Pr	−0.0	−9.7	−9.5	−4.0	+7.0	−13.7	+10.4	+0.8	+0.8
^{s}Bu	+0.5	−10.8	−10.2	−2.9	−12.4	−12.4	+12.4	2.5	+2.5
^{t}Bu	+1.1	−10.0	−9.4	−0.3	−12.0	−11.3	+15.6	3.6	+4.2
^{t}Bu^{F}	+17.5	+7.0	+7.6	+20.4	9.4	+10.1	NA	NA	NA

L*SnOC$O_2{}^{i}$Pr is shown in Figure 4, and includes the relative energies of the reactants (**Alk-a**), transition state (**TS-a**), intermediate (**INT-a**) and carbonate (**Carb-a**).

Because of the low reactivity of the tin alkoxides with aliphatic electrophiles, we initially examined a nonnucleophilic pathway in which carbon dioxide coordinates directly to the metal center, and insertion of carbon dioxide into the Sn−O bond would follow. Although rare, coordination of carbon dioxide to coordinatively unsaturated metal centers has been observed, most commonly in an η^2-fashion,[32−35] but end-on coordination has also been found.[36] A high energy transition state (**TS^{NP}**, $\Delta G^{‡}$ = 56.6 kcal mol^{-1}) was located in which carbon dioxide coordinates in an η^2-fashion to the tin center of isoproxide **Alk-a**. This interaction involves the tin 5*s* lone pair binding to an antibonding orbital located on the carbon dioxide molecule. As a result, there is a predictable decrease in electron density at the metal center and an increase in electron density at the carbon atom (see Figure 5 for Mulliken charge distribution). The C−O2 bond length is significantly longer than experimentally derived η^2-CO_2 complexes,[32−35] opening up the possibility that this transition state structure is best described as a metallacycle in which there has been an oxidative addition of C=O to the metal center, generating a tin(IV) complex.

Because of both the high-energy nature of this structure and our inability to find a pathway from **TS^{NP}** to the corresponding carbonate (**Carb-a**), this transition state was deemed nonproductive. An alternative and more energetically accessible transition state was found arising from an interaction between the oxygen lone pair (HOMO −1) on the tin alkoxide and the LUMO of CO_2 (**TS-a**, $\Delta G^{‡}$ = 16.6 kcal mol^{-1}). This four-membered transition state involves formation of a new C−O1 bond, weakening of the C=O2 double bond, formation of a new Sn−O2 bond and a weakening of the Sn−O1 bond. The C···O1 interaction of 1.869 Å results in a slight C=O bond elongation of 0.017 Å (C−O2) and 0.039 Å (C−O3), a decrease in the O2−C−O3 bond angle to 151° and an elongation of the Sn−O bond by 0.121 Å. The Wiberg bond index (WBI) of the formation C−O1 bond is 0.33, whereas the WBI of the Sn−O1 bond has decreased by 0.19− 0.37, indicating that although there has been minimal geometric change within the Sn−O1 bond, there has been significant weakening.

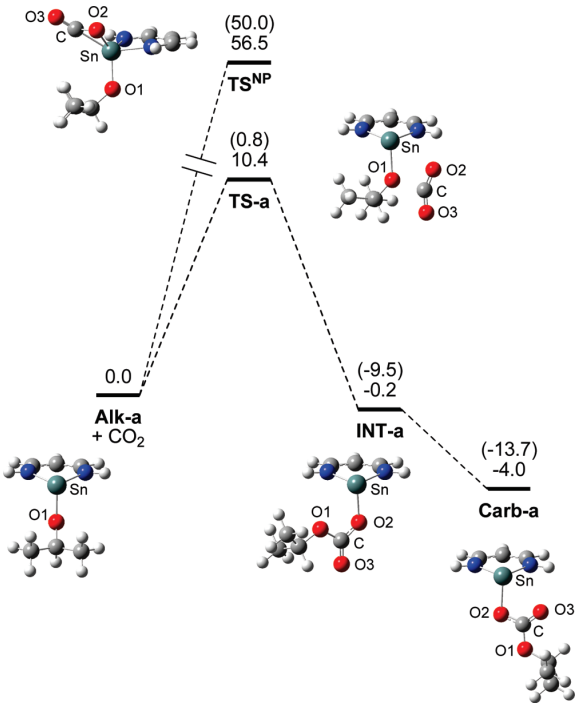

Figure 4. Gibbs free energy diagram (kcal mol^{-1}) and drawings for the reaction of L*SnO^{i}Pr with CO_2 at the B3LYP level. Electronic energy values are given in parentheses.

The Sn···O2 interaction of 2.733 Å is well within their combined Van der Waal radii of 3.69 Å and is shorter than the long-range interaction observed for maleate **4**. Although the WBI of 0.09 shows very little direct electronic interaction, the Mulliken population analysis shows there is a build-up of negative charge on O2 (−0.45 for the O2 atom in the **TS-a** compared to −0.33 fro the free carbon dioxide). Taken with the increase of positive charge from +0.71 to +0.83 of the tin atom, there could be an electrostatic Sn−O2 interaction that has not been accounted for in our calculations. Once **TS-a** is formed, a smooth transition to the metallo-alkylcarbonate intermediate, **INT-a**, is observed and no intermediates between **TS-a** and **INT-a** were calculated during an Intrinsic Reaction Coordinate (IRC) calculations.

INT-a possesses a formal Sn−O2 bond, the Sn···O1 distance is 2.913 Å, which is shorter than the sum of the combined van der Waals radii (WBI = 0.05) and no interaction exists between Sn and O3. A similar intermediate has also been observed by Wakamatsu and Otera.[37] After formation of **INT-a**, the Sn−O2 bond rotates such that the bulky alkyl group projects away from the metal center and a new Sn···O3 interaction is formed (2.728 Å, WBI = 0.11). The final product, **Carb-a**, is analogous to that reported for the lead isopropoxide system, in which there is a long distance Pb···O3 interaction.

The corresponding calculations were performed on the other alkoxide complexes, *sec*-butoxide **Alk-b**, *tert*-butoxide **Alk-c** and nonafluoro-*tert*-butoxide **Alk-d**, and their corresponding metallo-alkylcarbonates **Carb-b-d**. The $\Delta G°_{298}$

(32) Hirano, M.; Akita, M.; Tani, K.; Kumagai, K.; Kasuga, N. C.; Fukuoka, A.; Komiya, S. *Organometallics* **1997**, *16*, 4206.
(33) Fu, P. F.; Khan, M. A.; Nicholas, K. M. *J. Organomet. Chem.* **1996**, *506*, 49.
(34) Alvarez, R.; Carmona, E.; Marin, J. M.; Poveda, M. L.; Gutierrezpuebla, E.; Monge, A. *J. Am. Chem. Soc.* **1986**, *108*, 2286.
(35) Gambarotta, S.; Strologo, S.; Floriani, C.; Chiesivilla, A.; Guastini, C. *J. Am. Chem. Soc.* **1985**, *107*, 6278.
(36) Castro-Rodriguez, I.; Nakai, H.; Zakharov, L. N.; Rheingold, A. L.; Meyer, K. *Science* **2004**, *305*, 1757.
(37) Wakamatsu, K.; Orita, A.; Otera, J. *Organometallics* **2010**, *29*, 1290.

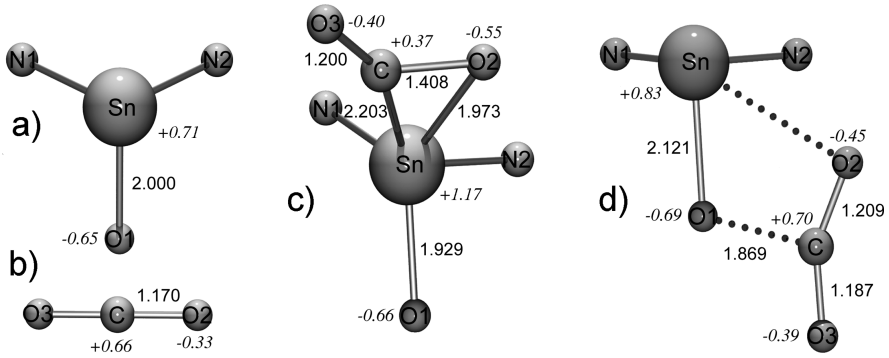

Figure 5. Optimized geometries and Mulliken charges for (a) **Alk-a**, (b) CO_2, (c) TS^{NP}, and (d) **TS-a**. Only Sn, N, O, and carbon dioxide atoms of the model complex are shown for clarity.

and ΔE° for the reactions follow the same trends as the larger systems (Table 4); that is, the isopropyl system as the most negative ΔG°_{298} and ΔE°, followed by the *sec*-butyl and *tert*-butyl system, respectively. The fluorinated system has a significantly positive ΔG°_{298} and ΔE°, which is in agreement with our experimental results in with the nonafluoro-*tert*-butoxide **2d** doe not react with carbon dioxide. A transition state was located for the *sec*-butyl system (**TS-b**) and the *tert*-butyl system (**TS-c**); however, no transition state was found for the fluorinate derivative (**TS-d**).

Discussion

The tin(II) alkoxide complexes **2a**−**2d** do not exhibit the standard reactivity as their transition metal counterparts; their lack of reactivity with methyl iodide indicates that the oxygen atom is essentially non-nucleophilic toward anything but very strong electrophiles such as methyl triflate. The notable difference in reactivity *between* the alkoxides **2a**−**2c** might be attributable to steric effects; the combination of the bulky β-diketiminate ligand as well as the *tert*-butoxide ligand of **2c** results in a more hindered approach to the oxygen atom than the corresponding isopropoxide system **2a**. However, there is also a compelling electronic argument as the reactivity trend mirrors the relative basicity of the alkoxide moieties; that is, the greater the basicity, or the greater the pK_a of the conjugate acid, the more reactive the alkoxide.[38,39] Because the reaction between the tin alkoxides and methyl triflate is irreversible, it is impossible to differentiate between steric and electronic arguments based solely on this reaction.

The activation of carbon dioxide by a seemingly nonnucleophilic metal alkoxide complex is counterintuitive. It has previously been show that the nucleophilicity of the alkoxide ligand drives insertion reactions.[1] Studies on rhenium alkoxide and aryloxide complexes, $(fac(CO)_3(PMe_3)_2ReOR$, revealed that only the alkoxide (R = Me) reacts with carbon dioxide, yet both alkoxide and aryloxide (R = 4-MeC_6H_4) react with carbon disulfide. Darensbourg observed that (*fac*)-$(CO)_3$(dppe)MnOMe reacts more readily with carbon dioxide than $(CO)_3$(dppe)$MnOCH_2CF_3$, a less nucleophilic alkoxide ligand.[9] The mechanism of carbon dioxide insertion in this case was postulated to proceed via a four-membered transition state, similar to what we observed in our calculations and have been proposed by others.[3,9,13,37]

A few transition metal systems have been reported to react with both methyl iodide and carbon dioxide, unfortunately most reports have been vague on the reaction conditions.[40,41] Vahrenkamp's pyrazolylborate-zinc methoxide complex, $(Tp^{Ph,Me})$ZnOMe, reacts readily with methyl iodide but very slowly with carbon dioxide, in sharp contrast to our results.[11] The former reaction is attributed to the nucleophilicity of the zinc-alkoxide. Thus, it can not only be the nucleophilicity of the alkoxide ligand that is governing the reactivity of alkoxides with carbon dioxide (vide infra). Interestingly, trispyrazolborate zinc *hydroxides* do react readily and reversibly with carbon dioxide,[42,43] although this could be because of hydrogen-bonding effects.

Another intriguing aspect about our results is the strong dependence on both the reaction rate as well as final equilibrium on minor variations of the alkyl group on the alkoxide ligand. This it true both with the tin and lead systems. The insertion of carbon dioxide into the Sn−O bond to generate metallo-alkylcarbonates is measurably reversible; as such, by using the equilibrium studies as well as the computational studies on the transition state, the factor governing the influence of the alkyl group can be examined. In order to normalize the different alkyl systems onto one scale, a "zero-point" was set by assuming that the alkyl group has a greater inductive influence on the ground state energy of the alkoxide **Alk** than the metallo-alkylcarbonate **Carb**. Electronic influences of the different alkyl groups are apparent upon considering the pK_a's of aliphatic alcohols;[39,44] however, these electronic influences are not apparent upon considering either the bond dissociation energies (BDE's) or pK_a's of the corresponding carboxylic acids,[45] and only minor variations within experimental error of each other are observed in the BDE's of the corresponding alcohols. As such, the relative energies of our metallo-alkylcarbonates **Carb-a-c** can be set to "zero" and all other energies can be compared to these metallo-alkylcarbonates (Figure 6).

(38) Bryndza, H. E.; Fong, L. K.; Paciello, R. A.; Tam, W.; Bercaw, J. E. *J. Am. Chem. Soc.* **1987**, *109*, 1444.
(39) Brauman, J. I.; Blair, L. K. *J. Am. Chem. Soc.* **1970**, *92*, 5986.
(40) Park, S.; Rheingold, A. L.; Roundhill, D. M. *Organometallics* **1991**, *10*, 615.
(41) Bryndza, H. E.; Tam, W. *Chem. Rev.* **1988**, *88*, 1163.
(42) Ruf, M.; Vahrenkamp, H. *Inorg. Chem.* **1996**, *35*, 6571.
(43) Looney, A.; Han, R.; McNeill, K.; Parkin, G. *J. Am. Chem. Soc.* **1993**, *115*, 4690.
(44) Olmstead, W. M.; Margolin, Z.; Bordwell, F. G. *J. Org. Chem.* **1980**, *45*, 3295.
(45) Blanksby, S. J.; Ellison, G. B. *Acc. Chem. Res.* **2003**, *36*, 255.

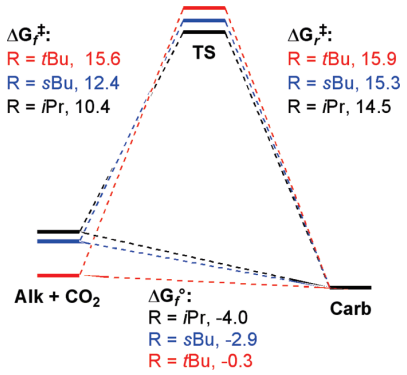

Figure 6. Energy diagram for the interconversion of **Alk** + CO_2 and **Carb** via transition state **TS**. Energies are reported in kcal mol^{-1}. ΔG_f° is the change in Gibbs free energy in the forward sense, $\Delta G_f^\ddagger$ is the activation energy in the forward reaction and $\Delta G_r^\ddagger$ is the activation energy for the reverse reaction.

In the isopropoxide system, the conversion from **Alk-a** to **Carb-a** has a relatively low activation barrier and the overall reaction is thermodynamically favored. In contrast, the conversion from **Alk-c**- to **Carb-c** in the *tert*-butoxide system is almost thermodynamically neutral and a significantly higher activation barrier is found. Steric arguments cannot fully explain the thermodynamic differences, these must be a consequence of the relative bond dissociation energies (BDE's) of the Sn-OR bond. If it is assumed that the Sn−O2 BDE for the metallo-alkylcarbonates is relatively similar due to reasons previously described, then the BDE of the Sn−O^{t}Bu bond is greater than that of the Sn−O^{s}Bu bond and the Sn−O^{i}Pr bond is the weakest of the three. Thus, in the forward sense of the reaction, in order to achieve the transition state, the energy required is greater for the *tert*-butoxide system than the isopropoxide system, thus the Sn−O bond of isopropoxide **Alk-a** must be weaker than the Sn−O bond of *tert*-butoxide **Alk-c**. Although the activation barriers to the reverse reaction follow a similar pattern in which the *tert*-butoxide system has a greater activation barrier than the isopropoxide system, the difference is not as great and can be attributed to a combination of steric arguments and the differences in the O1−C bond strengths. For the real molecule, (BDI)SnOR, the reverse reaction should be more affected by the sterics of the alkoxide group due to the interactions of both the BDI *N*-aryl groups and the alkoxide.

Although nonafluoro-*tert*-butoxide tin complex **2d** is nonreactive with carbon dioxide, the calculations show that the postulated carbon dioxide insertion product is significantly higher in energy than just **2d** and carbon dioxide. However, a direct comparison with the other alkoxide complexes **2a**−**2c** cannot be made because, in contrast to the nonfluorinated derivatives, the pK_a of the fluorinated alcohol and carboxylic acid are heavily influenced by the nearby fluorine atoms.[46]

The contrast between the reactivity of group 14 alkoxides and Vahrenkamp's zinc alkoxides is striking and reveals that it is not just the nucleophilicity of the alkoxide ligand that determines its reactivity with carbon dioxide. Although there are too many variables between group 14 alkoxides and (Tp^{Ph,Me})ZnOMe to make a meaningful comparison, the tin and lead systems can be compared. The higher reactivity of the lead system can be attributed to a combination of a more polarized and weaker Pb−O bond, resulting in a more nucleophilic alkoxide ligand and a more Lewis acidic lead metal center, which forms a more stable four-membered transition state due to a greater interaction with the CO_2 oxygen atom. The tin system suffers both from a stronger Sn−O bond, low nucleophilicity of the alkoxide ligand, as well as a smaller Lewis acidity of the metal center, thus requiring a higher activation barrier in its reaction with carbon dioxide.

Conclusions

Tin alkoxide complexes **2** are weakly nucleophilic species that only react with highly reactive aliphatic electrophiles; however, these complexes do react reversibly with carbon dioxide, due to a combination of a weakly nucleophilic alkoxide ligand and a Lewis acidic metal center that can help support the four-membered transition state. The rate of reaction as well as the relative equilibrium between reactants and products is dependent upon the alkoxide ligand. The isopropoxide complex **2a** reacts with carbon dioxide faster than the bulkier *tert*-butoxide complex **2c**, and the former reaction has a greater equilibrium constant than the latter. Although the sterics of the alkoxide ligand might play a role in these results, computational studies have shown that there is a significant electronic contribution to both the activation barrier as well as the established equilibrium. If it is assumed that the Sn−O BDE of the metallo-alkylcarbonate **5** complexes are less influenced by the alkyl substituent than the Sn−O BDE of the alkoxide complexes **2**, then a relative ordering of the Sn−O BDE can be made, with the *tert*-butoxide complex **2c** possessing the strongest Sn−O BDE, and the isopropoxide complex **2a** possessing the weakest Sn−O BDE. Interestingly, the *tert*-butoxide complex **2c** has the longest Sn−O bond and the isopropoxide complex **2a** has the shortest Sn−O bond.

Experimental Section

General. All manipulations were carried out under an atmosphere of dry nitrogen using standard Schlenk techniques or in an inert-atmosphere glovebox. Solvents were dried from the appropriate drying agent, distilled, degassed, and stored over 4 Å sieves. (BDI)SnCl and (BDI)SnO^{i}Pr were prepared according to the literature.[15,23] Potassium alkoxide salts were prepared by the slow addition of the relevant alcohol (dried and distilled) to a suspension of potassium hydride, except NaO^{t}Bu^F that was prepared by the treatment of a water solution of $(CF_3)_3COH$ with 1eq of NaOH and dried overnight under vacuum over P_2O_5. Methyl trifluoromethanesulfonate was freshly dried and distilled before use. Carbon dioxide was used as received (Union Carbide, 99.999%), and $^{13}CO_2$ was 99 atom %. ^{1}H, ^{13}C and ^{119}Sn NMR spectra were recorded on a Varian 400 MHz or Varian 500 MHz spectrometer. ^{1}H and ^{13}C NMR spectroscopy chemical shifts are given relative to residual solvent peaks and ^{119}Sn was externally referenced to $SnMe_4$. The UV spectra were recorded in Varian Cary 50 UV−vis spectrophotometer. The data for X-ray structures were collected at 173 K on a Nonius KappaCCD diffractometer, k(Mo−Kα) = 0.71073 Å and refined using the *SHELXL-97* software package.[47]

[CH{(CH$_3$)CN-2,6-^{i}Pr$_2$C$_6$H$_3$}$_2$SnO^{i}Pr] (2a). (BDI)SnOiPr was prepared following literature procedures. The ^{1}H and ^{13}C NMR spectra were identical to the ones reported earlier.[15]

(46) Arnett, E. M.; Venkatasubramaniam, K. G. *J. Org. Chem.* **1983**, *48*, 1569.

(47) Sheldrick, G. M. *SHELXL-97, Program for the Refinement of Crystal Structures*; University of Göttingen: Göttingen, Germany, 1997.

UV−vis (benzene): λ_{max} (ε, L mol^{-1} cm^{-1}) 366 nm (11000). IR (CCl_4, ν/cm^{-1}): 2964 (s), 2925 (s), 1464 (s), 1430, 1359, 1315 (s), 1170, 1101 (s).

[CH{(CH$_3$)CN-2,6-^{i}Pr$_2$C$_6$H$_3$}$_2$SnO^{s}Bu] (2b). A suspension of KO^{s}Bu (98 mg, 0.87 mmol) in THF (5 mL) was added to a solution of (BDI)SnCl (0.50 g, 0.87 mmol) in THF (5 mL) at room temperature, and the reaction mixture was stirred for 3 d. The solvent was removed under vacuum, the yellow crude product was extracted with toluene and the solution was filtered through Celite. Removal of the volatiles and recrystallization from pentane overnight afforded yellow crystals of (BDI)SnO^{s}Bu (0.42 g, 80%). ^{1}H NMR (400 MHz, C_6D_6, 303 K): δ 7.22 (d, J = 7.6, 2H, Ar*H*), 7.14 (t, J = 7.6, 2H, Ar*H*), 7.07 (d, J = 7.7, 2H, Ar*H*), 4.71 (s, 1H, $\gamma\sigma$-C*H*), 3.81 (m, 3H, C*H*Me$_2$ + OC*H*(Me)Et), 3.22 (m, 2H, C*H*Me$_2$), 1.55 (s, 3H, NC*Me*), 1.54 (s, 3H, NC*Me*), 1.50 (d, J = 6.1, 3H, CH*Me*), 1.48 (d, J = 6.1, 3H, CH*Me*), 1.25 (d, J = 6.8, 6H, CH*Me*), 1.19 (d, J = 6.9, 6H, CH*Me*), 1.11 (d, J = 6.8, 6H, CH*Me*), 0.75 (d, J = 6.0, 3H, OCH(*Me*)Et, 0.46 (t, J = 7.4, OCH(Me)CH$_2$*Me*). ^{13}C{^{1}H} NMR (500 MHz, C_6D_6, 303 K): δ 164.6 (N*C*Me), 144.9 (*ipso-C*), 142.6 (*o-C*), 141.1 (*o-C*), 126.2 (*p-C*), 124.3 (*m-C*), 123.8 (*m-C*), 96.3 (γ-*C*H), 70.7 (O*C*H(Me)Et), 34.9 (OCH(Me)*C*H$_2$Me), 28.2 (NC*Me*), 28.1 (NC*Me*), 26.6 (*C*HMe), 26.0 (*C*HMe), 24.6 (CH*Me*), 24.4 (CH*Me*), 24.3 (CH*Me*), 24.2 (CH*Me*), 23.1 (OCH(*Me*)Et), 10.3 (OCH(Me)CH$_2$*Me*). ^{119}Sn NMR (400 MHz, C_6D_6, 303 K): δ −181.5. UV−vis (benzene): λ_{max} (ε, L mol^{-1} cm^{-1}) 366 nm (12000). IR (Nujol, ν/cm^{-1}): 1554 (s), 1518 (s), 1260 (s), 1098, 1018 (s), 795 (s). IR (CCl_4, ν/cm^{-1}): 2966 (s), 2925 (s), 1463 (s), 1423, 1314 (s), 1172, 1104. Anal. Calcd for $C_{33}H_{50}N_2OSn$: C, 65.03; H, 8.27; N, 4.60. Found: C, 64.96; H, 8.23; N, 4.57.

[CH{(CH$_3$)CN-2,6-^{i}Pr$_2$C$_6$H$_3$}$_2$SnO^{t}Bu] (2c). Yellow crystals of (BDI)SnO^{t}Bu can be obtained in good yield (76%) using a similar methodology as used in the preparation of (BDI)SnO^{s}Bu **2b**. ^{1}H NMR (400 MHz, C_6D_6, 303 K): δ 7.18 (d, J = 7.6, 2H, Ar*H*), 7.14−7.06 (m, J = 7.6, 2H, Ar*H*), 7.03 (d, J = 7.6, 2H, Ar*H*), 4.61 (s, 1H, γ-C*H*), 3.86−3.71 (m, 2H, C*H*Me$_2$), 3.29−3.14 (m, 2H, C*H*Me$_2$), 1.54 (s, 6H, NC*Me*), 1.53 (d, J = 6.9, 6H, CH*Me*), 1.28 (d, J = 6.8, 6H, CH*Me*), 1.17 (d, J = 6.9, 6H, CH*Me*), 1.12 (d, J = 6.8, 6H, CH*Me*), 0.86 (s, 9H, OC(*Me*)$_3$). ^{13}C{^{1}H} NMR (400 MHz, C_6D_6, 303 K): δ 169.4 (N*C*Me), 165.0 (N*C*Me), 144.9 (*ipso-C*), 142.6 (*o-C*), 140.9 (*o-C*), 126.1 (*p-C*), 123.9 (*m-C*), 123.8 (*m-C*), 95.5 (γ-CH), 69.4 (O*C*(Me)$_3$), 34.9 (OC(*Me*)$_3$), 28.2 (NC*Me*), 28.2 (NC*Me*), 26.1 (*C*HMe), 24.4 (CH*Me*), 24.3 (CH*Me*), 24.2 (CH*Me*), 23.0 (CH*Me*). ^{119}Sn NMR (400 MHz, C_6D_6, 303 K): δ −149.1. UV−vis (benzene): λ_{max} (ε, L mol^{-1} cm^{-1}) 365 nm (13000). IR (Nujol, ν/cm^{-1}): 1555 (s), 1261 (s), 1093, 1018 (s), 939 (s), 796 (s). IR (CCl_4, ν/cm^{-1}): 2965 (s), 2927 (s), 1463 (s), 1424, 1361, 1171 (w). Anal. Calcd for $C_{33}H_{50}N_2OSn$: C, 65.03; H, 8.27; N, 4.60. Found: C, 64.97; H, 8.32; N, 4.55.

[CH{(CH$_3$)CN-2,6-^{i}Pr$_2$C$_6$H$_3$}$_2$SnOC(CF$_3$)$_3$] (2d). A solution of NaO^{t}Bu^F (0.14 g, 0.55 mmol) in THF (5 mL) was added to a solution of (BDI)SnCl (0.31 g, 0.55 mmol) in THF (5 mL) at room temperature, and the reaction mixture was stirred for 3 d. The solvent was removed under vacuum, the yellow crude product was extracted with toluene and the solution was filtered through Celite. The volatiles were removed and the yellow/green solid was washed with pentane. Recrystallization from THF overnight afforded green crystals of (BDI)SnO^{t}Bu^F (0.29 g, 69%). ^{1}H NMR (400 MHz, C_6D_6, 303 K): δ 7.16 (d, J = 7.6, 2H, Ar*H*), 7.09 (d, J = 7.7, 2H, Ar*H*), 7.03 (d, J = 7.7, 2H, Ar*H*), 4.55 (s, 1H, γ-C*H*), 3.80 − 3.34 (m, 2H, C*H*Me$_2$), 3.16 − 2.76 (m, 2H, C*H*Me$_2$), 1.45 (d, J = 5.7, 6H, CH*Me*), 1.44 (s, 6H, NC*Me*), 1.23 (d, J = 6.8, 6H, CH*Me*), 1.10 (d, J = 6.7, 6H, CH*Me*), 1.09 (d, J = 6.5, 6H, CH*Me*). ^{13}C{^{1}H} NMR (500 MHz, C_6D_6, 303 K): δ 166.0 (N*C*Me), 143.8 (*ipso-C*), 142.2 (*o-C*), 139.7 (*o-C*), 127.5 (*p-C*), 126.8 (*m-C*), 124.3 (*m-C*), 96.4 (γ-*C*H), 67.4 (O*C*(CF$_3$)$_3$), 28.6 (OC(*C*F$_3$)$_3$), 28.3 (NC*Me*), 25.4 (*C*HMe), 24.6 (CH*Me*), 24.3 (CH*Me*), 23.0 (CH*Me*), 23.0 (CH*Me*). ^{19}F NMR (400 MHz, C_6D_6, 303 K): δ −73.0. ^{119}Sn NMR (400 MHz, C_6D_6, 303 K): δ −256.3. UV−vis (benzene): λ_{max} (ε, L mol^{-1} cm^{-1}) 320 nm (22000). IR (Nujol, ν/cm^{-1}): 2024, 1945, 1548, 1518, 1319, 1262 (s), 1233 (s), 1167 (s), 1017, 966 (s), 795. Anal. Calcd for $C_{33}H_{41}F_9N_2OSn$: C, 51.38; H, 5.36; N, 3.63. Found: C, 51.41 ; H, 5.30; N, 3.64.

[CH{(CH$_3$)CN-2,6-^{i}Pr$_2$C$_6$H$_3$}$_2$SnO(CO)C$_2$H$_2$CO$_2$^{i}Pr] (4). A solid mixture of (BDI)SnO^{i}Pr (250 mg, 0.41 mmol) and maleic anhydride (40 mg, 0.41 mmol) was dissolved in toluene (10 mL) and stirred for 2 h, affording an orange solution. After evaporation of the solvent, the residue was dissolved in the minimum amount of hexane. Storage at −32 °C for 3 days afforded deep red crystals of (BDI)Sn(Ma)^{i}Pr (248 mg, 87%). ^{1}H NMR (400 MHz, C_6D_6, 303 K): δ 7.21 − 6.93 (m, 6H, Ar*H*), 5.96 (d, J = 11.9 Hz, 1H, COC*H*CHCO$_2$), 5.83 (d, J = 12.0 Hz, 1H, COCHC*H*CO$_2$), 5.09 (sept, 6.0 Hz, 1H, CO$_2$C*H*Me$_2$), 4.91 (s, 1H, γ-C*H*), 3.62 (sept, J = 6.7 Hz, 2H, C*H*Me$_2$), 3.04 (sept, J = 6.7 Hz, 2H, C*H*Me$_2$), 1.59 (s, 6H, NC*Me*), 1.37 (d, J = 6.6 Hz, 6H, CH*Me*$_2$), 1.27 (d, J = 6.7 Hz, 6H, CH*Me*$_2$), 1.12 (d, J = 6.8 Hz, 6H, CH*Me*$_2$), 1.07 (d, J = 6.2 Hz, 6H, CH*Me*$_2$), 1.04 (d, J = 6.8 Hz, 6H, CH*Me*$_2$). ^{13}C{^{1}H} NMR (400 MHz, C_6D_6, 303 K): δ 170.0 (SnO*C*O), 169.3 (*C*O$_2$^{i}Pr), 165.40 (N*C*Me), 145.31 (*ipso-C*), 142.43 (*o-C*), 141.27 (*o-C*), 131.0 (C*H*=CH), 130.0 (CH=C*H*), 127.1 (*p-C*), 124.8 (*m-C*), 123.7 (*m-C*), 99.8 (γ-*C*H), 67.5 (CO$_2$*C*HMe$_2$), 28.7 (NC*Me*), 27.7 (NC*Me*), 26.4 (*C*HMe), 24.6 (*C*HMe), 24.1 (CH*Me*), 23.60 (CH*Me*), 21.4 (CH*Me*). ^{119}Sn NMR (400 MHz, C_6D_6, 303 K): δ −374.2. IR (Nujol, v/cm^{-1}): 1735 (s), 1600, 1552, 1524, 1261 (s), 1211, 1172, 1102 (s), 1019 (s), 797(s). Anal. Calcd for $C_{36}H_{50}N_2O_4Sn$: C, 62.35; H, 7.27; N, 4.04. Found: C, 62.39; H, 7.15; N, 3.94.

Generation of Metallocarbonates 5a, 5b, and 5c: General Procedure. (BDI)SnO^{i}Pr (8.5 mg, 0.014 mmol) was dissolved in C_6D_6 (400 μL) in an NMR tube sealed with a Young's tap. The NMR tube was submerged in a dry ice/ethanol bath, the gas inside the NMR tube was evacuated and CO_2 was introduced at a pressure of 1 atm. A pale yellow solution mixture was observed, the reaction mixture was kept at room temperature for 48 h and was monitored by ^{1}H NMR spectroscopy. To generate samples for IR spectroscopy, a similar procedure was followed using CCl_4 as solvent.

[CH{(CH$_3$)CN-2,6-^{i}Pr$_2$C$_6$H$_3$}$_2$SnO(CO$_2$)^{i}Pr] (5a). ^{1}H NMR (400 MHz, C_6D_6, 303 K): δ 7.27−6.95 (m, 6H, Ar*H*), 4.95 (s, 1H, γ-C*H*), 4.89 (dq, J = 6.2, 1H, CO$_2$C*H*Me$_2$), 3.71 (hept, J = 6.7, 2H, C*H*Me$_2$), 3.07 (hept, 2H, J = 6.9, C*H*Me$_2$), 1.59 (s, 6H, NC*Me*), 1.44 (d, J = 6.7, 6H, CH*Me*), 1.22 (d, J = 6.8, 6H, CH*Me*), 1.18 (d, J = 6.3, 6H, CH*Me*), 1.16 (d, J = 7.0, 6H, CH*Me*), 1.06 (d, J = 6.8, 6H, CO$_2$CH*Me*). ^{13}C{^{1}H} NMR (400 MHz, C_6D_6, 303 K): δ 165.2 (N*C*Me), 158.7 (O*C*O$_2$), 145.4 (*ipso-C*), 142.5 (*o-C*), 141.3 (*o-C*), 127.1 (*p-C*), 124.7 (*m-C*), 123.6 (*m-C*), 99.7 (γ-*C*H), 68.5 (OCO$_2$-*C*HMe$_2$), 28.7 (OCO$_2$CH*Me*$_2$), 27.7 (NC*Me*), 26.0 (NC*Me*), 24.5 (*C*HMe), 24.1 (CH*Me*), 23.9 (CH*Me*), 23.5 (CH*Me*), 22.0 (CH*Me*). ^{119}Sn NMR (400 MHz, C_6D_6, 303 K): δ −379.7. UV−vis (benzene): λ_{max} 321 nm. IR (CCl_4, ν/cm^{-1}): 3963, 2963 (s), 2927, 2871, 2339 (s), 1718 (w), 1621, 1463, 1437, 1385, 1318.

[CH{(CH$_3$)CN-2,6-^{i}Pr$_2$C$_6$H$_3$}$_2$SnO(CO$_2$)^{s}Bu] (5b). ^{1}H NMR (400 MHz, C_6D_6, 303 K): δ 7.27−7.01 (m, 6H, Ar*H*), 4.93 (s, 1H, γ-C*H*), 4.72 (m, 1H, CO$_2$C*H*(Me)Et), 3.72 (hept, J = 6.8, 2H, C*H*Me$_2$), 3.06 (m, 2H, C*H*Me$_2$), 1.59 (s, 3H, NC*Me*), 1.58 (s, 3H, NC*Me*), 1.47 (d, J = 6.7, 3H, CH*Me*), 1.45 (d, J = 6.7, 3H, CH*Me*), 1.27−1.20 (m, 11H, CO$_2$CH(Me)C*H*$_2$Me + CO$_2$CH-(*Me*)CH$_2$Me+ CH*Me*), 1.16(d, J = 6.9 6H, CH*Me*), 1.06 (d, J = 6.8, 6H, CH*Me*), 0.85 (t, J = 7.5, 3H, CO$_2$CH(Me)CH$_2$*Me*). ^{13}C{^{1}H} NMR (400 MHz, C_6D_6, 303 K): δ 167.0 (N*C*Me), 165.2 (N*C*Me), 158.8 (O*C*O$_2$), 145.4 (*ipso-C*), 142.5 (*o-C*), 141.2 (*o-C*), 127.0 (*p-C*), 124.7 (*m-C*), 123.6 (*m-C*), 99.8 (γ-*C*H), 73.3 (OCO$_2$*C*(Me)Et), 29.0 (OCH(Me)*C*H$_2$Me), 28.7 (NC*Me*), 27.6 (NC*Me*), 26.1 (*C*HMe), 24.5 (*C*HMe), 24.0 (CH*Me*), 23.8 (CH*Me*), 23.4 (CH*Me*), 22.9 (CH*Me*), 19.4 (OCH(*Me*)Et), 9.6 (OCH(Me)CH$_2$*Me*). ^{119}Sn NMR (400 MHz, C_6D_6, 303 K): δ −379.1. UV−vis (benzene): λ_{max} 321 nm. IR (CCl_4, ν/cm^{-1}): 2965 (s), 2928, 2869, 2336 (s), 1720 (w), 1621, 1463, 1437, 1385, 1319, 1101.

[CH{(CH$_3$)CN-2,6-^{i}Pr$_2$C$_6$H$_3$}$_2$SnO(CO$_2$)^{t}Bu] (5c). ^{1}H NMR (400 MHz, C_6D_6, 303 K): δ 7.23−7.06 (m, 6H, Ar*H*), 4.89 (s, 1H, γ-C*H*), 3.68 (hept, J = 6.8, 2H, C*H*Me$_2$), 3.05 (hept, 2H, J = 6.8, C*H*Me$_2$), 1.44 (d, J = 6.7, 6H, CH*Me*), 1.42 (s, 6H, NC*Me*), 1.18 (d, J = 6.8, 6H, CH*Me*), 1.13 (d, J = 6.8, 6H, CH*Me*), 1.02 (d, J = 7.0, 6H, CH*Me*), 0.87 (s, 9H, OC*Me$_3$*). ^{13}C{^{1}H} NMR (400 MHz, C_6D_6, 303 K): δ 167.0 (N*C*Me), 165.3 (N*C*Me), 157.9 (O*C*O$_2$), 145.3 (*ipso-C*), 142.4 (*o-C*), 141.3 (*o-C*), 127.0 (*p-C*), 124.6 (*m-C*), 123.6 (*m-C*), 99.7 (γ-*C*H), 77.1 (O*C*(Me)$_3$), 34.8 (OC(*Me*)$_3$), 28.7 (NC*Me*), 28.0 (NC*Me*), 27.6 (*C*HMe), 26.3 (*C*HMe), 24.4 (CH*Me*), 24.1 (CH*Me*), 23.8 (CH*Me*), 23.4 (CH*Me*). ^{119}Sn NMR (400 MHz, C_6D_6, 303 K): δ −377.4. UV−vis (benzene): λ_{max} 325 nm. IR (CCl_4, ν/cm^{-1}): 2966, 2928, 2870, 2337 (s), 1717 (w), 1621, 1463, 1438, 1386, 1318.

Determination of $t_{1/2}$ for the Reaction of 2a−2c with MeOTf: General Procedure. A sealable NMR tube was charged with 1.7×10^{-5} mol of (BDI)SnOR in 0.25 mL in C_6D_6, 1.1 μL of dichloromethane (1.7×10^{-5} mol) and 1.9 μL of MeOTf (1.7×10^{-5} mol) to give a total volume of 0.25 mL. The NMR tube was then placed in the thermostatted probe (298.1 K) of a Varian 400 MHz spectrometer. The conversion was monitored by ^{1}H NMR spectroscopy. NMR spectra were acquired in 5 min intervals. In order to ensure accurate integration, a 10s delay between 30° pulses was utilized (number of scans = 4, acquisition time = 4). The $t_{1/2}$ was determined by comparing the γ-C*H* signal integration of (BDI)SnOR and (BDI)SnOTf, using the DCM peak as standard.

Equilibrium Studies of the Reaction of 2a−2c with CO_2: General Procedure. A 0.45 mL C_6D_6 solution consisting of 1.64×10^{-5} mol of (BDI)SnOR and 2.68×10^{-6} mol of ferrocene was added to a sealable NMR tube with a 50 cm^3 headspace. The solution was submerged in a dry ice/ethanol bath, the gas inside the NMR tube was evacuated and CO_2 was introduced at a pressure of 1 atm. The reaction mixture was kept at 313.1 K in a thermostatted bath for 72 h and the **2**/**5** ratio was monitored by comparing the γ-C*H* ^{1}H NMR signal to the internal standard ferrocene. In order to ensure accurate integration, a 10s delay between 30° pulses was utilized (number of scans = 4, acquisition time = 4).

Computational Details. All the calculations were carried out using density functional theory (DFT) in the Gaussian 03 program.[30] Geometry optimization for the full complexes ((BDI)SnOR) was performed at the b3lyp level by using a double-ζ basis set (Lanl2dz) plus a d type polarization function (d exponent 0.183) along with the effective core potential (Lanl2 ECP)[48] for Sn atoms and 3-21 g for all other atoms. Geometry optimization for the model complexes (L$^{\#}$SnOR) was performed at the b3lyp level by using a double-ζ basis set (Lanl2dz) plus a d type polarization function (d exponent 0.183) along with the effective core potential (Lanl2 ECP)[48] for Sn atoms and 6-31+g* for all other atom. Single point calculations were carried on all the found saddle points with the larger basis set [4333111/433111/43] plus two d polarization function (d exponents 0.253 and 0.078) for Sn[49,50] and 6-31 g(d, p) for all the other atoms. Zero-point vibrational energy corrections were also included. All the transition structures (TS) were located on the potential energy surfaces and verified by one imaginary frequency. Intrinsic reaction coordinates (IRC) calculations confirmed the connectivity of TS with reactants and products.

Acknowledgment. The authors are grateful for the financial support from the EPSRC (LF, grant no EP/E032575/1).

Supporting Information Available: Cartesian coordinates and total energies of all the structures, basis set information for the large basis set single-point calculations, crystallographic data for **2b**, **2c**, **4**, and **6** (CIF), and full citation for ref 30. This material is available free of charge via the Internet at http://pubs.acs.org.

(48) Wadt, W. R.; Hay, P. J. *J. Chem. Phys.* **1985**, *82*, 284.

(49) Takagi, N.; Nagase, S. *Organometallics* **2007**, *26*, 469.

(50) *Gaussian Basis Sets for Molecular Calculations*; Elsevier: Amsterdam, 1984.

Appendix B – (capo)GeCl synthesis and structure

$[CH_3C(O)CH\{(CH_3)CN\text{-}C_6H_{11}\}]GeCl$. (capo)H (1.45 g, 8.00 mmol) was dissolved in diethyl ether (40 mL) and treated dropwise with 2.37 M ^{n}BuLi in hexanes (3.37 mL). The resulting orange solution was stirred for 15 minutes at room temperature and added dropwise to a stirring suspension of $GeCl_2$(diox) (1.86 g, 8.00 mmol) in diethyl ether (10 mL) and the reaction mixture was stirred overnight. Filtration through celite and washings with cold pentane afforded a pale orange powder of (capo)GeCl (1.82) in 79% yield. Colourless crystals suitable for X-ray crystallography were obtained storing a concentrated diethyl ether solution at -27°C for 3 days. ^{1}H NMR (400 MHz, C_6D_6): δ 4.93 (s, 1H, γ-C*H*), 3.20 (m, 1H, NC*H*), 1.91 (m, 2H, ^{cy}CH_2), 1.76 (s, 3H, C*Me*), 1.43 (m, 4H, ^{cy}CH_2), 1.29 (s, 3H, C*Me*), 0.81 (m, 4H, ^{cy}CH_2). ^{13}C{^{1}H} NMR (400 MHz, C_6D_6): δ 173.7 (C*Me*), 166.6 (C*Me*), 102.0 (γ-*C*H), 60.5 (N*C*H), 35.1 (^{cy}C), 32.7 (^{cy}C), 25.6 (^{cy}C), 25.4 (^{cy}C), 24.8 (C*Me*), 21.3 (^{cy}C). MS (EI+): *m/z* 289, 254, 220, 207, 180, 154, 138, 109, 81, 67, 55.

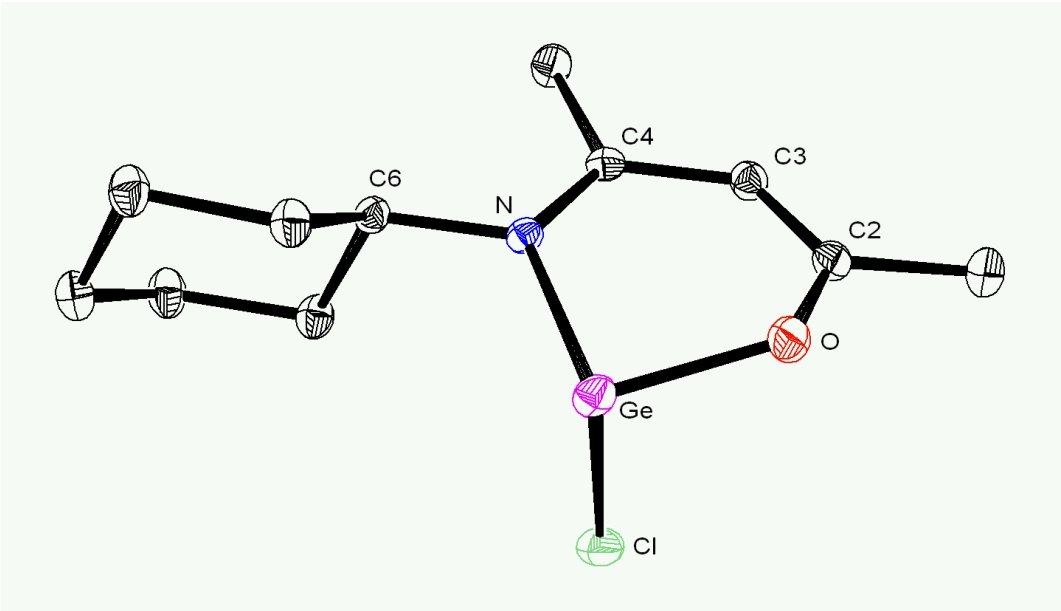

Table 1. Crystal data and structure refinement for (capo)GeCl.

Identification code	jun709	
Empirical formula	C11 H18 Cl Ge N O	
Formula weight	288.30	
Temperature	173(2) K	
Wavelength	0.71073 Å	
Crystal system	Monoclinic	
Space group	P 21/c (No.14)	
Unit cell dimensions	a = 8.8083(3) Å	a= 90°.
	b = 9.9713(3) Å	b= 90.748(2)°.
	c = 14.4029(5) Å	g = 90°.
Volume	1264.90(7) $Å^3$	
Z	4	
Density (calculated)	1.51 Mg/m^3	
Absorption coefficient	2.61 mm^{-1}	
F(000)	592	
Crystal size	0.16 x 0.14 x 0.12 mm^3	
Theta range for data collection	3.41 to 27.48°.	
Index ranges	-11<=h<=11, -12<=k<=12, -18<=l<=17	
Reflections collected	18977	
Independent reflections	2880 [R(int) = 0.053]	
Reflections with I>2sigma(I)	2598	
Completeness to theta = 27.48°	99.4 %	
Absorption correction	Semi-empirical from equivalents	
Tmax. and Tmin.	0.7369 and 0.6118	
Refinement method	Full-matrix least-squares on F^2	
Data / restraints / parameters	2880 / 0 / 138	
Goodness-of-fit on F^2	1.047	
Final R indices [I>2sigma(I)]	R1 = 0.026, wR2 = 0.063	
R indices (all data)	R1 = 0.032, wR2 = 0.066	
Largest diff. peak and hole	0.35 and -0.50 $e.Å^{-3}$	

Data collection KappaCCD , Program package WinGX , Abs correction MULTISCAN

Refinement using SHELXL-97 , Drawing using ORTEP-3 for Windows

Table 2. Atomic coordinates (x 10^4) and equivalent isotropic displacement parameters ($Å^2$x 10^3) for jun709. U(eq) is defined as one third of the trace of the orthogonalized U^{ij} tensor.

	x	y	z	U(eq)
Ge	2976(1)	716(1)	3394(1)	26(1)
Cl	2600(1)	2998(1)	3592(1)	36(1)
O	1487(2)	549(1)	2463(1)	31(1)
N	4650(2)	970(1)	2464(1)	21(1)
C(1)	86(2)	1104(2)	1107(2)	38(1)
C(2)	1586(2)	972(2)	1600(1)	27(1)
C(3)	2909(2)	1266(2)	1174(1)	25(1)
C(4)	4399(2)	1203(2)	1577(1)	22(1)
C(5)	5681(2)	1442(2)	919(1)	32(1)
C(6)	6230(2)	958(2)	2845(1)	22(1)
C(7)	6652(2)	2326(2)	3253(1)	28(1)
C(8)	8294(2)	2327(2)	3612(2)	33(1)
C(9)	8586(2)	1191(2)	4300(1)	33(1)
C(10)	8110(2)	-163(2)	3897(2)	32(1)
C(11)	6452(2)	-141(2)	3573(1)	28(1)

Table 3. Bond lengths [Å] and angles [°] for jun709.

Ge-O	1.8705(14)
Ge-N	2.0196(15)
Ge-Cl	2.3170(5)
O-C(2)	1.316(2)
N-C(4)	1.314(2)
N-C(6)	1.490(2)
C(1)-C(2)	1.498(3)
C(2)-C(3)	1.356(3)
C(3)-C(4)	1.430(2)
C(4)-C(5)	1.503(3)
C(6)-C(11)	1.528(3)
C(6)-C(7)	1.529(3)
C(7)-C(8)	1.530(3)

C(8)-C(9)	1.524(3)
C(9)-C(10)	1.526(3)
C(10)-C(11)	1.528(3)

O-Ge-N	92.70(6)
O-Ge-Cl	94.34(4)
N-Ge-Cl	93.77(4)
C(2)-O-Ge	126.43(12)
C(4)-N-C(6)	120.22(15)
C(4)-N-Ge	123.49(12)
C(6)-N-Ge	116.21(11)
O-C(2)-C(3)	124.37(18)
O-C(2)-C(1)	114.05(18)
C(3)-C(2)-C(1)	121.58(18)
C(2)-C(3)-C(4)	126.58(17)
N-C(4)-C(3)	122.96(16)
N-C(4)-C(5)	121.57(16)
C(3)-C(4)-C(5)	115.46(16)
N-C(6)-C(11)	111.65(14)
N-C(6)-C(7)	110.84(14)
C(11)-C(6)-C(7)	110.36(15)
C(6)-C(7)-C(8)	110.77(15)
C(9)-C(8)-C(7)	111.74(16)
C(8)-C(9)-C(10)	111.49(17)
C(9)-C(10)-C(11)	111.10(17)
C(10)-C(11)-C(6)	109.44(15)

Appendix C – Crystallographic Data

Table 1. Crystal data and structure refinement for compound **4**.

Identification code	dec107	
Empirical formula	C33 H50 N2 O Pb	
Formula weight	697.94	
Temperature	173(2) K	
Wavelength	0.71073 Å	
Crystal system	Triclinic	
Space group	$P\bar{1}$ (No.2)	
Unit cell dimensions	a = 8.5515(3) Å	α= 103.184(2)°.
	b = 11.9654(3) Å	β= 101.586(2)°.
	c = 16.9123(6) Å	γ = 96.650(2)°.
Volume	1626.69(9) $Å^3$	
Z	2	
Density (calculated)	1.43 Mg/m^3	
Absorption coefficient	5.21 mm^{-1}	
F(000)	704	
Crystal size	0.20 x 0.15 x 0.08 mm^3	
Theta range for data collection	3.45 to 25.98°.	
Index ranges	-10<=h<=10, -14<=k<=14, -20<=l<=20	
Reflections collected	22226	
Independent reflections	6353 [R(int) = 0.042]	
Reflections with I>2sigma(I)	5674	
Completeness to theta = 25.98°	99.4 %	
Tmax. and Tmin.	0.5178 and 0.4169	
Refinement method	Full-matrix least-squares on F^2	
Data / restraints / parameters	6353 / 5 / 341	
Goodness-of-fit on F^2	1.046	
Final R indices [I>2sigma(I)]	R1 = 0.028, wR2 = 0.060	
R indices (all data)	R1 = 0.036, wR2 = 0.063	
Largest diff. peak and hole	0.63 and -0.90 $e.Å^{-3}$	

The butyl group is disordered over two overlapping orientations which were included with isotropic C atoms and with their geometry restrained using the SAME instruction.

Data collection KappaCCD , Program package WinGX , Abs correction MULTISCAN

Refinement using SHELXL-97 , Drawing using ORTEP-3 for Windows

Table 2. Atomic coordinates (x 10^4) and equivalent isotropic displacement parameters ($Å^2$x 10^3) for dec107. U(eq) is defined as one third of the trace of the orthogonalized U^{ij} tensor.

	x	y	z	U(eq)
Pb	3731(1)	1798(1)	1876(1)	31(1)
O	6200(4)	1781(3)	1866(2)	47(1)
N(1)	4223(3)	3702(2)	2664(2)	24(1)
N(2)	4020(4)	1479(2)	3187(2)	27(1)
C(1)	3731(4)	4039(3)	3356(2)	26(1)
C(2)	3287(4)	3292(3)	3839(2)	30(1)
C(3)	3562(4)	2150(3)	3801(2)	27(1)
C(4)	3632(5)	5311(3)	3685(3)	38(1)
C(5)	3327(6)	1687(4)	4542(3)	42(1)
C(6)	4883(4)	4526(3)	2268(2)	28(1)
C(7)	3887(5)	4802(3)	1594(2)	33(1)
C(8)	4590(6)	5567(4)	1202(3)	47(1)
C(9)	6209(6)	6050(4)	1467(3)	49(1)
C(10)	7170(5)	5753(3)	2111(3)	42(1)
C(11)	6557(5)	4976(3)	2524(2)	30(1)
C(12)	2099(5)	4287(3)	1274(2)	36(1)
C(13)	1757(6)	3477(4)	387(3)	53(1)
C(14)	1031(6)	5225(4)	1281(3)	47(1)
C(15)	7667(5)	4635(4)	3206(3)	44(1)
C(16)	8115(10)	5556(8)	4016(4)	138(4)
C(17)	9178(7)	4287(6)	2967(4)	82(2)
C(18)	4534(5)	394(3)	3247(2)	30(1)
C(19)	3471(5)	-660(3)	2841(2)	35(1)
C(20)	4075(6)	-1694(4)	2842(3)	46(1)
C(21)	5627(6)	-1698(4)	3238(3)	46(1)
C(22)	6645(5)	-667(4)	3643(3)	45(1)
C(23)	6143(5)	406(3)	3660(3)	37(1)
C(24)	1731(5)	-708(3)	2400(3)	39(1)
C(25)	1412(7)	-1277(4)	1463(3)	60(1)
C(26)	549(6)	-1344(4)	2786(3)	58(1)
C(27)	7319(6)	1532(4)	4115(3)	57(1)
C(28)	7897(8)	1609(6)	5051(4)	81(2)
C(29)	8747(7)	1658(6)	3721(4)	82(2)

C(30)	6502(10)	983(7)	1173(5)	52(2)a
C(31)	7564(12)	1620(9)	769(7)	79(3)a
C(32)	6754(12)	2585(8)	461(6)	62(3)a
C(33)	7165(15)	-83(10)	1382(7)	79(3)a
C(30A)	6484(14)	1416(10)	986(8)	45(3)b
C(31A)	7507(17)	486(11)	1017(10)	69(5)b
C(32A)	6558(19)	-545(13)	1254(10)	66(4)b
C(33A)	7390(20)	2457(14)	758(12)	79(5)b

occupancy: a , b

Table 3. Bond lengths [Å] and angles [°] for dec107.

Pb-O	2.117(3)
Pb-N(2)	2.304(3)
Pb-N(1)	2.305(3)
O-C(30)	1.421(8)
O-C(30A)	1.529(12)
N(1)-C(1)	1.317(4)
N(1)-C(6)	1.436(4)
N(2)-C(3)	1.316(5)
N(2)-C(18)	1.437(4)
C(1)-C(2)	1.410(5)
C(1)-C(4)	1.515(5)
C(2)-C(3)	1.403(5)
C(3)-C(5)	1.521(5)
C(6)-C(7)	1.407(5)
C(6)-C(11)	1.412(5)
C(7)-C(8)	1.396(6)
C(7)-C(12)	1.519(6)
C(8)-C(9)	1.378(7)
C(9)-C(10)	1.368(6)
C(10)-C(11)	1.399(5)
C(11)-C(15)	1.505(6)
C(12)-C(14)	1.526(6)
C(12)-C(13)	1.540(6)
C(15)-C(16)	1.497(7)
C(15)-C(17)	1.505(7)
C(18)-C(19)	1.407(5)
C(18)-C(23)	1.409(6)
C(19)-C(20)	1.394(6)
C(19)-C(24)	1.512(6)
C(20)-C(21)	1.362(7)
C(21)-C(22)	1.369(6)
C(22)-C(23)	1.397(6)
C(23)-C(27)	1.523(6)
C(24)-C(25)	1.529(6)
C(24)-C(26)	1.529(6)
C(27)-C(29)	1.512(7)

C(27)-C(28)	1.539(8)
C(30)-C(31)	1.484(11)
C(30)-C(33)	1.537(12)
C(31)-C(32)	1.549(13)
C(30A)-C(31A)	1.497(14)
C(30A)-C(33A)	1.556(16)
C(31A)-C(32A)	1.571(16)

O-Pb-N(2)	94.08(11)
O-Pb-N(1)	93.33(10)
N(2)-Pb-N(1)	80.76(10)
C(30)-O-Pb	115.8(4)
C(30A)-O-Pb	113.3(5)
C(1)-N(1)-C(6)	121.7(3)
C(1)-N(1)-Pb	123.5(2)
C(6)-N(1)-Pb	114.1(2)
C(3)-N(2)-C(18)	122.0(3)
C(3)-N(2)-Pb	123.4(2)
C(18)-N(2)-Pb	114.1(2)
N(1)-C(1)-C(2)	124.5(3)
N(1)-C(1)-C(4)	119.8(3)
C(2)-C(1)-C(4)	115.7(3)
C(3)-C(2)-C(1)	128.9(3)
N(2)-C(3)-C(2)	125.0(3)
N(2)-C(3)-C(5)	119.1(3)
C(2)-C(3)-C(5)	115.9(3)
C(7)-C(6)-C(11)	121.1(3)
C(7)-C(6)-N(1)	119.8(3)
C(11)-C(6)-N(1)	118.8(3)
C(8)-C(7)-C(6)	118.1(4)
C(8)-C(7)-C(12)	119.3(4)
C(6)-C(7)-C(12)	122.6(3)
C(9)-C(8)-C(7)	121.4(4)
C(10)-C(9)-C(8)	119.9(4)
C(9)-C(10)-C(11)	122.0(4)
C(10)-C(11)-C(6)	117.5(4)
C(10)-C(11)-C(15)	120.4(4)
C(6)-C(11)-C(15)	122.2(3)

C(7)-C(12)-C(14)	112.2(3)
C(7)-C(12)-C(13)	111.1(3)
C(14)-C(12)-C(13)	109.6(3)
C(16)-C(15)-C(11)	113.0(4)
C(16)-C(15)-C(17)	109.6(5)
C(11)-C(15)-C(17)	113.0(4)
C(19)-C(18)-C(23)	121.2(3)
C(19)-C(18)-N(2)	119.7(3)
C(23)-C(18)-N(2)	119.0(3)
C(20)-C(19)-C(18)	117.7(4)
C(20)-C(19)-C(24)	119.6(4)
C(18)-C(19)-C(24)	122.7(3)
C(21)-C(20)-C(19)	121.9(4)
C(20)-C(21)-C(22)	119.9(4)
C(21)-C(22)-C(23)	121.8(4)
C(22)-C(23)-C(18)	117.5(4)
C(22)-C(23)-C(27)	120.0(4)
C(18)-C(23)-C(27)	122.5(4)
C(19)-C(24)-C(25)	111.7(4)
C(19)-C(24)-C(26)	111.4(4)
C(25)-C(24)-C(26)	110.1(4)
C(29)-C(27)-C(23)	111.3(5)
C(29)-C(27)-C(28)	110.7(4)
C(23)-C(27)-C(28)	111.3(4)
O-C(30)-C(31)	109.0(7)
O-C(30)-C(33)	114.4(7)
C(31)-C(30)-C(33)	112.2(8)
C(30)-C(31)-C(32)	110.9(8)
C(31A)-C(30A)-O	104.7(9)
C(31A)-C(30A)-C(33A)	110.2(11)
O-C(30A)-C(33A)	111.2(10)
C(30A)-C(31A)-C(32A)	108.9(11)

```
 Least-squares planes (x,y,z in crystal coordinates) and deviations
from them
 (* indicates atom used to define plane)

  8.5262 (0.0008) x - 1.2978 (0.0160) y - 2.1910 (0.0210) z = 2.5370
(0.0037)

 *    0.0000 (0.0000)  Pb
 *    0.0000 (0.0000)  N1
 *    0.0000 (0.0000)  N2

 Rms deviation of fitted atoms =   0.0000


  7.2065 (0.0113) x + 0.4903 (0.0157) y + 4.8628 (0.0352) z = 4.5196
(0.0090)

 Angle to previous plane (with approximate esd) = 28.23 ( 0.15 )

 *    0.0008 (0.0015)  N1
 *   -0.0008 (0.0015)  N2
 *   -0.0009 (0.0017)  C1
 *    0.0009 (0.0018)  C3
     -0.1229 (0.0052)  C2
     -0.8304 (0.0054)  Pb

 Rms deviation of fitted atoms =   0.0008


  6.1253 (0.0437) x + 1.2244 (0.0341) y + 7.5310 (0.0923) z = 5.3074
(0.0260)

 Angle to previous plane (with approximate esd) = 11.68 ( 0.72 )

 *    0.0000 (0.0000)  C1
 *    0.0000 (0.0000)  C2
 *    0.0000 (0.0000)  C3

 Rms deviation of fitted atoms =   0.0000
```

Table 1. Crystal data and structure refinement for compound **8**.

Identification code	mar108	
Empirical formula	C37 H52 N2 O4 Pb	
Formula weight	796.00	
Temperature	173(2) K	
Wavelength	0.71073 Å	
Crystal system	Triclinic	
Space group	$P\bar{1}$ (No.2)	
Unit cell dimensions	a = 9.8835(3) Å	α= 78.263(2)°.
	b = 13.8766(5) Å	β= 83.056(2)°.
	c = 14.0242(5) Å	γ = 75.675(2)°.
Volume	1819.59(11) $Å^3$	
Z	2	
Density (calculated)	1.45 Mg/m^3	
Absorption coefficient	4.67 mm^{-1}	
F(000)	804	
Crystal size	0.15 x 0.15 x 0.08 mm^3	
Theta range for data collection	3.42 to 26.08°.	
Index ranges	-12<=h<=11, -17<=k<=17, -17<=l<=17	
Reflections collected	26325	
Independent reflections	7153 [R(int) = 0.072]	
Reflections with I>2sigma(I)	5977	
Completeness to theta = 26.08°	99.2 %	
Tmax. and Tmin.	0.6154 and 0.4711	
Refinement method	Full-matrix least-squares on F^2	
Data / restraints / parameters	7153 / 0 / 409	
Goodness-of-fit on F^2	1.057	
Final R indices [I>2sigma(I)]	R1 = 0.048, wR2 = 0.112	
R indices (all data)	R1 = 0.065, wR2 = 0.120	
Largest diff. peak and hole	2.14 and -1.50 $e.Å^{-3}$ (near Pb)	

Data collection KappaCCD , Program package WinGX , Abs correction MULTISCAN

Refinement using SHELXL-97 , Drawing using ORTEP-3 for Windows

Table 2. Atomic coordinates (x 10^4) and equivalent isotropic displacement parameters ($Å^2$x 10^3) for mar108. U(eq) is defined as one third of the trace of the orthogonalized U^{ij} tensor.

	x	y	z	U(eq)
Pb	5753(1)	3438(1)	2101(1)	31(1)
O(1)	7664(5)	2146(4)	2429(4)	40(1)
O(2)	8664(6)	3459(4)	2057(5)	56(2)
O(3)	8694(7)	213(5)	4001(5)	69(2)
O(4)	9101(7)	-256(5)	2522(5)	67(2)
N(1)	5048(5)	2400(4)	1287(4)	26(1)
N(2)	4586(6)	2650(4)	3424(4)	31(1)
C(1)	4532(7)	1595(5)	1694(5)	31(2)
C(2)	4241(7)	1287(5)	2692(5)	36(2)
C(3)	4190(7)	1791(5)	3492(5)	33(2)
C(4)	4159(9)	983(6)	1032(6)	45(2)
C(5)	3592(11)	1312(7)	4461(6)	55(2)
C(6)	5104(7)	2762(5)	249(5)	30(1)
C(7)	3969(7)	3469(6)	-152(5)	36(2)
C(8)	4066(9)	3865(7)	-1139(6)	50(2)
C(9)	5260(9)	3589(7)	-1725(6)	58(2)
C(10)	6366(9)	2862(7)	-1326(6)	56(2)
C(11)	6338(8)	2427(6)	-336(5)	40(2)
C(12)	2626(7)	3833(6)	464(6)	41(2)
C(13)	2419(9)	4988(7)	461(7)	61(2)
C(14)	1350(9)	3638(8)	101(8)	67(3)
C(15)	7604(7)	1649(6)	80(6)	44(2)
C(16)	7949(10)	741(7)	-430(8)	66(3)
C(17)	8871(9)	2120(7)	-31(7)	56(2)
C(18)	4317(7)	3185(5)	4223(5)	32(2)
C(19)	5295(8)	2970(6)	4926(6)	43(2)
C(20)	5015(11)	3512(8)	5678(7)	66(3)
C(21)	3821(11)	4263(8)	5720(7)	72(3)
C(22)	2869(10)	4493(7)	5032(7)	60(2)
C(23)	3103(8)	3975(6)	4240(6)	43(2)
C(24)	6645(8)	2162(6)	4902(6)	44(2)
C(25)	7930(8)	2639(7)	4721(7)	54(2)
C(26)	6802(11)	1350(7)	5840(6)	67(3)

C(27)	2049(8)	4238(6)	3480(6)	48(2)
C(28)	1542(12)	5352(8)	3168(8)	79(3)
C(29)	850(13)	3757(10)	3824(10)	95(4)
C(30)	8722(8)	2544(6)	2312(6)	45(2)
C(31)	10125(8)	1839(7)	2463(7)	56(2)
C(32)	10331(9)	864(7)	2823(7)	63(3)
C(33)	9273(9)	270(7)	3180(8)	60(2)
C(34)	8168(11)	-958(7)	2824(7)	67(3)
C(35)	9003(14)	-1952(9)	3199(14)	131(6)
C(36)	7545(13)	-990(9)	1867(9)	85(3)
C(37)	6500(20)	-1667(13)	2048(13)	151(7)

Table 3. Bond lengths [Å] and angles [°] for mar108.

Pb-O(1)	2.279(5)
Pb-N(1)	2.284(5)
Pb-N(2)	2.291(5)
O(1)-C(30)	1.278(9)
O(2)-C(30)	1.236(10)
O(3)-C(33)	1.219(11)
O(4)-C(33)	1.337(12)
O(4)-C(34)	1.470(11)
N(1)-C(1)	1.337(8)
N(1)-C(6)	1.438(8)
N(2)-C(3)	1.326(8)
N(2)-C(18)	1.430(9)
C(1)-C(2)	1.394(10)
C(1)-C(4)	1.510(9)
C(2)-C(3)	1.427(10)
C(3)-C(5)	1.507(10)
C(6)-C(7)	1.386(10)
C(6)-C(11)	1.417(10)
C(7)-C(8)	1.383(10)
C(7)-C(12)	1.528(10)
C(8)-C(9)	1.373(12)
C(9)-C(10)	1.377(12)
C(10)-C(11)	1.398(11)
C(11)-C(15)	1.524(11)
C(12)-C(14)	1.518(11)
C(12)-C(13)	1.564(12)
C(15)-C(16)	1.519(11)
C(15)-C(17)	1.529(11)
C(18)-C(19)	1.401(10)
C(18)-C(23)	1.413(10)
C(19)-C(20)	1.379(11)
C(19)-C(24)	1.517(11)
C(20)-C(21)	1.372(13)
C(21)-C(22)	1.365(12)
C(22)-C(23)	1.408(11)
C(23)-C(27)	1.509(11)

C(24)-C(26)	1.544(11)
C(24)-C(25)	1.544(11)
C(27)-C(29)	1.485(14)
C(27)-C(28)	1.492(13)
C(30)-C(31)	1.496(11)
C(31)-C(32)	1.318(13)
C(32)-C(33)	1.468(13)
C(34)-C(35)	1.451(14)
C(34)-C(36)	1.556(16)
C(36)-C(37)	1.528(18)

O(1)-Pb-N(1)	86.07(18)
O(1)-Pb-N(2)	87.62(18)
N(1)-Pb-N(2)	83.76(19)
C(30)-O(1)-Pb	106.7(5)
C(33)-O(4)-C(34)	117.2(7)
C(1)-N(1)-C(6)	122.0(5)
C(1)-N(1)-Pb	126.1(4)
C(6)-N(1)-Pb	111.7(4)
C(3)-N(2)-C(18)	121.2(6)
C(3)-N(2)-Pb	126.4(5)
C(18)-N(2)-Pb	112.4(4)
N(1)-C(1)-C(2)	125.6(6)
N(1)-C(1)-C(4)	118.4(6)
C(2)-C(1)-C(4)	116.0(6)
C(1)-C(2)-C(3)	130.6(7)
N(2)-C(3)-C(2)	124.5(6)
N(2)-C(3)-C(5)	119.3(7)
C(2)-C(3)-C(5)	116.2(6)
C(7)-C(6)-C(11)	121.3(6)
C(7)-C(6)-N(1)	119.1(6)
C(11)-C(6)-N(1)	119.6(6)
C(8)-C(7)-C(6)	118.8(7)
C(8)-C(7)-C(12)	119.1(7)
C(6)-C(7)-C(12)	122.1(6)
C(9)-C(8)-C(7)	121.8(8)
C(8)-C(9)-C(10)	118.9(8)
C(9)-C(10)-C(11)	122.3(8)

C(10)-C(11)-C(6)	116.8(7)
C(10)-C(11)-C(15)	120.4(7)
C(6)-C(11)-C(15)	122.7(7)
C(14)-C(12)-C(7)	112.3(7)
C(14)-C(12)-C(13)	110.0(7)
C(7)-C(12)-C(13)	109.2(6)
C(16)-C(15)-C(11)	110.5(7)
C(16)-C(15)-C(17)	109.9(7)
C(11)-C(15)-C(17)	110.5(7)
C(19)-C(18)-C(23)	121.5(7)
C(19)-C(18)-N(2)	120.0(6)
C(23)-C(18)-N(2)	118.3(6)
C(20)-C(19)-C(18)	118.6(7)
C(20)-C(19)-C(24)	118.4(7)
C(18)-C(19)-C(24)	123.0(7)
C(21)-C(20)-C(19)	120.6(8)
C(22)-C(21)-C(20)	121.6(8)
C(21)-C(22)-C(23)	120.6(8)
C(22)-C(23)-C(18)	117.1(7)
C(22)-C(23)-C(27)	120.2(7)
C(18)-C(23)-C(27)	122.6(7)
C(19)-C(24)-C(26)	113.4(7)
C(19)-C(24)-C(25)	110.9(7)
C(26)-C(24)-C(25)	109.1(7)
C(29)-C(27)-C(28)	110.4(8)
C(29)-C(27)-C(23)	111.3(8)
C(28)-C(27)-C(23)	112.5(7)
O(2)-C(30)-O(1)	124.5(7)
O(2)-C(30)-C(31)	118.6(7)
O(1)-C(30)-C(31)	116.9(7)
C(32)-C(31)-C(30)	125.0(8)
C(31)-C(32)-C(33)	127.9(8)
O(3)-C(33)-O(4)	124.3(9)
O(3)-C(33)-C(32)	123.8(11)
O(4)-C(33)-C(32)	111.8(9)
C(35)-C(34)-O(4)	108.6(10)
C(35)-C(34)-C(36)	109.5(10)
O(4)-C(34)-C(36)	104.7(8)

C(37)-C(36)-C(34)	112.1(11)

Table 1. Crystal data and structure refinement for compound **9**.

Identification code	mar1408	
Empirical formula	C30 H43 F3 N2 O3 S	
Formula weight	568.72	
Temperature	173(2) K	
Wavelength	0.71073 Å	
Crystal system	Monoclinic	
Space group	$P2_1/n$ (No.14)	
Unit cell dimensions	a = 10.1750(2) Å	α= 90°.
	b = 27.5131(6) Å	β= 98.252(1)°.
	c = 11.5138(2) Å	γ = 90°.
Volume	3189.87(11) $Å^3$	
Z	4	
Density (calculated)	1.18 Mg/m^3	
Absorption coefficient	0.15 mm^{-1}	
F(000)	1216	
Crystal size	0.40 x 0.30 x 0.25 mm^3	
Theta range for data collection	3.46 to 26.00°.	
Index ranges	-12<=h<=12, -33<=k<=33, -14<=l<=13	
Reflections collected	35361	
Independent reflections	6239 [R(int) = 0.067]	
Reflections with I>2sigma(I)	4710	
Completeness to theta = 26.00°	99.4 %	
Refinement method	Full-matrix least-squares on F^2	
Data / restraints / parameters	6239 / 0 / 370	
Goodness-of-fit on F^2	0.934	
Final R indices [I>2sigma(I)]	R1 = 0.046, wR2 = 0.112	
R indices (all data)	R1 = 0.068, wR2 = 0.125	
Largest diff. peak and hole	0.23 and -0.36 e.$Å^{-3}$	

H atoms on N were refined.

Data collection KappaCCD , Program package WinGX , Abs correction not applied ,
Refinement using SHELXL-97 , Drawing using ORTEP-3 for Windows

Table 2. Atomic coordinates (x 10^4) and equivalent isotropic displacement parameters ($Å^2$x 10^3) for mar1408. U(eq) is defined as one third of the trace of the orthogonalized U^{ij} tensor.

	x	y	z	U(eq)
S	2985(1)	5148(1)	7135(1)	38(1)
F(1)	980(2)	4648(1)	6086(1)	77(1)
F(2)	2043(2)	4296(1)	7591(1)	89(1)
F(3)	748(2)	4894(1)	7819(2)	82(1)
O(1)	3871(2)	4906(1)	6471(1)	59(1)
O(2)	2328(2)	5568(1)	6580(1)	49(1)
O(3)	3480(2)	5211(1)	8359(1)	53(1)
N(1)	2733(1)	5910(1)	4320(1)	29(1)
N(2)	3248(1)	5819(1)	306(1)	29(1)
C(1)	2798(2)	5623(1)	3399(1)	27(1)
C(2)	2993(2)	5823(1)	2321(1)	27(1)
C(3)	3160(2)	5575(1)	1296(1)	27(1)
C(4)	2626(2)	5094(1)	3645(2)	37(1)
C(5)	3273(2)	5034(1)	1169(2)	38(1)
C(6)	3022(2)	6421(1)	4401(1)	28(1)
C(7)	4228(2)	6565(1)	5051(2)	35(1)
C(8)	4481(2)	7060(1)	5151(2)	44(1)
C(9)	3583(2)	7397(1)	4633(2)	48(1)
C(10)	2387(2)	7247(1)	4007(2)	42(1)
C(11)	2072(2)	6755(1)	3888(1)	32(1)
C(12)	5235(2)	6202(1)	5658(2)	40(1)
C(13)	6525(2)	6216(1)	5152(2)	63(1)
C(14)	5473(3)	6282(1)	6982(2)	70(1)
C(15)	710(2)	6590(1)	3316(2)	36(1)
C(16)	-192(2)	6531(1)	4264(2)	49(1)
C(17)	81(2)	6927(1)	2341(2)	58(1)
C(18)	3038(2)	6330(1)	102(1)	29(1)
C(19)	1860(2)	6472(1)	-611(2)	35(1)
C(20)	1692(2)	6965(1)	-847(2)	48(1)
C(21)	2631(2)	7300(1)	-394(2)	55(1)
C(22)	3785(2)	7151(1)	296(2)	49(1)
C(23)	4029(2)	6660(1)	545(2)	34(1)
C(24)	818(2)	6101(1)	-1083(2)	45(1)

C(25)	-61(2)	5977(1)	-157(2)	64(1)
C(26)	-31(3)	6256(1)	-2231(2)	76(1)
C(27)	5360(2)	6493(1)	1185(2)	35(1)
C(28)	6293(2)	6385(1)	289(2)	54(1)
C(29)	5989(2)	6856(1)	2100(2)	60(1)
C(30)	1627(2)	4724(1)	7159(2)	55(1)

Table 3. Bond lengths [Å] and angles [°] for mar1408.

S-O(1)	1.4286(15)
S-O(3)	1.4370(13)
S-O(2)	1.4379(15)
S-C(30)	1.812(2)
F(1)-C(30)	1.331(3)
F(2)-C(30)	1.324(3)
F(3)-C(30)	1.339(3)
N(1)-C(1)	1.331(2)
N(1)-C(6)	1.436(2)
N(2)-C(3)	1.337(2)
N(2)-C(18)	1.437(2)
C(1)-C(2)	1.397(2)
C(1)-C(4)	1.498(2)
C(2)-C(3)	1.395(2)
C(3)-C(5)	1.500(2)
C(6)-C(7)	1.400(2)
C(6)-C(11)	1.401(2)
C(7)-C(8)	1.389(3)
C(7)-C(12)	1.526(3)
C(8)-C(9)	1.376(3)
C(9)-C(10)	1.385(3)
C(10)-C(11)	1.395(3)
C(11)-C(15)	1.516(2)
C(12)-C(13)	1.512(3)
C(12)-C(14)	1.525(3)
C(15)-C(17)	1.524(3)
C(15)-C(16)	1.532(3)
C(18)-C(23)	1.398(2)
C(18)-C(19)	1.408(2)
C(19)-C(20)	1.388(3)
C(19)-C(24)	1.516(3)
C(20)-C(21)	1.375(3)
C(21)-C(22)	1.382(3)
C(22)-C(23)	1.395(3)
C(23)-C(27)	1.517(2)
C(24)-C(25)	1.525(3)

C(24)-C(26)	1.532(3)
C(27)-C(29)	1.523(3)
C(27)-C(28)	1.528(3)

O(1)-S-O(3)	114.94(9)
O(1)-S-O(2)	115.20(9)
O(3)-S-O(2)	114.47(9)
O(1)-S-C(30)	104.41(11)
O(3)-S-C(30)	102.93(10)
O(2)-S-C(30)	102.56(10)
C(1)-N(1)-C(6)	126.82(14)
C(3)-N(2)-C(18)	127.19(14)
N(1)-C(1)-C(2)	120.21(15)
N(1)-C(1)-C(4)	113.85(14)
C(2)-C(1)-C(4)	125.93(15)
C(3)-C(2)-C(1)	127.44(16)
N(2)-C(3)-C(2)	120.43(15)
N(2)-C(3)-C(5)	113.50(14)
C(2)-C(3)-C(5)	126.06(15)
C(7)-C(6)-C(11)	122.56(16)
C(7)-C(6)-N(1)	117.84(15)
C(11)-C(6)-N(1)	119.51(15)
C(8)-C(7)-C(6)	117.39(17)
C(8)-C(7)-C(12)	119.98(17)
C(6)-C(7)-C(12)	122.62(16)
C(9)-C(8)-C(7)	121.45(18)
C(8)-C(9)-C(10)	120.24(18)
C(9)-C(10)-C(11)	120.86(18)
C(10)-C(11)-C(6)	117.46(16)
C(10)-C(11)-C(15)	121.10(16)
C(6)-C(11)-C(15)	121.23(16)
C(13)-C(12)-C(14)	111.05(19)
C(13)-C(12)-C(7)	111.68(16)
C(14)-C(12)-C(7)	111.32(17)
C(11)-C(15)-C(17)	113.47(16)
C(11)-C(15)-C(16)	109.08(15)
C(17)-C(15)-C(16)	110.98(17)
C(23)-C(18)-C(19)	122.80(16)

C(23)-C(18)-N(2)	119.52(15)
C(19)-C(18)-N(2)	117.54(15)
C(20)-C(19)-C(18)	117.14(17)
C(20)-C(19)-C(24)	121.89(17)
C(18)-C(19)-C(24)	120.96(17)
C(21)-C(20)-C(19)	121.38(19)
C(20)-C(21)-C(22)	120.4(2)
C(21)-C(22)-C(23)	121.13(19)
C(22)-C(23)-C(18)	117.10(17)
C(22)-C(23)-C(27)	120.80(17)
C(18)-C(23)-C(27)	121.92(16)
C(19)-C(24)-C(25)	110.52(16)
C(19)-C(24)-C(26)	113.60(19)
C(25)-C(24)-C(26)	110.6(2)
C(23)-C(27)-C(29)	113.27(17)
C(23)-C(27)-C(28)	109.20(15)
C(29)-C(27)-C(28)	110.84(18)
F(2)-C(30)-F(1)	107.30(19)
F(2)-C(30)-F(3)	107.51(19)
F(1)-C(30)-F(3)	107.5(2)
F(2)-C(30)-S	112.06(17)
F(1)-C(30)-S	111.36(15)
F(3)-C(30)-S	110.90(16)

Hydrogen bonds with H..A < r(A) + 2.000 Angstroms and <DHA > 110 deg.

D-H	d(D-H)	d(H..A)	<DHA	d(D..A)	A
N1-H1X	0.83	2.02	172	2.852	O2
N2-H2X	0.85	1.99	176	2.834	O3 [x, y, z-1]

Table 1. Crystal data and structure refinement for compound **11b**.

Identification code	jun1408	
Empirical formula	C33 H50 N2 O Sn	
Formula weight	609.44	
Temperature	173(2) K	
Wavelength	0.71073 Å	
Crystal system	Triclinic	
Space group	$P\bar{1}$ (No.2)	
Unit cell dimensions	a = 8.7788(2) Å	α= 92.884(2)°.
	b = 9.8810(2) Å	β= 90.071(2)°.
	c = 20.5060(4) Å	γ = 113.948(1)°.
Volume	1623.12(6) $Å^3$	
Z	2	
Density (calculated)	1.25 Mg/m^3	
Absorption coefficient	0.81 mm^{-1}	
F(000)	640	
Crystal size	0.4 x 0.3 x 0.3 mm^3	
Theta range for data collection	3.64 to 26.06°.	
Index ranges	-10<=h<=10, -12<=k<=12, -24<=l<=25	
Reflections collected	23390	
Independent reflections	6364 [R(int) = 0.043]	
Reflections with I>2sigma(I)	5816	
Completeness to theta = 26.06°	99.0 %	
Tmax. and Tmin.	0.7235 and 0.8002	
Refinement method	Full-matrix least-squares on F^2	
Data / restraints / parameters	6364 / 0 / 331	
Goodness-of-fit on F^2	1.110	
Final R indices [I>2sigma(I)]	R1 = 0.045, wR2 = 0.117	
R indices (all data)	R1 = 0.050, wR2 = 0.121	
Largest diff. peak and hole	2.63 and -1.13 e.$Å^{-3}$	

The isobutyl group attached to O is disordered over two partially overlapping orientations with the C30 and C31 alternative positions resolved, and was included with isotropic C atoms.

Data collection KappaCCD , Program package WinGX , Abs correction MULTISCAN

Refinement using SHELXL-97 , Drawing using ORTEP-3 for Windows

Table 2. Atomic coordinates (x 10^4) and equivalent isotropic displacement parameters ($Å^2$x 10^3) for jun1408. U(eq) is defined as one third of the trace of the orthogonalized U^{ij} tensor.

	x	y	z	U(eq)
Sn	4432(1)	6822(1)	2437(1)	29(1)
O	6666(4)	6698(3)	2436(2)	44(1)
N(1)	5149(4)	8565(3)	3231(1)	27(1)
N(2)	5228(4)	8735(3)	1816(1)	27(1)
C(1)	4828(4)	9762(4)	3191(2)	28(1)
C(2)	4555(5)	10296(4)	2600(2)	31(1)
C(3)	4897(4)	9907(4)	1965(2)	29(1)
C(4)	4780(5)	10641(5)	3809(2)	39(1)
C(5)	4904(6)	10910(5)	1435(2)	41(1)
C(6)	5630(5)	8203(4)	3844(2)	30(1)
C(7)	4426(5)	7319(4)	4269(2)	33(1)
C(8)	4958(6)	6937(5)	4843(2)	41(1)
C(9)	6629(6)	7449(5)	5003(2)	45(1)
C(10)	7806(6)	8312(5)	4585(2)	43(1)
C(11)	7351(5)	8692(5)	3993(2)	34(1)
C(12)	2562(5)	6764(5)	4119(2)	37(1)
C(13)	1776(6)	5093(5)	3965(3)	51(1)
C(14)	1657(6)	7176(6)	4688(2)	50(1)
C(15)	8661(5)	9567(5)	3516(2)	40(1)
C(16)	9183(8)	11231(6)	3622(3)	68(2)
C(17)	10209(7)	9219(8)	3546(3)	71(2)
C(18)	5819(5)	8508(4)	1183(2)	31(1)
C(19)	4698(5)	7664(4)	691(2)	35(1)
C(20)	5332(7)	7374(5)	101(2)	47(1)
C(21)	7031(7)	7941(6)	5(2)	55(1)
C(22)	8114(6)	8784(6)	492(2)	53(1)
C(23)	7555(5)	9091(5)	1096(2)	42(1)
C(24)	2808(5)	7026(5)	765(2)	39(1)
C(25)	2051(7)	5336(6)	740(3)	59(1)
C(26)	1973(7)	7578(6)	245(2)	56(1)
C(27)	8799(5)	10054(7)	1627(2)	59(1)
C(28)	9471(8)	11675(8)	1500(4)	79(2)
C(29)	10239(8)	9598(9)	1720(4)	96(3)

C(30)	6731(9)	5320(8)	2206(4)	42(1)a	
C(31)	7636(11)	4885(10)	2719(4)	58(2)a	
C(32)	6884(9)	4842(8)	3357(3)	76(2)	
C(33)	7461(9)	5292(8)	1496(3)	81(2)	
C(30A)	6627(16)	5225(14)	2592(7)	42(1)b	
C(31A)	7880(19)	5045(18)	2146(7)	58(2)b	
Occupancy:	a	0.64		b	0.36

Table 3. Bond lengths [Å] and angles [°] for jun1408.

Sn-O	2.013(3)
Sn-N(1)	2.202(3)
Sn-N(2)	2.203(3)
O-C(30)	1.442(7)
O-C(30A)	1.494(13)
N(1)-C(1)	1.328(5)
N(1)-C(6)	1.434(5)
N(2)-C(3)	1.326(5)
N(2)-C(18)	1.439(5)
C(1)-C(2)	1.404(5)
C(1)-C(4)	1.509(5)
C(2)-C(3)	1.406(5)
C(3)-C(5)	1.506(5)
C(6)-C(7)	1.402(5)
C(6)-C(11)	1.414(5)
C(7)-C(8)	1.390(6)
C(7)-C(12)	1.525(6)
C(8)-C(9)	1.377(7)
C(9)-C(10)	1.375(7)
C(10)-C(11)	1.393(6)
C(11)-C(15)	1.521(6)
C(12)-C(13)	1.524(6)
C(12)-C(14)	1.541(6)
C(15)-C(16)	1.521(7)
C(15)-C(17)	1.533(7)
C(18)-C(19)	1.390(6)
C(18)-C(23)	1.409(6)
C(19)-C(20)	1.396(6)
C(19)-C(24)	1.528(6)
C(20)-C(21)	1.383(7)
C(21)-C(22)	1.366(8)
C(22)-C(23)	1.397(6)
C(23)-C(27)	1.528(7)
C(24)-C(25)	1.524(7)
C(24)-C(26)	1.534(6)
C(27)-C(28)	1.502(9)

C(27)-C(29)	1.519(8)
C(30)-C(31)	1.498(11)
C(30)-C(33)	1.596(10)
C(31)-C(32)	1.461(10)
C(30A)-C(31A)	1.49(2)

O-Sn-N(1)	94.08(12)
O-Sn-N(2)	94.29(12)
N(1)-Sn-N(2)	82.79(11)
C(30)-O-Sn	118.1(3)
C(30A)-O-Sn	114.9(5)
C(1)-N(1)-C(6)	120.4(3)
C(1)-N(1)-Sn	121.6(2)
C(6)-N(1)-Sn	116.5(2)
C(3)-N(2)-C(18)	121.6(3)
C(3)-N(2)-Sn	121.8(2)
C(18)-N(2)-Sn	115.6(2)
N(1)-C(1)-C(2)	123.8(3)
N(1)-C(1)-C(4)	119.4(3)
C(2)-C(1)-C(4)	116.7(3)
C(1)-C(2)-C(3)	127.9(3)
N(2)-C(3)-C(2)	123.7(3)
N(2)-C(3)-C(5)	119.3(3)
C(2)-C(3)-C(5)	117.0(3)
C(7)-C(6)-C(11)	120.9(4)
C(7)-C(6)-N(1)	120.8(3)
C(11)-C(6)-N(1)	118.2(3)
C(8)-C(7)-C(6)	118.6(4)
C(8)-C(7)-C(12)	119.2(4)
C(6)-C(7)-C(12)	122.2(3)
C(9)-C(8)-C(7)	120.9(4)
C(10)-C(9)-C(8)	120.2(4)
C(9)-C(10)-C(11)	121.4(4)
C(10)-C(11)-C(6)	117.8(4)
C(10)-C(11)-C(15)	121.0(4)
C(6)-C(11)-C(15)	121.2(3)
C(13)-C(12)-C(7)	111.4(4)
C(13)-C(12)-C(14)	110.1(4)

C(7)-C(12)-C(14)	111.3(4)
C(11)-C(15)-C(16)	112.3(4)
C(11)-C(15)-C(17)	111.9(4)
C(16)-C(15)-C(17)	109.4(4)
C(19)-C(18)-C(23)	121.7(4)
C(19)-C(18)-N(2)	120.3(3)
C(23)-C(18)-N(2)	117.9(4)
C(18)-C(19)-C(20)	118.4(4)
C(18)-C(19)-C(24)	123.2(3)
C(20)-C(19)-C(24)	118.4(4)
C(21)-C(20)-C(19)	120.7(5)
C(22)-C(21)-C(20)	120.1(4)
C(21)-C(22)-C(23)	121.7(5)
C(22)-C(23)-C(18)	117.3(4)
C(22)-C(23)-C(27)	120.4(4)
C(18)-C(23)-C(27)	122.3(4)
C(25)-C(24)-C(19)	111.8(4)
C(25)-C(24)-C(26)	110.2(4)
C(19)-C(24)-C(26)	111.2(4)
C(28)-C(27)-C(29)	109.5(5)
C(28)-C(27)-C(23)	112.2(4)
C(29)-C(27)-C(23)	112.4(5)
O-C(30)-C(31)	107.5(6)
O-C(30)-C(33)	116.1(6)
C(31)-C(30)-C(33)	112.7(6)
C(32)-C(31)-C(30)	111.4(7)
C(31A)-C(30A)-O	103.2(10)

Least-squares planes (x,y,z in crystal coordinates) and deviations from them
(* indicates atom used to define plane)

7.1515 (0.0126) x + 1.9381 (0.0240) y + 0.6316 (0.0239) z = 5.5464 (0.0169)

*	0.0002	(0.0015)	N1
*	-0.0002	(0.0015)	N2
*	-0.0002	(0.0017)	C1
*	0.0002	(0.0017)	C3
	-0.9005	(0.0051)	Sn
	-0.1295	(0.0053)	C2
	0.6727	(0.0086)	O

Rms deviation of fitted atoms = 0.0002

Table 1. Crystal data and structure refinement for compound **11c**.

Identification code	oct2507	
Empirical formula	C33 H50 N2 O Sn	
Formula weight	609.44	
Temperature	173(2) K	
Wavelength	0.71073 Å	
Crystal system	Monoclinic	
Space group	$P2_1/n$ (No.14)	
Unit cell dimensions	a = 13.3880(2) Å	α= 90°.
	b = 16.7487(3) Å	β= 107.654(1)°.
	c = 15.2140(2) Å	γ = 90°.
Volume	3250.80(9) $Å^3$	
Z	4	
Density (calculated)	1.25 Mg/m^3	
Absorption coefficient	0.81 mm^{-1}	
F(000)	1280	
Crystal size	0.15 x 0.10 x 0.10 mm^3	
Theta range for data collection	3.42 to 26.01°.	
Index ranges	-16<=h<=16, -20<=k<=20, -18<=l<=18	
Reflections collected	45959	
Independent reflections	6387 [R(int) = 0.051]	
Reflections with I>2sigma(I)	5479	
Completeness to theta = 26.01°	99.6 %	
Tmax. and Tmin.	0.944 and 0.883	
Refinement method	Full-matrix least-squares on F^2	
Data / restraints / parameters	6387 / 0 / 347	
Goodness-of-fit on F^2	1.057	
Final R indices [I>2sigma(I)]	R1 = 0.029, wR2 = 0.067	
R indices (all data)	R1 = 0.037, wR2 = 0.071	
Largest diff. peak and hole	0.56 and -0.50 e.$Å^{-3}$	

Data collection KappaCCD , Program package WinGX , Abs correction MULTISCAN

Refinement using SHELXL-97 , Drawing using ORTEP-3 for Windows

Table 2. Atomic coordinates (x 10^4) and equivalent isotropic displacement parameters ($Å^2$x 10^3) for oct2507. U(eq) is defined as one third of the trace of the orthogonalized U^{ij} tensor.

	x	y	z	U(eq)
Sn	9091(1)	1636(1)	5651(1)	24(1)
O	7866(1)	1442(1)	4513(1)	32(1)
N(1)	8064(2)	1967(1)	6481(1)	24(1)
N(2)	9105(1)	2938(1)	5423(1)	24(1)
C(1)	8238(2)	2613(1)	7011(2)	26(1)
C(2)	8850(2)	3256(1)	6884(2)	26(1)
C(3)	9154(2)	3450(1)	6102(2)	25(1)
C(4)	7739(2)	2678(2)	7773(2)	37(1)
C(5)	9526(2)	4296(2)	6051(2)	36(1)
C(6)	7294(2)	1378(1)	6527(2)	26(1)
C(7)	6243(2)	1488(2)	5984(2)	31(1)
C(8)	5544(2)	860(2)	5935(2)	38(1)
C(9)	5860(2)	159(2)	6419(2)	43(1)
C(10)	6880(2)	77(2)	6974(2)	41(1)
C(11)	7617(2)	681(2)	7048(2)	32(1)
C(12)	5856(2)	2266(2)	5476(2)	39(1)
C(13)	5061(3)	2686(2)	5875(3)	66(1)
C(14)	5371(3)	2134(2)	4454(2)	59(1)
C(15)	8724(2)	563(2)	7701(2)	39(1)
C(16)	9262(2)	-154(2)	7427(2)	57(1)
C(17)	8708(3)	477(2)	8701(2)	58(1)
C(18)	9336(2)	3197(1)	4599(2)	30(1)
C(19)	10376(2)	3205(2)	4581(2)	37(1)
C(20)	10560(3)	3440(2)	3761(2)	53(1)
C(21)	9752(3)	3648(2)	3001(2)	61(1)
C(22)	8733(3)	3623(2)	3022(2)	55(1)
C(23)	8496(2)	3389(2)	3817(2)	38(1)
C(24)	11298(2)	2963(2)	5401(2)	46(1)
C(25)	11795(3)	2187(2)	5206(3)	66(1)
C(26)	12141(3)	3623(2)	5679(3)	67(1)
C(27)	7366(2)	3335(2)	3826(2)	45(1)
C(28)	7018(3)	4077(2)	4233(3)	72(1)
C(29)	6590(3)	3175(2)	2869(2)	69(1)

C(30)	7800(2)	759(2)	3946(2)	46(1)
C(31)	7638(7)	35(2)	4481(3)	169(4)
C(32)	6842(3)	839(2)	3122(2)	60(1)
C(33)	8723(3)	690(5)	3625(4)	185(4)

Table 3. Bond lengths [Å] and angles [°] for oct2507.

Sn-O	2.0179(16)
Sn-N(1)	2.2015(19)
Sn-N(2)	2.2100(19)
O-C(30)	1.419(3)
N(1)-C(1)	1.328(3)
N(1)-C(6)	1.443(3)
N(2)-C(3)	1.328(3)
N(2)-C(18)	1.445(3)
C(1)-C(2)	1.401(3)
C(1)-C(4)	1.507(3)
C(2)-C(3)	1.406(3)
C(3)-C(5)	1.513(3)
C(6)-C(11)	1.404(3)
C(6)-C(7)	1.411(3)
C(7)-C(8)	1.393(4)
C(7)-C(12)	1.524(4)
C(8)-C(9)	1.382(4)
C(9)-C(10)	1.378(4)
C(10)-C(11)	1.394(4)
C(11)-C(15)	1.527(4)
C(12)-C(14)	1.509(4)
C(12)-C(13)	1.545(4)
C(15)-C(16)	1.521(4)
C(15)-C(17)	1.536(4)
C(18)-C(19)	1.402(4)
C(18)-C(23)	1.404(4)
C(19)-C(20)	1.399(4)
C(19)-C(24)	1.520(4)
C(20)-C(21)	1.368(5)
C(21)-C(22)	1.375(5)
C(22)-C(23)	1.396(4)
C(23)-C(27)	1.520(4)
C(24)-C(25)	1.529(5)
C(24)-C(26)	1.544(4)
C(27)-C(28)	1.522(5)
C(27)-C(29)	1.533(4)

C(30)-C(33)	1.464(5)
C(30)-C(32)	1.503(4)
C(30)-C(31)	1.512(6)

O-Sn-N(1)	92.66(7)
O-Sn-N(2)	93.89(7)
N(1)-Sn-N(2)	83.02(7)
C(30)-O-Sn	122.40(16)
C(1)-N(1)-C(6)	121.62(19)
C(1)-N(1)-Sn	121.89(15)
C(6)-N(1)-Sn	115.82(14)
C(3)-N(2)-C(18)	120.58(19)
C(3)-N(2)-Sn	120.98(15)
C(18)-N(2)-Sn	116.51(14)
N(1)-C(1)-C(2)	123.0(2)
N(1)-C(1)-C(4)	119.2(2)
C(2)-C(1)-C(4)	117.7(2)
C(1)-C(2)-C(3)	128.7(2)
N(2)-C(3)-C(2)	123.4(2)
N(2)-C(3)-C(5)	120.2(2)
C(2)-C(3)-C(5)	116.4(2)
C(11)-C(6)-C(7)	121.3(2)
C(11)-C(6)-N(1)	119.5(2)
C(7)-C(6)-N(1)	118.9(2)
C(8)-C(7)-C(6)	117.9(2)
C(8)-C(7)-C(12)	119.9(2)
C(6)-C(7)-C(12)	122.2(2)
C(9)-C(8)-C(7)	121.4(2)
C(10)-C(9)-C(8)	119.8(2)
C(9)-C(10)-C(11)	121.5(3)
C(10)-C(11)-C(6)	118.0(2)
C(10)-C(11)-C(15)	118.8(2)
C(6)-C(11)-C(15)	123.2(2)
C(14)-C(12)-C(7)	111.8(2)
C(14)-C(12)-C(13)	109.8(3)
C(7)-C(12)-C(13)	111.0(2)
C(16)-C(15)-C(11)	111.8(2)
C(16)-C(15)-C(17)	110.3(3)

C(11)-C(15)-C(17)	110.7(2)
C(19)-C(18)-C(23)	121.7(2)
C(19)-C(18)-N(2)	119.6(2)
C(23)-C(18)-N(2)	118.5(2)
C(20)-C(19)-C(18)	117.7(3)
C(20)-C(19)-C(24)	119.2(3)
C(18)-C(19)-C(24)	123.1(2)
C(21)-C(20)-C(19)	121.2(3)
C(20)-C(21)-C(22)	120.5(3)
C(21)-C(22)-C(23)	121.1(3)
C(22)-C(23)-C(18)	117.7(3)
C(22)-C(23)-C(27)	120.9(3)
C(18)-C(23)-C(27)	121.5(2)
C(19)-C(24)-C(25)	111.1(3)
C(19)-C(24)-C(26)	112.2(3)
C(25)-C(24)-C(26)	109.7(3)
C(23)-C(27)-C(28)	112.6(3)
C(23)-C(27)-C(29)	113.0(3)
C(28)-C(27)-C(29)	109.0(3)
O-C(30)-C(33)	111.2(3)
O-C(30)-C(32)	108.3(2)
C(33)-C(30)-C(32)	108.8(3)
O-C(30)-C(31)	108.2(3)
C(33)-C(30)-C(31)	113.0(5)
C(32)-C(30)-C(31)	107.2(4)

```
 Least-squares planes (x,y,z in crystal coordinates) and deviations
from them
 (* indicates atom used to define plane)

  7.7899 (0.0095) x + 1.4977 (0.0138) y + 9.0346 (0.0108) z = 12.4321
(0.0030)

 *    0.0000 (0.0000)  Sn
 *    0.0000 (0.0000)  N1
 *    0.0000 (0.0000)  N2

 Rms deviation of fitted atoms =   0.0000


  10.1318 (0.0067) x - 6.3569 (0.0208) y + 4.2238 (0.0179) z = 9.6528
(0.0137)

 Angle to previous plane (with approximate esd) = 33.2 ( 0.1 )

 *   -0.0059 (0.0011)  C1
 *    0.0059 (0.0011)  C3
 *    0.0051 (0.0010)  N1
 *   -0.0051 (0.0010)  N2
      0.9048 (0.0032)  Sn
      0.1517 (0.0033)  C2

 Rms deviation of fitted atoms =   0.0055


  10.0957 (0.0125) x - 9.2910 (0.0499) y + 1.6181 (0.0520) z = 7.0236
(0.0540)

 Angle to previous plane (with approximate esd) = 14.5 ( 0.3 )

 *    0.0000 (0.0000)  C1
 *    0.0000 (0.0000)  C2
 *    0.0000 (0.0000)  C3

 Rms deviation of fitted atoms =   0.0000
```

Table 1. Crystal data and structure refinement for compound **11d**.

Identification code	oct809	
Empirical formula	C33 H41 F9 N2 O Sn	
Formula weight	771.37	
Temperature	173(2) K	
Wavelength	0.71073 Å	
Crystal system	Monoclinic	
Space group	$P\,2_1/m$	
Unit cell dimensions	a = 8.9128(2) Å	α= 90°.
	b = 19.8833(5) Å	β= 113.349(1)°.
	c = 10.4482(2) Å	γ = 90°.
Volume	1699.96(7) $Å^3$	
Z	2	
Density (calculated)	1.51 Mg/m^3	
Absorption coefficient	0.83 mm^{-1}	
F(000)	784	
Crystal size	0.16 x 0.08 x 0.06 mm^3	
Theta range for data collection	3.74 to 27.11°.	
Index ranges	-11<=h<=11, -25<=k<=25, -13<=l<=13	
Reflections collected	27173	
Independent reflections	3861 [R(int) = 0.063]	
Reflections with I>2sigma(I)	3446	
Completeness to theta = 27.11°	99.6 %	
Absorption correction	Semi-empirical from equivalents	
Tmax. and Tmin.	0.9733 and 0.8682	
Refinement method	Full-matrix least-squares on F^2	
Data / restraints / parameters	3861 / 0 / 263	
Goodness-of-fit on F^2	1.023	
Final R indices [I>2sigma(I)]	R1 = 0.028, wR2 = 0.059	
R indices (all data)	R1 = 0.035, wR2 = 0.062	
Largest diff. peak and hole	0.36 and -0.35 $e.Å^{-3}$	

The molecule lies on a mirror plane with the alkoxide group disordered over two positions

Data collection KappaCCD , Program package WinGX , Abs correction MULTISCAN

Refinement using SHELXL-97 , Drawing using ORTEP-3 for Windows

Table 2. Atomic coordinates (x 10^4) and equivalent isotropic displacement parameters ($Å^2$x 10^3) for oct809. U(eq) is defined as one third of the trace of the orthogonalized U^{ij} tensor.

	x	y	z	U(eq)
Sn	10502(1)	2500	3202(1)	18(1)
F(1)	9250(30)	3504(12)	5265(18)	56(3)
F(2)	10386(4)	2654(5)	6357(3)	66(3)
F(3)	8287(13)	3072(5)	6585(9)	64(2)
F(4)	5414(3)	2500	4974(3)	67(1)
F(5)	5047(2)	2500	2823(2)	51(1)
F(6)	5934(6)	3386(2)	3905(5)	59(1)
F(7)	6744(6)	1371(2)	4151(5)	55(1)
F(8)	7939(13)	1688(4)	6255(9)	56(2)
F(9)	9330(30)	1460(11)	4961(16)	48(2)
O	8188(2)	2500	3309(2)	24(1)
N	9780(2)	3232(1)	1505(2)	17(1)
C(1)	10226(2)	3133(1)	442(2)	19(1)
C(2)	10579(3)	2500	49(3)	22(1)
C(3)	10364(3)	3733(1)	-391(2)	26(1)
C(4)	9257(2)	3883(1)	1764(2)	20(1)
C(5)	7570(3)	4018(1)	1233(2)	25(1)
C(6)	7080(3)	4640(1)	1550(3)	32(1)
C(7)	8203(3)	5102(1)	2378(3)	36(1)
C(8)	9843(3)	4959(1)	2899(2)	33(1)
C(9)	10418(3)	4348(1)	2603(2)	24(1)
C(10)	6325(3)	3506(1)	351(3)	32(1)
C(11)	4650(3)	3587(2)	417(3)	47(1)
C(12)	6088(3)	3523(2)	-1175(3)	53(1)
C(13)	12252(3)	4220(1)	3187(2)	28(1)
C(14)	12960(3)	4158(1)	4778(3)	42(1)
C(15)	13159(3)	4775(1)	2754(3)	41(1)
C(16)	7819(4)	2500	4454(3)	27(1)
C(17)	8918(8)	2945(3)	5635(6)	47(1)
C(18)	6021(6)	2723(3)	4027(5)	41(1)
C(19)	7952(8)	1744(3)	4989(6)	41(1)

Table 3. Bond lengths [Å] and angles [°] for oct809.

Sn-O	2.110(2)
Sn-N	2.1837(16)
F(1)-C(17)	1.25(2)
F(2)-C(17)	1.354(8)
F(3)-C(17)	1.345(11)
F(4)-C(18)	1.376(5)
F(5)-C(18)	1.291(5)
F(6)-C(18)	1.322(7)
F(7)-C(19)	1.315(8)
F(8)-C(19)	1.332(11)
F(9)-C(19)	1.36(2)
O-C(16)	1.360(3)
N-C(1)	1.334(2)
N-C(4)	1.439(2)
C(1)-C(2)	1.398(2)
C(1)-C(3)	1.511(3)
C(4)-C(9)	1.405(3)
C(4)-C(5)	1.407(3)
C(5)-C(6)	1.394(3)
C(5)-C(10)	1.519(3)
C(6)-C(7)	1.381(4)
C(7)-C(8)	1.372(3)
C(8)-C(9)	1.399(3)
C(9)-C(13)	1.523(3)
C(10)-C(12)	1.524(4)
C(10)-C(11)	1.530(3)
C(13)-C(14)	1.531(3)
C(13)-C(15)	1.538(3)
C(16)-C(17)	1.518(6)
C(16)-C(18)	1.549(5)
C(16)-C(19)	1.592(6)
O-Sn-N	93.65(6)
N'-Sn-N	83.53(8)
C(16)-O-Sn	128.97(18)
C(1)-N-C(4)	120.96(16)

C(1)-N-Sn	119.29(13)
C(4)-N-Sn	117.41(12)
N-C(1)-C(2)	123.51(19)
N-C(1)-C(3)	118.88(18)
C(2)-C(1)-C(3)	117.61(18)
C(1)'-C(2)-C(1)	128.5(2)
C(9)-C(4)-C(5)	121.86(19)
C(9)-C(4)-N	119.78(18)
C(5)-C(4)-N	118.24(18)
C(6)-C(5)-C(4)	117.5(2)
C(6)-C(5)-C(10)	121.1(2)
C(4)-C(5)-C(10)	121.41(19)
C(7)-C(6)-C(5)	121.4(2)
C(8)-C(7)-C(6)	120.3(2)
C(7)-C(8)-C(9)	121.2(2)
C(8)-C(9)-C(4)	117.7(2)
C(8)-C(9)-C(13)	119.0(2)
C(4)-C(9)-C(13)	123.22(19)
C(5)-C(10)-C(12)	112.7(2)
C(5)-C(10)-C(11)	113.2(2)
C(12)-C(10)-C(11)	108.2(2)
C(9)-C(13)-C(14)	111.29(19)
C(9)-C(13)-C(15)	111.6(2)
C(14)-C(13)-C(15)	109.80(19)
O-C(16)-C(17)	114.3(3)
O-C(16)-C(18)	109.3(3)
C(17)-C(16)-C(18)	109.1(3)
O-C(16)-C(19)	107.4(2)
C(17)-C(16)-C(19)	109.3(4)
C(18)-C(16)-C(19)	107.2(3)
F(1)-C(17)-F(3)	106.2(10)
F(1)-C(17)-F(2)	104.9(13)
F(3)-C(17)-F(2)	105.3(6)
F(1)-C(17)-C(16)	114.9(10)
F(3)-C(17)-C(16)	112.7(7)
F(2)-C(17)-C(16)	112.0(5)
F(5)-C(18)-F(6)	104.9(4)
F(5)-C(18)-F(4)	106.6(4)

F(6)-C(18)-F(4)	111.5(4)
F(5)-C(18)-C(16)	113.7(3)
F(6)-C(18)-C(16)	109.1(4)
F(4)-C(18)-C(16)	110.9(4)
F(7)-C(19)-F(8)	106.7(6)
F(7)-C(19)-F(9)	105.1(11)
F(8)-C(19)-F(9)	110.4(9)
F(7)-C(19)-C(16)	111.8(4)
F(8)-C(19)-C(16)	113.5(6)
F(9)-C(19)-C(16)	109.0(9)

Symmetry transformations used to generate equivalent atoms:

‘ x,-y+1/2,z

Table 1. Crystal data and structure refinement for compound **13**.

Identification code	dec809	
Empirical formula	C36 H50 N2 O4 Sn	
Formula weight	693.47	
Temperature	173(2) K	
Wavelength	0.71073 Å	
Crystal system	Triclinic	
Space group	$P\bar{1}$ (No.2)	
Unit cell dimensions	a = 14.7295(3) Å	α= 110.624(1)°.
	b = 16.2188(2) Å	β= 99.628(1)°.
	c = 17.6171(2) Å	γ = 108.961(1)°.
Volume	3531.49(9) $Å^3$	
Z	4	
Density (calculated)	1.30 Mg/m^3	
Absorption coefficient	0.76 mm^{-1}	
F(000)	1448	
Crystal size	0.23 x 0.20 x 0.10 mm^3	
Theta range for data collection	3.40 to 27.10°.	
Index ranges	-18<=h<=18, -20<=k<=20, -22<=l<=22	
Reflections collected	56849	
Independent reflections	15530 [R(int) = 0.058]	
Reflections with I>2sigma(I)	12240	
Completeness to theta = 27.10°	99.8 %	
Absorption correction	Semi-empirical from equivalents	
Tmax. and Tmin.	0.8976 and 0.8300	
Refinement method	Full-matrix least-squares on F^2	
Data / restraints / parameters	15530 / 0 / 779	
Goodness-of-fit on F^2	1.011	
Final R indices [I>2sigma(I)]	R1 = 0.033, wR2 = 0.070	
R indices (all data)	R1 = 0.051, wR2 = 0.076	
Largest diff. peak and hole	0.44 and -1.10 $e.Å^{-3}$	

There are two independent molecules in the unit cell that differ in the conformation of the alkoxide ligand

Data collection KappaCCD , Program package WinGX , Abs correction MULTISCAN

Refinement using SHELXL-97 , Drawing using ORTEP-3 for Windows

Table 2. Atomic coordinates (x 10^4) and equivalent isotropic displacement parameters ($Å^2$x 10^3) for dec809. U(eq) is defined as one third of the trace of the orthogonalized U^{ij} tensor.

	x	y	z	U(eq)
Sn	6547(1)	9004(1)	1733(1)	19(1)
Sn(1B)	3128(1)	5810(1)	3051(1)	20(1)
O(1)	7834(1)	8758(1)	1471(1)	26(1)
O(2)	6686(2)	7321(1)	460(1)	46(1)
O(3)	9891(2)	10007(1)	1359(1)	44(1)
O(4)	10384(2)	9371(1)	2210(1)	43(1)
N(1)	7382(1)	10508(1)	1987(1)	19(1)
N(2)	7309(2)	9490(1)	3082(1)	20(1)
C(1)	8255(2)	11126(2)	2601(1)	21(1)
C(2)	8628(2)	10991(2)	3313(1)	23(1)
C(3)	8147(2)	10291(2)	3574(1)	22(1)
C(4)	8879(2)	12040(2)	2560(2)	32(1)
C(5)	8616(2)	10495(2)	4489(2)	33(1)
C(6)	6913(2)	10789(2)	1392(1)	21(1)
C(7)	7121(2)	10629(2)	616(1)	22(1)
C(8)	6594(2)	10846(2)	37(2)	27(1)
C(9)	5904(2)	11229(2)	221(2)	32(1)
C(10)	5716(2)	11391(2)	990(2)	32(1)
C(11)	6207(2)	11174(2)	1589(2)	24(1)
C(12)	7899(2)	10239(2)	400(2)	25(1)
C(13)	7390(2)	9220(2)	-327(2)	38(1)
C(14)	8704(2)	10905(2)	177(2)	41(1)
C(15)	6000(2)	11380(2)	2442(2)	28(1)
C(16)	4877(2)	11006(3)	2337(2)	53(1)
C(17)	6527(3)	12459(2)	3031(2)	46(1)
C(18)	6843(2)	8861(2)	3451(1)	22(1)
C(19)	7228(2)	8200(2)	3540(2)	25(1)
C(20)	6793(2)	7655(2)	3946(2)	33(1)
C(21)	5999(2)	7736(2)	4235(2)	37(1)
C(22)	5592(2)	8345(2)	4096(2)	34(1)
C(23)	5995(2)	8912(2)	3693(2)	26(1)
C(24)	8050(2)	8042(2)	3171(2)	29(1)
C(25)	7578(2)	7087(2)	2353(2)	37(1)

C(26)	8898(2)	8039(2)	3803(2)	47(1)
C(27)	5532(2)	9579(2)	3552(2)	32(1)
C(28)	4375(2)	9098(3)	3251(2)	53(1)
C(29)	5950(3)	10536(2)	4340(2)	56(1)
C(30)	7565(2)	7928(2)	829(2)	29(1)
C(31)	8385(2)	7716(2)	532(2)	36(1)
C(32)	9361(2)	8303(2)	821(2)	38(1)
C(33)	9873(2)	9321(2)	1482(2)	33(1)
C(34)	11044(3)	10342(2)	2893(2)	46(1)
C(35)	12042(3)	10671(3)	2763(2)	70(1)
C(36)	11063(3)	10253(3)	3714(2)	66(1)
O(1B)	1981(1)	5873(1)	3655(1)	25(1)
O(2B)	3311(2)	7017(2)	4784(1)	54(1)
O(3B)	128(2)	4534(1)	3954(1)	43(1)
O(4B)	-570(2)	5331(1)	3402(1)	41(1)
N(1B)	2006(2)	5349(1)	1833(1)	20(1)
N(2B)	2594(1)	4270(1)	2746(1)	18(1)
C(1B)	1276(2)	4465(2)	1341(1)	21(1)
C(2B)	1168(2)	3654(2)	1492(1)	19(1)
C(3B)	1805(2)	3543(2)	2097(1)	20(1)
C(4B)	527(2)	4298(2)	542(2)	32(1)
C(5B)	1581(2)	2517(2)	1965(2)	31(1)
C(6B)	2144(2)	6085(2)	1523(2)	24(1)
C(7B)	1689(2)	6733(2)	1775(2)	28(1)
C(8B)	1827(2)	7423(2)	1452(2)	39(1)
C(9B)	2392(3)	7472(2)	909(2)	46(1)
C(10B)	2865(2)	6852(2)	694(2)	45(1)
C(11B)	2758(2)	6151(2)	993(2)	33(1)
C(12B)	1068(2)	6714(2)	2377(2)	30(1)
C(13B)	1603(3)	7635(2)	3225(2)	47(1)
C(14B)	-4(2)	6588(2)	1981(2)	45(1)
C(15B)	3316(2)	5506(2)	759(2)	39(1)
C(16B)	4456(3)	6089(3)	1170(2)	59(1)
C(17B)	3058(3)	4956(2)	-212(2)	56(1)
C(18B)	3271(2)	4063(2)	3275(1)	20(1)
C(19B)	3075(2)	3949(2)	3995(2)	24(1)
C(20B)	3759(2)	3760(2)	4484(2)	30(1)
C(21B)	4605(2)	3692(2)	4276(2)	33(1)

C(22B)	4790(2)	3823(2)	3580(2)	30(1)
C(23B)	4139(2)	4017(2)	3064(2)	24(1)
C(24B)	2154(2)	4013(2)	4252(2)	25(1)
C(25B)	2480(2)	4855(2)	5134(2)	36(1)
C(26B)	1486(2)	3075(2)	4259(2)	38(1)
C(27B)	4387(2)	4160(2)	2302(2)	29(1)
C(28B)	5362(2)	5049(2)	2587(2)	50(1)
C(29B)	4454(3)	3274(2)	1673(2)	60(1)
C(30B)	2393(2)	6562(2)	4430(2)	31(1)
C(31B)	1693(2)	6798(2)	4899(2)	37(1)
C(32B)	725(3)	6256(2)	4703(2)	43(1)
C(33B)	94(2)	5276(2)	3982(2)	36(1)
C(34B)	-1345(2)	4413(2)	2718(2)	41(1)
C(35B)	-2242(3)	4620(3)	2452(2)	58(1)
C(36B)	-941(3)	4050(2)	2000(2)	52(1)

Table 3. Bond lengths [Å] and angles [°] for dec809.

Sn-O(1)	2.1489(16)
Sn-N(2)	2.1784(18)
Sn-N(1)	2.1812(18)
O(1)-C(30)	1.296(3)
O(2)-C(30)	1.228(3)
O(3)-C(33)	1.199(3)
O(4)-C(33)	1.335(3)
O(4)-C(34)	1.466(3)
N(1)-C(1)	1.327(3)
N(1)-C(6)	1.444(3)
N(2)-C(3)	1.331(3)
N(2)-C(18)	1.447(3)
C(1)-C(2)	1.402(3)
C(1)-C(4)	1.502(3)
C(2)-C(3)	1.399(3)
C(3)-C(5)	1.512(3)
C(6)-C(7)	1.404(3)
C(6)-C(11)	1.407(3)
C(7)-C(8)	1.391(3)
C(7)-C(12)	1.519(3)
C(8)-C(9)	1.380(4)
C(9)-C(10)	1.380(4)
C(10)-C(11)	1.390(3)
C(11)-C(15)	1.526(3)
C(12)-C(13)	1.522(3)
C(12)-C(14)	1.533(4)
C(15)-C(16)	1.519(4)
C(15)-C(17)	1.520(4)
C(18)-C(23)	1.403(3)
C(18)-C(19)	1.408(3)
C(19)-C(20)	1.391(3)
C(19)-C(24)	1.517(4)
C(20)-C(21)	1.377(4)
C(21)-C(22)	1.378(4)
C(22)-C(23)	1.395(3)
C(23)-C(27)	1.521(3)

C(24)-C(26)	1.531(4)
C(24)-C(25)	1.535(3)
C(27)-C(29)	1.514(4)
C(27)-C(28)	1.528(4)
C(30)-C(31)	1.485(4)
C(31)-C(32)	1.325(4)
C(32)-C(33)	1.480(4)
C(34)-C(35)	1.479(5)
C(34)-C(36)	1.501(4)
Sn(1B)-O(1B)	2.1534(16)
Sn(1B)-N(1B)	2.1851(18)
Sn(1B)-N(2B)	2.1866(17)
O(1B)-C(30B)	1.299(3)
O(2B)-C(30B)	1.227(3)
O(3B)-C(33B)	1.205(3)
O(4B)-C(33B)	1.340(3)
O(4B)-C(34B)	1.464(4)
N(1B)-C(1B)	1.333(3)
N(1B)-C(6B)	1.450(3)
N(2B)-C(3B)	1.328(3)
N(2B)-C(18B)	1.449(3)
C(1B)-C(2B)	1.397(3)
C(1B)-C(4B)	1.513(3)
C(2B)-C(3B)	1.400(3)
C(3B)-C(5B)	1.508(3)
C(6B)-C(7B)	1.408(3)
C(6B)-C(11B)	1.410(4)
C(7B)-C(8B)	1.398(3)
C(7B)-C(12B)	1.513(4)
C(8B)-C(9B)	1.376(4)
C(9B)-C(10B)	1.383(4)
C(10B)-C(11B)	1.390(4)
C(11B)-C(15B)	1.520(4)
C(12B)-C(14B)	1.531(4)
C(12B)-C(13B)	1.534(4)
C(15B)-C(16B)	1.522(4)
C(15B)-C(17B)	1.534(4)
C(18B)-C(23B)	1.408(3)

C(18B)-C(19B)	1.408(3)
C(19B)-C(20B)	1.394(3)
C(19B)-C(24B)	1.523(3)
C(20B)-C(21B)	1.382(4)
C(21B)-C(22B)	1.372(4)
C(22B)-C(23B)	1.396(3)
C(23B)-C(27B)	1.522(3)
C(24B)-C(26B)	1.526(4)
C(24B)-C(25B)	1.531(3)
C(27B)-C(28B)	1.515(4)
C(27B)-C(29B)	1.520(4)
C(30B)-C(31B)	1.486(4)
C(31B)-C(32B)	1.316(4)
C(32B)-C(33B)	1.492(4)
C(34B)-C(36B)	1.502(4)
C(34B)-C(35B)	1.506(4)

O(1)-Sn-N(2)	87.90(7)
O(1)-Sn-N(1)	87.32(7)
N(2)-Sn-N(1)	84.88(7)
C(30)-O(1)-Sn	111.82(16)
C(33)-O(4)-C(34)	117.0(2)
C(1)-N(1)-C(6)	120.86(19)
C(1)-N(1)-Sn	125.64(15)
C(6)-N(1)-Sn	113.46(14)
C(3)-N(2)-C(18)	118.92(18)
C(3)-N(2)-Sn	125.86(15)
C(18)-N(2)-Sn	115.22(13)
N(1)-C(1)-C(2)	123.5(2)
N(1)-C(1)-C(4)	119.5(2)
C(2)-C(1)-C(4)	117.0(2)
C(3)-C(2)-C(1)	129.0(2)
N(2)-C(3)-C(2)	124.4(2)
N(2)-C(3)-C(5)	119.3(2)
C(2)-C(3)-C(5)	116.3(2)
C(7)-C(6)-C(11)	121.4(2)
C(7)-C(6)-N(1)	120.2(2)
C(11)-C(6)-N(1)	118.4(2)

C(8)-C(7)-C(6)	118.0(2)
C(8)-C(7)-C(12)	119.8(2)
C(6)-C(7)-C(12)	122.3(2)
C(9)-C(8)-C(7)	121.5(2)
C(8)-C(9)-C(10)	119.7(2)
C(9)-C(10)-C(11)	121.4(2)
C(10)-C(11)-C(6)	118.0(2)
C(10)-C(11)-C(15)	120.2(2)
C(6)-C(11)-C(15)	121.7(2)
C(7)-C(12)-C(13)	110.9(2)
C(7)-C(12)-C(14)	112.1(2)
C(13)-C(12)-C(14)	110.3(2)
C(16)-C(15)-C(17)	110.2(2)
C(16)-C(15)-C(11)	112.6(2)
C(17)-C(15)-C(11)	110.4(2)
C(23)-C(18)-C(19)	121.5(2)
C(23)-C(18)-N(2)	118.7(2)
C(19)-C(18)-N(2)	119.8(2)
C(20)-C(19)-C(18)	117.5(2)
C(20)-C(19)-C(24)	120.6(2)
C(18)-C(19)-C(24)	121.8(2)
C(21)-C(20)-C(19)	121.8(2)
C(20)-C(21)-C(22)	119.9(3)
C(21)-C(22)-C(23)	121.1(3)
C(22)-C(23)-C(18)	118.0(2)
C(22)-C(23)-C(27)	119.9(2)
C(18)-C(23)-C(27)	122.1(2)
C(19)-C(24)-C(26)	112.9(2)
C(19)-C(24)-C(25)	109.5(2)
C(26)-C(24)-C(25)	109.9(2)
C(29)-C(27)-C(23)	111.2(2)
C(29)-C(27)-C(28)	111.8(2)
C(23)-C(27)-C(28)	112.2(2)
O(2)-C(30)-O(1)	124.1(2)
O(2)-C(30)-C(31)	119.1(2)
O(1)-C(30)-C(31)	116.8(2)
C(32)-C(31)-C(30)	127.2(2)
C(31)-C(32)-C(33)	128.2(3)

O(3)-C(33)-O(4)	124.8(3)
O(3)-C(33)-C(32)	124.7(3)
O(4)-C(33)-C(32)	110.3(2)
O(4)-C(34)-C(35)	109.3(3)
O(4)-C(34)-C(36)	105.6(3)
C(35)-C(34)-C(36)	115.1(3)
O(1B)-Sn(1B)-N(1B)	88.54(7)
O(1B)-Sn(1B)-N(2B)	88.78(6)
N(1B)-Sn(1B)-N(2B)	86.09(7)
C(30B)-O(1B)-Sn(1B)	109.74(16)
C(33B)-O(4B)-C(34B)	116.8(2)
C(1B)-N(1B)-C(6B)	118.66(19)
C(1B)-N(1B)-Sn(1B)	126.67(15)
C(6B)-N(1B)-Sn(1B)	114.51(14)
C(3B)-N(2B)-C(18B)	119.52(18)
C(3B)-N(2B)-Sn(1B)	126.95(15)
C(18B)-N(2B)-Sn(1B)	113.14(13)
N(1B)-C(1B)-C(2B)	124.4(2)
N(1B)-C(1B)-C(4B)	119.0(2)
C(2B)-C(1B)-C(4B)	116.5(2)
C(1B)-C(2B)-C(3B)	130.1(2)
N(2B)-C(3B)-C(2B)	124.3(2)
N(2B)-C(3B)-C(5B)	119.4(2)
C(2B)-C(3B)-C(5B)	116.3(2)
C(7B)-C(6B)-C(11B)	121.5(2)
C(7B)-C(6B)-N(1B)	119.5(2)
C(11B)-C(6B)-N(1B)	118.9(2)
C(8B)-C(7B)-C(6B)	117.8(2)
C(8B)-C(7B)-C(12B)	119.4(2)
C(6B)-C(7B)-C(12B)	122.8(2)
C(9B)-C(8B)-C(7B)	121.3(3)
C(8B)-C(9B)-C(10B)	120.1(3)
C(9B)-C(10B)-C(11B)	121.5(3)
C(10B)-C(11B)-C(6B)	117.8(2)
C(10B)-C(11B)-C(15B)	119.5(2)
C(6B)-C(11B)-C(15B)	122.8(2)
C(7B)-C(12B)-C(14B)	112.2(2)
C(7B)-C(12B)-C(13B)	110.6(2)

C(14B)-C(12B)-C(13B)	110.2(2)
C(11B)-C(15B)-C(16B)	111.0(2)
C(11B)-C(15B)-C(17B)	112.3(2)
C(16B)-C(15B)-C(17B)	109.8(3)
C(23B)-C(18B)-C(19B)	121.5(2)
C(23B)-C(18B)-N(2B)	118.1(2)
C(19B)-C(18B)-N(2B)	120.3(2)
C(20B)-C(19B)-C(18B)	117.7(2)
C(20B)-C(19B)-C(24B)	119.4(2)
C(18B)-C(19B)-C(24B)	122.9(2)
C(21B)-C(20B)-C(19B)	121.6(2)
C(22B)-C(21B)-C(20B)	119.7(2)
C(21B)-C(22B)-C(23B)	121.8(2)
C(22B)-C(23B)-C(18B)	117.7(2)
C(22B)-C(23B)-C(27B)	119.4(2)
C(18B)-C(23B)-C(27B)	122.9(2)
C(19B)-C(24B)-C(26B)	111.9(2)
C(19B)-C(24B)-C(25B)	110.7(2)
C(26B)-C(24B)-C(25B)	109.3(2)
C(28B)-C(27B)-C(29B)	110.0(3)
C(28B)-C(27B)-C(23B)	111.3(2)
C(29B)-C(27B)-C(23B)	111.7(2)
O(2B)-C(30B)-O(1B)	123.8(2)
O(2B)-C(30B)-C(31B)	119.4(2)
O(1B)-C(30B)-C(31B)	116.8(2)
C(32B)-C(31B)-C(30B)	126.8(3)
C(31B)-C(32B)-C(33B)	128.3(3)
O(3B)-C(33B)-O(4B)	124.8(3)
O(3B)-C(33B)-C(32B)	124.9(3)
O(4B)-C(33B)-C(32B)	110.2(2)
O(4B)-C(34B)-C(36B)	110.1(2)
O(4B)-C(34B)-C(35B)	105.8(2)
C(36B)-C(34B)-C(35B)	113.2(3)

Table 1. Crystal data and structure refinement for compound **15a**.

Identification code	dec307	
Empirical formula	C32 H48 Ge N2 O	
Formula weight	549.31	
Temperature	173(2) K	
Wavelength	0.71073 Å	
Crystal system	Monoclinic	
Space group	$P2_1/n$ (No.14)	
Unit cell dimensions	a = 13.1504(5) Å	α= 90°.
	b = 16.3912(3) Å	β= 107.328(1)°.
	c = 15.2918(6) Å	γ = 90°.
Volume	3146.56(18) $Å^3$	
Z	4	
Density (calculated)	1.16 Mg/m^3	
Absorption coefficient	1.00 mm^{-1}	
F(000)	1176	
Crystal size	0.25 x 0.20 x 0.15 mm^3	
Theta range for data collection	3.48 to 26.15°.	
Index ranges	-16<=h<=13, -20<=k<=18, -18<=l<=18	
Reflections collected	18604	
Independent reflections	6127 [R(int) = 0.056]	
Reflections with I>2sigma(I)	4769	
Completeness to theta = 26.15°	97.6 %	
Tmax. and Tmin.	0.9071 and 0.7045	
Refinement method	Full-matrix least-squares on F^2	
Data / restraints / parameters	6127 / 0 / 337	
Goodness-of-fit on F^2	1.022	
Final R indices [I>2sigma(I)]	R1 = 0.048, wR2 = 0.100	
R indices (all data)	R1 = 0.069, wR2 = 0.111	
Largest diff. peak and hole	0.54 and -0.82 e.$Å^{-3}$	

Isomorphous with the Pb analoge (DEC307)

Data collection KappaCCD , Program package WinGX , Abs correction MULTISCAN

Refinement using SHELXL-97 , Drawing using ORTEP-3 for Windows

Table 2. Atomic coordinates (x 10^4) and equivalent isotropic displacement parameters ($Å^2$x 10^3) for dec307. U(eq) is defined as one third of the trace of the orthogonalized U^{ij} tensor.

	x	y	z	U(eq)
Ge	4173(1)	6670(1)	5704(1)	31(1)
O	3069(2)	6504(1)	4669(1)	39(1)
N(1)	4313(2)	7879(1)	5517(2)	32(1)
N(2)	3233(2)	6948(1)	6490(2)	28(1)
C(1)	4412(2)	8407(2)	6196(2)	32(1)
C(2)	4086(2)	8232(2)	6964(2)	33(1)
C(3)	3429(2)	7585(2)	7051(2)	30(1)
C(4)	4881(3)	9249(2)	6163(3)	50(1)
C(5)	2903(3)	7626(2)	7807(2)	43(1)
C(6)	4576(3)	8113(2)	4697(2)	43(1)
C(7)	5638(3)	8050(2)	4685(3)	53(1)
C(8)	5854(5)	8275(3)	3874(3)	79(2)
C(9)	5076(5)	8547(3)	3136(3)	87(2)
C(10)	4041(5)	8591(3)	3151(3)	78(1)
C(11)	3759(4)	8373(2)	3932(3)	56(1)
C(12)	6531(3)	7736(3)	5480(3)	60(1)
C(13)	6948(4)	6920(3)	5259(4)	86(2)
C(14)	7451(4)	8354(3)	5785(4)	89(2)
C(15)	2610(4)	8406(2)	3926(3)	67(1)
C(16)	2341(5)	9210(4)	4291(4)	108(2)
C(17)	1811(5)	8249(3)	2986(4)	104(2)
C(18)	2426(2)	6357(2)	6507(2)	33(1)
C(19)	2725(3)	5636(2)	7014(2)	41(1)
C(20)	1945(3)	5043(2)	6948(3)	53(1)
C(21)	913(3)	5154(2)	6408(3)	53(1)
C(22)	629(3)	5874(2)	5936(2)	44(1)
C(23)	1372(2)	6492(2)	5975(2)	35(1)
C(24)	3847(3)	5477(2)	7633(3)	52(1)
C(25)	4366(4)	4764(3)	7295(3)	76(1)
C(26)	3864(4)	5338(3)	8631(3)	74(1)
C(27)	1021(3)	7284(2)	5456(2)	44(1)
C(28)	264(4)	7760(3)	5859(4)	87(2)
C(29)	503(4)	7155(3)	4452(3)	80(1)

C(30)	3104(3)	5780(2)	4154(3)	52(1)
C(31)	2161(5)	5260(3)	4127(5)	124(3)
C(32)	3116(6)	6024(4)	3218(4)	122(2)

Table 3. Bond lengths [Å] and angles [°] for dec307.

Ge-O	1.821(2)
Ge-N(2)	2.016(2)
Ge-N(1)	2.020(2)
O-C(30)	1.432(4)
N(1)-C(1)	1.328(4)
N(1)-C(6)	1.447(4)
N(2)-C(3)	1.327(4)
N(2)-C(18)	1.443(4)
C(1)-C(2)	1.394(4)
C(1)-C(4)	1.519(4)
C(2)-C(3)	1.397(4)
C(3)-C(5)	1.515(4)
C(6)-C(11)	1.398(5)
C(6)-C(7)	1.406(5)
C(7)-C(8)	1.402(5)
C(7)-C(12)	1.507(6)
C(8)-C(9)	1.354(7)
C(9)-C(10)	1.369(7)
C(10)-C(11)	1.399(6)
C(11)-C(15)	1.509(6)
C(12)-C(13)	1.520(6)
C(12)-C(14)	1.540(6)
C(15)-C(16)	1.514(6)
C(15)-C(17)	1.529(6)
C(18)-C(23)	1.401(4)
C(18)-C(19)	1.405(4)
C(19)-C(20)	1.395(4)
C(19)-C(24)	1.520(5)
C(20)-C(21)	1.374(5)
C(21)-C(22)	1.374(5)
C(22)-C(23)	1.397(4)
C(23)-C(27)	1.519(4)
C(24)-C(25)	1.519(5)
C(24)-C(26)	1.538(5)
C(27)-C(29)	1.497(5)
C(27)-C(28)	1.532(5)

C(30)-C(32)	1.491(6)
C(30)-C(31)	1.495(6)

O-Ge-N(2)	94.63(10)
O-Ge-N(1)	96.10(10)
N(2)-Ge-N(1)	87.74(9)
C(30)-O-Ge	117.0(2)
C(1)-N(1)-C(6)	120.8(2)
C(1)-N(1)-Ge	121.31(19)
C(6)-N(1)-Ge	116.00(19)
C(3)-N(2)-C(18)	121.3(2)
C(3)-N(2)-Ge	121.87(18)
C(18)-N(2)-Ge	116.32(17)
N(1)-C(1)-C(2)	122.8(3)
N(1)-C(1)-C(4)	120.7(3)
C(2)-C(1)-C(4)	116.4(3)
C(1)-C(2)-C(3)	126.2(3)
N(2)-C(3)-C(2)	122.8(3)
N(2)-C(3)-C(5)	118.9(2)
C(2)-C(3)-C(5)	118.4(3)
C(11)-C(6)-C(7)	122.0(3)
C(11)-C(6)-N(1)	118.9(3)
C(7)-C(6)-N(1)	119.1(3)
C(8)-C(7)-C(6)	117.2(4)
C(8)-C(7)-C(12)	119.2(4)
C(6)-C(7)-C(12)	123.6(3)
C(9)-C(8)-C(7)	121.5(5)
C(8)-C(9)-C(10)	120.8(4)
C(9)-C(10)-C(11)	121.2(5)
C(6)-C(11)-C(10)	117.4(4)
C(6)-C(11)-C(15)	122.2(3)
C(10)-C(11)-C(15)	120.4(4)
C(7)-C(12)-C(13)	111.6(4)
C(7)-C(12)-C(14)	111.9(4)
C(13)-C(12)-C(14)	110.1(4)
C(11)-C(15)-C(16)	111.9(4)
C(11)-C(15)-C(17)	114.0(4)
C(16)-C(15)-C(17)	108.8(4)

C(23)-C(18)-C(19)	121.3(3)
C(23)-C(18)-N(2)	119.3(3)
C(19)-C(18)-N(2)	119.3(3)
C(20)-C(19)-C(18)	117.9(3)
C(20)-C(19)-C(24)	118.9(3)
C(18)-C(19)-C(24)	123.2(3)
C(21)-C(20)-C(19)	121.6(3)
C(20)-C(21)-C(22)	119.7(3)
C(21)-C(22)-C(23)	121.5(3)
C(22)-C(23)-C(18)	118.0(3)
C(22)-C(23)-C(27)	119.8(3)
C(18)-C(23)-C(27)	122.2(3)
C(25)-C(24)-C(19)	111.8(3)
C(25)-C(24)-C(26)	110.4(3)
C(19)-C(24)-C(26)	111.5(3)
C(29)-C(27)-C(23)	113.0(3)
C(29)-C(27)-C(28)	109.4(3)
C(23)-C(27)-C(28)	111.0(3)
O-C(30)-C(32)	108.5(3)
O-C(30)-C(31)	109.0(3)
C(32)-C(30)-C(31)	111.9(4)

Least-squares planes (x,y,z in crystal coordinates) and deviations from them
(* indicates atom used to define plane)

7.7570 (0.0126) x + 0.5061 (0.0206) y + 9.0925 (0.0146) z = 8.7606 (0.0138)

* 0.0000 (0.0000) Ge
* 0.0000 (0.0000) N1
* 0.0000 (0.0000) N2

Rms deviation of fitted atoms = 0.0000

9.7165 (0.0088) x - 6.9861 (0.0261) y + 4.2538 (0.0236) z = 1.0406 (0.0317)

Angle to previous plane (with approximate esd) = 32.45 (0.15)

* -0.0076 (0.0013) N1
* 0.0076 (0.0013) N2
* 0.0085 (0.0014) C1
* -0.0085 (0.0014) C3
    0.1406 (0.0044) C2
    0.7807 (0.0039) Ge

Rms deviation of fitted atoms = 0.0081

- 9.6148 (0.0158) x + 9.5059 (0.0578) y - 1.9151 (0.0654) z = 2.5632 (0.0907)

Angle to previous plane (with approximate esd) = 12.86 (0.40)

* 0.0000 (0.0000) C1
* 0.0000 (0.0000) C2
* 0.0000 (0.0000) C3

Rms deviation of fitted atoms = 0.0000

Table 1. Crystal data and structure refinement for compound **15b**.

Identification code	jul310	
Empirical formula	C33 H50 Ge N2 O	
Formula weight	563.34	
Temperature	173(2) K	
Wavelength	0.71073 Å	
Crystal system	Triclinic	
Space group	$P\bar{1}$ (No.2)	
Unit cell dimensions	a = 8.5920(1) Å	α= 102.907(1)°.
	b = 11.7494(3) Å	β= 102.097(2)°.
	c = 16.6858(4) Å	γ = 95.886(1)°.
Volume	1585.59(6) $Å^3$	
Z	2	
Density (calculated)	1.18 Mg/m^3	
Absorption coefficient	0.99 mm^{-1}	
F(000)	604	
Crystal size	0.21 x 0.16 x 0.12 mm^3	
Theta range for data collection	3.46 to 27.10°.	
Index ranges	-11<=h<=11, -15<=k<=15, -21<=l<=21	
Reflections collected	26337	
Independent reflections	6947 [R(int) = 0.050]	
Reflections with I>2sigma(I)	6133	
Completeness to theta = 27.10°	99.6 %	
Tmax. and Tmin.	0.8838 and 0.8031	
Refinement method	Full-matrix least-squares on F^2	
Data / restraints / parameters	6947 / 22 / 401	
Goodness-of-fit on F^2	1.023	
Final R indices [I>2sigma(I)]	R1 = 0.032, wR2 = 0.076	
R indices (all data)	R1 = 0.040, wR2 = 0.080	
Largest diff. peak and hole	0.39 and -0.40 e.$Å^{-3}$	

The *sec*-butyl group and one of the isopropyl groups are disordered and were modeled over two positions with loose restraints applied to C-C distances

Data collection KappaCCD , Program package WinGX , Abs correction MULTISCAN

Refinement using SHELXL-97 , Drawing using ORTEP-3 for Windows

Table 2. Atomic coordinates (x 10^4) and equivalent isotropic displacement parameters ($Å^2$x 10^3) for jul310. U(eq) is defined as one third of the trace of the orthogonalized U^{ij} tensor.

	x	y	z	U(eq)
Ge	1098(1)	3044(1)	2955(1)	21(1)
O	-971(2)	3140(1)	3050(1)	30(1)
N(1)	840(2)	3440(1)	1819(1)	21(1)
N(2)	678(2)	1319(1)	2320(1)	18(1)
C(1)	1350(2)	2816(2)	1186(1)	22(1)
C(2)	1669(2)	1663(2)	1143(1)	23(1)
C(3)	1214(2)	926(1)	1633(1)	20(1)
C(4)	1569(3)	3344(2)	465(1)	33(1)
C(5)	1334(2)	-369(2)	1351(1)	31(1)
C(6)	325(2)	4558(2)	1783(1)	23(1)
C(7)	-1267(2)	4575(2)	1365(1)	29(1)
C(8)	-1762(3)	5667(2)	1384(1)	36(1)
C(9)	-731(3)	6711(2)	1806(1)	40(1)
C(10)	826(3)	6677(2)	2206(1)	36(1)
C(11)	1403(2)	5609(2)	2201(1)	27(1)
C(12)	-2446(2)	3444(2)	898(2)	43(1)
C(13)	-3016(4)	3391(3)	-54(2)	67(1)
C(14)	-3878(3)	3329(3)	1282(2)	63(1)
C(15)	3147(2)	5624(2)	2643(1)	32(1)
C(16)	3455(3)	6133(2)	3601(1)	49(1)
C(17)	4320(3)	6315(2)	2279(2)	46(1)
C(18)	74(2)	507(1)	2756(1)	21(1)
C(19)	-1574(2)	49(2)	2519(1)	24(1)
C(20)	-2140(2)	-725(2)	2956(1)	33(1)
C(21)	-1118(3)	-1008(2)	3614(1)	38(1)
C(22)	483(3)	-519(2)	3856(1)	35(1)
C(23)	1123(2)	243(2)	3432(1)	25(1)
C(27)	2909(2)	760(2)	3721(1)	28(1)
C(28)	3304(3)	1637(2)	4594(1)	43(1)
C(29)	3974(2)	-206(2)	3740(1)	37(1)
C(24)	-2746(11)	368(10)	1781(7)	32(3)[a]
C(25)	-3329(15)	-749(11)	1052(6)	70(3)[a]
C(26)	-4158(14)	813(12)	2115(8)	60(3)[a]

C(24A)	-2699(14)	406(12)	1866(8)	35(4)[b]
C(25A)	-2822(11)	-253(11)	947(5)	49(2)[b]
C(26A)	-4431(14)	443(13)	1955(8)	46(3)[b]
C(30)	-1710(13)	5085(6)	3559(6)	55(2)[c]
C(31)	-1161(6)	3974(4)	3777(3)	32(1)[c]
C(32)	-2324(5)	3373(3)	4169(2)	41(1)[c]
C(33)	-1728(11)	2358(8)	4503(5)	46(2)[c]
C(30A)	-1670(20)	2463(12)	4261(8)	63(3)[d]
C(31A)	-1130(9)	3509(6)	3934(4)	36(2)[d]
C(32A)	-2278(7)	4406(5)	3951(3)	41(2)[d]
C(33A)	-1686(16)	5508(7)	3716(7)	46(2)[d]

---

a = 53.9%, *b* = 46.1% *c* = 58.8%, *d* = 41.2%

Table 3. Bond lengths [Å] and angles [°] for jul310.

Ge-O	1.8294(12)
Ge-N(2)	2.0234(14)
Ge-N(1)	2.0244(14)
O-C(31)	1.429(4)
N(1)-C(1)	1.326(2)
N(1)-C(6)	1.439(2)
N(2)-C(3)	1.328(2)
N(2)-C(18)	1.441(2)
C(1)-C(2)	1.399(2)
C(1)-C(4)	1.507(2)
C(2)-C(3)	1.397(2)
C(3)-C(5)	1.510(2)
C(6)-C(7)	1.404(3)
C(6)-C(11)	1.406(2)
C(7)-C(8)	1.389(3)
C(7)-C(12)	1.526(3)
C(8)-C(9)	1.384(3)
C(9)-C(10)	1.373(3)
C(10)-C(11)	1.395(3)
C(11)-C(15)	1.521(3)
C(12)-C(14)	1.509(3)
C(12)-C(13)	1.547(3)
C(15)-C(16)	1.531(3)
C(15)-C(17)	1.534(3)
C(18)-C(19)	1.402(2)
C(18)-C(23)	1.404(2)
C(19)-C(20)	1.396(3)
C(19)-C(24)	1.560(10)
C(20)-C(21)	1.381(3)
C(21)-C(22)	1.374(3)
C(22)-C(23)	1.396(3)
C(23)-C(27)	1.524(3)
C(27)-C(29)	1.531(3)
C(27)-C(28)	1.532(3)
C(24)-C(26)	1.529(10)
C(24)-C(25)	1.533(10)

C(30)-C(31)	1.525(7)
C(31)-C(32)	1.503(5)
C(32)-C(33)	1.516(8)

O-Ge-N(2)	96.31(6)
O-Ge-N(1)	96.70(6)
N(2)-Ge-N(1)	87.48(5)
C(31)-O-Ge	116.4(2)
C(1)-N(1)-C(6)	120.75(14)
C(1)-N(1)-Ge	122.77(11)
C(6)-N(1)-Ge	115.63(10)
C(3)-N(2)-C(18)	120.63(14)
C(3)-N(2)-Ge	122.70(11)
C(18)-N(2)-Ge	115.34(10)
N(1)-C(1)-C(2)	122.79(15)
N(1)-C(1)-C(4)	119.61(15)
C(2)-C(1)-C(4)	117.58(15)
C(3)-C(2)-C(1)	126.36(15)
N(2)-C(3)-C(2)	122.74(15)
N(2)-C(3)-C(5)	119.88(15)
C(2)-C(3)-C(5)	117.38(15)
C(7)-C(6)-C(11)	121.60(16)
C(7)-C(6)-N(1)	119.04(15)
C(11)-C(6)-N(1)	119.28(16)
C(8)-C(7)-C(6)	117.90(18)
C(8)-C(7)-C(12)	119.82(18)
C(6)-C(7)-C(12)	122.28(17)
C(9)-C(8)-C(7)	121.44(19)
C(10)-C(9)-C(8)	119.82(19)
C(9)-C(10)-C(11)	121.52(19)
C(10)-C(11)-C(6)	117.71(18)
C(10)-C(11)-C(15)	119.29(17)
C(6)-C(11)-C(15)	123.00(16)
C(14)-C(12)-C(7)	111.6(2)
C(14)-C(12)-C(13)	110.1(2)
C(7)-C(12)-C(13)	110.90(19)
C(11)-C(15)-C(16)	111.30(17)
C(11)-C(15)-C(17)	111.47(17)

C(16)-C(15)-C(17)	110.31(17)
C(19)-C(18)-C(23)	121.67(16)
C(19)-C(18)-N(2)	118.71(15)
C(23)-C(18)-N(2)	119.54(15)
C(20)-C(19)-C(18)	117.84(17)
C(20)-C(19)-C(24)	120.5(5)
C(18)-C(19)-C(24)	121.6(5)
C(21)-C(20)-C(19)	121.13(18)
C(22)-C(21)-C(20)	120.21(18)
C(21)-C(22)-C(23)	121.17(18)
C(22)-C(23)-C(18)	117.92(17)
C(22)-C(23)-C(27)	119.30(16)
C(18)-C(23)-C(27)	122.78(15)
C(23)-C(27)-C(29)	111.85(16)
C(23)-C(27)-C(28)	111.47(16)
C(29)-C(27)-C(28)	109.71(16)
C(26)-C(24)-C(25)	111.0(7)
C(26)-C(24)-C(19)	107.9(9)
C(25)-C(24)-C(19)	108.3(7)
O-C(31)-C(32)	108.4(3)
O-C(31)-C(30)	112.1(4)
C(32)-C(31)-C(30)	111.6(5)
C(31)-C(32)-C(33)	113.7(4)

Table 1. Crystal data and structure refinement for compound **15c**.

Identification code	nov507	
Empirical formula	C33 H50 Ge N2 O	
Formula weight	563.34	
Temperature	173(2) K	
Wavelength	0.71073 Å	
Crystal system	Monoclinic	
Space group	$P2_1/n$ (No.14)	
Unit cell dimensions	a = 13.3507(3) Å	α= 90°.
	b = 16.6088(3) Å	β= 107.101(1)°.
	c = 15.0981(3) Å	γ = 90°.
Volume	3199.82(11) $Å^3$	
Z	4	
Density (calculated)	1.17 Mg/m^3	
Absorption coefficient	0.98 mm^{-1}	
F(000)	1208	
Crystal size	0.15 x 0.10 x 0.10 mm^3	
Theta range for data collection	3.42 to 25.86°.	
Index ranges	-16<=h<=16, -20<=k<=20, -18<=l<=18	
Reflections collected	44895	
Independent reflections	6043 [R(int) = 0.061]	
Reflections with I>2sigma(I)	5144	
Completeness to theta = 25.86°	97.4 %	
Tmax. and Tmin.	0.8046 and 0.7359	
Refinement method	Full-matrix least-squares on F^2	
Data / restraints / parameters	6043 / 0 / 347	
Goodness-of-fit on F^2	1.029	
Final R indices [I>2sigma(I)]	R1 = 0.034, wR2 = 0.079	
R indices (all data)	R1 = 0.045, wR2 = 0.084	
Largest diff. peak and hole	0.58 and -0.50 e.$Å^{-3}$	

The structure is isomorphous with the Sn analogue.

Data collection KappaCCD , Program package WinGX , Abs correction MULTISCAN

Refinement using SHELXL-97 , Drawing using ORTEP-3 for Windows

Table 2. Atomic coordinates (x 10^4) and equivalent isotropic displacement parameters ($Å^2$x 10^3) for nov507. U(eq) is defined as one third of the trace of the orthogonalized U^{ij} tensor.

	x	y	z	U(eq)
Ge	8940(1)	1761(1)	5625(1)	22(1)
O	7859(1)	1568(1)	4578(1)	30(1)
N(1)	7996(1)	2026(1)	6415(1)	22(1)
N(2)	9034(1)	2959(1)	5412(1)	23(1)
C(1)	8190(2)	2649(1)	6989(1)	24(1)
C(2)	8831(2)	3289(1)	6893(2)	25(1)
C(3)	9133(2)	3477(1)	6102(2)	24(1)
C(4)	7678(2)	2688(2)	7756(2)	35(1)
C(5)	9558(2)	4314(1)	6054(2)	35(1)
C(6)	7227(2)	1424(1)	6445(1)	24(1)
C(7)	6181(2)	1540(1)	5915(2)	29(1)
C(8)	5481(2)	903(2)	5860(2)	35(1)
C(9)	5801(2)	189(2)	6322(2)	40(1)
C(10)	6816(2)	104(1)	6870(2)	38(1)
C(11)	7552(2)	717(1)	6953(2)	29(1)
C(12)	5792(2)	2332(2)	5426(2)	37(1)
C(13)	5005(3)	2743(2)	5848(2)	65(1)
C(14)	5295(2)	2217(2)	4395(2)	58(1)
C(15)	8655(2)	595(1)	7602(2)	35(1)
C(16)	9228(2)	-95(2)	7290(2)	53(1)
C(17)	8633(2)	451(2)	8602(2)	54(1)
C(18)	9289(2)	3198(1)	4583(2)	29(1)
C(19)	10335(2)	3152(1)	4569(2)	35(1)
C(20)	10546(3)	3374(2)	3745(2)	49(1)
C(21)	9765(3)	3621(2)	2985(2)	57(1)
C(22)	8741(3)	3647(2)	3006(2)	51(1)
C(23)	8472(2)	3428(1)	3798(2)	36(1)
C(24)	11231(2)	2879(2)	5387(2)	41(1)
C(25)	11680(2)	2075(2)	5188(2)	61(1)
C(26)	12104(2)	3513(2)	5675(2)	63(1)
C(27)	7337(2)	3433(2)	3808(2)	43(1)
C(28)	7044(3)	4201(2)	4228(2)	68(1)
C(29)	6557(3)	3300(2)	2846(2)	65(1)

C(30)	7879(2)	903(2)	3981(2)	45(1)
C(31)	7926(7)	151(2)	4480(3)	226(5)
C(32)	6897(3)	934(2)	3185(2)	71(1)
C(33)	8767(3)	1038(4)	3567(4)	177(4)

Table 3. Bond lengths [Å] and angles [°] for nov507.

Ge-O	1.8287(15)
Ge-N(1)	2.0222(16)
Ge-N(2)	2.0263(17)
O-C(30)	1.432(3)
N(1)-C(1)	1.325(3)
N(1)-C(6)	1.442(3)
N(2)-C(3)	1.327(3)
N(2)-C(18)	1.446(3)
C(1)-C(2)	1.398(3)
C(1)-C(4)	1.510(3)
C(2)-C(3)	1.404(3)
C(3)-C(5)	1.511(3)
C(6)-C(11)	1.400(3)
C(6)-C(7)	1.404(3)
C(7)-C(8)	1.398(3)
C(7)-C(12)	1.522(3)
C(8)-C(9)	1.378(4)
C(9)-C(10)	1.371(4)
C(10)-C(11)	1.396(3)
C(11)-C(15)	1.524(3)
C(12)-C(14)	1.514(4)
C(12)-C(13)	1.540(4)
C(15)-C(16)	1.528(3)
C(15)-C(17)	1.537(3)
C(18)-C(19)	1.405(3)
C(18)-C(23)	1.406(3)
C(19)-C(20)	1.403(3)
C(19)-C(24)	1.515(4)
C(20)-C(21)	1.367(4)
C(21)-C(22)	1.377(4)
C(22)-C(23)	1.394(3)
C(23)-C(27)	1.520(4)
C(24)-C(25)	1.529(4)
C(24)-C(26)	1.536(4)
C(27)-C(28)	1.526(4)
C(27)-C(29)	1.533(4)

C(30)-C(31)	1.450(5)
C(30)-C(32)	1.496(4)
C(30)-C(33)	1.511(5)

O-Ge-N(1)	94.44(7)
O-Ge-N(2)	95.98(7)
N(1)-Ge-N(2)	87.62(7)
C(30)-O-Ge	121.57(15)
C(1)-N(1)-C(6)	121.70(17)
C(1)-N(1)-Ge	121.28(13)
C(6)-N(1)-Ge	116.09(12)
C(3)-N(2)-C(18)	120.54(17)
C(3)-N(2)-Ge	120.53(14)
C(18)-N(2)-Ge	116.62(13)
N(1)-C(1)-C(2)	122.32(18)
N(1)-C(1)-C(4)	119.24(18)
C(2)-C(1)-C(4)	118.41(19)
C(1)-C(2)-C(3)	126.45(19)
N(2)-C(3)-C(2)	122.48(19)
N(2)-C(3)-C(5)	120.67(19)
C(2)-C(3)-C(5)	116.83(19)
C(11)-C(6)-C(7)	121.56(19)
C(11)-C(6)-N(1)	119.30(19)
C(7)-C(6)-N(1)	119.01(19)
C(8)-C(7)-C(6)	117.7(2)
C(8)-C(7)-C(12)	119.9(2)
C(6)-C(7)-C(12)	122.3(2)
C(9)-C(8)-C(7)	121.2(2)
C(10)-C(9)-C(8)	119.9(2)
C(9)-C(10)-C(11)	121.6(2)
C(10)-C(11)-C(6)	117.8(2)
C(10)-C(11)-C(15)	118.8(2)
C(6)-C(11)-C(15)	123.32(19)
C(14)-C(12)-C(7)	111.9(2)
C(14)-C(12)-C(13)	109.6(2)
C(7)-C(12)-C(13)	111.0(2)
C(11)-C(15)-C(16)	112.2(2)
C(11)-C(15)-C(17)	111.05(19)

C(16)-C(15)-C(17)	110.0(2)
C(19)-C(18)-C(23)	122.0(2)
C(19)-C(18)-N(2)	119.1(2)
C(23)-C(18)-N(2)	118.8(2)
C(20)-C(19)-C(18)	117.3(2)
C(20)-C(19)-C(24)	119.0(2)
C(18)-C(19)-C(24)	123.7(2)
C(21)-C(20)-C(19)	121.4(3)
C(20)-C(21)-C(22)	120.5(2)
C(21)-C(22)-C(23)	121.3(3)
C(22)-C(23)-C(18)	117.5(3)
C(22)-C(23)-C(27)	121.0(2)
C(18)-C(23)-C(27)	121.5(2)
C(19)-C(24)-C(25)	111.3(2)
C(19)-C(24)-C(26)	112.1(2)
C(25)-C(24)-C(26)	110.3(2)
C(23)-C(27)-C(28)	112.7(2)
C(23)-C(27)-C(29)	113.0(2)
C(28)-C(27)-C(29)	109.1(2)
O-C(30)-C(31)	110.1(3)
O-C(30)-C(32)	107.8(2)
C(31)-C(30)-C(32)	110.0(4)
O-C(30)-C(33)	107.9(3)
C(31)-C(30)-C(33)	115.0(5)
C(32)-C(30)-C(33)	105.7(3)

```
 Least-squares planes (x,y,z in crystal coordinates) and deviations
from them
 (* indicates atom used to define plane)

  7.8406 (0.0092) x + 0.9970 (0.0140) y + 9.0404 (0.0103) z = 12.2708
(0.0031)

 *    0.0000 (0.0000)  Ge
 *    0.0000 (0.0000)  N1
 *    0.0000 (0.0000)  N2

 Rms deviation of fitted atoms =   0.0000


  10.0330 (0.0062) x - 6.9936 (0.0185) y + 3.9926 (0.0165) z = 9.1610
(0.0131)

 Angle to previous plane (with approximate esd) = 34.31 ( 0.11 )

 *   -0.0065 (0.0010)  C1
 *    0.0065 (0.0010)  C3
 *    0.0058 (0.0009)  N1
 *   -0.0058 (0.0009)  N2
      0.8234 (0.0027)  Ge
      0.1510 (0.0031)  C2

 Rms deviation of fitted atoms =   0.0062


  9.9007 (0.0121) x - 9.6981 (0.0425) y + 1.4740 (0.0469) z = 6.5694
(0.0489)

 Angle to previous plane (with approximate esd) = 13.85 ( 0.28 )

 *    0.0000 (0.0000)  C1
 *    0.0000 (0.0000)  C2
 *    0.0000 (0.0000)  C3

 Rms deviation of fitted atoms =   0.0000
```

Table 1. Crystal data and structure refinement for compound **17**.

Identification code	aug908	
Empirical formula	C34 H53 Ge I N2 O	
Formula weight	705.27	
Temperature	173(2) K	
Wavelength	0.71073 Å	
Crystal system	Orthorhombic	
Space group	Pnma (No.62)	
Unit cell dimensions	a = 21.2060(4) Å	α= 90°.
	b = 18.5239(7) Å	β= 90°.
	c = 8.9409(3) Å	γ = 90°.
Volume	3512.15(19) $Å^3$	
Z	4	
Density (calculated)	1.33 Mg/m^3	
Absorption coefficient	1.78 mm^{-1}	
F(000)	1456	
Crystal size	0.40 x 0.30 x 0.25 mm^3	
Theta range for data collection	3.67 to 26.04°.	
Index ranges	-26<=h<=23, -22<=k<=17, -11<=l<=9	
Reflections collected	15322	
Independent reflections	3538 [R(int) = 0.065]	
Reflections with I>2sigma(I)	2763	
Completeness to theta = 26.04°	98.8 %	
Tmax. and Tmin.	0.6589 and 0.4773	
Refinement method	Full-matrix least-squares on F^2	
Data / restraints / parameters	3538 / 6 / 208	
Goodness-of-fit on F^2	1.019	
Final R indices [I>2sigma(I)]	R1 = 0.040, wR2 = 0.086	
R indices (all data)	R1 = 0.058, wR2 = 0.095	
Largest diff. peak and hole	0.53 and -0.91 e.$Å^{-3}$	

The tBu group was included as disordered across the mirror plane and with restraints on the C-C(Me) and C(Me)…C(Me) distances.

Data collection KappaCCD , Program package WinGX , Abs correction MULTISCAN

Refinement using SHELXL-97 , Drawing using ORTEP-3 for Windows

Table 2. Atomic coordinates (x 10^4) and equivalent isotropic displacement parameters ($Å^2$x 10^3) for aug908. U(eq) is defined as one third of the trace of the orthogonalized U^{ij} tensor.

	x	y	z	U(eq)
I	6362(1)	2500	7175(1)	40(1)
Ge	3576(1)	2500	1258(1)	25(1)
O	3398(1)	2500	3137(3)	40(1)
N	4141(1)	3269(1)	968(2)	24(1)
C(1)	4633(1)	3173(2)	36(3)	26(1)
C(2)	4813(2)	2500	-500(4)	31(1)
C(3)	5020(1)	3811(2)	-429(3)	36(1)
C(4)	4033(1)	3965(2)	1670(3)	27(1)
C(5)	3688(1)	4499(2)	918(3)	33(1)
C(6)	3621(1)	5166(2)	1621(4)	39(1)
C(7)	3882(1)	5301(2)	3000(4)	43(1)
C(8)	4212(1)	4766(2)	3717(3)	42(1)
C(9)	4301(1)	4091(2)	3090(3)	32(1)
C(10)	3383(1)	4377(2)	-597(3)	44(1)
C(11)	2660(2)	4429(2)	-471(4)	70(1)
C(12)	3617(2)	4922(2)	-1775(4)	62(1)
C(13)	4679(2)	3519(2)	3904(3)	44(1)
C(14)	5382(2)	3558(2)	3509(4)	58(1)
C(15)	4614(2)	3563(2)	5607(4)	65(1)
C(16)	2795(2)	2500	3944(5)	45(1)
C(20)	2940(2)	2500	-246(5)	47(1)
C(17)	2965(3)	2740(7)	5485(7)	160(7)
C(18)	2374(4)	3045(5)	3239(12)	147(5)
C(19)	2501(6)	1789(5)	3927(12)	128(5)

Table 3. Bond lengths [Å] and angles [°] for aug908.

Ge-O	1.723(3)
Ge-N	1.877(2)
Ge-C(20)	1.905(4)
O-C(16)	1.469(4)
N-C(1)	1.347(3)
N-C(4)	1.452(3)
C(1)-C(2)	1.389(3)
C(1)-C(3)	1.498(4)
C(4)-C(5)	1.403(4)
C(4)-C(9)	1.410(4)
C(5)-C(6)	1.394(4)
C(5)-C(10)	1.518(4)
C(6)-C(7)	1.375(4)
C(7)-C(8)	1.372(4)
C(8)-C(9)	1.383(4)
C(9)-C(13)	1.515(4)
C(10)-C(11)	1.540(4)
C(10)-C(12)	1.542(5)
C(13)-C(15)	1.531(4)
C(13)-C(14)	1.534(5)
C(16)-C(19)	1.457(8)
C(16)-C(18)	1.486(8)
C(16)-C(17)	1.492(7)
O-Ge-N	105.94(8)
N-Ge-N’	98.63(12)
O-Ge-C(20)	122.21(16)
N-Ge-C(20)	110.72(10)
C(16)-O-Ge	132.1(2)
C(1)-N-C(4)	120.3(2)
C(1)-N-Ge	118.63(17)
C(4)-N-Ge	120.95(15)
N-C(1)-C(2)	123.0(3)
N-C(1)-C(3)	119.5(2)
C(2)-C(1)-C(3)	117.5(2)
C(1)-C(2)-C(1)’	127.6(3)

C(5)-C(4)-C(9)	121.6(3)
C(5)-C(4)-N	120.1(2)
C(9)-C(4)-N	118.3(2)
C(6)-C(5)-C(4)	117.5(3)
C(6)-C(5)-C(10)	119.4(3)
C(4)-C(5)-C(10)	123.1(3)
C(7)-C(6)-C(5)	121.7(3)
C(8)-C(7)-C(6)	119.5(3)
C(7)-C(8)-C(9)	122.3(3)
C(8)-C(9)-C(4)	117.4(3)
C(8)-C(9)-C(13)	120.7(3)
C(4)-C(9)-C(13)	121.9(3)
C(5)-C(10)-C(11)	110.5(3)
C(5)-C(10)-C(12)	112.0(3)
C(11)-C(10)-C(12)	109.2(3)
C(9)-C(13)-C(15)	113.1(3)
C(9)-C(13)-C(14)	111.8(3)
C(15)-C(13)-C(14)	108.3(3)
C(19)-C(16)-O	111.6(5)
C(19)-C(16)-C(18)	110.7(6)
O-C(16)-C(18)	108.3(4)
C(19)-C(16)-C(17)	112.5(6)
O-C(16)-C(17)	104.0(4)
C(18)-C(16)-C(17)	109.6(6)

Symmetry transformations used to generate equivalent atoms:

‘ x,-y+1/2,z

```
 Least-squares planes (x,y,z in crystal coordinates) and deviations
from them
 (* indicates atom used to define plane)

  4.4911 (0.0336) x - 0.0000 (0.0000) y + 8.7381 (0.0031) z = 2.7053
(0.0117)

 *    0.0000 (0.0000)  Ge
 *    0.0000 (0.0000)  N
 *    0.0000 (0.0000)  N'

 Rms deviation of fitted atoms =   0.0000


  13.2265 (0.0376) x - 0.0000 (0.0000) y + 6.9887 (0.0126) z = 6.1528
(0.0156)

 Angle to previous plane (with approximate esd) = 26.36 ( 0.18 )

 *    0.0000 (0.0000)  N
 *    0.0000 (0.0000)  C1
 *    0.0000 (0.0000)  N'
 *    0.0000 (0.0000)  C1'
     -0.5435 (0.0040)  Ge
     -0.1360 (0.0051)  C2

 Rms deviation of fitted atoms =   0.0000


  16.5736 (0.0924) x - 0.0000 (0.0001) y + 5.5777 (0.0487) z = 7.6985
(0.0440)

 Angle to previous plane (with approximate esd) = 12.82 ( 0.67 )

 *    0.0000 (0.0000)  C1
 *    0.0000 (0.0000)  C2
 *    0.0000 (0.0000)  C1'

 Rms deviation of fitted atoms =   0.0000
```

Table 1. Crystal data and structure refinement for compound **18b**.

Identification code	may209	
Empirical formula	C82 H130 F6 Ge2 N4 O11 S2	
Formula weight	1671.26	
Temperature	173(2) K	
Wavelength	0.71073 Å	
Crystal system	Triclinic	
Space group	$P\bar{1}$ (No.2)	
Unit cell dimensions	a = 12.7878(4) Å	α= 86.982(2)°.
	b = 13.0690(3) Å	β= 83.786(2)°.
	c = 13.4060(5) Å	γ = 83.477(2)°.
Volume	2211.03(12) $Å^3$	
Z	1	
Density (calculated)	1.26 Mg/m^3	
Absorption coefficient	0.796 mm^{-1}	
F(000)	888	
Crystal size	0.34 x 0.25 x 0.18 mm^3	
Theta range for data collection	3.43 to 27.48°.	
Index ranges	-16<=h<=16, -16<=k<=16, -17<=l<=17	
Reflections collected	36161	
Independent reflections	10017 [R(int) = 0.048]	
Reflections with I>2sigma(I)	8565	
Completeness to theta = 27.48°	98.9 %	
Tmax. and Tmin.	0.8228 and 0.7350	
Refinement method	Full-matrix least-squares on F^2	
Data / restraints / parameters	10017 / 42 / 520	
Goodness-of-fit on F^2	1.053	
Final R indices [I>2sigma(I)]	R1 = 0.042, wR2 = 0.106	
R indices (all data)	R1 = 0.054, wR2 = 0.113	
Largest diff. peak and hole	0.53 and -0.36 $e.Å^{-3}$	

The sec-butoxy group was disordered over two positions. It was not possible to distinguish between the carbon and oxygen atom positions on either THF solvate; they were therefore refined with carbon at 80 % occupancy and oxygen at 20 % occupancy for each position. The THF molecule on the inversion centre was also modelled with all atoms left isotropic

Data collection KappaCCD , Program package WinGX , Abs correction MULTISCAN

Refinement using SHELXL-97 , Drawing using ORTEP-3 for Windows

Table 2. Atomic coordinates (x 10^4) and equivalent isotropic displacement parameters ($Å^2$x 10^3) for may209. U(eq) is defined as one third of the trace of the orthogonalized U^{ij} tensor.

	x	y	z	U(eq)
Ge	8914(1)	2900(1)	3208(1)	25(1)
S	10808(1)	2576(1)	6283(1)	42(1)
F(1)	12522(2)	1311(2)	5995(3)	131(1)
F(2)	12791(2)	2820(2)	6343(2)	109(1)
F(3)	12381(2)	2549(2)	4865(2)	113(1)
O(1)	8070(1)	3567(1)	2402(1)	35(1)
O(2)	10739(3)	2234(2)	7306(2)	92(1)
O(3)	10623(2)	3668(1)	6104(2)	60(1)
O(4)	10306(2)	1978(1)	5644(2)	52(1)
N(1)	9641(1)	1776(1)	2513(1)	27(1)
N(2)	8074(1)	2169(1)	4155(1)	27(1)
C(1)	9730(2)	827(2)	2957(2)	29(1)
C(2)	9231(2)	595(2)	3905(2)	31(1)
C(3)	8413(2)	1189(2)	4439(2)	29(1)
C(4)	10371(2)	-44(2)	2415(2)	42(1)
C(5)	7853(2)	712(2)	5358(2)	42(1)
C(6)	10164(2)	1956(2)	1503(2)	31(1)
C(7)	11230(2)	2139(2)	1398(2)	37(1)
C(8)	11714(2)	2276(2)	420(2)	48(1)
C(9)	11166(2)	2239(2)	-399(2)	49(1)
C(10)	10116(2)	2071(2)	-277(2)	43(1)
C(11)	9583(2)	1925(2)	676(2)	35(1)
C(12)	11888(2)	2181(2)	2273(2)	49(1)
C(13)	12768(3)	1282(3)	2278(3)	74(1)
C(14)	12383(3)	3197(3)	2243(3)	69(1)
C(15)	8430(2)	1724(2)	776(2)	41(1)
C(16)	8318(3)	599(3)	608(3)	73(1)
C(17)	7776(3)	2432(3)	82(3)	80(1)
C(18)	7026(2)	2641(2)	4537(2)	32(1)
C(19)	6153(2)	2385(2)	4098(2)	40(1)
C(20)	5157(2)	2871(2)	4434(2)	49(1)
C(21)	5039(2)	3570(2)	5177(2)	54(1)
C(22)	5911(2)	3800(2)	5608(2)	48(1)

C(23)	6925(2)	3339(2)	5307(2)	37(1)
C(24)	6225(2)	1607(2)	3279(2)	53(1)
C(25)	5824(2)	2112(3)	2318(3)	65(1)
C(26)	5612(3)	686(3)	3641(3)	75(1)
C(27)	7848(2)	3609(2)	5818(2)	43(1)
C(28)	7940(3)	4767(2)	5699(3)	67(1)
C(29)	7766(3)	3247(3)	6932(2)	70(1)
C(30)	9850(2)	3725(2)	3736(2)	36(1)
C(35)	12195(3)	2296(3)	5842(3)	71(1)
C(31)	6593(6)	4882(8)	2684(9)	59(2) [a]
C(32)	7769(4)	4683(3)	2467(3)	38(1) [a]
C(33)	8207(5)	5193(3)	1510(4)	65(2) [a]
C(34)	9403(6)	5085(6)	1351(6)	75(2) [a]
C(31A)	9093(9)	4711(10)	1151(10)	69(3) [b]
C(32A)	8250(6)	4657(5)	2045(6)	41(2) [b]
C(33A)	7189(6)	5120(6)	1750(7)	60(3) [b]
C(34A)	6330(12)	5141(15)	2613(14)	68(5) [b]
C(1S)	14026(4)	1764(5)	8352(5)	147(2)
C(2S)	14987(5)	1863(5)	7651(5)	143(2)
C(3S)	15829(5)	1343(6)	8139(7)	202(4)
C(4S)	15352(7)	1032(7)	9125(7)	228(5)
C(5S)	14336(5)	1234(7)	9215(5)	181(3)
C(6S)	14564(10)	4156(8)	10130(8)	112(4)
C(8S)	15754(11)	5083(9)	9132(11)	146(5)
C(7S)	15358(8)	4120(7)	9263(7)	111(3)
C(9S)	15012(13)	5754(10)	9744(12)	157(6)
C(10S)	14346(13)	5194(10)	10449(12)	159(6)
O(1S)	14026(4)	1764(5)	8352(5)	147(2)
O(2S)	14987(5)	1863(5)	7651(5)	143(2)
O(3S)	15829(5)	1343(6)	8139(7)	202(4)
O(4S)	15352(7)	1032(7)	9125(7)	228(5)
O(5S)	14336(5)	1234(7)	9215(5)	181(3)
O(6S)	14564(10)	4156(8)	10130(8)	112(4)
O(8S)	15754(11)	5083(9)	9132(11)	146(5)
O(7S)	15358(8)	4120(7)	9263(7)	111(3)
O(9S)	15012(13)	5754(10)	9744(12)	157(6)
O(10S)	14346(13)	5194(10)	10449(12)	159(6)

a 63.5 %, 36.5 %

Table 3. Bond lengths [Å] and angles [°] for may209.

Ge-O(1)	1.7418(15)
Ge-N(2)	1.8684(16)
Ge-N(1)	1.8809(16)
Ge-C(30)	1.910(2)
S-O(2)	1.416(2)
S-O(3)	1.4320(19)
S-O(4)	1.4353(18)
S-C(35)	1.811(4)
F(1)-C(35)	1.320(4)
F(2)-C(35)	1.334(4)
F(3)-C(35)	1.336(5)
O(1)-C(32)	1.470(4)
N(1)-C(1)	1.345(3)
N(1)-C(6)	1.464(3)
N(2)-C(3)	1.354(3)
N(2)-C(18)	1.461(3)
C(1)-C(2)	1.393(3)
C(1)-C(4)	1.498(3)
C(2)-C(3)	1.385(3)
C(3)-C(5)	1.499(3)
C(6)-C(7)	1.402(3)
C(6)-C(11)	1.404(3)
C(7)-C(8)	1.399(3)
C(7)-C(12)	1.523(4)
C(8)-C(9)	1.371(4)
C(9)-C(10)	1.376(4)
C(10)-C(11)	1.396(3)
C(11)-C(15)	1.518(3)
C(12)-C(13)	1.531(4)
C(12)-C(14)	1.532(4)
C(15)-C(17)	1.524(4)
C(15)-C(16)	1.525(4)
C(18)-C(19)	1.398(3)
C(18)-C(23)	1.400(3)
C(19)-C(20)	1.396(3)
C(19)-C(24)	1.523(4)

C(20)-C(21)	1.372(4)
C(21)-C(22)	1.378(4)
C(22)-C(23)	1.393(3)
C(23)-C(27)	1.511(3)
C(24)-C(25)	1.528(4)
C(24)-C(26)	1.540(4)
C(27)-C(28)	1.531(4)
C(27)-C(29)	1.539(4)
C(31)-C(32)	1.496(8)
C(32)-C(33)	1.498(6)
C(33)-C(34)	1.512(8)

O(1)-Ge-N(2)	106.87(8)
O(1)-Ge-N(1)	107.11(7)
N(2)-Ge-N(1)	98.39(7)
O(1)-Ge-C(30)	114.56(9)
N(2)-Ge-C(30)	115.93(9)
N(1)-Ge-C(30)	112.48(9)
O(2)-S-O(3)	115.52(16)
O(2)-S-O(4)	114.79(14)
O(3)-S-O(4)	114.63(12)
O(2)-S-C(35)	104.30(19)
O(3)-S-C(35)	102.76(15)
O(4)-S-C(35)	102.40(15)
C(32)-O(1)-Ge	121.29(19)
C(32A)-O(1)-Ge	119.2(3)
C(1)-N(1)-C(6)	120.21(17)
C(1)-N(1)-Ge	120.57(14)
C(6)-N(1)-Ge	119.12(12)
C(3)-N(2)-C(18)	120.50(17)
C(3)-N(2)-Ge	119.94(14)
C(18)-N(2)-Ge	119.46(13)
N(1)-C(1)-C(2)	123.26(18)
N(1)-C(1)-C(4)	119.71(19)
C(2)-C(1)-C(4)	117.02(18)
C(3)-C(2)-C(1)	127.27(19)
N(2)-C(3)-C(2)	123.16(18)
N(2)-C(3)-C(5)	118.32(19)

C(2)-C(3)-C(5)	118.49(19)
C(7)-C(6)-C(11)	122.5(2)
C(7)-C(6)-N(1)	118.68(19)
C(11)-C(6)-N(1)	118.82(19)
C(8)-C(7)-C(6)	117.1(2)
C(8)-C(7)-C(12)	118.6(2)
C(6)-C(7)-C(12)	124.2(2)
C(9)-C(8)-C(7)	121.4(2)
C(8)-C(9)-C(10)	120.5(2)
C(9)-C(10)-C(11)	121.3(2)
C(10)-C(11)-C(6)	117.2(2)
C(10)-C(11)-C(15)	119.6(2)
C(6)-C(11)-C(15)	123.2(2)
C(7)-C(12)-C(13)	111.5(2)
C(7)-C(12)-C(14)	111.3(2)
C(13)-C(12)-C(14)	109.0(3)
C(11)-C(15)-C(17)	112.7(2)
C(11)-C(15)-C(16)	111.4(2)
C(17)-C(15)-C(16)	110.4(3)
C(19)-C(18)-C(23)	122.2(2)
C(19)-C(18)-N(2)	117.95(19)
C(23)-C(18)-N(2)	119.89(19)
C(20)-C(19)-C(18)	117.8(2)
C(20)-C(19)-C(24)	118.4(2)
C(18)-C(19)-C(24)	123.8(2)
C(21)-C(20)-C(19)	121.1(2)
C(20)-C(21)-C(22)	120.0(2)
C(21)-C(22)-C(23)	121.6(2)
C(22)-C(23)-C(18)	117.2(2)
C(22)-C(23)-C(27)	119.3(2)
C(18)-C(23)-C(27)	123.5(2)
C(19)-C(24)-C(25)	111.2(2)
C(19)-C(24)-C(26)	110.9(3)
C(25)-C(24)-C(26)	110.5(2)
C(23)-C(27)-C(28)	110.5(2)
C(23)-C(27)-C(29)	111.7(2)
C(28)-C(27)-C(29)	111.1(2)
F(1)-C(35)-F(2)	106.3(3)

F(1)-C(35)-F(3)	109.0(4)
F(2)-C(35)-F(3)	108.0(3)
F(1)-C(35)-S	111.2(3)
F(2)-C(35)-S	110.8(3)
F(3)-C(35)-S	111.4(2)
O(1)-C(32)-C(31)	109.1(5)
O(1)-C(32)-C(33)	107.7(3)
C(31)-C(32)-C(33)	114.2(5)
C(32)-C(33)-C(34)	113.9(5)

Symmetry transformations used to generate equivalent atoms:

Table 1. Crystal data and structure refinement for compound **20**.

Identification code	jun910	
Empirical formula	C33 H50 I2 N2 O Sn	
Formula weight	863.24	
Temperature	173(2) K	
Wavelength	0.71073 Å	
Crystal system	Orthorhombic	
Space group	*P* 2_1 2_1 2_1 (No.19)	
Unit cell dimensions	a = 11.7659(2) Å	α= 90°.
	b = 16.2783(3) Å	β= 90°.
	c = 17.9140(2) Å	γ = 90°.
Volume	3431.05(9) $Å^3$	
Z	4	
Density (calculated)	1.67 Mg/m^3	
Absorption coefficient	2.57 mm^{-1}	
F(000)	1704	
Crystal size	0.20 x 0.10 x 0.05 mm^3	
Theta range for data collection	3.46 to 27.11°.	
Index ranges	-15<=h<=15, -20<=k<=20, -22<=l<=22	
Reflections collected	54654	
Independent reflections	7552 [R(int) = 0.064]	
Reflections with I>2sigma(I)	6898	
Completeness to theta = 27.11°	99.7 %	
Tmax. and Tmin.	0.7821 and 0.6951	
Refinement method	Full-matrix least-squares on F^2	
Data / restraints / parameters	7552 / 0 / 354	
Goodness-of-fit on F^2	1.069	
Final R indices [I>2sigma(I)]	R1 = 0.034, wR2 = 0.078	
R indices (all data)	R1 = 0.042, wR2 = 0.081	
Absolute structure parameter	0.01(3)	
Largest diff. peak and hole	0.55 and -1.51 e.$Å^{-3}$	

Data collection KappaCCD , Program package WinGX , Abs correction MULTISCAN

Refinement using SHELXL-97 , Drawing using ORTEP-3 for Windows

Table 2. Atomic coordinates (x 10^4) and equivalent isotropic displacement parameters ($Å^2$x 10^3) for jun910. U(eq) is defined as one third of the trace of the orthogonalized U^{ij} tensor.

	x	y	z	U(eq)
I(1)	1187(1)	1578(1)	7053(1)	30(1)
I(2)	2789(1)	2237(1)	8960(1)	46(1)
Sn	1855(1)	815(1)	8324(1)	17(1)
O	770(3)	627(2)	9144(2)	29(1)
N(1)	3547(3)	369(3)	8077(2)	18(1)
N(2)	1257(3)	-417(2)	8019(2)	17(1)
C(1)	3723(4)	-232(3)	7582(3)	19(1)
C(2)	2894(4)	-729(3)	7259(3)	23(1)
C(3)	1773(4)	-861(3)	7496(3)	20(1)
C(4)	4933(5)	-438(4)	7354(4)	34(1)
C(5)	1198(5)	-1612(3)	7170(3)	26(1)
C(6)	4525(4)	803(3)	8370(3)	23(1)
C(7)	4867(5)	647(3)	9103(3)	28(1)
C(8)	5803(5)	1089(4)	9375(3)	36(2)
C(9)	6354(5)	1659(4)	8945(4)	40(2)
C(10)	5994(5)	1820(4)	8224(4)	34(1)
C(11)	5068(4)	1398(3)	7909(3)	27(1)
C(12)	4284(5)	18(4)	9596(3)	35(1)
C(13)	4946(9)	-774(5)	9632(6)	77(3)
C(14)	4082(6)	363(5)	10380(4)	51(2)
C(15)	4715(5)	1604(4)	7128(3)	33(1)
C(16)	5728(6)	1499(6)	6571(4)	62(2)
C(17)	4303(7)	2468(4)	7050(5)	61(2)
C(18)	236(4)	-783(3)	8353(3)	20(1)
C(19)	397(4)	-1286(3)	8980(3)	23(1)
C(20)	-555(5)	-1634(4)	9307(3)	27(1)
C(21)	-1645(5)	-1477(4)	9033(3)	32(1)
C(22)	-1770(5)	-993(4)	8410(3)	32(1)
C(23)	-843(4)	-642(3)	8052(3)	23(1)
C(24)	1560(5)	-1495(4)	9290(3)	33(1)
C(25)	1701(7)	-1218(5)	10086(4)	53(2)
C(26)	1783(8)	-2415(5)	9245(5)	69(2)
C(27)	-1047(5)	-128(4)	7356(3)	27(1)

C(28)	-1730(5)	-591(5)	6762(3)	43(2)
C(29)	-1661(6)	656(4)	7545(4)	43(2)
C(30)	128(5)	1091(4)	9641(3)	24(1)
C(31)	-909(6)	595(4)	9837(4)	43(2)
C(32)	813(6)	1266(4)	10363(3)	42(2)
C(33)	-272(5)	1918(4)	9324(4)	35(1)

Table 3. Bond lengths [Å] and angles [°] for jun910.

I(1)-Sn	2.7104(5)
I(2)-Sn	2.8047(5)
Sn-O	1.971(4)
Sn-N(1)	2.165(4)
Sn-N(2)	2.194(4)
O-C(30)	1.390(7)
N(1)-C(1)	1.337(6)
N(1)-C(6)	1.447(6)
N(2)-C(3)	1.329(6)
N(2)-C(18)	1.469(6)
C(1)-C(2)	1.393(7)
C(1)-C(4)	1.519(7)
C(2)-C(3)	1.401(7)
C(3)-C(5)	1.515(7)
C(6)-C(7)	1.397(8)
C(6)-C(11)	1.425(8)
C(7)-C(8)	1.403(8)
C(7)-C(12)	1.516(9)
C(8)-C(9)	1.370(10)
C(9)-C(10)	1.383(9)
C(10)-C(11)	1.406(8)
C(11)-C(15)	1.498(8)
C(12)-C(13)	1.508(10)
C(12)-C(14)	1.531(9)
C(15)-C(17)	1.493(10)
C(15)-C(16)	1.563(9)
C(18)-C(23)	1.398(7)
C(18)-C(19)	1.402(7)
C(19)-C(20)	1.385(7)
C(19)-C(24)	1.516(8)
C(20)-C(21)	1.398(8)
C(21)-C(22)	1.375(9)
C(22)-C(23)	1.387(8)
C(23)-C(27)	1.521(7)
C(24)-C(25)	1.504(9)
C(24)-C(26)	1.523(10)

C(27)-C(29)	1.506(8)
C(27)-C(28)	1.531(8)
C(30)-C(31)	1.504(9)
C(30)-C(33)	1.534(8)
C(30)-C(32)	1.550(8)

O-Sn-N(1)	134.13(16)
O-Sn-N(2)	80.59(15)
N(1)-Sn-N(2)	86.44(15)
O-Sn-I(1)	120.64(12)
N(1)-Sn-I(1)	104.40(11)
N(2)-Sn-I(1)	96.69(11)
O-Sn-I(2)	94.51(11)
N(1)-Sn-I(2)	89.96(11)
N(2)-Sn-I(2)	168.87(11)
I(1)-Sn-I(2)	94.401(17)
C(30)-O-Sn	138.2(3)
C(1)-N(1)-C(6)	118.3(4)
C(1)-N(1)-Sn	121.5(3)
C(6)-N(1)-Sn	119.6(3)
C(3)-N(2)-C(18)	116.1(4)
C(3)-N(2)-Sn	121.7(3)
C(18)-N(2)-Sn	122.1(3)
N(1)-C(1)-C(2)	126.3(5)
N(1)-C(1)-C(4)	119.0(5)
C(2)-C(1)-C(4)	114.6(5)
C(1)-C(2)-C(3)	128.5(5)
N(2)-C(3)-C(2)	124.0(5)
N(2)-C(3)-C(5)	120.5(5)
C(2)-C(3)-C(5)	115.3(5)
C(7)-C(6)-C(11)	122.6(5)
C(7)-C(6)-N(1)	118.7(5)
C(11)-C(6)-N(1)	118.6(5)
C(6)-C(7)-C(8)	117.4(6)
C(6)-C(7)-C(12)	122.7(5)
C(8)-C(7)-C(12)	119.9(5)
C(9)-C(8)-C(7)	121.5(6)
C(8)-C(9)-C(10)	120.6(6)

C(9)-C(10)-C(11)	121.3(6)
C(10)-C(11)-C(6)	116.6(5)
C(10)-C(11)-C(15)	118.7(5)
C(6)-C(11)-C(15)	124.7(5)
C(13)-C(12)-C(7)	111.6(6)
C(13)-C(12)-C(14)	110.8(6)
C(7)-C(12)-C(14)	111.0(6)
C(17)-C(15)-C(11)	112.8(6)
C(17)-C(15)-C(16)	107.0(6)
C(11)-C(15)-C(16)	111.1(5)
C(23)-C(18)-C(19)	121.8(5)
C(23)-C(18)-N(2)	121.3(5)
C(19)-C(18)-N(2)	116.9(4)
C(20)-C(19)-C(18)	118.0(5)
C(20)-C(19)-C(24)	118.8(5)
C(18)-C(19)-C(24)	123.2(5)
C(19)-C(20)-C(21)	121.2(5)
C(22)-C(21)-C(20)	119.3(5)
C(21)-C(22)-C(23)	121.8(5)
C(22)-C(23)-C(18)	118.0(5)
C(22)-C(23)-C(27)	118.7(5)
C(18)-C(23)-C(27)	123.3(5)
C(25)-C(24)-C(19)	112.4(5)
C(25)-C(24)-C(26)	109.1(6)
C(19)-C(24)-C(26)	110.9(6)
C(29)-C(27)-C(23)	111.0(5)
C(29)-C(27)-C(28)	108.8(5)
C(23)-C(27)-C(28)	112.4(5)
O-C(30)-C(31)	107.4(5)
O-C(30)-C(33)	114.0(4)
C(31)-C(30)-C(33)	108.0(5)
O-C(30)-C(32)	110.5(5)
C(31)-C(30)-C(32)	109.0(5)
C(33)-C(30)-C(32)	107.9(5)

Table 1. Crystal data and structure refinement for compound **21**.

Identification code	dec1109b	
Empirical formula	C66 H100 Cu2 Ge2 I2 N4 O2, 3(C7 H8)	
Formula weight	1784.02	
Temperature	173(2) K	
Wavelength	0.71073 Å	
Crystal system	Monoclinic	
Space group	*C* 2/m (No.12)	
Unit cell dimensions	a = 15.7342(5) Å	α= 90°.
	b = 16.4339(7) Å	β= 102.306(2)°.
	c = 16.7541(7) Å	γ = 90°.
Volume	4232.6(3) $Å^3$	
Z	2	
Density (calculated)	1.40 Mg/m^3	
Absorption coefficient	1.98 mm^{-1}	
F(000)	1836	
Crystal size	0.14 x 0.06 x 0.04 mm^3	
Theta range for data collection	3.51 to 27.11°.	
Index ranges	-18<=h<=20, -21<=k<=21, -21<=l<=21	
Reflections collected	22306	
Independent reflections	4843 [R(int) = 0.089]	
Completeness to theta = 27.11°	99.7 %	
Absorption correction	Semi-empirical from equivalents	
Max. and min. transmission	0.9089and 0.7904	
Refinement method	Full-matrix least-squares on F^2	
Data / restraints / parameters	4843 / 67 / 239	
Goodness-of-fit on F^2	1.002	
Final R indices [I>2sigma(I)]	R1 = 0.052, wR2 = 0.091	
R indices (all data)	R1 = 0.095, wR2 = 0.103	
Largest diff. peak and hole	1.01 and -0.59 e.$Å^{-3}$	

The ^{t}Bu group disordered abouta mirror plane and was refined with carbon atoms left isotropic. One of the ^{i}Pr groups is disordered over two positions; the toluene solvates are disordered about special positions

Data collection KappaCCD , Program package WinGX , Abs correction MULTISCAN

Refinement using SHELXL-97 , Drawing using ORTEP-3 for Windows

Table 2. Atomic coordinates (x 10^4) and equivalent isotropic displacement parameters ($Å^2$x 10^3) for dec1109b. U(eq) is defined as one third of the trace of the orthogonalized U^{ij} tensor.

	x	y	z	U(eq)
I	507(1)	5000	3988(1)	34(1)
Ge	-2252(1)	5000	3405(1)	22(1)
Cu	-999(1)	5000	4442(1)	32(1)
O	-3393(3)	5000	3360(3)	31(1)
N	-2254(2)	5854(2)	2585(2)	23(1)
C(1)	-1746(3)	5763(3)	2049(3)	27(1)
C(2)	-1455(4)	5000	1855(4)	29(2)
C(3)	-1494(3)	6490(3)	1611(3)	37(1)
C(4)	-2672(3)	6621(2)	2687(3)	24(1)
C(5)	-2255(3)	7181(2)	3277(3)	29(1)
C(6)	-2709(3)	7882(3)	3401(3)	43(1)
C(7)	-3528(4)	8033(3)	2961(4)	49(1)
C(8)	-3920(3)	7490(3)	2367(4)	45(1)
C(9)	-3520(3)	6769(3)	2227(3)	34(1)
C(10)	-1338(3)	7058(3)	3777(3)	34(1)
C(11)	-739(3)	7745(3)	3611(3)	47(1)
C(12)	-1332(4)	7006(3)	4683(3)	46(1)
C(13)	-4051(10)	6136(10)	1669(10)	37(4)[a]
C(14)	-3811(8)	6191(17)	841(10)	61(5)[a]
C(15)	-5035(11)	6199(13)	1584(14)	48(4)[a]
C(13A)	-3875(14)	6252(12)	1466(10)	33(5)[b]
C(14A)	-3886(13)	6683(17)	654(10)	53(5)[b]
C(15A)	-4796(16)	5995(14)	1492(16)	45(5)[b]
C(16)	-3797(4)	5000	4060(4)	32(2)
C(17)	-4774(5)	4863(8)	3694(5)	45(3)
C(18)	-3429(8)	4371(7)	4673(8)	51(3)
C(19)	-3696(7)	5865(6)	4416(7)	33(2)
C(1S)	-2762(4)	4374(4)	-1061(4)	71(4)
C(2S)	-2839(5)	4479(4)	-1897(4)	78(4)
C(3S)	-2812(4)	5256(4)	-2217(3)	76(4)
C(4S)	-2709(5)	5928(4)	-1703(5)	66(3)
C(5S)	-2632(6)	5824(4)	-867(5)	74(4)
C(6S)	-2658(4)	5046(5)	-546(3)	73(3)

C(7S)	-2623(8)	3597(5)	-650(6)	73(4)
C(8S)	-34(11)	4405(5)	-55(9)	66(5)
C(9S)	-411(10)	4951(6)	-662(8)	96(9)
C(10S)	-333(11)	5783(6)	-518(8)	38(5)
C(11S)	123(11)	6070(5)	232(8)	46(5)
C(12S)	500(10)	5525(7)	839(8)	82(10)
C(13S)	421(10)	4692(6)	695(9)	59(9)
C(14S)	-165(15)	3460(5)	-296(13)	67(7)

a 56.7 %, *b* 43.3 %

Table 3. Bond lengths [Å] and angles [°] for dec1109b.

I-Cu'	2.5791(9)
I-Cu	2.6382(9)
Ge-O	1.781(4)
Ge-N	1.964(3)
Ge-Cu	2.3341(10)
O-C(16)	1.447(7)
N-C(1)	1.332(5)
N-C(4)	1.449(5)
C(1)-C(2)	1.397(5)
C(1)-C(3)	1.499(6)
C(4)-C(5)	1.406(6)
C(4)-C(9)	1.413(6)
C(5)-C(6)	1.395(6)
C(5)-C(10)	1.518(6)
C(6)-C(7)	1.365(7)
C(7)-C(8)	1.380(7)
C(8)-C(9)	1.385(6)
C(9)-C(13)	1.522(12)
C(10)-C(12)	1.519(7)
C(10)-C(11)	1.534(6)
C(13)-C(14)	1.517(12)
C(13)-C(15)	1.527(11)
C(16)-C(18)	1.485(12)
C(16)-C(19)	1.537(10)
C(16)-C(17)	1.546(10)
Cu'-I-Cu	78.37(3)
O-Ge-N	96.87(14)
N-Ge-N"	91.3(2)
O-Ge-Cu	135.71(14)
N-Ge-Cu	113.29(10)
Ge-Cu-I'	141.37(4)
Ge-Cu-I	116.99(4)
I'-Cu-I	101.63(3)
C(16)-O-Ge	125.3(4)
C(1)-N-C(4)	122.0(3)

C(1)-N-Ge	118.7(3)
C(4)-N-Ge	118.2(3)
N-C(1)-C(2)	122.1(4)
N-C(1)-C(3)	120.0(4)
C(2)-C(1)-C(3)	117.9(4)
C(1)-C(2)-C(1)"	127.7(5)
C(5)-C(4)-C(9)	121.1(4)
C(5)-C(4)-N	119.7(4)
C(9)-C(4)-N	119.0(4)
C(6)-C(5)-C(4)	117.9(4)
C(6)-C(5)-C(10)	118.9(4)
C(4)-C(5)-C(10)	123.2(4)
C(7)-C(6)-C(5)	121.6(5)
C(6)-C(7)-C(8)	119.9(5)
C(7)-C(8)-C(9)	121.7(5)
C(8)-C(9)-C(4)	117.7(4)
C(8)-C(9)-C(13)	118.6(8)
C(4)-C(9)-C(13)	123.3(7)
C(5)-C(10)-C(12)	111.2(4)
C(5)-C(10)-C(11)	110.5(4)
C(12)-C(10)-C(11)	110.5(4)
C(14)-C(13)-C(9)	108.0(10)
C(14)-C(13)-C(15)	110.8(12)
C(9)-C(13)-C(15)	115.1(12)
O-C(16)-C(18)	112.8(6)
O-C(16)-C(19)	106.7(4)
C(18)-C(16)-C(19)	112.5(9)
O-C(16)-C(17)	104.5(6)
C(18)-C(16)-C(17)	112.4(7)
C(19)-C(16)-C(17)	107.5(7)

Symmetry transformations used to generate equivalent atoms:

' -x,-y+1,-z+1 " x,-y+1,z

Table 1. Crystal data and structure refinement for compound **22**.

Identification code	feb310b	
Empirical formula	C58 H82 Hg1 N4, 0.33(C H2 Cl2)	
Formula weight	1064.03	
Temperature	173(2) K	
Wavelength	0.71073 Å	
Crystal system	Trigonal	
Space group	$R\bar{3}$ (No.148)	
Unit cell dimensions	a = 33.4216(10) Å	α= 90°.
	b = 33.4216(10) Å	β= 90°.
	c = 12.6432(3) Å	γ = 120°.
Volume	12230.4(6) $Å^3$	
Z	9	
Density (calculated)	1.30 Mg/m^3	
Absorption coefficient	2.90 mm^{-1}	
F(000)	4968	
Crystal size	0.19 x 0.16 x 0.16 mm^3	
Theta range for data collection	3.47 to 26.72°.	
Index ranges	-41<=h<=29, -38<=k<=42, -15<=l<=12	
Reflections collected	17578	
Independent reflections	5739 [R(int) = 0.048]	
Reflections with I>2sigma(I)	5079	
Completeness to theta = 26.72°	99.7 %	
Absorption correction	Semi-empirical from equivalents	
Tmax. and Tmin.	0.4145 and 0.3498	
Refinement method	Full-matrix least-squares on F^2	
Data / restraints / parameters	5739 / 0 / 296	
Goodness-of-fit on F^2	1.031	
Final R indices [I>2sigma(I)]	R1 = 0.036, wR2 = 0.071	
R indices (all data)	R1 = 0.046, wR2 = 0.075	
Largest diff. peak and hole	1.77 and -1.27 $e.Å^{-3}$ (near disordered solvate)	

The molecule sits on an inversion centre; the dichloromethane solvate is disordered over across an inversion and sits on a 3-fold rotation axis

Data collection KappaCCD , Program package WinGX , Abs correction MULTISCAN

Refinement using SHELXL-97 , Drawing using ORTEP-3 for Windows

Table 2. Atomic coordinates (x 10^4) and equivalent isotropic displacement parameters ($Å^2$x 10^3) for feb310b. U(eq) is defined as one third of the trace of the orthogonalized U^{ij} tensor.

	x	y	z	U(eq)
Hg	5000	0	0	23(1)
N(1)	5560(1)	1247(1)	783(2)	24(1)
N(2)	4584(1)	568(1)	-695(2)	20(1)
C(1)	5673(1)	994(1)	256(3)	24(1)
C(2)	5351(1)	688(1)	-591(3)	23(1)
C(3)	5006(1)	823(1)	-949(2)	22(1)
C(4)	6100(1)	956(1)	422(3)	33(1)
C(5)	5196(1)	1259(1)	-1601(3)	34(1)
C(6)	5842(1)	1520(1)	1643(3)	26(1)
C(7)	6249(1)	1941(1)	1458(3)	32(1)
C(8)	6508(1)	2189(2)	2332(3)	44(1)
C(9)	6369(2)	2029(2)	3349(3)	47(1)
C(10)	5960(1)	1629(2)	3510(3)	38(1)
C(11)	5683(1)	1367(1)	2671(3)	29(1)
C(12)	6395(1)	2129(1)	344(3)	38(1)
C(13)	6174(2)	2413(2)	33(4)	67(2)
C(14)	6919(2)	2414(2)	193(4)	52(1)
C(15)	5230(1)	925(1)	2848(3)	34(1)
C(16)	4972(2)	940(2)	3843(4)	57(1)
C(17)	5300(2)	510(2)	2883(4)	51(1)
C(18)	4237(1)	680(1)	-988(2)	21(1)
C(19)	4183(1)	1011(1)	-414(3)	25(1)
C(20)	3807(1)	1066(1)	-664(3)	32(1)
C(21)	3497(1)	813(1)	-1453(3)	35(1)
C(22)	3562(1)	497(1)	-2017(3)	34(1)
C(23)	3926(1)	420(1)	-1798(3)	27(1)
C(24)	4516(1)	1300(1)	457(3)	29(1)
C(25)	4727(2)	1816(1)	252(3)	42(1)
C(26)	4277(2)	1175(1)	1534(3)	43(1)
C(27)	4001(1)	81(1)	-2439(3)	31(1)
C(28)	4287(2)	315(2)	-3421(3)	57(1)
C(29)	3557(2)	-357(2)	-2727(4)	57(1)
C(1S)	6530(30)	3620(20)	3320(50)	118(17)

Cl(1)	6620(20)	3400(20)	2207(7)	236(7)

Table 3. Bond lengths [Å] and angles [°] for feb310b.

Hg-C(2)	2.127(3)
N(1)-C(1)	1.275(4)
N(1)-C(6)	1.429(4)
N(2)-C(3)	1.272(4)
N(2)-C(18)	1.430(4)
C(1)-C(2)	1.500(5)
C(1)-C(4)	1.507(5)
C(2)-C(3)	1.503(5)
C(3)-C(5)	1.509(5)
C(6)-C(11)	1.401(5)
C(6)-C(7)	1.405(5)
C(7)-C(8)	1.391(5)
C(7)-C(12)	1.520(5)
C(8)-C(9)	1.381(6)
C(9)-C(10)	1.369(6)
C(10)-C(11)	1.392(5)
C(11)-C(15)	1.512(5)
C(12)-C(13)	1.517(6)
C(12)-C(14)	1.530(6)
C(15)-C(17)	1.518(6)
C(15)-C(16)	1.540(6)
C(18)-C(23)	1.408(5)
C(18)-C(19)	1.410(5)
C(19)-C(20)	1.393(5)
C(19)-C(24)	1.518(5)
C(20)-C(21)	1.381(5)
C(21)-C(22)	1.378(5)
C(22)-C(23)	1.393(5)
C(23)-C(27)	1.513(5)
C(24)-C(25)	1.525(5)
C(24)-C(26)	1.527(5)
C(27)-C(29)	1.519(5)
C(27)-C(28)	1.523(6)
C(2)-Hg-C(2)’	180.00(12)
C(1)-N(1)-C(6)	120.1(3)

C(3)-N(2)-C(18)	122.1(3)
N(1)-C(1)-C(2)	118.3(3)
N(1)-C(1)-C(4)	126.2(3)
C(2)-C(1)-C(4)	115.5(3)
C(1)-C(2)-C(3)	114.1(3)
C(1)-C(2)-Hg	107.8(2)
C(3)-C(2)-Hg	109.8(2)
N(2)-C(3)-C(2)	118.9(3)
N(2)-C(3)-C(5)	125.1(3)
C(2)-C(3)-C(5)	116.0(3)
C(11)-C(6)-C(7)	121.3(3)
C(11)-C(6)-N(1)	117.7(3)
C(7)-C(6)-N(1)	120.9(3)
C(8)-C(7)-C(6)	117.9(4)
C(8)-C(7)-C(12)	120.9(3)
C(6)-C(7)-C(12)	121.2(3)
C(9)-C(8)-C(7)	121.4(4)
C(10)-C(9)-C(8)	119.7(4)
C(9)-C(10)-C(11)	121.8(4)
C(10)-C(11)-C(6)	117.8(3)
C(10)-C(11)-C(15)	121.9(3)
C(6)-C(11)-C(15)	120.3(3)
C(13)-C(12)-C(7)	110.0(3)
C(13)-C(12)-C(14)	110.2(4)
C(7)-C(12)-C(14)	113.8(3)
C(11)-C(15)-C(17)	111.0(3)
C(11)-C(15)-C(16)	113.2(3)
C(17)-C(15)-C(16)	110.5(4)
C(23)-C(18)-C(19)	120.9(3)
C(23)-C(18)-N(2)	118.2(3)
C(19)-C(18)-N(2)	120.6(3)
C(20)-C(19)-C(18)	117.7(3)
C(20)-C(19)-C(24)	120.2(3)
C(18)-C(19)-C(24)	122.1(3)
C(21)-C(20)-C(19)	122.2(4)
C(22)-C(21)-C(20)	119.1(4)
C(21)-C(22)-C(23)	121.6(3)
C(22)-C(23)-C(18)	118.5(3)

C(22)-C(23)-C(27)	121.3(3)
C(18)-C(23)-C(27)	120.2(3)
C(19)-C(24)-C(25)	111.9(3)
C(19)-C(24)-C(26)	110.9(3)
C(25)-C(24)-C(26)	110.0(3)
C(23)-C(27)-C(29)	113.6(3)
C(23)-C(27)-C(28)	110.4(3)
C(29)-C(27)-C(28)	111.0(3)

Symmetry transformations used to generate equivalent atoms:

‘ -x+1,-y,-z

Appendix D – Calculations

L#SnOiPr (Alk)

Center Number	Atomic Number	Atomic Type	Coordinates (Angstroms) X	Y	Z
1	8	0	1.013416	0.001524	0.836332
2	7	0	-1.472426	-1.441654	-0.054731
3	7	0	-1.472246	1.441469	-0.060530
4	6	0	-2.480347	-1.238891	0.782781
5	6	0	-2.970406	0.002540	1.205354
6	1	0	-3.805779	0.003980	1.896387
7	6	0	-2.480201	1.242198	0.777784
8	6	0	3.083466	1.271330	0.540040
9	1	0	2.583648	2.163041	0.935950
10	1	0	3.035026	1.307254	-0.557154
11	1	0	4.141633	1.312614	0.830805
12	6	0	2.406037	0.001743	1.078362
13	6	0	3.083704	-1.268646	0.542230
14	1	0	2.584286	-2.159804	0.939904
15	1	0	4.141947	-1.309047	0.832836
16	1	0	3.035040	-1.306633	-0.554882
17	1	0	2.523453	0.002686	2.174608
18	50	0	-0.020307	-0.001813	-0.876033
19	1	0	-2.990829	2.127827	1.165246
20	1	0	-2.991076	-2.122894	1.173807
21	1	0	-1.295192	-2.426395	-0.234603
22	1	0	-1.294927	2.425454	-0.244414

$L^{\#}SnOiPr+CO_2$ (^{NP}TS)

Center Number	Atomic Number	Atomic Type	Coordinates (Angstroms) X	Y	Z
1	8	0	0.743146	-1.413958	-0.458162
2	7	0	-1.689430	-0.034188	-1.395146
3	7	0	-1.546757	-0.068492	1.460274
4	6	0	-2.903833	-0.501563	-1.153642
5	6	0	-3.438370	-0.790371	0.110822
6	1	0	-4.448955	-1.178802	0.153988
7	6	0	-2.784369	-0.546022	1.316956
8	6	0	2.371873	-1.904504	1.313274
9	1	0	1.603526	-2.475307	1.847533
10	1	0	2.409484	-0.888067	1.727433
11	1	0	3.343368	-2.376137	1.507196
12	6	0	2.073908	-1.878509	-0.188287
13	6	0	3.117939	-1.087590	-0.979622
14	1	0	2.864554	-1.079953	-2.045412
15	1	0	4.110868	-1.540951	-0.866448
16	1	0	3.182408	-0.048738	-0.633330
17	1	0	2.071119	-2.914499	-0.555241
18	50	0	-0.091896	0.274251	-0.040489
19	6	0	1.111485	2.057799	0.433613
20	8	0	0.548346	1.954854	-0.852553
21	8	0	1.768584	3.028808	0.691401
22	1	0	-1.266834	0.093181	2.423683
23	1	0	-3.339728	-0.743321	2.235568
24	1	0	-3.554311	-0.656807	-2.016178
25	1	0	-1.499818	0.162548	-2.374428

$L^{\#}SnOiPr+CO_2$ (TS)

Center Number	Atomic Number	Atomic Type	Coordinates (Angstroms) X	Y	Z
1	8	0	1.225997	0.236780	0.098276
2	7	0	-1.336381	-1.255962	0.899440
3	7	0	-1.784542	1.075805	-0.720554
4	6	0	-2.216175	-0.641593	1.674152
5	6	0	-2.842209	0.585480	1.412375
6	1	0	-3.554236	0.952682	2.142643
7	6	0	-2.626258	1.358721	0.267661
8	6	0	1.104000	2.321506	1.351029
9	1	0	1.142751	1.754568	2.287280
10	1	0	0.052455	2.510693	1.107280
11	1	0	1.601090	3.286540	1.514450
12	6	0	1.798653	1.541151	0.232274
13	6	0	1.795163	2.286944	-1.105926
14	1	0	2.292121	1.694211	-1.882448
15	1	0	2.328590	3.241193	-1.013753
16	1	0	0.772691	2.511492	-1.437075
17	1	0	2.841507	1.366777	0.527926
18	50	0	-0.382916	-0.642563	-0.967542
19	6	0	2.183326	-1.238890	0.729878
20	8	0	1.429929	-2.135858	0.430237
21	8	0	3.197151	-0.849149	1.209305
22	1	0	-0.978091	-2.124566	1.287777
23	1	0	-2.486434	-1.138361	2.609336
24	1	0	-3.211550	2.278189	0.181304
25	1	0	-1.812236	1.761727	-1.471050

$L^{\#}SnOiPr+CO_2$ (INT)

Center Number	Atomic Number	Atomic Type	Coordinates (Angstroms) X	Y	Z
1	8	0	0.003567	-0.001839	-0.006885
2	7	0	-0.004293	-0.002362	4.668131
3	7	0	2.048570	0.007544	2.637578
4	6	0	0.769877	-0.960972	5.159400
5	6	0	1.960299	-1.435548	4.595478
6	1	0	2.483194	-2.226748	5.120330
7	6	0	2.538811	-0.947089	3.419238
8	6	0	1.144268	-1.166133	-1.822765
9	1	0	0.844798	-2.141463	-1.428080
10	1	0	2.133046	-0.907403	-1.422897
11	1	0	1.228263	-1.249222	-2.913333
12	6	0	0.115956	-0.099812	-1.453767
13	6	0	0.483627	1.292342	-1.954281
14	1	0	-0.268782	2.028331	-1.651267
15	1	0	0.545565	1.293155	-3.048772
16	1	0	1.456487	1.609821	-1.558797
17	1	0	-0.866949	-0.394961	-1.832448
18	50	0	0.107793	1.006127	2.723987
19	6	0	-0.858330	-0.887450	0.634553
20	8	0	-0.861578	-0.659105	1.918560
21	8	0	-1.490958	-1.731722	0.029712
22	1	0	-0.816465	0.192043	5.247805
23	1	0	0.460636	-1.416952	6.102940
24	1	0	3.492299	-1.390748	3.122640
25	1	0	2.631144	0.206363	1.829101

$L^{\#}SnO(CO_2)iPr$ (Carb)

Center Number	Atomic Number	Atomic Type	Coordinates (Angstroms) X	Y	Z
1	8	0	2.521531	0.437340	-0.689223
2	7	0	-1.466216	0.677137	1.368721
3	7	0	-2.629673	0.034077	-1.183866
4	6	0	-2.132794	1.804262	1.161406
5	6	0	-2.923565	2.109727	0.047388
6	1	0	-3.406409	3.079982	0.024170
7	6	0	-3.129924	1.254005	-1.041728
8	6	0	4.546712	1.647231	-0.381928
9	1	0	3.984408	2.586478	-0.347917
10	1	0	4.844369	1.461852	-1.420538
11	1	0	5.454084	1.763714	0.222270
12	6	0	3.708483	0.493249	0.154285
13	6	0	4.431047	-0.850433	0.109133
14	1	0	3.787613	-1.649096	0.490653
15	1	0	5.334252	-0.813504	0.730546
16	1	0	4.728426	-1.093293	-0.918058
17	1	0	3.376680	0.700519	1.175980
18	50	0	-1.179482	-1.058694	0.086604
19	1	0	-3.772227	1.629257	-1.842709
20	1	0	-2.057829	2.573306	1.934289
21	1	0	-0.909382	0.677310	2.218925
22	1	0	-2.911080	-0.411921	-2.053270
23	6	0	1.393298	-0.063335	-0.156260
24	8	0	1.309743	-0.454839	1.025620
25	8	0	0.397832	-0.097078	-0.985437

L#SnOsBu

Center Number	Atomic Number	Atomic Type	Coordinates (Angstroms) X	Y	Z
1	8	0	-0.989904	-0.080986	0.425320
2	7	0	1.445165	1.426828	-0.532937
3	7	0	1.838634	-1.177910	0.629550
4	6	0	2.253121	1.771445	0.461079
5	6	0	2.796252	0.912256	1.423249
6	1	0	3.442146	1.346531	2.177936
7	6	0	2.590510	-0.471962	1.463281
8	6	0	-3.216492	0.802953	0.717886
9	1	0	-2.980095	1.055540	1.761197
10	1	0	-4.276927	0.511552	0.690659
11	6	0	-2.362368	-0.411742	0.317549
12	6	0	-2.678785	-1.631004	1.193319
13	1	0	-2.087697	-2.498527	0.874534
14	1	0	-3.741590	-1.901988	1.136691
15	1	0	-2.427061	-1.416748	2.239290
16	1	0	-2.619239	-0.668636	-0.730486
17	50	0	0.428963	-0.488068	-0.918818
18	1	0	3.113502	-1.020145	2.251359
19	1	0	2.536265	2.824914	0.532379
20	1	0	1.185452	2.211252	-1.125144
21	1	0	1.844091	-2.173604	0.834913
22	6	0	-2.996491	2.029378	-0.172495
23	1	0	-3.629241	2.868418	0.142631
24	1	0	-1.951611	2.354981	-0.125688
25	1	0	-3.237981	1.807350	-1.221412

$L^{\#}SnOsBu+CO_2$ (TS)

Center Number	Atomic Number	Atomic Type	Coordinates (Angstroms) X	Y	Z
1	8	0	-0.985069	-0.014533	0.164846
2	7	0	1.600928	1.344665	-0.959111
3	7	0	1.918758	-0.868248	0.854778
4	6	0	2.393758	1.931182	-0.069165
5	6	0	2.890952	1.348967	1.101742
6	1	0	3.524050	1.957704	1.737243
7	6	0	2.651909	0.026074	1.499556
8	6	0	-1.575983	1.289454	0.313075
9	6	0	-1.406704	1.794973	1.748109
10	50	0	0.689017	-0.693735	-0.945168
11	6	0	-1.505520	-1.514156	1.075511
12	8	0	-0.656065	-2.294536	0.698573
13	8	0	-2.472171	-1.294397	1.731454
14	1	0	1.393712	1.940373	-1.757067
15	1	0	2.697189	2.962505	-0.268457
16	1	0	3.120612	-0.295412	2.433004
17	1	0	1.849759	-1.763892	1.331054
18	1	0	-1.003336	1.953774	-0.353379
19	6	0	-3.215257	0.890063	-1.625122
20	1	0	-2.666485	1.566919	-2.295014
21	1	0	-2.851580	-0.127989	-1.803646
22	1	0	-4.271685	0.922749	-1.916690
23	6	0	-3.038628	1.292054	-0.157112
24	1	0	-3.433921	2.306758	-0.004951
25	1	0	-3.620409	0.625092	0.488854
26	1	0	-1.766587	2.828416	1.832855
27	1	0	-1.971185	1.174276	2.450679
28	1	0	-0.349494	1.776640	2.035698

$L^{\#}SnO(CO_2)sBu$

Center Number	Atomic Number	Atomic Type	Coordinates (Angstroms) X	Y	Z
1	8	0	-2.310885	0.215306	0.615972
2	7	0	1.796883	1.051630	-1.032391
3	7	0	2.804015	-0.442651	1.211315
4	6	0	2.452764	2.026967	-0.418910
5	6	0	3.174821	1.920191	0.775482
6	1	0	3.657583	2.814350	1.152997
7	6	0	3.314453	0.741880	1.519348
8	50	0	1.424071	-1.006399	-0.429113
9	1	0	3.909537	0.809418	2.433820
10	1	0	2.427865	3.013051	-0.889474
11	1	0	1.294553	1.351217	-1.863522
12	1	0	3.032932	-1.163037	1.891496
13	6	0	-1.153331	-0.085235	0.002237
14	8	0	-1.005012	-0.051072	-1.235870
15	8	0	-0.205526	-0.421665	0.820370
16	6	0	-4.700599	0.194629	0.534202
17	1	0	-4.715962	0.680739	1.519341
18	1	0	-5.562957	0.585262	-0.023472
19	6	0	-3.364562	2.141385	-0.432251
20	1	0	-4.207721	2.473104	-1.050378
21	1	0	-3.404018	2.677081	0.523671
22	1	0	-2.437964	2.410424	-0.949065
23	6	0	-3.437726	0.633314	-0.207721
24	1	0	-3.357271	0.110270	-1.166068
25	6	0	-4.831448	-1.324021	0.695761
26	1	0	-4.843993	-1.827291	-0.279782
27	1	0	-3.995826	-1.730820	1.274744
28	1	0	-5.761436	-1.581898	1.216237

L#SnOtBu

Center Number	Atomic Number	Atomic Type	Coordinates (Angstroms) X	Y	Z
1	8	0	-0.941404	0.519710	-0.046030
2	7	0	1.654141	-0.002048	-1.439089
3	7	0	1.638870	0.052872	1.443114
4	6	0	2.512622	0.991249	-1.252128
5	6	0	2.920861	1.513930	-0.019150
6	1	0	3.632502	2.331754	-0.031132
7	6	0	2.500132	1.038204	1.228505
8	6	0	-2.886461	-0.007494	1.323055
9	1	0	-2.632055	-1.071010	1.422021
10	1	0	-3.978135	0.082062	1.397461
11	6	0	-2.361084	0.564615	-0.009830
12	6	0	-2.960947	-0.223732	-1.192186
13	1	0	-2.565058	0.160951	-2.139798
14	1	0	-4.055211	-0.139787	-1.217963
15	1	0	-2.710178	-1.290256	-1.122115
16	50	0	0.340324	-1.010569	0.012686
17	1	0	2.937772	1.520428	2.106691
18	1	0	2.958804	1.440557	-2.143324
19	1	0	1.514968	-0.229566	-2.420061
20	1	0	1.491236	-0.139848	2.430333
21	6	0	-2.752686	2.048647	-0.124929
22	1	0	-2.369612	2.466356	-1.062871
23	1	0	-3.842456	2.180407	-0.102052
24	1	0	-2.313638	2.617177	0.702662
25	1	0	-2.439602	0.533279	2.165890

$L^{\#}SnOtBu+CO_2$ (TS)

Center Number	Atomic Number	Atomic Type	Coordinates (Angstroms) X	Y	Z
1	8	0	-1.088367	0.002263	0.123264
2	7	0	1.839443	1.423487	-0.459140
3	7	0	1.730682	-1.170573	0.728666
4	6	0	2.628202	1.661970	0.581305
5	6	0	2.960711	0.745888	1.584989
6	1	0	3.612819	1.081477	2.383197
7	6	0	2.520805	-0.583091	1.615110
8	6	0	-1.371191	2.350329	-0.456110
9	1	0	-1.135378	2.171556	-1.513943
10	1	0	-0.455555	2.634519	0.070700
11	1	0	-2.065401	3.198157	-0.416129
12	6	0	-2.019393	1.115061	0.190079
13	6	0	-2.315648	1.410276	1.669430
14	1	0	-2.777745	0.547013	2.153767
15	1	0	-2.996236	2.266449	1.761285
16	1	0	-1.386369	1.650841	2.198956
17	50	0	0.681769	-0.411431	-1.029942
18	6	0	-1.602789	-1.735838	0.578643
19	8	0	-0.720907	-2.368292	0.039309
20	8	0	-2.588915	-1.717458	1.239063
21	1	0	1.756654	2.223475	-1.081791
22	1	0	3.067312	2.660186	0.663509
23	1	0	2.865896	-1.195038	2.452294
24	1	0	1.508717	-2.136789	0.952832
25	6	0	-3.302921	0.758689	-0.579721
26	1	0	-3.810263	-0.098429	-0.130916
27	1	0	-3.997754	1.607810	-0.575130
28	1	0	-3.067167	0.518117	-1.623665

L#SnOCOOtBu

Center Number	Atomic Number	Atomic Type	Coordinates (Angstroms) X	Y	Z
1	8	0	-2.313680	0.201964	0.843423
2	7	0	1.605762	0.810173	-1.284818
3	7	0	2.854706	-0.033871	1.165876
4	6	0	2.240609	1.934773	-0.984339
5	6	0	3.047837	2.159950	0.136719
6	1	0	3.498161	3.140198	0.243647
7	6	0	3.309149	1.211205	1.133426
8	6	0	-4.542207	0.799103	1.244474
9	1	0	-4.199002	1.745051	1.677147
10	1	0	-4.587831	0.052583	2.044630
11	1	0	-5.552123	0.944179	0.844569
12	6	0	-3.596122	0.340094	0.130303
13	6	0	-4.038932	-1.016326	-0.430673
14	1	0	-3.367126	-1.358344	-1.220722
15	1	0	-5.051089	-0.928534	-0.843748
16	1	0	-4.061705	-1.768762	0.366156
17	50	0	1.409574	-1.052662	-0.174891
18	1	0	3.956990	1.530900	1.953894
19	1	0	2.121517	2.771130	-1.677725
20	1	0	1.029317	0.872834	-2.119402
21	1	0	3.171762	-0.551264	1.981870
22	6	0	-1.188309	-0.190785	0.226064
23	8	0	-1.108712	-0.467490	-0.989041
24	8	0	-0.168152	-0.260020	1.024762
25	6	0	-3.486475	1.412581	-0.959838
26	1	0	-3.119643	2.353633	-0.533516
27	1	0	-2.812495	1.097447	-1.759123
28	1	0	-4.477663	1.598758	-1.390521

$L^{\#}SnOtBu^{F}$

Center Number	Atomic Number	Atomic Type	Coordinates (Angstroms) X	Y	Z
1	8	0	0.039222	0.074502	-0.409744
2	7	0	2.757849	0.007460	-1.484437
3	7	0	2.508245	0.327978	1.368257
4	6	0	3.333761	1.198247	-1.363521
5	6	0	3.508578	1.917722	-0.176938
6	1	0	3.998080	2.882497	-0.242787
7	6	0	3.120991	1.473174	1.091601
8	6	0	-1.437599	0.375962	1.476631
9	6	0	-1.269773	0.146774	-0.075784
10	6	0	-2.039984	-1.168914	-0.489133
11	50	0	1.667779	-1.151600	0.000611
12	1	0	3.355898	2.127640	1.934048
13	1	0	3.721177	1.656494	-2.276155
14	1	0	2.746600	-0.336512	-2.441020
15	1	0	2.325053	0.199957	2.360087
16	6	0	-1.893070	1.373318	-0.846567
17	9	0	-1.078760	1.625528	1.827601
18	9	0	-0.619418	-0.468699	2.157464
19	9	0	-2.689235	0.164720	1.923556
20	9	0	-3.380146	-1.035463	-0.482960
21	9	0	-1.726482	-2.180482	0.356957
22	9	0	-1.670546	-1.561989	-1.721418
23	9	0	-2.019934	1.092433	-2.159650
24	9	0	-3.116730	1.711316	-0.380690
25	9	0	-1.104262	2.453538	-0.739883

$L^{\#}SnOtBu^{F}$ +CO_2 (TS)

Center Number	Atomic Number	Atomic Type	Coordinates (Angstroms) X	Y	Z
1	8	0	0.415994	-0.406474	0.164389
2	7	0	-3.981691	-0.623138	-0.168038
3	7	0	-1.999941	1.362733	0.178788
4	6	0	-4.612250	0.105507	0.716025
5	6	0	-4.138717	1.276765	1.303577
6	1	0	-4.764687	1.779877	2.013701
7	6	0	-2.899923	1.833251	1.008012
8	6	0	1.751899	0.697552	-1.417963
9	6	0	1.664765	0.082523	0.011110
10	6	0	2.759026	-1.026955	0.136179
11	50	0	-1.943644	-0.440855	-0.939204
12	6	0	-0.292111	-1.615280	1.373958
13	8	0	-1.407262	-1.617162	0.939617
14	8	0	0.496587	-1.974941	2.122700
15	1	0	-4.509114	-1.419195	-0.467859
16	1	0	-5.597859	-0.219004	1.015084
17	1	0	-2.651524	2.752135	1.516768
18	1	0	-1.165689	1.912814	0.145401
19	6	0	1.929357	1.193984	1.064613
20	9	0	0.672747	1.421646	-1.676809
21	9	0	1.804644	-0.254702	-2.326005
22	9	0	2.792999	1.485698	-1.586462
23	9	0	1.217185	2.278114	0.775729
24	9	0	3.194587	1.558054	1.119489
25	9	0	3.861506	-0.700012	-0.517027
26	9	0	2.318945	-2.159133	-0.365677
27	9	0	3.099631	-1.238145	1.388742
28	9	0	1.563052	0.804423	2.263033

$L^{\#}SnO(CO_2)tBu^{F}$

Center Number	Atomic Number	Atomic Type	Coordinates (Angstroms) X	Y	Z
1	8	0	0.957533	0.036646	-0.722725
2	7	0	-3.017817	0.684074	1.316096
3	7	0	-4.139077	0.238282	-1.299020
4	6	0	-3.425865	1.919937	1.060519
5	6	0	-4.066371	2.357035	-0.105546
6	1	0	-4.338428	3.404388	-0.166058
7	6	0	-4.389976	1.539405	-1.192202
8	6	0	3.027412	0.995840	-1.131796
9	6	0	2.229118	0.069918	-0.131029
10	6	0	2.866356	-1.366884	-0.114080
11	50	0	-2.993197	-1.061838	0.030677
12	1	0	-4.909220	2.015230	-2.027062
13	1	0	-3.248038	2.669697	1.834540
14	1	0	-2.539566	0.585999	2.207866
15	1	0	-4.473907	-0.162827	-2.171111
16	6	0	-0.211834	-0.384836	-0.079697
17	8	0	-0.235670	-0.714193	1.098731
18	8	0	-1.192696	-0.347881	-0.906844
19	6	0	2.280173	0.720642	1.313863
20	9	0	3.468664	1.336198	1.505393
21	9	0	2.147751	-0.174991	2.298292
22	9	0	1.319932	1.651283	1.436095
23	9	0	2.657417	2.279460	-0.961443
24	9	0	4.356292	0.909209	-0.944690
25	9	0	3.121308	-1.783442	-1.369074
26	9	0	4.026483	-1.375186	0.570602
27	9	0	2.770919	0.664048	-2.403108
28	9	0	2.040109	-2.259912	0.445150

LSnO^{i}Pr

Center Number	Atomic Number	Atomic Type	Coordinates (Angstroms) X	Y	Z
1	8	0	0.000973	1.026454	1.611529
2	7	0	-1.481100	-0.347016	-0.888229
3	7	0	1.480474	-0.347379	-0.888880
4	6	0	-1.264377	-0.448963	-2.210731
5	6	0	-0.000753	-0.577020	-2.807967
6	1	0	-0.001007	-0.692950	-3.882391
7	6	0	1.263166	-0.449289	-2.211286
8	6	0	-2.460063	-0.411818	-3.155452
9	1	0	-2.926762	0.578062	-3.138723
10	1	0	-3.219337	-1.132955	-2.839268
11	1	0	-2.149593	-0.637664	-4.177054
12	6	0	2.458454	-0.412517	-3.156527
13	1	0	3.217740	-1.133722	-2.840520
14	1	0	2.925332	0.577282	-3.140225
15	1	0	2.147504	-0.638528	-4.177948
16	6	0	-2.822819	-0.073927	-0.392454
17	6	0	-3.303868	1.257343	-0.369750
18	6	0	-4.554266	1.507951	0.206574
19	1	0	-4.926469	2.525119	0.241108
20	6	0	-5.324395	0.476701	0.738784
21	1	0	-6.289162	0.692113	1.184038
22	6	0	-4.854394	-0.831439	0.688566
23	1	0	-5.463712	-1.635191	1.086390
24	6	0	-3.607449	-1.132168	0.124298
25	6	0	-2.493430	2.427410	-0.934633
26	1	0	-1.637187	2.018766	-1.476901
27	6	0	-1.940178	3.296411	0.220994
28	1	0	-2.763302	3.683809	0.832750
29	1	0	-1.375923	4.145884	-0.183654

30	1	0	-1.277495	2.686824	0.840804
31	6	0	-3.325966	3.280950	-1.922955
32	1	0	-3.730589	2.667093	-2.735918
33	1	0	-2.692298	4.061770	-2.358946
34	1	0	-4.162417	3.771370	-1.413697
35	6	0	-3.168360	-2.597372	0.041826
36	1	0	-2.166393	-2.628697	-0.393963
37	6	0	-4.119270	-3.397109	-0.885935
38	1	0	-5.136650	-3.404541	-0.480201
39	1	0	-3.774819	-4.433920	-0.976030
40	1	0	-4.151805	-2.952749	-1.886303
41	6	0	-3.103985	-3.254252	1.441982
42	1	0	-2.383455	-2.729578	2.077450
43	1	0	-2.789056	-4.300502	1.352316
44	1	0	-4.084771	-3.230005	1.928619
45	6	0	2.822343	-0.074036	-0.393675
46	6	0	3.303128	1.257344	-0.371160
47	6	0	4.553625	1.508237	0.204816
48	1	0	4.925621	2.525486	0.239210
49	6	0	5.324081	0.477182	0.736935
50	1	0	6.288903	0.692824	1.181957
51	6	0	4.854299	-0.831045	0.686987
52	1	0	5.463846	-1.634636	1.084785
53	6	0	3.607279	-1.132062	0.123032
54	6	0	2.492198	2.427265	-0.935638
55	1	0	1.636353	2.018467	-1.478412
56	6	0	1.938098	3.295287	0.220318
57	1	0	1.274513	2.685324	0.838801
58	1	0	1.374647	4.145435	-0.184034
59	1	0	2.760760	3.681686	0.833333
60	6	0	3.324560	3.281880	-1.923178
61	1	0	4.160734	3.772237	-1.413403
62	1	0	2.690656	4.062788	-2.358668
63	1	0	3.729563	2.668816	-2.736550

64	6	0	3.168385	-2.597340	0.040911
65	1	0	2.166647	-2.628931	-0.395388
66	6	0	4.119843	-3.397342	-0.886053
67	1	0	4.152754	-2.953420	-1.886603
68	1	0	3.775601	-4.434250	-0.975841
69	1	0	5.137041	-3.404425	-0.479858
70	6	0	3.103357	-3.253655	1.441298
71	1	0	4.083922	-3.229239	1.928371
72	1	0	2.788431	-4.299930	1.351921
73	1	0	2.382560	-2.728692	2.076228
74	6	0	-1.267581	1.716658	3.599274
75	1	0	-2.156608	1.227448	3.189489
76	1	0	-1.270167	2.762832	3.277853
77	1	0	-1.310244	1.680508	4.694275
78	6	0	0.002125	1.020731	3.089354
79	6	0	1.274804	1.712630	3.597372
80	1	0	2.161704	1.220509	3.186434
81	1	0	1.318882	1.676490	4.692320
82	1	0	1.280331	2.758739	3.275801
83	1	0	0.000789	-0.018369	3.459553
84	50	0	-0.000011	-0.757828	0.696573

LSnO(CO_2)^{i}Pr

Center Number	Atomic Number	Atomic Type	Coordinates (Angstroms) X	Y	Z
1	7	0	1.457973	-0.831307	0.711775
2	7	0	-1.505056	-0.736784	0.694362
3	6	0	1.225918	-1.156529	1.996285
4	6	0	-0.045701	-1.243372	2.579345
5	1	0	-0.060994	-1.525650	3.622210

6	6	0	-1.300627	-1.131678	1.966082
7	6	0	2.405921	-1.524663	2.887093
8	1	0	2.904073	-2.421409	2.504179
9	1	0	2.072546	-1.711710	3.909065
10	1	0	3.145898	-0.720302	2.890367
11	6	0	-2.498255	-1.557155	2.806637
12	1	0	-3.253970	-0.770283	2.832737
13	1	0	-2.187562	-1.793369	3.825566
14	1	0	-2.968094	-2.442100	2.364407
15	6	0	2.813879	-0.954451	0.181473
16	6	0	3.695762	0.150103	0.215346
17	6	0	4.980580	-0.005062	-0.322061
18	1	0	5.665247	0.834927	-0.300465
19	6	0	5.386084	-1.210001	-0.888290
20	1	0	6.384093	-1.309542	-1.299790
21	6	0	4.501156	-2.284159	-0.935552
22	1	0	4.814335	-3.217537	-1.389385
23	6	0	3.209156	-2.178395	-0.407435
24	6	0	3.279338	1.509174	0.779365
25	1	0	2.239023	1.451652	1.100199
26	6	0	4.158819	1.925081	1.983511
27	1	0	4.096157	1.188206	2.791343
28	1	0	3.821963	2.892587	2.372989
29	1	0	5.209159	2.020039	1.685444
30	6	0	3.340837	2.595688	-0.326465
31	1	0	4.378419	2.855052	-0.566222
32	1	0	2.803781	3.486514	0.010565
33	1	0	2.855714	2.238983	-1.241513
34	6	0	2.262648	-3.377531	-0.500293
35	1	0	1.321361	-3.104226	-0.016576
36	6	0	1.958655	-3.716725	-1.981365
37	1	0	1.519725	-2.851871	-2.489592
38	1	0	1.251918	-4.553049	-2.041031
39	1	0	2.875798	-4.000688	-2.508791

40	6	0	2.842728	-4.612481	0.233161
41	1	0	3.780959	-4.932919	-0.232183
42	1	0	2.133550	-5.447119	0.187413
43	1	0	3.041814	-4.382599	1.285362
44	6	0	-2.855796	-0.792221	0.138456
45	6	0	-3.714449	0.329639	0.227123
46	6	0	-4.996808	0.229706	-0.329343
47	1	0	-5.667897	1.077494	-0.260806
48	6	0	-5.420621	-0.928686	-0.972850
49	1	0	-6.416371	-0.981523	-1.398031
50	6	0	-4.556716	-2.014536	-1.079430
51	1	0	-4.882697	-2.910945	-1.594383
52	6	0	-3.269755	-1.968254	-0.531472
53	6	0	-3.305274	1.640197	0.909629
54	1	0	-2.244984	1.578675	1.168791
55	6	0	-4.133934	1.875418	2.200272
56	1	0	-5.197877	1.971776	1.956226
57	1	0	-3.806770	2.799972	2.689506
58	1	0	-4.018797	1.052021	2.911061
59	6	0	-3.492488	2.851090	-0.042643
60	1	0	-2.853395	2.760538	-0.923128
61	1	0	-3.213901	3.771217	0.487022
62	1	0	-4.537980	2.945919	-0.354757
63	6	0	-2.353043	-3.184623	-0.687677
64	1	0	-1.404338	-2.961514	-0.192447
65	6	0	-2.965007	-4.440281	-0.017216
66	1	0	-3.161018	-4.259400	1.044927
67	1	0	-2.276591	-5.288838	-0.104670
68	1	0	-3.909636	-4.712658	-0.499806
69	6	0	-2.058548	-3.459391	-2.184052
70	1	0	-2.981734	-3.700885	-2.721849
71	1	0	-1.368480	-4.305531	-2.283623
72	1	0	-1.603394	-2.580984	-2.653144
73	8	0	0.159591	1.774478	0.164824

74	8	0	-0.724926	2.808717	-1.678723
75	8	0	0.352591	4.001471	-0.021657
76	6	0	-0.118353	2.836587	-0.589328
77	6	0	-0.002150	5.257456	-0.756258
78	1	0	-1.051237	5.177011	-1.052607
79	6	0	0.877565	5.390292	-2.001443
80	1	0	1.933682	5.392800	-1.714143
81	1	0	0.647197	6.325038	-2.524132
82	1	0	0.676439	4.548410	-2.666815
83	6	0	0.217060	6.365636	0.270509
84	1	0	-0.043393	7.337069	-0.162256
85	1	0	1.267661	6.380729	0.576222
86	50	0	0.005836	-0.087686	-0.733275
87	1	0	-0.401137	6.188383	1.155088

LSnO^{s}Bu

Center Number	Atomic Number	Atomic Type	Coordinates (Angstroms) X	Y	Z
1	8	0	0.018990	-1.097515	1.453446
2	7	0	1.549596	0.467874	-0.908175
3	7	0	-1.415365	0.447986	-0.970289
4	6	0	1.360694	0.693741	-2.218692
5	6	0	0.107680	0.864534	-2.827537
6	1	0	0.128196	1.079215	-3.886396
7	6	0	-1.166404	0.664597	-2.273988
8	6	0	2.575733	0.760001	-3.137100
9	1	0	3.050998	-0.222872	-3.216484
10	1	0	3.321457	1.449486	-2.730202
11	1	0	2.284142	1.090758	-4.135528
12	6	0	-2.337691	0.689855	-3.249311
13	1	0	-3.105907	1.389145	-2.906469

14	1	0	-2.803527	-0.298818	-3.308880
15	1	0	-2.001798	0.982011	-4.245639
16	6	0	2.871347	0.116261	-0.412692
17	6	0	3.332110	-1.217213	-0.538999
18	6	0	4.553001	-1.563031	0.050160
19	1	0	4.908575	-2.583440	-0.030498
20	6	0	5.313960	-0.621924	0.740642
21	1	0	6.254260	-0.911158	1.195991
22	6	0	4.867147	0.692187	0.833896
23	1	0	5.470206	1.427834	1.353690
24	6	0	3.651108	1.086606	0.259487
25	6	0	2.520798	-2.287825	-1.273581
26	1	0	1.716613	-1.789059	-1.819627
27	6	0	1.863095	-3.247283	-0.252622
28	1	0	2.632133	-3.751115	0.345102
29	1	0	1.274020	-4.010035	-0.776908
30	1	0	1.205634	-2.675297	0.407876
31	6	0	3.381631	-3.068235	-2.297039
32	1	0	3.854122	-2.391149	-3.018071
33	1	0	2.749189	-3.775104	-2.846166
34	1	0	4.169402	-3.640895	-1.796118
35	6	0	3.242067	2.560629	0.328762
36	1	0	2.256270	2.661449	-0.132888
37	6	0	4.238554	3.435802	-0.475161
38	1	0	5.242514	3.372903	-0.041650
39	1	0	3.918860	4.484294	-0.459134
40	1	0	4.293020	3.104169	-1.517471
41	6	0	3.140531	3.061683	1.789529
42	1	0	2.398661	2.476799	2.342618
43	1	0	2.833311	4.113890	1.804775
44	1	0	4.106128	2.977627	2.299648
45	6	0	-2.772738	0.145806	-0.536658
46	6	0	-3.253329	-1.183802	-0.606330
47	6	0	-4.528255	-1.463618	-0.100076

48	1	0	-4.901065	-2.480492	-0.139605
49	6	0	-5.320646	-0.461731	0.454521
50	1	0	-6.303669	-0.699055	0.845025
51	6	0	-4.847683	0.845655	0.500036
52	1	0	-5.471581	1.626689	0.919394
53	6	0	-3.578063	1.174688	0.007528
54	6	0	-2.417861	-2.322721	-1.196830
55	1	0	-1.525457	-1.888141	-1.654128
56	6	0	-1.948289	-3.277082	-0.071324
57	1	0	-1.311334	-2.721854	0.622185
58	1	0	-1.372812	-4.107507	-0.498489
59	1	0	-2.810809	-3.689686	0.464741
60	6	0	-3.196325	-3.095874	-2.289944
61	1	0	-4.069444	-3.602900	-1.865423
62	1	0	-2.546893	-3.857607	-2.736299
63	1	0	-3.541352	-2.423934	-3.084065
64	6	0	-3.130959	2.639257	0.040319
65	1	0	-2.115769	2.694830	-0.360964
66	6	0	-4.048624	3.510901	-0.855452
67	1	0	-4.051012	3.141528	-1.886323
68	1	0	-3.697320	4.549302	-0.858208
69	1	0	-5.078305	3.495183	-0.482484
70	6	0	-3.106219	3.193111	1.485961
71	1	0	-4.105817	3.160552	1.932703
72	1	0	-2.763306	4.234387	1.483282
73	1	0	-2.424751	2.605168	2.108920
74	6	0	1.564101	-1.898416	3.196275
75	1	0	2.374948	-1.339887	2.718668
76	1	0	1.565380	-2.916364	2.794944
77	1	0	1.746599	-1.941271	4.276584
78	6	0	0.212272	-1.224889	2.912345
79	6	0	-0.955617	-2.019589	3.526342
80	1	0	-0.737243	-2.177846	4.590941
81	1	0	-0.990480	-3.002202	3.041140

82	1	0	0.219747	-0.224513	3.380156
83	50	0	0.027294	0.749841	0.674177
84	6	0	-2.312232	-1.305785	3.372835
85	1	0	-2.283906	-0.319952	3.854458
86	1	0	-2.549863	-1.167877	2.315795
87	1	0	-3.116546	-1.887910	3.836485

LSnO(CO_2)^{s}Bu

Center Number	Atomic Number	Atomic Type	Coordinates (Angstroms) X	Y	Z
1	7	0	-1.738053	-0.303584	0.714099
2	7	0	0.501067	1.642003	0.682834
3	6	0	-1.754644	0.064982	2.007950
4	6	0	-0.870216	0.985007	2.587246
5	1	0	-1.025023	1.180671	3.638506
6	6	0	0.113259	1.766761	1.967068
7	6	0	-2.841471	-0.493541	2.917765
8	1	0	-3.829652	-0.185151	2.561024
9	1	0	-2.705551	-0.140218	3.941074
10	1	0	-2.820989	-1.586397	2.907850
11	6	0	0.728023	2.872100	2.816544
12	1	0	1.815945	2.784789	2.838206
13	1	0	0.342975	2.832262	3.836656
14	1	0	0.490936	3.849824	2.384228
15	6	0	-2.823337	-1.137569	0.201589
16	6	0	-2.706761	-2.546626	0.214496
17	6	0	-3.765264	-3.308897	-0.297375
18	1	0	-3.685998	-4.389854	-0.290302
19	6	0	-4.904456	-2.703984	-0.819607
20	1	0	-5.712435	-3.311298	-1.211529

21	6	0	-4.997806	-1.314888	-0.848823
22	1	0	-5.880476	-0.846284	-1.268783
23	6	0	-3.968249	-0.511412	-0.344963
24	6	0	-1.454354	-3.259086	0.727292
25	1	0	-0.725612	-2.509367	1.036054
26	6	0	-1.771136	-4.183844	1.928207
27	1	0	-2.195229	-3.616222	2.763443
28	1	0	-0.852581	-4.671149	2.274552
29	1	0	-2.488024	-4.961941	1.642566
30	6	0	-0.792836	-4.076120	-0.413845
31	1	0	-1.378622	-4.972586	-0.647753
32	1	0	0.219662	-4.361799	-0.116034
33	1	0	-0.714378	-3.471200	-1.323481
34	6	0	-4.104103	1.011495	-0.416140
35	1	0	-3.215260	1.451021	0.043580
36	6	0	-4.166320	1.484889	-1.890378
37	1	0	-3.275388	1.158747	-2.436837
38	1	0	-4.222534	2.579159	-1.934604
39	1	0	-5.049600	1.073060	-2.390419
40	6	0	-5.346465	1.505969	0.365934
41	1	0	-6.266232	1.106949	-0.075166
42	1	0	-5.399170	2.600557	0.338296
43	1	0	-5.300776	1.187134	1.412692
44	6	0	1.452546	2.604145	0.129099
45	6	0	2.843344	2.345847	0.178194
46	6	0	3.714135	3.292558	-0.378445
47	1	0	4.781760	3.111905	-0.340440
48	6	0	3.236709	4.451100	-0.982825
49	1	0	3.929747	5.167196	-1.409429
50	6	0	1.865717	4.682179	-1.046388
51	1	0	1.494968	5.579631	-1.528216
52	6	0	0.955380	3.772576	-0.496160
53	6	0	3.435357	1.086371	0.821194
54	1	0	2.614725	0.413781	1.084375

55	6	0	4.232885	1.442534	2.103370
56	1	0	5.080783	2.091592	1.856618
57	1	0	4.621070	0.528395	2.566927
58	1	0	3.607397	1.960271	2.836229
59	6	0	4.367095	0.335121	-0.166186
60	1	0	3.819405	0.008642	-1.052661
61	1	0	4.774098	-0.555110	0.330198
62	1	0	5.209342	0.966915	-0.468208
63	6	0	-0.544061	4.063256	-0.604388
64	1	0	-1.082780	3.264763	-0.087593
65	6	0	-0.911938	5.407297	0.072194
66	1	0	-0.609730	5.410317	1.124861
67	1	0	-1.994551	5.571060	0.021006
68	1	0	-0.414677	6.243308	-0.431026
69	6	0	-0.992723	4.062003	-2.087780
70	1	0	-0.480898	4.853303	-2.646061
71	1	0	-2.073761	4.232281	-2.156456
72	1	0	-0.760179	3.100527	-2.557106
73	8	0	0.965955	-1.311190	0.039121
74	8	0	2.243658	-1.426235	-1.860312
75	8	0	2.350354	-3.055102	-0.228728
76	6	0	1.866500	-1.877478	-0.761542
77	6	0	3.448408	-3.705729	-1.013404
78	1	0	4.120857	-2.911921	-1.350800
79	6	0	2.848161	-4.426410	-2.222117
80	1	0	2.112643	-5.166445	-1.891602
81	1	0	3.638685	-4.933909	-2.785616
82	1	0	2.365965	-3.689381	-2.867897
83	6	0	4.139282	-4.634766	-0.012362
84	1	0	4.943053	-5.166010	-0.537020
85	1	0	3.407687	-5.378646	0.324639
86	50	0	-0.218724	0.186840	-0.768685
87	6	0	4.699726	-3.863880	1.199722
88	1	0	5.457923	-3.138829	0.878603

89	1	0	3.884204	-3.321362	1.684082
90	1	0	5.159337	-4.545487	1.923044

LSnO^{t}Bu

Center Number	Atomic Number	Atomic Type	Coordinates (Angstroms) X	Y	Z
1	8	0	-0.006025	1.016818	1.529870
2	7	0	-1.470822	-0.330700	-0.987355
3	7	0	1.505021	-0.314058	-0.962764
4	6	0	-1.238101	-0.423816	-2.307441
5	6	0	0.032884	-0.536462	-2.892747
6	1	0	0.042496	-0.644668	-3.967945
7	6	0	1.292568	-0.407727	-2.286846
8	6	0	-2.424129	-0.399006	-3.265549
9	1	0	-2.911933	0.580489	-3.244118
10	1	0	-3.171321	-1.139485	-2.964981
11	1	0	-2.098451	-0.608445	-4.285870
12	6	0	2.492964	-0.365625	-3.226216
13	1	0	3.242245	-1.101481	-2.919636
14	1	0	2.971334	0.617981	-3.189049
15	1	0	2.185050	-0.570085	-4.253019
16	6	0	-2.821577	-0.082078	-0.505403
17	6	0	-3.330024	1.239264	-0.494727
18	6	0	-4.587829	1.469894	0.073542
19	1	0	-4.979686	2.479749	0.099977
20	6	0	-5.341749	0.426786	0.606440
21	1	0	-6.312997	0.626075	1.044882
22	6	0	-4.847445	-0.872446	0.563800
23	1	0	-5.444572	-1.685995	0.959905
24	6	0	-3.590943	-1.152103	0.009782

25	6	0	-2.534779	2.419733	-1.058525
26	1	0	-1.689456	2.022007	-1.625151
27	6	0	-1.957191	3.262905	0.103589
28	1	0	-2.768762	3.642310	0.736001
29	1	0	-1.392881	4.116964	-0.291091
30	1	0	-1.288648	2.634864	0.698659
31	6	0	-3.385564	3.291791	-2.013973
32	1	0	-3.811880	2.691473	-2.826027
33	1	0	-2.757625	4.075594	-2.452822
34	1	0	-4.206956	3.779696	-1.478639
35	6	0	-3.125428	-2.609378	-0.065144
36	1	0	-2.113650	-2.622948	-0.478468
37	6	0	-4.042929	-3.422638	-1.014673
38	1	0	-5.069504	-3.442193	-0.633090
39	1	0	-3.682997	-4.454961	-1.095710
40	1	0	-4.056860	-2.978994	-2.015766
41	6	0	-3.080746	-3.267860	1.334929
42	1	0	-2.406453	-2.714703	1.996249
43	1	0	-2.718267	-4.299264	1.254066
44	1	0	-4.077605	-3.287672	1.788035
45	6	0	2.850184	-0.063834	-0.463874
46	6	0	3.353977	1.258774	-0.436150
47	6	0	4.608923	1.487233	0.139085
48	1	0	4.997147	2.498085	0.178036
49	6	0	5.363843	0.441306	0.664423
50	1	0	6.332749	0.639024	1.108743
51	6	0	4.872941	-0.858713	0.608008
52	1	0	5.470239	-1.674413	0.999428
53	6	0	3.620070	-1.136752	0.044942
54	6	0	2.556784	2.443555	-0.987559
55	1	0	1.710344	2.050458	-1.555881
56	6	0	1.982731	3.274624	0.185062
57	1	0	1.317422	2.640155	0.776645
58	1	0	1.415350	4.131467	-0.198965

59	1	0	2.796291	3.649258	0.817683
60	6	0	3.405105	3.325272	-1.936307
61	1	0	4.226906	3.808827	-1.397662
62	1	0	2.775787	4.112556	-2.366928
63	1	0	3.830651	2.732965	-2.754616
64	6	0	3.160435	-2.595058	-0.046217
65	1	0	2.154348	-2.609561	-0.473110
66	6	0	4.093451	-3.399412	-0.988218
67	1	0	4.122994	-2.947402	-1.985210
68	1	0	3.735539	-4.431201	-1.083600
69	1	0	5.113924	-3.421947	-0.590791
70	6	0	3.098784	-3.262927	1.348905
71	1	0	4.087567	-3.272833	1.819691
72	1	0	2.751167	-4.298366	1.254872
73	1	0	2.405424	-2.722703	2.001103
74	6	0	-1.452401	0.566292	3.490101
75	1	0	-1.519949	-0.508391	3.283377
76	1	0	-2.269312	1.070499	2.964648
77	1	0	-1.568420	0.720712	4.568958
78	6	0	-0.099763	1.130029	3.004528
79	6	0	-0.013712	2.628859	3.355306
80	1	0	-0.085367	2.764318	4.440501
81	1	0	-0.829168	3.174478	2.873259
82	50	0	0.008309	-0.765130	0.600952
83	1	0	0.937248	3.041182	3.007217
84	6	0	1.074029	0.383826	3.675458
85	1	0	1.010529	-0.693220	3.482001
86	1	0	2.020193	0.755021	3.268952
87	1	0	1.060960	0.544174	4.759513

LSnO(CO_2)^{t}Bu

Center Number	Atomic Number	Atomic Type	Coordinates (Angstroms) X	Y	Z
1	7	0	1.743816	0.021573	0.693750
2	7	0	-0.772092	-1.541040	0.698215
3	6	0	1.753948	-0.412562	1.969409
4	6	0	0.717864	-1.132188	2.578395
5	1	0	0.863424	-1.362900	3.623867
6	6	0	-0.412312	-1.709616	1.984072
7	6	0	2.999516	-0.184955	2.817097
8	1	0	3.835192	-0.764888	2.410544
9	1	0	2.823303	-0.496255	3.847998
10	1	0	3.297369	0.864722	2.801612
11	6	0	-1.233803	-2.644190	2.863062
12	1	0	-2.284274	-2.343542	2.864421
13	1	0	-0.856298	-2.639623	3.886772
14	1	0	-1.189856	-3.665484	2.470746
15	6	0	2.960098	0.611404	0.137429
16	6	0	3.183049	2.005774	0.221997
17	6	0	4.364221	2.524881	-0.325402
18	1	0	4.551076	3.590128	-0.260822
19	6	0	5.294770	1.703626	-0.953784
20	1	0	6.201089	2.127720	-1.370684
21	6	0	5.051441	0.337175	-1.055027
22	1	0	5.770431	-0.300022	-1.557160
23	6	0	3.890391	-0.230389	-0.517709
24	6	0	2.192513	2.968021	0.886275
25	1	0	1.301455	2.404114	1.175498
26	6	0	2.812143	3.621580	2.149039
27	1	0	3.128643	2.869268	2.877638
28	1	0	2.075670	4.276618	2.628316
29	1	0	3.685045	4.225739	1.877885

30	6	0	1.751131	4.075728	-0.105213
31	1	0	2.615562	4.639530	-0.471712
32	1	0	1.082098	4.776905	0.408003
33	1	0	1.205675	3.649148	-0.949671
34	6	0	3.665124	-1.737053	-0.669230
35	1	0	2.710860	-1.988224	-0.198708
36	6	0	3.580030	-2.129564	-2.165789
37	1	0	2.775368	-1.577817	-2.662583
38	1	0	3.379930	-3.202899	-2.263573
39	1	0	4.521692	-1.905866	-2.678700
40	6	0	4.779527	-2.546604	0.040174
41	1	0	5.754658	-2.341186	-0.414450
42	1	0	4.579120	-3.620918	-0.045386
43	1	0	4.834265	-2.287120	1.102568
44	6	0	-1.866060	-2.348202	0.162063
45	6	0	-3.195568	-1.870702	0.213506
46	6	0	-4.215495	-2.674750	-0.312729
47	1	0	-5.238304	-2.318073	-0.276319
48	6	0	-3.936958	-3.911024	-0.887565
49	1	0	-4.740049	-4.518332	-1.289365
50	6	0	-2.620385	-4.358372	-0.958315
51	1	0	-2.402864	-5.313934	-1.421869
52	6	0	-1.568646	-3.592195	-0.442066
53	6	0	-3.548756	-0.494743	0.779247
54	1	0	-2.630020	0.011248	1.078252
55	6	0	-4.492059	-0.599652	2.002631
56	1	0	-5.438736	-1.076427	1.724078
57	1	0	-4.710736	0.402094	2.389752
58	1	0	-4.035306	-1.186610	2.806400
59	6	0	-4.201782	0.385109	-0.318305
60	1	0	-3.605894	0.357028	-1.237150
61	1	0	-4.235165	1.420949	0.027860
62	1	0	-5.214488	0.037822	-0.552359
63	6	0	-0.135982	-4.116338	-0.563277

64	1	0	0.534279	-3.376791	-0.117459
65	6	0	0.040413	-5.453393	0.199041
66	1	0	-0.218887	-5.337002	1.256568
67	1	0	1.080371	-5.793582	0.131276
68	1	0	-0.603974	-6.228733	-0.229416
69	6	0	0.259634	-4.283121	-2.051954
70	1	0	-0.379876	-5.025013	-2.542066
71	1	0	1.300441	-4.618245	-2.130967
72	1	0	0.158223	-3.331663	-2.584214
73	8	0	-0.971050	1.382119	0.200807
74	8	0	-0.826201	2.793354	-1.595943
75	8	0	-2.389967	3.101858	0.094241
76	6	0	-1.344821	2.445520	-0.515687
77	6	0	-2.960751	4.347333	-0.539154
78	6	0	-1.877352	5.432427	-0.616070
79	1	0	-1.459659	5.612155	0.380093
80	1	0	-2.319152	6.362640	-0.988521
81	1	0	-1.083606	5.106354	-1.288331
82	6	0	-4.064253	4.727712	0.455088
83	1	0	-4.558299	5.648393	0.128614
84	1	0	-3.629398	4.881201	1.446921
85	50	0	0.094896	-0.131212	-0.722405
86	1	0	-4.803969	3.924132	0.517216
87	6	0	-3.531672	4.012043	-1.925047
88	1	0	-2.727629	3.650626	-2.567260
89	1	0	-4.301166	3.238453	-1.836497
90	1	0	-3.981677	4.910068	-2.361209

LSnOtBu^F

Center Number	Atomic Number	Atomic Type	Coordinates (Angstroms) X	Y	Z
1	8	0	-0.145050	1.065484	0.233160
2	7	0	1.667631	-1.532037	0.259682
3	7	0	-1.283098	-1.837709	0.214410
4	6	0	1.563974	-2.793966	0.724130
5	6	0	0.364826	-3.517447	0.824940
6	1	0	0.464212	-4.537330	1.167734
7	6	0	-0.953284	-3.048923	0.691533
8	6	0	2.826961	-3.516439	1.176248
9	1	0	3.275784	-3.001672	2.030452
10	1	0	3.570982	-3.517284	0.374314
11	1	0	2.599520	-4.545181	1.459673
12	6	0	-2.063821	-3.992136	1.135218
13	1	0	-2.833029	-4.061034	0.359802
14	1	0	-2.548811	-3.613853	2.040708
15	1	0	-1.663601	-4.986519	1.340352
16	6	0	2.964152	-0.862891	0.312987
17	6	0	3.317124	-0.116073	1.460890
18	6	0	4.590970	0.463210	1.516377
19	1	0	4.877435	1.026762	2.396038
20	6	0	5.486189	0.341277	0.457443
21	1	0	6.468202	0.796117	0.519942
22	6	0	5.105677	-0.344690	-0.691749
23	1	0	5.790917	-0.409530	-1.528999
24	6	0	3.847654	-0.952250	-0.788619
25	6	0	2.341597	0.103772	2.619722
26	1	0	1.354125	-0.227091	2.290086
27	6	0	2.242579	1.607165	2.975758
28	1	0	3.182382	1.966651	3.409544
29	1	0	1.445221	1.760514	3.710718

30	1	0	2.006958	2.196504	2.092486
31	6	0	2.756997	-0.707338	3.872534
32	1	0	2.795552	-1.780446	3.661945
33	1	0	2.037472	-0.541238	4.682825
34	1	0	3.746429	-0.387615	4.219102
35	6	0	3.458105	-1.639473	-2.099251
36	1	0	2.467620	-2.084543	-1.971211
37	6	0	4.445106	-2.769005	-2.482587
38	1	0	5.450034	-2.366477	-2.648465
39	1	0	4.115277	-3.257619	-3.406550
40	1	0	4.502550	-3.524300	-1.691565
41	6	0	3.367641	-0.587248	-3.236280
42	1	0	2.698379	0.230148	-2.952489
43	1	0	2.990541	-1.052553	-4.154316
44	1	0	4.357480	-0.164650	-3.441993
45	6	0	-2.656607	-1.362739	0.306407
46	6	0	-3.139871	-0.858122	1.537619
47	6	0	-4.432093	-0.323290	1.579241
48	1	0	-4.808293	0.079820	2.511770
49	6	0	-5.238344	-0.292368	0.444073
50	1	0	-6.235569	0.129290	0.497074
51	6	0	-4.759353	-0.805079	-0.756442
52	1	0	-5.390475	-0.787186	-1.637447
53	6	0	-3.470175	-1.344615	-0.849583
54	6	0	-2.282689	-0.841739	2.806553
55	1	0	-1.422008	-1.496200	2.647676
56	6	0	-1.742501	0.586829	3.057333
57	1	0	-1.076988	0.876343	2.246227
58	1	0	-1.190657	0.622250	4.005147
59	1	0	-2.565118	1.308953	3.100923
60	6	0	-3.056662	-1.367395	4.040146
61	1	0	-3.882633	-0.698603	4.304018
62	1	0	-2.381272	-1.421726	4.901565
63	1	0	-3.467742	-2.366687	3.855846

64	6	0	-3.004403	-1.916858	-2.191109
65	1	0	-1.969512	-2.251227	-2.077643
66	6	0	-3.856483	-3.149547	-2.586045
67	1	0	-3.804075	-3.921618	-1.810642
68	1	0	-3.492127	-3.575184	-3.528245
69	1	0	-4.906057	-2.865273	-2.717682
70	6	0	-3.043977	-0.844298	-3.309481
71	1	0	-4.077439	-0.540959	-3.511346
72	1	0	-2.620304	-1.252223	-4.234378
73	1	0	-2.475510	0.042511	-3.021763
74	6	0	0.985416	2.902433	-0.842020
75	6	0	-0.333509	2.351327	-0.278042
76	6	0	-0.819093	3.282873	0.846457
77	50	0	0.107328	-0.607743	-0.944041
78	6	0	-1.394914	2.391859	-1.396666
79	9	0	-0.171922	3.035468	2.021235
80	9	0	-0.618692	4.597132	0.514791
81	9	0	-2.159281	3.090527	1.064589
82	9	0	-1.897166	3.639395	-1.610743
83	9	0	-0.850668	1.935466	-2.585635
84	9	0	-2.427822	1.540849	-1.103282
85	9	0	0.791644	3.924045	-1.726013
86	9	0	1.675733	1.900693	-1.493475
87	9	0	1.792984	3.357596	0.169698

LSnO(CO_2)$^{t}Bu^{F}$

Center Number	Atomic Number	Atomic Type	Coordinates (Angstroms) X	Y	Z
1	7	0	-2.038637	-1.454622	0.715732
2	7	0	-1.970957	1.505082	0.720716

3	6	0	-2.510319	-1.227391	1.957460
4	6	0	-2.631674	0.037279	2.547124
5	1	0	-3.002486	0.043911	3.561743
6	6	0	-2.424390	1.297485	1.972189
7	6	0	-3.009386	-2.406326	2.781832
8	1	0	-3.845541	-2.893735	2.269735
9	1	0	-3.340783	-2.073417	3.766568
10	1	0	-2.224099	-3.155326	2.901502
11	6	0	-2.804775	2.501188	2.823857
12	1	0	-1.957937	3.184907	2.917877
13	1	0	-3.122757	2.183625	3.818025
14	1	0	-3.618469	3.058196	2.348108
15	6	0	-2.047887	-2.818751	0.185955
16	6	0	-0.932485	-3.666584	0.385330
17	6	0	-0.973557	-4.956687	-0.159980
18	1	0	-0.128052	-5.617760	-0.011714
19	6	0	-2.070757	-5.398891	-0.892606
20	1	0	-2.079057	-6.399879	-1.308369
21	6	0	-3.153268	-4.548436	-1.098186
22	1	0	-4.002613	-4.891716	-1.677477
23	6	0	-3.164173	-3.253446	-0.567092
24	6	0	0.310477	-3.230953	1.167298
25	1	0	0.207336	-2.172805	1.417678
26	6	0	0.466974	-4.051139	2.473977
27	1	0	-0.409812	-3.951981	3.120596
28	1	0	1.345566	-3.702728	3.028672
29	1	0	0.604544	-5.113200	2.242436
30	6	0	1.592259	-3.389354	0.314463
31	1	0	1.777590	-4.444741	0.084019
32	1	0	2.456371	-3.010072	0.866872
33	1	0	1.523673	-2.842122	-0.627866
34	6	0	-4.376838	-2.354383	-0.822981
35	1	0	-4.203588	-1.399551	-0.319387
36	6	0	-4.546411	-2.073416	-2.337548

37	1	0	-3.642700	-1.611102	-2.747839
38	1	0	-5.392006	-1.395189	-2.502697
39	1	0	-4.737760	-3.003049	-2.884095
40	6	0	-5.670805	-2.976940	-0.240854
41	1	0	-5.896808	-3.928522	-0.733660
42	1	0	-6.518313	-2.299416	-0.396297
43	1	0	-5.566490	-3.162547	0.833350
44	6	0	-1.948076	2.869849	0.193030
45	6	0	-0.794234	3.673715	0.339639
46	6	0	-0.817631	4.971183	-0.190419
47	1	0	0.058693	5.599117	-0.081740
48	6	0	-1.934854	5.459889	-0.860315
49	1	0	-1.929719	6.465604	-1.264691
50	6	0	-3.054969	4.648624	-1.020806
51	1	0	-3.918918	5.025996	-1.555788
52	6	0	-3.084437	3.349562	-0.501058
53	6	0	0.480766	3.176402	1.027756
54	1	0	0.350261	2.124196	1.285865
55	6	0	0.780591	3.982399	2.316688
56	1	0	0.932395	5.041836	2.081903
57	1	0	1.692167	3.599800	2.789393
58	1	0	-0.039723	3.904726	3.037522
59	6	0	1.686699	3.269142	0.061122
60	1	0	1.464748	2.778464	-0.889704
61	1	0	2.564139	2.784427	0.492105
62	1	0	1.935419	4.315992	-0.148161
63	6	0	-4.334248	2.490315	-0.710921
64	1	0	-4.176142	1.532539	-0.208321
65	6	0	-5.588744	3.155912	-0.092031
66	1	0	-5.442086	3.347942	0.976152
67	1	0	-6.460109	2.501744	-0.211547
68	1	0	-5.805238	4.108996	-0.586257
69	6	0	-4.557471	2.208270	-2.218463
70	1	0	-4.727513	3.142288	-2.764610

71	1	0	-5.432560	1.562061	-2.356589
72	1	0	-3.683473	1.709493	-2.650372
73	8	0	0.582365	0.004402	0.170335
74	8	0	1.817220	-0.538645	-1.698034
75	8	0	2.797188	0.060758	0.324463
76	6	0	1.672369	-0.191474	-0.531532
77	6	0	4.128456	-0.021677	-0.186144
78	6	0	4.617223	-1.462030	-0.323162
79	6	0	4.914488	0.675961	0.941024
80	50	0	-1.316599	0.013333	-0.706917
81	6	0	4.379871	0.727193	-1.513998
82	9	0	4.346198	-0.106011	-2.589651
83	9	0	3.460556	1.720582	-1.685342
84	9	0	5.626554	1.303908	-1.491676
85	9	0	3.833797	-2.218675	-1.137941
86	9	0	4.622798	-2.056585	0.918109
87	9	0	5.893072	-1.473819	-0.814934
88	9	0	4.499074	0.246957	2.160910
89	9	0	6.255005	0.443083	0.843085
90	9	0	4.698735	2.031901	0.872971
